Decrypting the Crustal Evolution of the Mozambique Belt in Malawi

Blackwell Chawala Manda

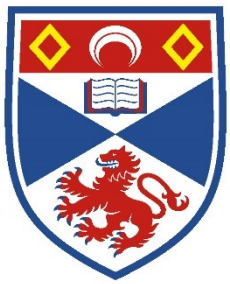

University of
St Andrews

This thesis is submitted in partial fulfilment for the degree of PhD

at the

University of St Andrews

26th February 2016

“One thing I have learned through my career in science is to never completely believe anything – as Einstein remarked, God is subtle; it’s easy to be wrong.” William M. White

Declarations

1. Candidate's declarations:

I, Blackwell C. Manda, hereby certify that this thesis, which is approximately thirty five thousand words in length, has been written by me, and that it is the record of work carried out by me, or principally by myself in collaboration with others as acknowledged, and that it has not been submitted in any previous application for a higher degree.

I was admitted as a research student in May 2011 and as a candidate for the degree of Doctor of Philosophy in May, 2013; the higher study for which this is a record was carried out in the University of St Andrews between 2013 and 2016.

I, Blackwell C. Manda, received assistance in the writing of this thesis in respect of language, grammar, spelling or syntax, which was provided by Professor Peter Cawood, Dr Ruth Robinson, Dr Anthony R. Prave and Dr Christopher J. Spencer.

Funding for this thesis was provided by the University of Malawi, University of St Andrews, and the National Environment Research Council (NERC).

Date …… signature of candidate ……

2. Supervisor's declaration:

I hereby certify that the candidate has fulfilled the conditions of the Resolution and Regulations appropriate for the degree of Doctor of Philosophy in the University of St Andrews and that the candidate is qualified to submit this thesis in application for that degree.

Date …..…… signature of supervisor ……

3. Permission for publication:

Permission for electronic publication:

In submitting this thesis to the University of St Andrews I understand that I am giving permission for it to be made available for use in accordance with the regulations of the University Library for the time being in force, subject to any copyright vested in the work not being affected thereby. I also understand that the title and the abstract will be published, and that a copy of the work may be made and supplied to any bona fide library or research worker, that my thesis will be electronically accessible for personal or research use unless exempt by award of an embargo as requested below, and that the library has the right to migrate my thesis into new electronic forms as required to ensure continued access to the thesis. I have obtained any third-party copyright permissions that may be required in order to allow such access and migration, or have requested the appropriate embargo below.

The following is an agreed request by candidate and supervisor regarding the publication of this thesis:

PRINTED COPY

a) Embargo on all or part of print copy for a period of 2 years (maximum five) on the following ground(s):
    - Publication would preclude future publication

ELECTRONIC COPY

a) Embargo on all or part of electronic copy for a period of 2 years (maximum five) on the following ground(s):
    - Publication would preclude future publication

Date …… signature of candidate …… signature of supervisor ……

ABSTRACT

Global paleogeography exerts a first order control on both the deep and surficial components of the Earth system. Temporal and spatial constraints on the Mozambique Belt of Eastern Africa are needed to understand its crustal evolution and its role in assembly of Gondwana. This thesis provides detailed data on the timing, sources and nature of tectono-thermal events responsible for magmatism in the Mozambique Belt in southern Malawi.

An integrated approach of petrography, geochemistry, radiogenic isotopes, and single zircon geochronology has been used to determine spatial and temporal constraints and to better constrain models of the assembly of East and West Gondwana, which occurred along the Mozambique Belt. In particular the thesis attempts to address key unresolved questions about the number and timing of accretionary pulses within the orogen.

LA-ICP-MS single zircon U-Pb results show tectono-thermal events in four periods: Mesoproterozoic from 1128 ± 30 Ma to 1033 ± 20 Ma; Neoproterozoic (956 ± 12 Ma – 594 ± 65 Ma); Cambrian (530 ± 3 Ma – 515 ± 12 Ma); and Cretaceous (118 ± 2 Ma). Metamorphism is dated from a charnockitic gneiss that yielded a lower intercept age of 515 ± 18 Ma.

The granitoids are intermediate to acidic with relative enrichment in LILEs and depletion in HFSEs with moderately negative anomalies in Th, Nb, P, Zr and Ti. REE spider plots show enrichment in LREEs and depleted HREEs with negative Eu anomalies. The meta-granites are largely metaluminous with a few peraluminous, I-type granites belonging to the calc-alkaline series.

Radiogenic isotope data reveals slight differences with older, Mesoproterozoic rocks showing positive εNd and εHf values signifying derivation from depleted mantle material, whilst the younger rocks display negative epsilon values suggestive of crustal material recycling and mixing for their source and origins.

Granitoids of southern Malawi display characteristics consistent with derivation in a continental Andean type arc with some aspects of the chemistry resembling tonalite-trondhjemite-granite (TTG) suites mapped in the Mozambique Belt in Kenya, Tanzania, Mozambique, and Antarctica although the data are not sufficiently compelling to assign the Malawi rocks to classic TTGs.

ACKNOWLEDGEMENTS

I would like to thank the University of Malawi (Chancellor College) and the University of St Andrews for sponsorship and the special opportunity that enabled me study for my PhD. I would also like to thank NERC Isotope Geology Laboratory (NIGL) in Nottingham UK for the award to carry out the isotope geochronology analyses for this research.

I would like to specially thank my supervisor Professor Peter Cawood whose clinical attention to detail and patience pushed me to finally rise up to the high bar. It was a very special privilege. Dr Ruth Robinson (St Andrews) and Professor John Saka (University of Malawi) are specially thanked for their academic guidance and moral encouragement during my studies. Heartfelt thanks go to Dr Anthony Prave who untiringly advised and supported me in the writing up of this thesis.

I am indebted to Dr Christopher Spencer and his family who combined academic advice and a home whilst I studied in St Andrews. Dr Nick Roberts of NIGL (UK) deserves special thanks for the technical expertise in geochronology dating.

German fellow PhD student "Batzi" will always be remembered for his untypical and untiring assistance. My fellow PhD students in Room 500 and 600 are thanked for encouragement and support in this journey.

I am indebted to Dr Gareth Izon and Dr Cheryl Wood for step by step advice in the laboratories at St Andrews. I would like to say "thank you" to the technical staff in the School of Geography and Geosciences at the University of St Andrews in Donald Herd, Colin Cameron, Stuart Allison and Andy Mackie, Angus Calder and many more for their technical assistance in my studies. Technical staff in the Department of Geography and Earth Sciences in Chancellor College are also thanked for their help in getting my samples prepared and exported to St Andrews for analysis. Jonathan Gwaligwali, Messrs Mpando and Namatingwi are specially thanked for this.

I found solace during this daunting and stressful journey from very dear Christian friends in Scotland & Malawi and across the horizons - "God bless you". Specially remembered will be Ron Borthwick (Glasgow) a friend and pastor who gave me untold spiritual backing but is now not in this world anymore – "Till we meet".

To my beloved wife Phelire - it's all priceless – not enough words will amount. My children Lusungu, Jireh and Tsidkenu "I love you too much". God bless you.

CONTENTS

LIST OF FIGURES

LIST OF TABLES

LIST OF APPENDICES

Chapter 1: Thesis Outline

1.0 Introduction

1.1 RATIONALE

The motivation to conduct this study lies in providing a detailed study of all (meta)igneous and related tectono-thermal events in the Mozambique Belt, Southern Malawi, through time. Their precise ages, tectonic settings and any other inherent information will address key paleogeographic questions with a potential to shed more light on the tectonic assembly of Gondwana. This dataset for Southern Malawi will be integrated with, and better constrain, models of assembly of East and West Gondwana along the Mozambique Belt, and in particular address the question of the number and timing of accretionary pulses within the orogen. In a more general sense the study will provide insight into the mechanisms of reworking of older cratonic fragments and orogenic belts caught within the suture zone. Previous geochronological work (whole-rock and mineral Rb-Sr and K-Ar, and U-Pb zircon conventional methods), indicates an Archean – Neoproterozoic crust for Malawi for the various supracrustals and calc-alkaline magmatism overlying the different sections forming this part of the Mozambique Belt (Andreolli, 1984; Kröner et al., 2001). However, the nature and timing of the tectono-thermal events are poorly understood, and hitherto not well constrained, which in turn compromises our understanding of the basic regional tectono-thermal dynamics of the Mozambique Belt. Malawi lying at the junction of the East African Orogen and the Kuunga Orogen (Meert, 2003) is critical to our understanding of Gondwana assembly as it partly has a record of collision, arc magmatism and subduction dynamics.

1.2 OBJECTIVES:

The main objectives of this part of the thesis are to enhance understanding of the Mesoproterozoic and Neoproterozoic tectonothermal events in the Mozambique Belt in Malawi as reflected in the record of calc-alkaline and related magmatism, and related intrusions into supracrustal rocks, employing modern approaches that provide increased precision, accuracy, and resolving power in geochronology, major and trace element geochemistry, and petrographic studies. Importantly in this study integration of new high precision U-Pb, Nd and Hf isotopic data will aid in:

1. Establishing crustal growth zones in the region;

2. Constraining the timing of granulite facies metamorphism; and

3. Helping define the boundaries of the Mozambique Belt in Malawi with the adjacent belts that are presumed to be Mesoproterozoic in age.

1.3 METHODS

The timing of metamorphism will be determined using U-Pb zircon geochronology and the analysis of cores (crystallisation) and rims (metamorphism), and on other uranium-bearing minerals present in granitoids or gneisses (e.g. rutile and monazite) which would provide metamorphic ages. Isotopic analyses (Nd whole rock and zircon Hf) will supply critical information on crustal growth and evolution during terrane amalgamation and will be used to discriminate old reworked and juvenile crust. The new datasets will be integrated to better constrain models of the assembly of East and West Gondwana along the Mozambique Belt, and in particular address key unresolved questions about the number and timing of accretionary

pulses within the orogen. In a more general sense, the study will provide insight into the mechanisms of reworking older cratonic fragments and orogenic belts caught within the east-west Gondwana suture zone.

Chapter Two presents a synopsis of the literature that was background to this research.

Chapter Three looks at the geology of the study area. The geology of southern Malawi is reviewed after reconnaissance mapping. The main lithological units were sampled for petrographic, geochemistry, and geochronological work.

Chapter Four is a presentation of XRF and ICP-MS whole rock major and trace element geochemistry of the southern Malawi granitoids with aim of characterising the rocks as well as their geotectonic settings. Comparisons are drawn between the granitoids with those of surrounding regions.

Chapter Five presents the LA-ICP-MS single zircon geochronological data, constraining the areas magmatism ages as well as placing some constraints on metamorphism.

Chapter Six is the radiogenic isotopes where whole rock samarium and neodymium (Sm-Nd) data is presented and analysed. Lutetium and Hafnium (Lu-Hf) data from single zircon spots are also presented.

Chapter Seven is a discussion chapter with conclusions, some perspectives and synopsis.

Chapter 2: Literature Review

2.1 INTRODUCTION

Geochronological and petrogenetic data for high grade biotite (± hornblende) gneisses along with associated metaigneous rocks in the Mozambique Belt, south-western Malawi (Fig. 2.1 & 2.2) will provide new constraints on the character of tectono-thermal events associated with the Neoproterozoic assembly of the supercontinent Gondwana, as well as provide more general insight into the processes of continental assembly. The timing and mechanism of Gondwana assembly remain enigmatic and the Malawi region has been selected so as to provide an enhanced understanding as to the nature of the bounding cratonic fragments and their associated continental margin and convergent plate margin assemblages. Better understanding of the history of the Mozambique Belt (Fig. 2.3), one of the principal sutures in Gondwana assembly, will help constrain global paleogeography during the Neoproterozoic, which is a first order control on the profound changes that the Earth system was undergoing with respect to surface and solid Earth processes during that key time in Earth history (Cawood and Buchan, 2007; Collins and Pisarevsky, 2005).

Fig. 2.1: Map showing the location of Malawi (inset) in Africa (Compiled by Blackwell Manda)

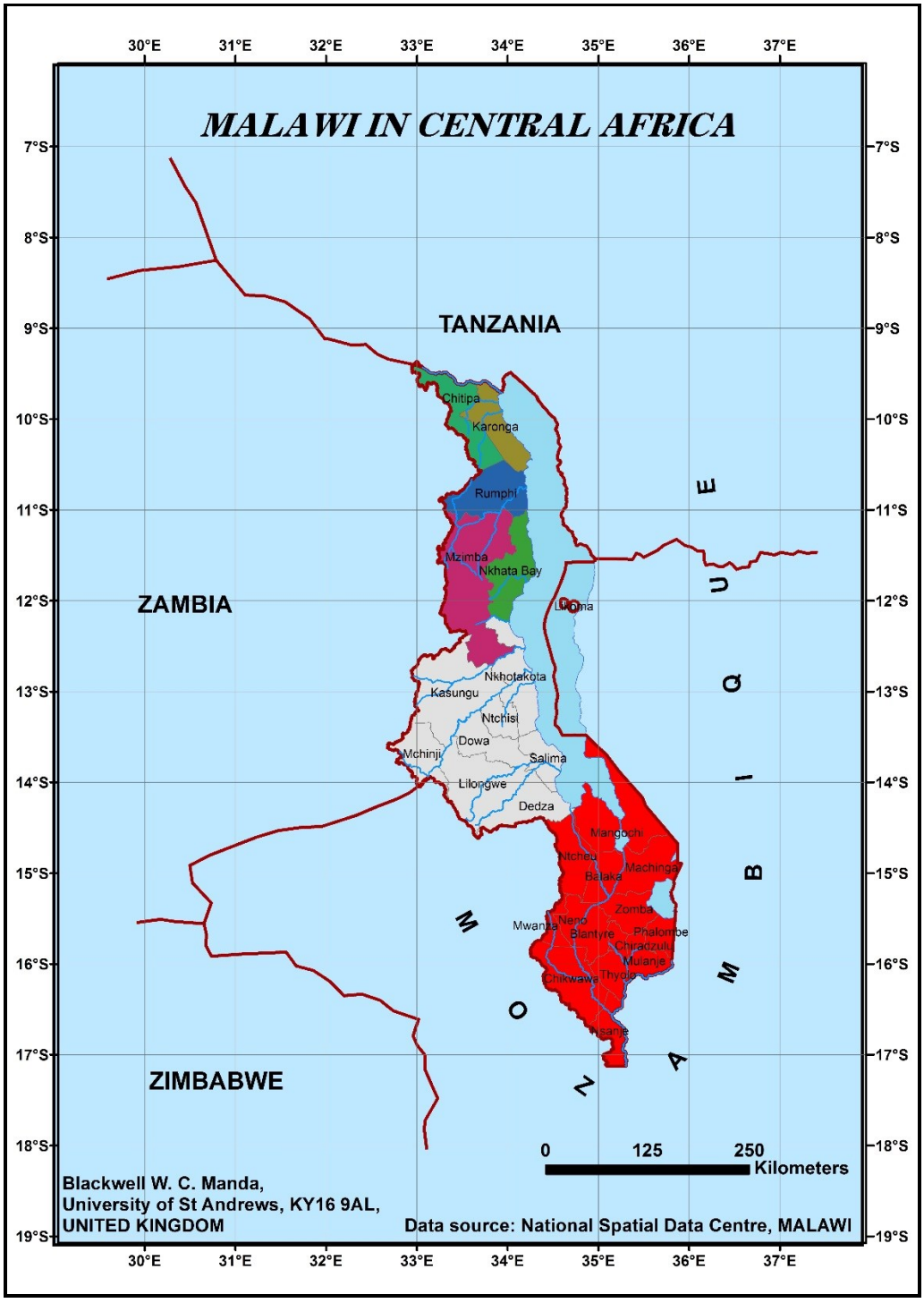

Fig. 2.2: Map showing Malawi in relation to neighbouring countries. Malawi is subdivided into three regions North, Central, and South which are shown in different colours on the map. (Compiled by Blackwell Manda).

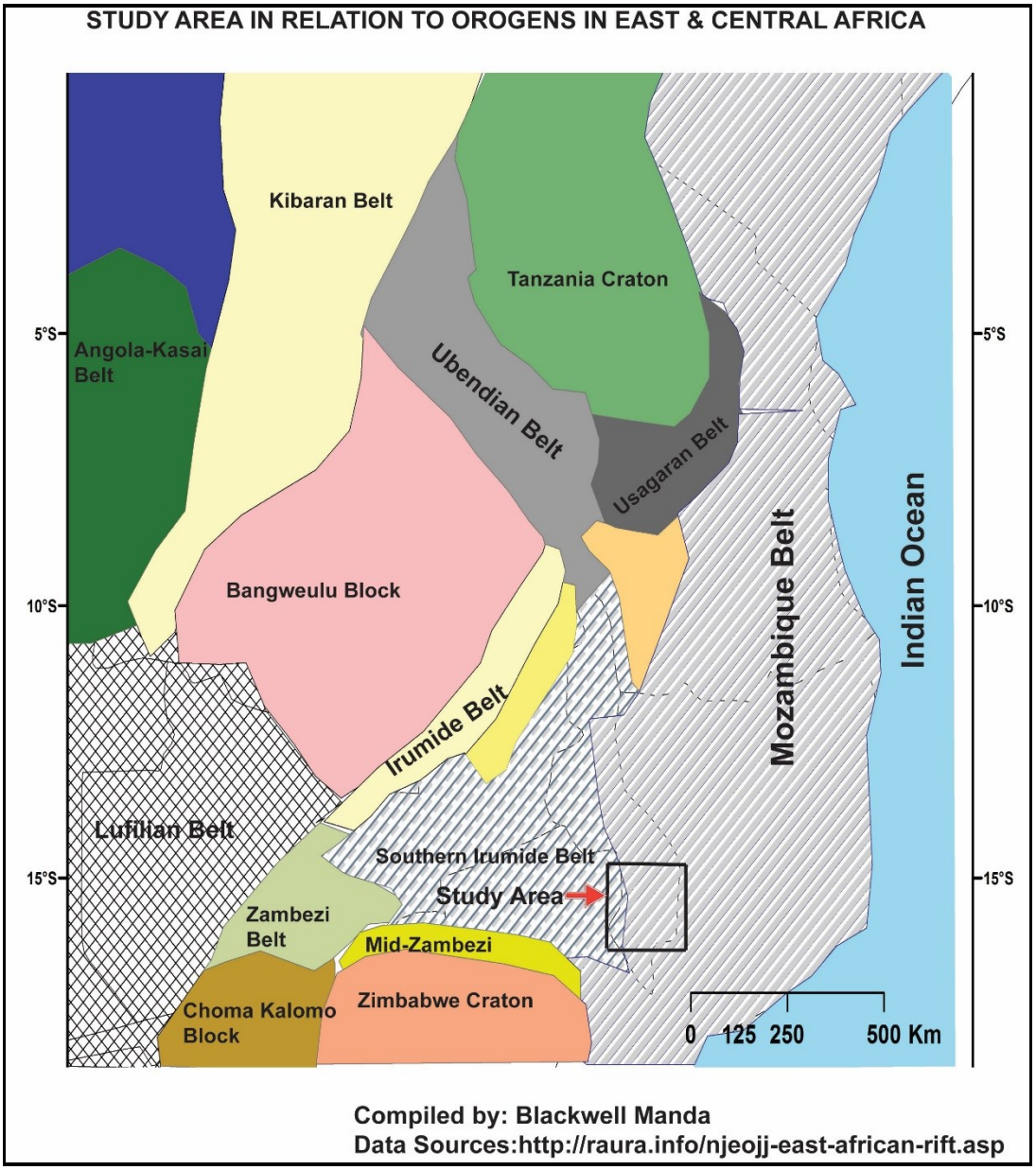

Fig. 2.3: Tectonic map showing Mozambique Belt in relationship with other belts. Study area is indicated in southern Malawi.

2.2 RODINIA SUPERCONTINENT

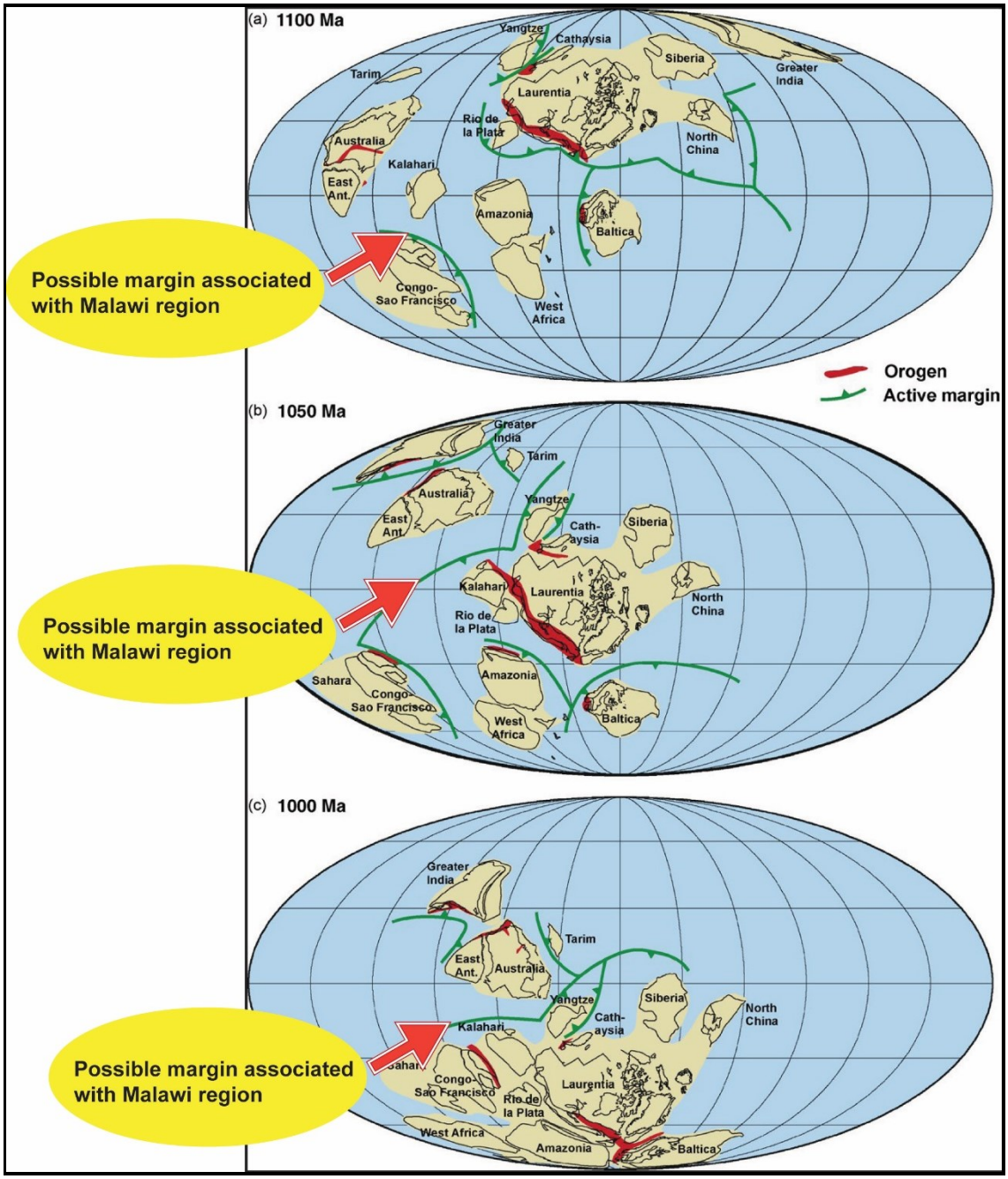

Fig. 2.4: Diagrams showing the assembly and break-up of Rodinia, and the formation of Gondwanaland and possible positions of the Malawi region in time. (a) 1100 Ma; (b) 1050 Ma; (c) 1000 Ma; (d) 900 Ma; (e) 825 Ma; (f) 780 Ma; (j) 600 Ma; (k) 550 Ma; (l) 530 Ma.

Sources: Adapted from Li et al., 2008, Precambrian Research 160 (2008) 179–210.

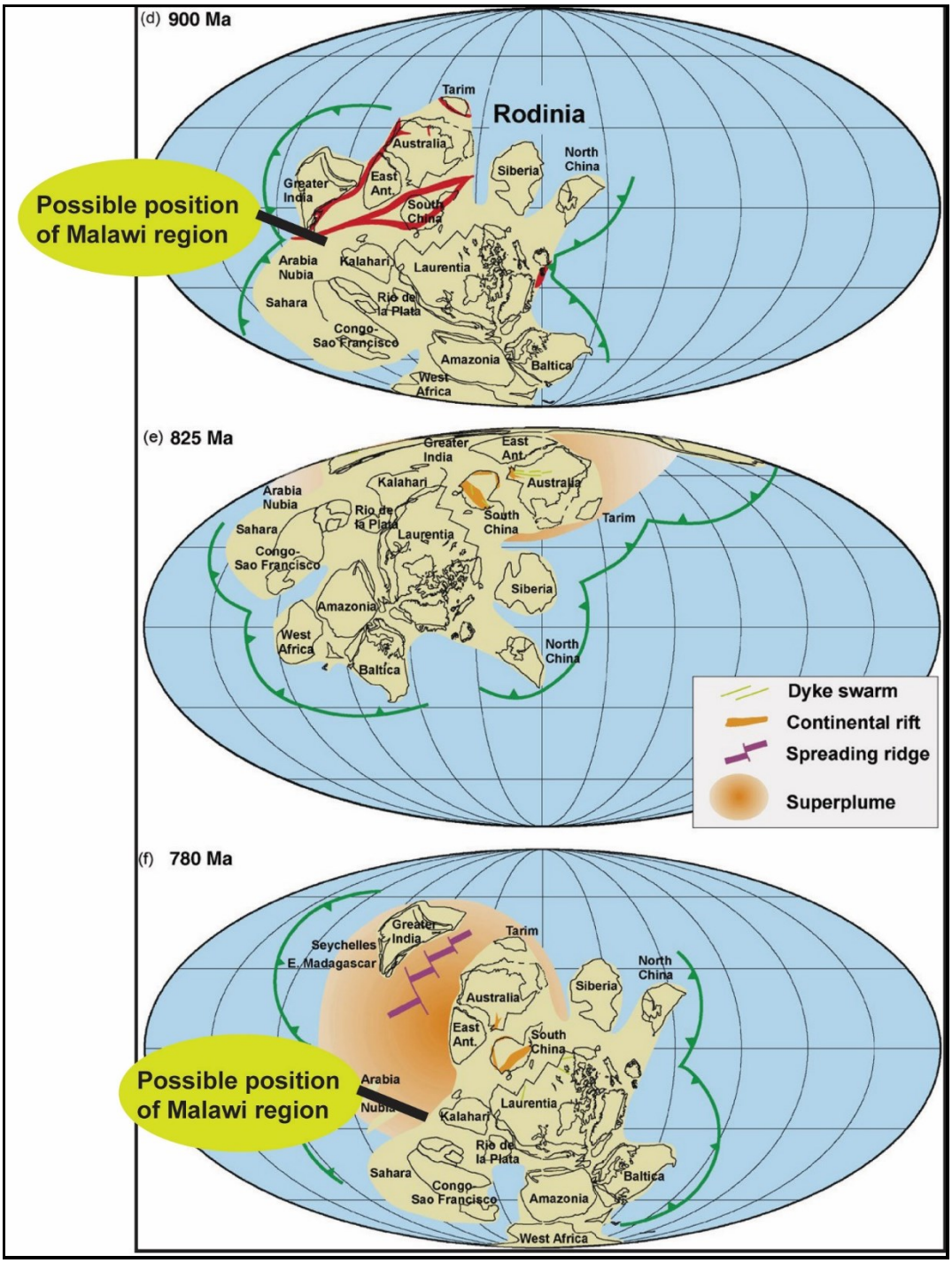

Fig. 2.4: (Continued)

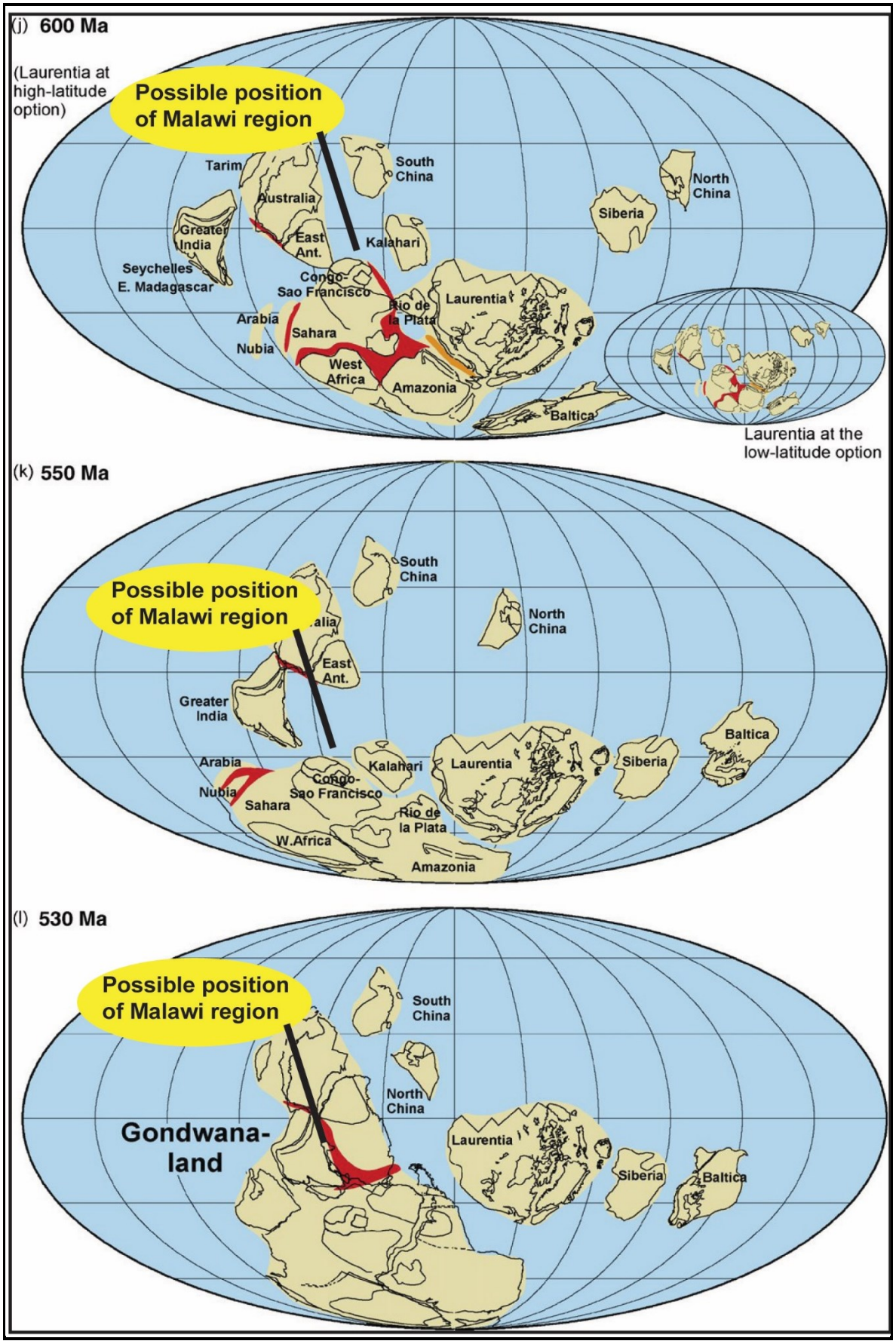

Fig. 2.4: (Continued)

The amalgamation of Laurentia, Siberia, North China, Cathaysia and possibly Rio de la Plata had taken place by 1000 Ma with Laurentia in the process of colliding with the Yangtze craton. All the other continental blocks were apart from Laurentia separated by oceans (Fig. 2.4 (a)) (Li et al., 2008). Kalahari may have collided with southern Laurentia by 1050 Ma with the development of convergent margins in between most of the continents by 1030 Ma (Fig. 2.4 (b) and (c)). India, Australia – East Antarctica and Tarim had amalgamated and collided with Laurentia by 1100 Ma. The known major continental blocks were all assembled together to form Rodinia supercontinent by 900 Ma (Fig. 2.4 (d)) (Li et al., 2008).

Superplume events (due to mantle avalanches surrounding the supercontinent) largely between 900 and 820 Ma and associated bimodal magmatism (750 Ma – 720 Ma) have been proposed as being responsible for the break-up of Rodinia (Li et al., 2008). Rodinia supercontinent break-up started with disintegration around Laurentia with continental bits drifting from Laurentia and colliding with other pieces to make up Gondwana supercontinent (Li et al., 2008). By 600 Ma much of Western Gondwana had amalgamated but oceans were still present between Australia–East Antarctica, India, eastern Africa and Kalahari (Fig. 2.4 (j)). The final assembly of Gondwana occurred by 540 – 530 Ma by the closing of the Mozambique Ocean and the collision of India with Australia-East Antarctica (Fig. 2.4 l) (Li et al., 2008).

2.3 GONDWANA ASSEMBLY

The African continent consists of a series of Archean cratons (e.g. Kaapvaal, Zimbabwe, Tanzania) sutured by a series of Mesoproterozoic and Neoproterozoic orogenic belts associated with the assembly of the Rodinia and Gondwana supercontinents, respectively, all bounded by Mesozoic to Tertiary rifts and passive margin successions that define the present day margins of Africa and formed during the breakup of Pangea/Gondwana (Johnstone et al., 2005; Muhongo et al., 2001).

Our understanding of the character and timing of Gondwana assembly has evolved, particularly over the last few decades, through a combination of renewed field investigations combined with analytical developments, notably in geochronology (compare McWilliams, 1981 with Meert, 2003). Reliable data that can be tied to a tectonic framework are available now for many of the cratons in Gondwana (Meert, 2003). Cooling histories of the orogenic belts have also been developed. However, events in some regions are better constrained than in others (e.g., Arabian–Nubian Shield vs. Kenya–India (Meert, 2003)).

Gondwana assembly (Fig. 2.5) occurred along a network of Pan-African–Brasiliano orogenic belts during the Neoproterozoic and Cambrian (Stern, 1994; de Wit et al., 2001; Meert, 2003; Cawood and Buchan, 2007; Jacobs and Thomas, 2004; Collins and Pisarevsky, 2005; Bingen et al., 2009). Three main pulses of assembly are recognized (Meert, et al 1997): the East African Orogeny (800 - 650 Ma), which formed the Mozambique Belt after the collision of India, Madagascar and Sri Lanka with East Africa; the Brasiliano orogeny (600 - 530 Ma) that amalgamated the South American nuclei and Africa; and the Kuunga orogeny (570 - 530 Ma) which was the collision between Australia and Antarctica with the rest of Gondwana (Meert, et al 1997; Meert, 2003).

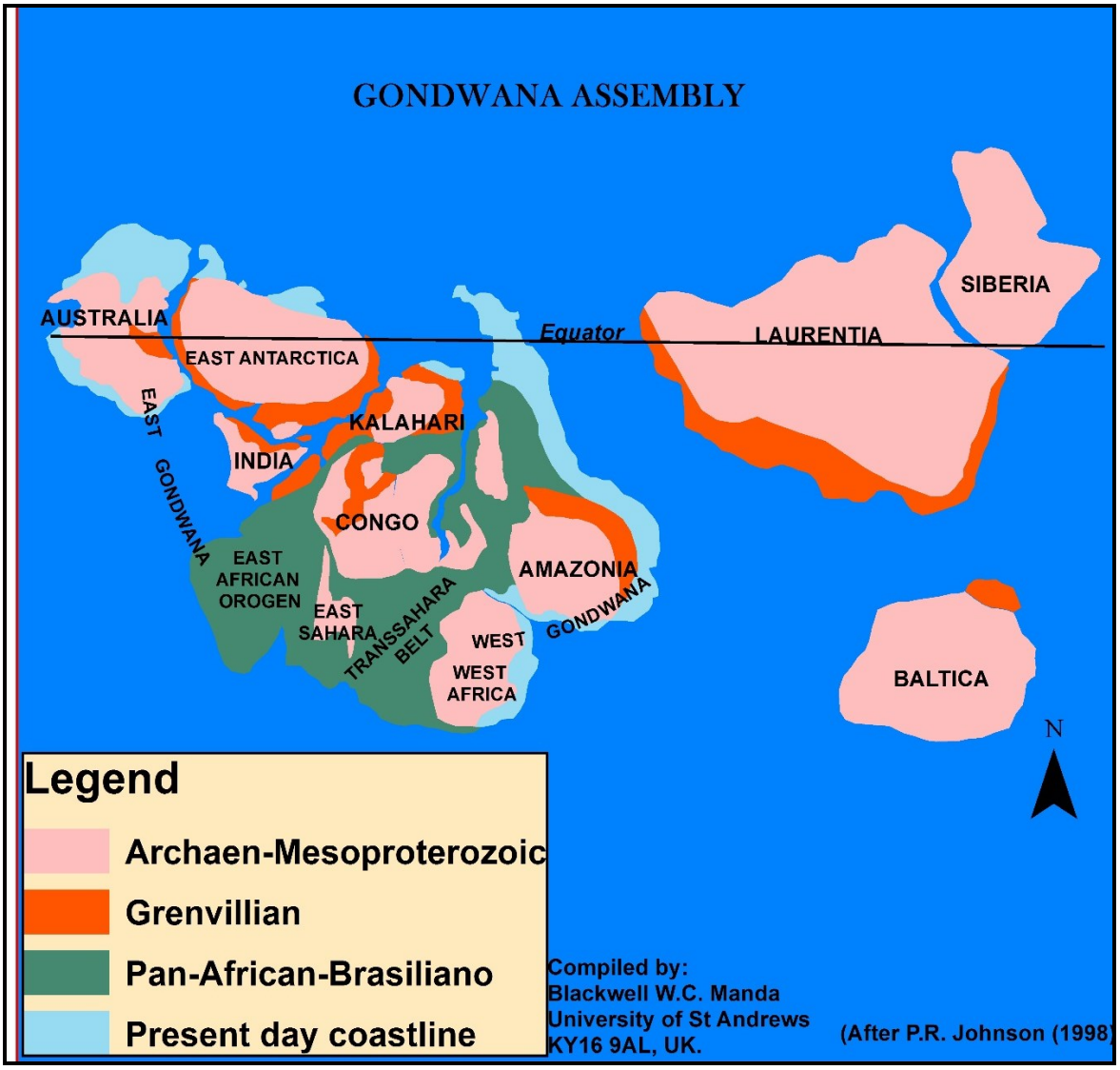

Fig. 2.5: Illustrating Gondwana Assembly during the Neoproterozoic and Cambrian (after Johnson P.R. (1998))

2.4 THE MOZAMBIQUE BELT

The Mozambique Belt (750 – 530 Ma) is the suture between East (India, Madagascar, Antarctica, Australia) and West (Africa, South America) Gondwana (Meert, et al 1997; Meert, 2003). It represents a zone of continent–continent collision comparable to the modern Alpine-Himalayan orogen (Meert, 2003) and is also referred to as "The East African–Antarctic orogen" (Jacobs et al., 1998). The belt stretches from Arabia in the north (the Arabian-Nubian shield), along the East African margin (the Mozambique belt), into East Antarctica, a distance over 8000 km and it is generally 1000 km wide (Muhongo and Lenoir, 1994; Stern, 1994; Jabobs et al., 2004). Holmes in 1951 was the first to name this region the Mozambique Belt upon realising the structural discontinuity between the Tanzanian craton and gneisses to the east (Grantham et al., 2003).

The geologic character of the Mozambique Belt varies considerably from north to south (Jabobs et al., 2004). The northern part of the belt (Arabian–Nubian Shield) is dominated by juvenile mid-Neoproterozoic island arc terranes bounded by suture zones with abundant ophiolites, and marked by low to medium grade deformation (Jacobs et al., 2004). The southern

part, from Kenya to Dronning Maud Land (East Antarctica), is underlain by high-grade rocks (up to granulites facies) of Neoproterozoic–Cambrian age with Archean –Mesoproterozoic protoliths. Neoproterozoic plutons intrude the gneisses, and this part of the orogen is considered as resulting from continent-continent collision (e.g., Muhongo and Lenoir, 1994; Jacobs et al., 1998; Kröner, 2001; Jacobs et al., 2004).

Variations in the models put forward in the assembly of Gondwana have often primarily been because of the lack of accurate geological information. For example, Stern (2002 and references therein) indicated that the northern part of the Mozambique Belt (i.e., in Egypt, Sudan, Eritrea, Ethiopia and northern Kenya) consists mainly of juvenile crust, whereas its southern portion (i.e., central-south Kenya and Tanzania) is made up of mainly reworked Neoarchean and Paleoproterozoic crust. Sacchi et al. (1984) described Mesoproterozoic events in the southern part of the Mozambique belt (what they termed the '1000 Ma-old Kibaran events') and Andreoli (1981, 1984) documented the same age 'Kibaran tectono-thermal events' in the Mozambique belt of southern Malawi. Later Daly (1986) argued that both the Mozambique and the Irumide Belts of central Africa were formed during the same (Mesoproterozoic) orogenic period (about 1100 Ma ago).

Muhongo et al., (2003) however, used single zircon evaporation dating and the SHRIMP technique to argue that there is no evidence for Mesoproterozoic (Kibaran) metamorphism and deformation in this region but rather that the only evidence for fragmentation of Rodinia is the calc-alkaline magmatism (~1200-950 Ma) in northern Mozambique, southern Malawi and southern Tanzania, and that there is no evidence for post-1300 Ma sedimentation along the purported passive margins of the Mozambique belt in East Africa. No isotopic ages are available for sedimentation in the Mesoproterozoic in the Mozambique Belt in Malawi (Muhongo et al., 2003).

In a review of carbonate rocks in the Mozambique Belt, Grantham et al. (2003) noted the occurrence of strongly deformed carbonate, quartzite, and phyllosilicate schists intruded by 1105 Ma dolerite dykes in the central Mozambique and eastern Zimbabwe area, including 1400 Ma carbonate rocks in the Zambezi Belt. In central Mozambique and eastern Zimbabwe 1100 Ma carbonate rocks are present (Grantham et al., 2003). These occurrences are important in that they define the development of continental shelves and, hence, potential plate boundaries.

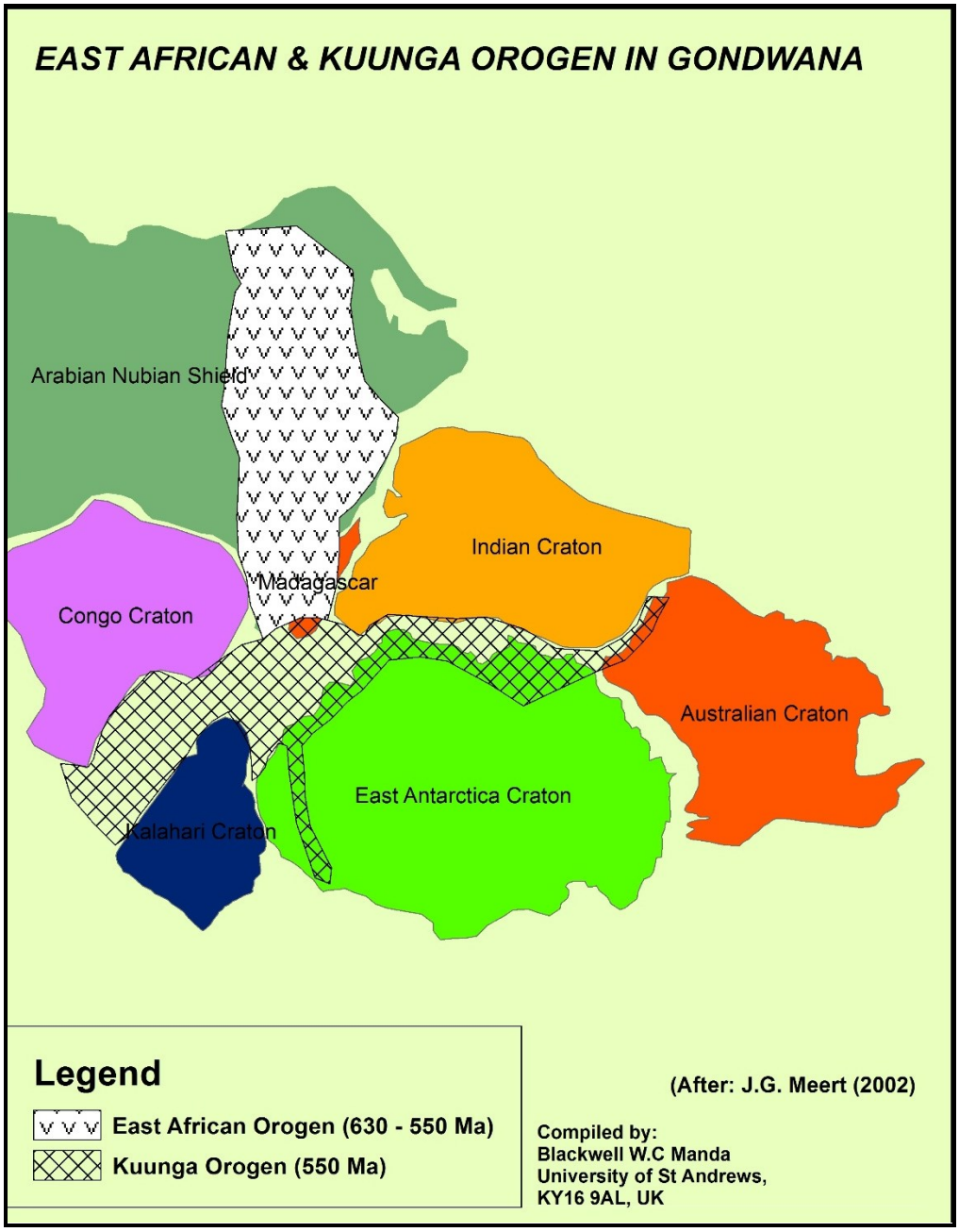

Fig. 2.6: Illustrating the East African Orogen and Kuunga Orogen in Eastern Gondwana (after J. G. Meert, 2003)

As highlighted by Bingen et al. (2009) enhanced understanding of Gondwana assembly dynamics requires detailed characterisation of individual terranes through the Pan-African orogenic belts. Malawi through its geographic location forms a potential keystone in furthering our knowledge of Gondwana assembly and in more general terms the processes of continental amalgamation. Malawi lies within the zone of intersection and overlap between two fundamental sutures associated with Gondwana assembly, the East African (Mozambique Belt) and Kuunga orogens (Fig 2.6) (Meert, et al., 1997; Meert, 2003).

Furthermore, older orogenic belts ascribed to Rodinia assembly, the Ubendian, Irumide (Kibaran), and Southern Irumide Belts, are overprinted by the Mozambique Belt in Malawi and in adjoining Mozambique (Kröner et al., 2001).

2.5 MOZAMBIQUE BELT – MALAWI

The northern part of Malawi appears to have been affected by three tectono-thermal-metamorphic events: Paleoproterozoic, Mesoproterozoic and the Pan African (Mozambique Belt) events. Magmatism is indicated as old as Archean (3.5 Ga) on the basis of a K-Ar hornblende date (Ray et al., 1974), with subsequent magmatic events in the Mesoproterozoic and Neoproterozoic. The region around southern Malawi experienced a Mesoproterozoic metamorphic event which Andreoli (1984) called "Kibaran" and Johnson et al., (2005) termed Southern Irumide Belt (SIB), and which was subsequently overprinted by the Neoproterozoic Mozambique Belt event. There is, however, a distinct area south of Malawi underlain by charnokitic gneisses that appear to record the Mozambique Belt event and that the earlier Mesoproterozoic event is absent.

The Precambrian geology of southern Malawi has long been considered as constituting a segment of the Pan-African Mozambique Belt (Kröner et al., 2001). However, Rb-Sr whole rock ages (1100 – 850 Ma) (Andreolli, 1984; Pinna, 1995) were considered as representing high-grade metamorphism thereby assigning this segment to the "Kibaran" Mesoproterozoic orogenic belt (Kröner et al., 2001). More recent high-precision zircon geochronology has failed to confirm the existence of a Mesoproterozoic event in southern Malawi or in northern Mozambique (Muhongo et al., 2003; Kröner et al., 2001).

The geology in southern Malawi (Fig. 2.7) consists basically of strongly foliated quartz–biotite–plagioclase, hornblende and microcline orthogneiss of tonalitic, trondhjemitic, or granodioritic (TTG) composition. These gneisses grade into massive, dark-olive-green charnockite, and in several places they show well preserved retrograde transitions from charnockite to hornblende biotite gneiss. In places, sillimanite facies metapelitic paragneisses are present (Andreoli, 1981, 1984). With no cross cutting relationships observed between these rocks, Kröner et al., (2001) assumed that the paragneisses represented a supracrustal succession that were the oldest units and these were intruded by a granitoid suite (the orthogneisses), and both were later tectonically transposed and metamorphosed to granulite facies (Kröner et al., 2001).

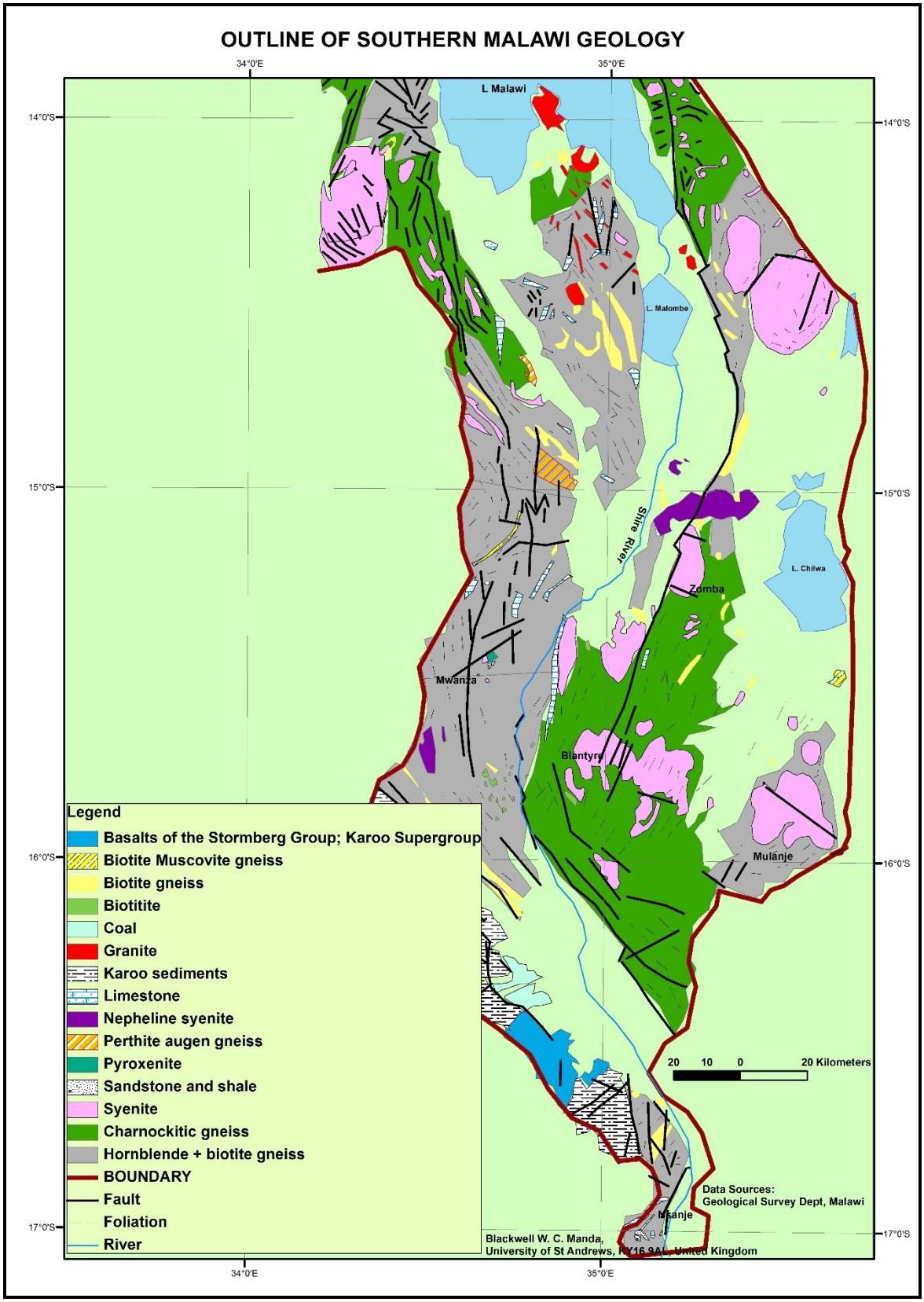

Fig. 2.7: Showing the outline geology of southern Malawi (after Geological Survey Dept., Malawi (1974)

The gneiss assemblages of southern Malawi reached peak metamorphic conditions at 900 ± 70°C and 9.5 ± 1.5 kbar, followed by an isobaric cooling path (Kröner et al., 2001). The first

of three distinct events (all data from Kröner et al., 2001) suggested for this region is late Mesoproterozoic to early Neoproterozoic (Kibaran) in age (ca. 1040 - 929 Ma) and is represented by intrusion of calc-alkaline granitoids. Nd isotope data indicate overall juvenile compositions consistent with a magmatic arc environment, or emplacement into thinned continental crust with little involvement of older basement. The second event is a Pan-African period of intrusion of calc-alkaline granitoids around 710 - 555 Ma and the Nd isotope data show crustal residence ages of 1.0 - 1.5 Ga suggesting either re-melting of 1.0-1.5 Ga (Kibaran) protoliths or mixing of juvenile material with subordinate amounts of older crust. The last event is a thermal peak of Pan-African high grade metamorphism around 571 - 549 Ma.

The late Mesoproterozoic and Pan-African magmatic events in Malawi may be linked to granitoid magmatism of similar ages in north-western Mozambique and the central Zambezi belt of northern Zimbabwe, and therefore East Gondwana was not a coherent block colliding with West Gondwana but consisted of individual terranes before being amalgamated into the supercontinent Gondwana some 550 - 530 Ma ago (Kröner et al., 2001). The MORB-like chemistry of mafic rocks together with the presence of Neoproterozoic continental-margin arc magmas in southern Malawi denotes Neoproterozoic oceanic crust between the Congo and Kalahari Cratons (Johnson et al., 2005).

2.6 CONCLUSION

Geochronological work (whole-rock and mineral Rb-Sr and K-Ar, and U-Pb zircon conventional methods), indicates an Archean – Neoproterozoic crust for Malawi for the various supracrustals and calc-alkaline magmatism overlying the different sections forming this part of the Mozambique Belt (Andreolli, 1984; Kröner et al., 2001). The character and scheduling of the tectono-thermal events during Rodinia and Gondwana amalgamation and break-up are poorly understood, and hitherto not well constrained. Our understanding, therefore, of the basic regional geodynamic evolution of the Mozambique Belt is compromised. Malawi lying at the junction of the East African Orogen and the Kuunga Orogen (Meert, 2003) is critical to our understanding of Gondwana assembly as it partly has a record of collision, arc magmatism and subduction dynamics.

2.7 REFERENCES

Andreoli, M. A. G. (1984). "Petrochemistry, tectonic evolution and metasomatic mineralizations of Mozambique Belt granulites from S Malawi and Tete (Mozambique)." Precambrian Research 25 (1-3): 161-186.

Ashwal L. D., R. A. Armstrong et al., (2006) Geochronology of zircon megacrysts from nepheline-bearing gneisses as constraints on tectonic setting: implications for resetting of the U-Pb and Lu-Hf isotopic systems, Contrib Mineral Petrol (2007) 153:389–403, DOI 10.1007/s00410-006-0153.

Bickford M. E., (1988), "The formation of continental crust: Part 1. A review of some principles; Part 2. An application to the Proterozoic evolution of southern North America", Geological Society of America Bulletin 1988;100, no. 9;1375-1391, doi: 10.1130/0016-7606(1988)100<1375:TFOCCP>2.3.CO;2

Bingen, B., J. Jacobs, et al. (2009), "Geochronology of the Precambrian crust in the Mozambique belt in NE Mozambique, and implications for Gondwana assembly." Precambrian Research 170(3–4): 231-255.

Boger, S. D. and J. M. Miller (2004), "Terminal suturing of Gondwana and the onset of the Ross–Delamerian Orogeny: the cause and effect of an Early Cambrian reconfiguration of plate motions." Earth and Planetary Science Letters 219(1–2): 35-48.

Cannon R. T., D.A. Hopkins, et al.,(1969), Polyphase Deformation in the Mozambique Belt, Northern Malawi, Geological Society of America Bulletin, vol. 80, pp 2615-2622. doi: 10.1130/0016-7606(1969)80[2615:PDITMB]2.0.CO;2

Cawood P.A., C. J. Hawkesworth, B. Dhuime (2013), "The continental record and the generation of continental crust." Geological Society of America Bulletin 125(no. 1-2): 14-32.

Collins, A. S. and S. A. Pisarevsky (2005), "Amalgamating eastern Gondwana: The evolution of the Circum-Indian Orogens." Earth-Science Reviews 71(3–4): 229-270.

Goldfarb, R. J., D. I. Groves, et al. (2001), "Orogenic gold and geologic time: a global synthesis." Ore Geology Reviews 18(1-2): 1-75.

Daly, M. C. (1986), "The intracratonic Irumide Belt of Zambia and its bearing on collision orogeny during the Proterozoic of Africa." Geological Society, London, Special Publications 19(1): 321-328.

De Wit, M. J., S. A. Bowring, et al. (2001), "Age and tectonic evolution of Neoproterozoic ductile shear zones in southwestern Madagascar, with implications for Gondwana studies." Tectonics 20(1): 1-45.

Grantham G. H., M. M., & Eglington B. M. (2003), "A review of the evolution of the Mozambique Belt and implications for the amalgamation and dispersal of Rodinia and Gondwana." Geological Society, London, Special Publications 2003 v.206: p401-425.

Hoffman, P. F. (1991), "Did the Breakout of Laurentia Turn Gondwanaland Inside-Out?" Science 252(5011): 1409-1412.

Jacobs, J., C. M. Fanning, et al. (1998), "Continuation of the Mozambique Belt into East Antarctica: Grenville-age metamorphism and polyphase Pan-African high-grade events in central Dronning Maud Land." Journal of Geology 106(4): 385-406

Jacobs, J. and R. J. Thomas (2004), "Himalayan-type indenter-escape tectonics model for the southern part of the late Neoproterozoic-early Palaeozoic East African-Antarctic orogen." Geology 32(8): 721-724.

Johnson, S. P., T. Rivers, et al. (2005), "A review of the Mesoproterozoic to early Palaeozoic magmatic and tectonothermal history of south-central Africa: implications for Rodinia and Gondwana." Journal of the Geological Society 162: 433-450.

Johnson, P. R. (1998), Tectonic map of Saudi Arabia and Adjacent Areas, Ministry of Petroleum and Mineral Resources, Deputy Ministry for Mineral Resource Technical Report USGS-TR-98-3 (IR 948).

Johnson, S. P., B. De Waele, et al. (2006), "U-Pb sensitive high-resolution ion microprobe (SHRIMP) zircon geochronology of granitoid rocks in eastern Zambia: Terrane subdivision of the Mesoproterozoic Southern Irumide Belt." Tectonics 25(6): TC6004.

Johnson, S. P., B. de Waele, et al. (2007), "Geochemistry, Geochronology and Isotopic Evolution of the Chewore–Rufunsa Terrane, Southern Irumide Belt: a Mesoproterozoic Continental Margin Arc." Journal of Petrology, 48(7): 1411-1441.

Kröner, A., A. P. Willner, et al. (2001), "Single zircon ages, PT evolution and Nd isotopic systematics of high-grade gneisses in southern Malawi and their bearing on the evolution of the Mozambique belt in southeastern Africa." Precambrian Research 109(3-4): 257-291.

Li, Z. X., S. V. Bogdanova, et al. (2008), "Assembly, configuration, and break-up history of Rodinia: A synthesis." Precambrian Research 160(1–2): 179-210.

Meert, J. G. and R. Van Der Voo (1997), "The assembly of Gondwana 800-550 Ma." Journal of Geodynamics 23(3–4): 223-235.

Meert, J. G. (2003), "A synopsis of events related to the assembly of eastern Gondwana." Tectonophysics 362(1–4): 1-40.

Muhongo, S., C. Hauzenberger, et al. (2003), "Vestiges of the mesoproterozoic events in the neoproterozoic Mozambique belt: The East African perspective in the Rodinia puzzle." Gondwana Research 6(3): 409-416.

Muhongo, S., A. Kröner, et al. (2001), "Single Zircon Evaporation and SHRIMP Ages for Granulite-Facies Rocks in the Mozambique Belt of Tanzania." The Journal of Geology 109(2): 171-189.

Pinna, P., G. Jourde, et al. (1993), "The Mozambique Belt in northern Mozambique: Neoproterozoic (1100–850 Ma) crustal growth and tectogenesis, and superimposed Pan-African (800–550 Ma) tectonism." Precambrian Research 62(1–2): 1-59.

Ray, G. E. (1974), "The structural and metamorphic geology of northern Malawi." Journal of the Geological Society 130(5): 427-440.

Ring U., Kroener A., Toulkeridis U. T., (1997), Paleoproterozoic granulite-facies metamorphism and granitoid intrusions in the Ubendian-Usagaran Orogen of northern Malawi, east-central Africa, Precambrian Research 85 (1997) 27-51

Ring, U., A. Kroner, et al. (1999), "Deformed A-type granites in northern Malawi, east-central Africa: pre- or syntectonic?" Journal of the Geological Society 156: 695-714.

Sacchi, R., J. Marques, et al., (1984), Kibaran events in the southernmost Mozambique belt. Precambrian Research, 25, 141–159.

Stern, R. J. (1994), "Arc-Assembly and Continental Collision in the Neoproterozoic African Orogen: Implications for the Consolidation of Gondwanaland." Annual Review of Earth And Planetary Sciences 22: 319-351.

Stern, R. J. (2002), "Crustal evolution in the East African Orogen: a neodymium isotopic perspective." Journal of African Earth Sciences 34(3–4): 109-117.

Wilde S. A., Valley J. W., Peck W. H., and Graham C. M., (2001), Evidence from detrital zircons for the existence of continental crust and oceans on the Earth 4.4 Gyr ago. Nature 409(6817), 175–178.

Zhao, G., P. A. Cawood, et al. (2002), "Review of global 2.1–1.8 Ga orogens: implications for a pre-Rodinia supercontinent." Earth-Science Reviews 59(1–4): 125-162.

Chapter 3: Geology of Southern Malawi

3.1 INTRODUCTION

The age, extent and character of the major lithotectonic units within the Mozambique Belt in Malawi remain poorly constrained and limited to, at best, preliminary regional sampling and reconnaissance mapping. This project aims at providing the first ever detailed analysis of the geological units in Southern Malawi to establish their tectonic relationship and refine their ages. The study area lies between 15°00'S and 16°30'S and includes the area west of Lake Chilwa, the Mulanje area southeast of Malawi and adjacent to Mozambique, the Neno, Mwanza

Boma and Kirk Range areas along Malawi's western border with Mozambique and the Shire Highlands that largely includes the Blantyre and Thyolo areas (Fig. 3.1).

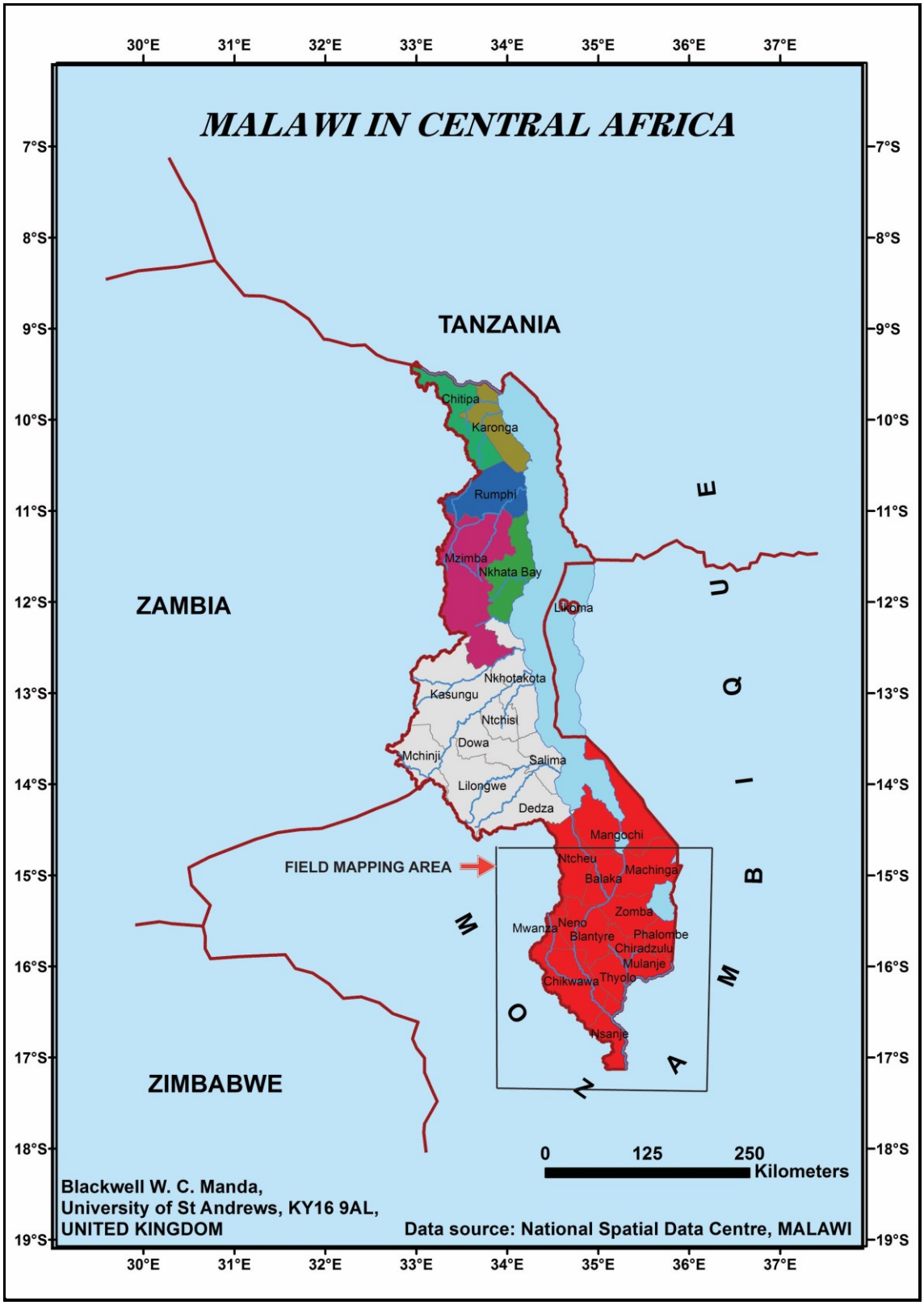

Fig. 3.1: Map of Malawi showing the field mapping area in southern Malawi. Malawi has three regions - North (Combined colours), Central (Pink) and South (Red)

3.2 METHODS

A 1:250,000 regional geology map sheet No. 2 was used as basis for field work and sampling. Other reference geological map sheets included the 1:100,000 scale maps of the Mulanje, Zomba, Shire Highlands, Mwanza, and the Kirk Range-Lisungwe Area. These maps are published by the Geological Survey Department of Malawi. Aster – DEM imagery has also been utilised to produce a remote sensing interpretation of the structural geology of the southern Malawi area (see Appendix 3.1 and 3.2). The field work took the form of road and track traverses with a GPS Garmin 60 to record spatial data. Linear and planar data were recorded using a Brunton compass. A Fuji Finepix SP2950 digital camera was used to capture field photographs. Thin sections were studied under a petrological microscope where point counting of minerals was conducted.

The aim of the fieldwork was to collect rock samples from the main lithological units for geochemical and geochronological analysis. To help guide sample selection, the geological maps available from the Malawian Geological Survey were digitised and at each sample locality the geology was checked and, if necessary, revised so that samples could be placed into their correct geological context. As a consequence, a revised geological map was constructed from both satellite imagery interpretation and by the field checks undertaken in the key sampled areas. Samples collected are shown in Appendix 3.3 and their locations are indicated in Appendix 3.4. ARCGIS 10.2 software was utilized for the satellite image interpretation and production of maps.

3.3 PREVIOUS WORK

Southern Malawi is a varied physiographic province: Mulanje mountain, the tallest mountain in Malawi rises to nearly 3000 m, and the Zomba Plateau is close to 2400 metres in average elevation whereas the upper and lower Shire Valley and Lake Chilwa plains are around 600 m elevation with the Shire Highlands and the Kirk Range forming intermediate areas between 1000 and 1250 m above sea level (Bloomfield, 1970).

Paragneisses (semi-pelitic and psammitic types), calcareous gneisses, metasomatites and anatexites of the Basement Complex are the major rock types in this area (Bloomfield, 1960; Garson et al., 1969). They were considered to be of Neoproterozoic – early Palaeozoic age and, because of relatively poor exposure and subsequent tectonic overprinting, many contact relationships are poorly known. The gneisses have generally been metamorphosed to amphibolite - granulite facies and migmatisation is not uncommon. The Basement Complex was intruded by various granitic rocks followed by alkali metasomatism giving rise to late-kinematic granites and syenites, and then cut by a swarm of NE-SW trending dolerite dykes known as the Stormberg dykes (Wooley, et al., 1979). The Chilwa Alkaline Province (Upper Jurassic to Lower Cretaceous in age) rocks include the syenite-granites (mostly in the Michese, Mulanje and Zomba Plateau areas), agglomerate and carbonatite vents, trachytes and nepheline-syenites and minor intrusions of lamprophyres, phonolites, microfoyaites, microgranites and microsyenites (Bloomfield, 1960, Garson et al., 1969). The preponderance of Na over K and relatively high amounts of Mg and Ca in the gneisses and granulites is interpreted as due to incorporation of calcareous and dolomitic shale horizons (Bloomfield, 1970). A group of interbanded pelitic and semipelitic schists occurs to the west and is mapped as the Kirk Schist Group (Bloomfield, 1970).

3.4 PRESENT WORK

Based on reconnaissance field work the study area of the South Malawi region in particular is underlain by supracrustal rocks including gneisses, schists, calc-silicates, limestones, amphibolites, metapyroxenites and various granitoids (Appendix 3.1). Various syenites, carbonatites, and pegmatite bodies intrude the area. A swarm of dolerite dykes, and solvsbergite dykes of the Chilwa Alkaline Province trending in a general NE-SW direction and lamprophyre dykes that trend NW-SE cut across the gneisses. Deformation has occurred to various degrees, and foliation is complex but generally NW-SE trending. Charnockitic and hornblende-biotite gneisses interbanded with quartzofeldspathic and calc-silicate gneisses dominate the Mulanje-Thyolo-Blantyre and Zomba area (which lies mostly to the east of the study area) in which foliation is NE-SW and is generally more uniform compared to that in the western Mwanza – Kirk Range area. Metagranites with fine grained dark enclaves extend in a belt about 30 km wide from the southeast of Mwanza northwestwardly to the Mozambique area; they define resistant hills that dot the landscape. Syenites and other granitic rocks intrude the gneissic rocks in several places like Mulanje, Blantyre and Zomba.

3.4.1 HORNBLENDE BIOTITE GNEISS

Leucocratic, coarsely crystalline a hornblende biotite gneisses are distributed widely across southern Malawi. They underlie much of the western areas from Mwanza towards the Kirk Range where they are concordantly banded with calc-silicate gneisses and marbles. To the east (Shire Highlands and Mulanje area) they are interbanded with charnockitic gneisses that have similar macroscopic features and can only be confidently differentiated petrographically. They are migmatised and patches of charnockitic gneisses occur within the hornblende biotite gneisses. In places the hornblende biotite gneisses grade into biotite and garnet biotite gneisses (Garson 1969). Evans (1965) argued that these hornblende biotite gneisses are retrogressed equivalents of the charnockites, comparing them to amphibolites facies rocks of Vijayan Series of Ceylon.

Minor faulting gives passage to late stage pegmatite veins (Fig. 3.2A) and some dark coloured inclusions. Ptygmatic folding is seen in the light coloured bands and these formed earlier than the faulting (Fig. 3.2B).

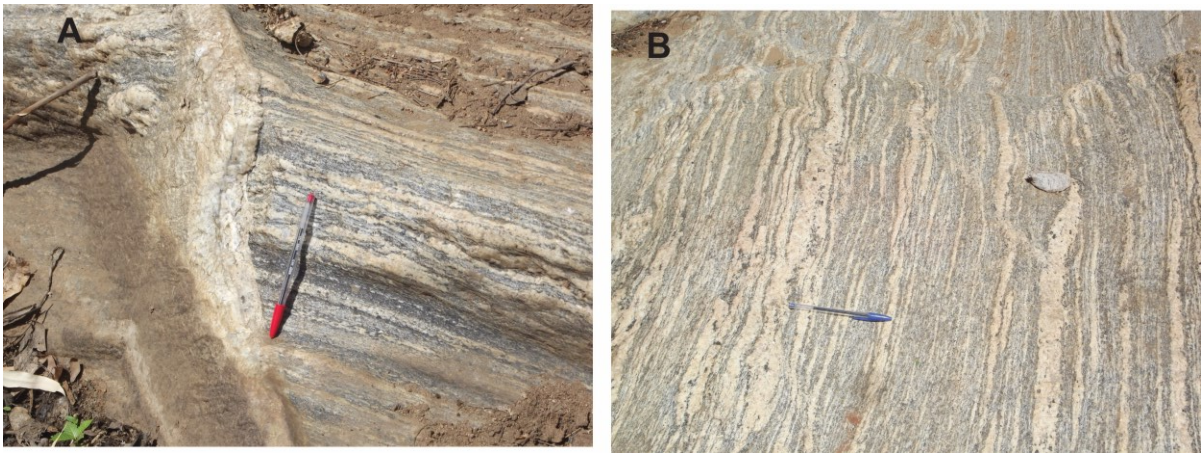

Fig. 3.2: Migmatitic hornblende biotite gneisses from southern Malawi showing compositional banding and pegmatite veins intruded along minor faults.

Hornblende, biotite, garnet, epidote, and locally clinopyroxene are visible in hand specimen; in thin section subhedral and euhedral green hornblende can be identified (14 - 24%). Biotite

(12%) appears as pleochroic, brown, elongated crystals. Accessory minerals include zircon, apatite and some opaque oxide minerals.

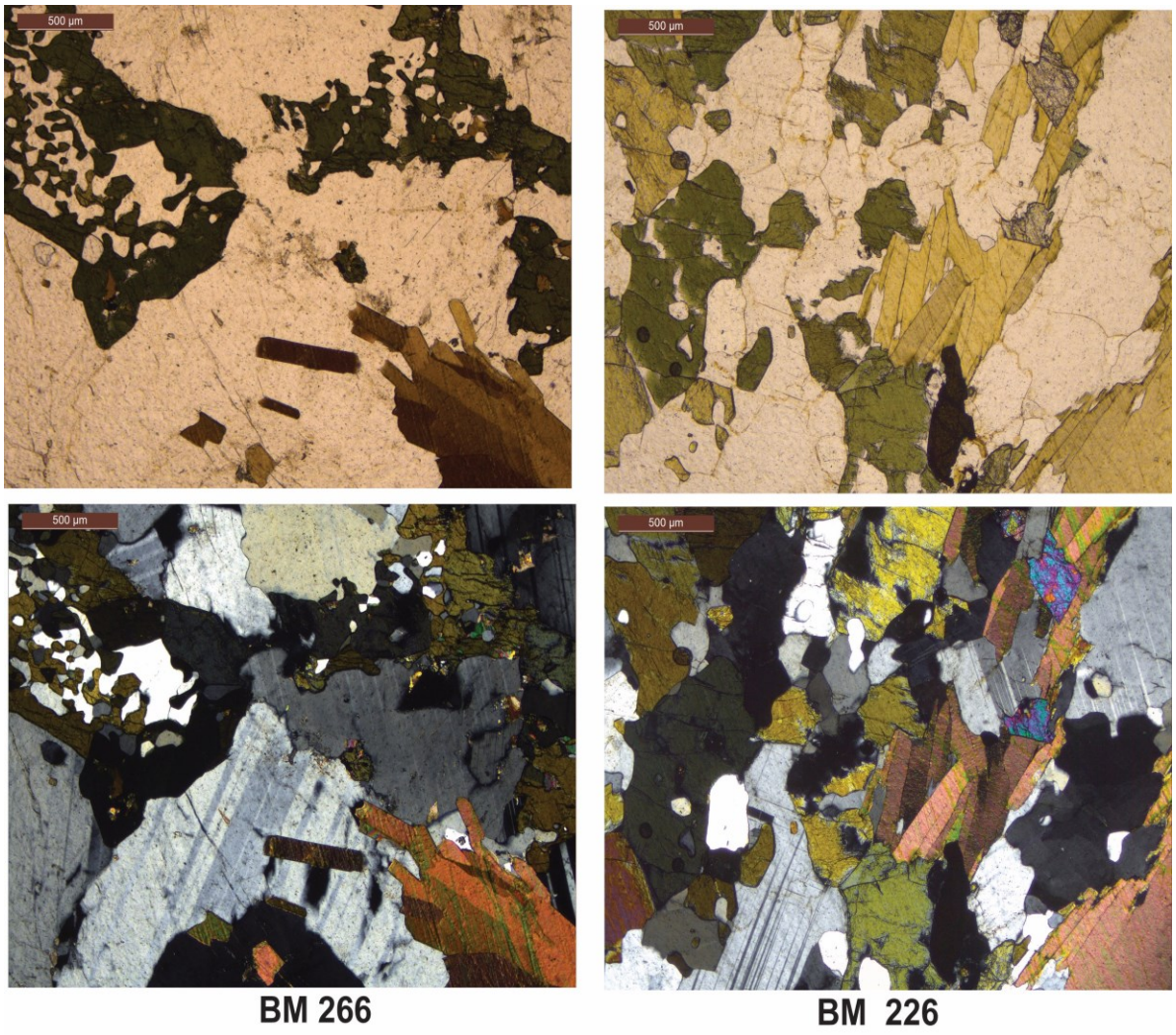

Fig. 3.3: Hornblende biotite gneisses from southern Malawi in thin section, plane polarised light (upper microphotographs) and cross polarised light (lower microphotographs).

3.4.2 CHARNOCKITIC GNEISS

The charnockitic gneisses (Fig. 3.4) in the Zomba, Shire Highlands and Mulanje mountain areas were observed as alternating leucocratic, mesocratic and locally melanocratic bands. No evidence is retained that the banding is indicative of original sedimentary bedding. They are coarse-grained and foliated and have been intruded by various phases of granites, microgranites, mafic bands and pegmatites. The charnockitic granulites are absent in the western parts of the region where hornblende biotite gneisses dominate but due to poor exposure a clear and distinct contact could not be established between these two areas.

Fig. 3.4: Grey charnockitic gneiss quarry face and a migmatitic charnockitic block representative of the bedrock in Mulanje, southern Malawi.

In thin section the charnockitic gneisses consist on average of 24% anhedral quartz with undulose extinction and as much as 41% subhedral to anhedral plagioclase. Hypersthene occurs in subhedral and euhedral crystals and together with diopside they comprise anywhere up to 28% of the rock. Hornblende (5 – 11%) occurs as light green euhedral crystals. Occasionally the hornblende is seen replacing pyroxenes. Accessory minerals include apatite, magnetite, and zircon.

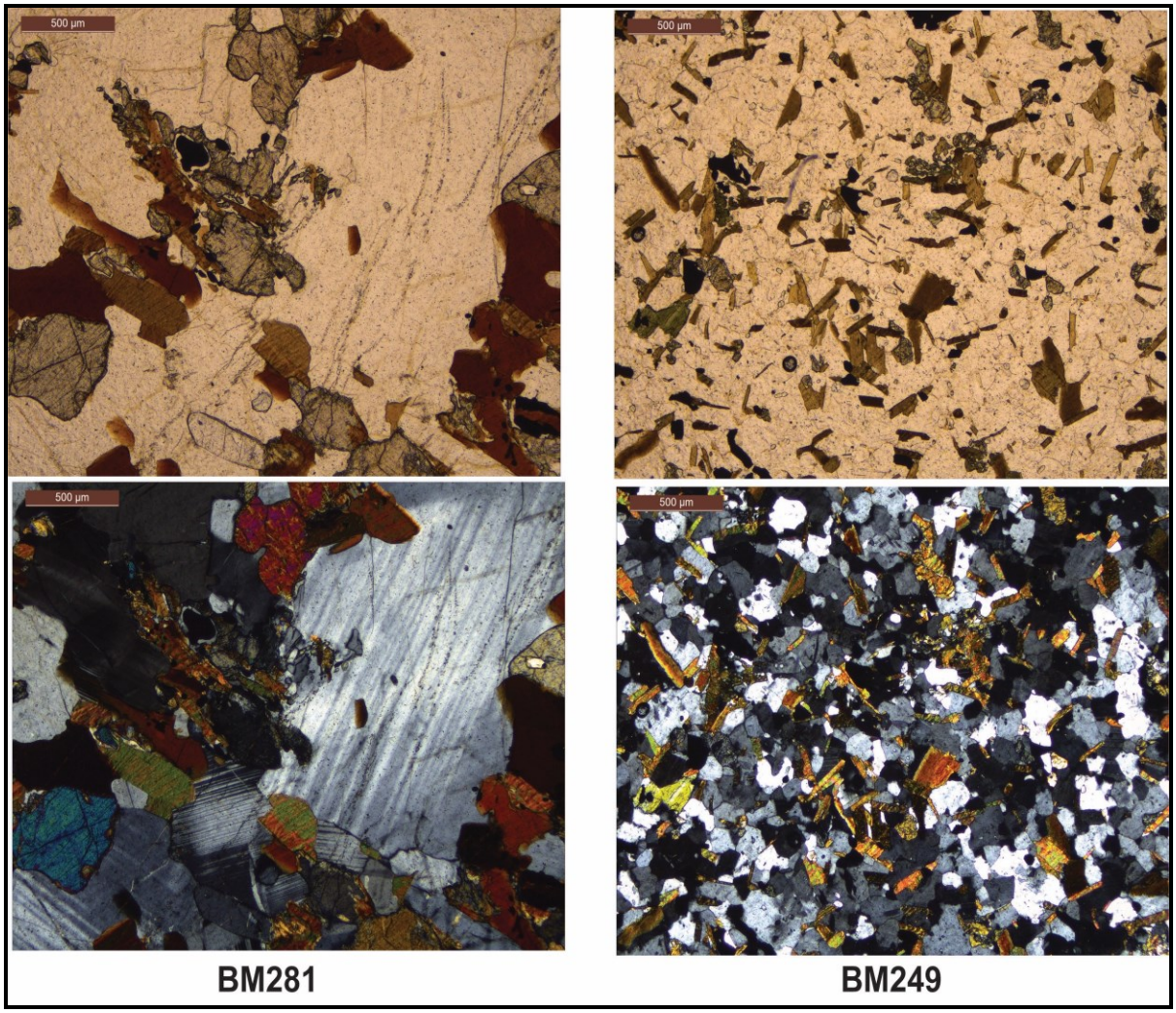

Fig. 3.5: Charnockitic gneiss from Mulanje (Malawi) in plane polarised (upper microphotographs) and crossed polarised light (lower microphotographs).

3.4.3 MARBLES AND CALC-SILICATES

White, pink, grey and, in places, blue-tinted marbles occur interbanded with calc-silicate gneisses at Chenkumbi near Balaka, Lirangwe west of Blantyre and in the Kirk Range area. The marbles are both calcitic and dolomitic, occurring as coarse grained, narrow bands. They are weakly foliated and contain minor amounts of graphite and phlogopite. The calc-silicates appear as concordant bands, but at Chenkumbi they also occur as irregular, angular fragments that may reflect an original sedimentary texture as rudites. Calc-silicate gneisses also occur as narrow concordant bands with the charnockitic gneisses. Relict stratification was observed in

boulders that had been excavated as part of a road construction near Thondwe in Zomba. Isoclinal folding is common in the calc-silicates (Fig. 3.6).

Fig. 3.6: Calc-silicate and marble showing isoclinal folding in Balaka and Chiradzulu southern Malawi

3.4.4 AMPHIBOLITE

Amphibolites occur as narrow (a few centimetres up to 30 metres) bands across most of the north-western portion of the study area. In the Kirk Range area and surrounding areas they comprise the most abundant mafic rock and can be identified by blocky jointing and tendency to withstand erosion by forming lengthy (up to five kilometers) ridges. They are mesocratic to leucocratic, medium to coarsely crystalline bodies that are concordant to the foliation and banding in the biotite and hornblende gneisses. Near Ndzama Mission (Ntcheu), angular xenoliths of foliated leucocratic quartzofeldspathic gneisses occur in the amphibolites (Fig. 3.7).

Fig. 3.7: Amphibolite containing leucocratic hornblende gneiss xenoliths near Ndzama (Ntcheu) in southern Malawi.

3.4.5 MICA SCHIST

Mica (muscovite) schists occur in the northwest part of the field area as narrow (up to 20 meters wide) but extensive layers interbanded with quartzofeldspathic and biotite gneisses. Graphite is present in the Ndzama Mission area of the Ntcheu District.

3.4.6 QUARTZFELDSPATHIC GNEISS

Narrow (3 to 30 meters wide and often extending for several kilometers) bands of quartzofeldspathic rocks occur concordant to the gneisses and granulites. Some appear to have been leucogranites that have been metamorphosed whereas in other places they exhibit a layering that is reminiscent of sedimentary bedding and could be considered as paragneisses (Fig. 3.8).

Fig. 3.8: Weathered quartzofeldspathic paragneiss showing relics of original sedimentary layering, Neno area southern Malawi.

3.4.7 GRANITES (META):

The metagranites are buff but also pinkish, and coarsely crystalline with biotite as the predominant mafic mineral. They display both foliated and unfoliated textures. The metagranites extend in a belt about 30 km wide from the south east of Mwanza in a north-westerly direction into Mozambique. These rocks are re-classified in this mapping as they occur more widely than previously recognized. They were previously mapped as cafemic gneiss occurring as rare small bands concordant/interbanded with semipelitic hornblende-biotite gneiss (Bloomfield, 1970). They form resistant hill outcrops in hornblende biotite gneisses (Fig. 3.9). Contacts between the gneisses and granitoids are varied: in many places they appear sharp and commonly sheared whereas in others the contacts are transitional/gradational, i.e. there is a systematic decrease of foliation that occurs over distances a couple to several meters. Fine grained mafic enclaves and “xenoliths” (Fig. 3.10) occur in the hill outcrops. The enclaves are often mesocratic and finer, occurring as oval shaped blebs or angular bodies with sharp margins. In some bodies the margins appear diffused. They appear in various sizes from a few centimetres to 30 centimetres across but sometimes appear as small dykes about 45 centimetres wide. Some of the granitic bodies are deformed and appear concordant to the gneissic foliation.

Fig. 3.9: Field photographs of typical granite hill outcrops in Mwanza - southern Malawi

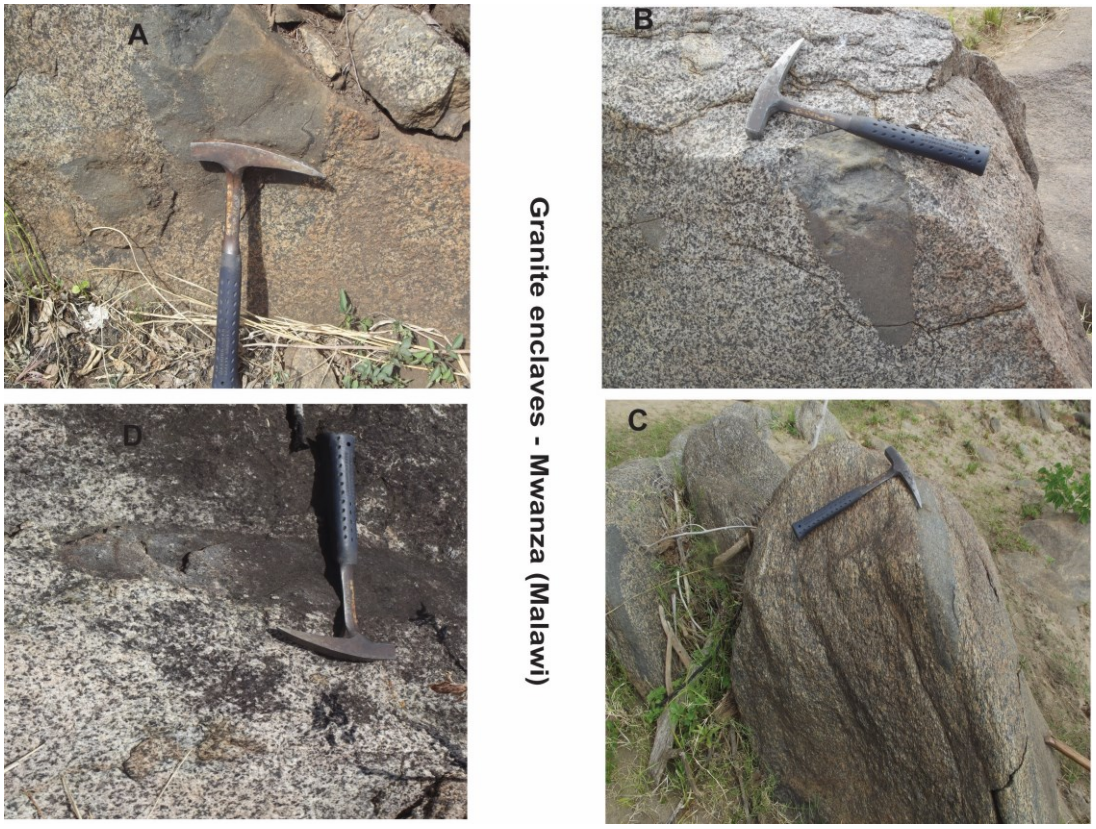

Fig. 3.10: Granite bodies at various localities in Mwanza - southern Malawi. Some appear undeformed (A and B) others appear deformed and concordant to foliation (D).

In thin section (Fig. 3.11) the metagranites show a typical granular texture with variable amounts of anhedral quartz (between 26 - 51%) with typical wavy extinction and subordinate subhedral and anhedral lamellae twinned plagioclase feldspar (11- 27%). In some sections K-feldspar appears with an average of 23%. Euhedral and subhedral pleochroic (yellow-green) hornblende occurs in various percentages to as much as 20% and in places replaces pyroxene. Biotite with characteristic brown to greenish pleochroism comprises c. 5 - 13%. Accessory minerals include ilmenite and zircon, as well as other unidentified opaque oxide minerals. In one sample BM 213GX the thin section shows that the mineralogical composition of the enclave is the same as the parent rock and the only difference is the grain size. The contact is sharp with no chilled margins.

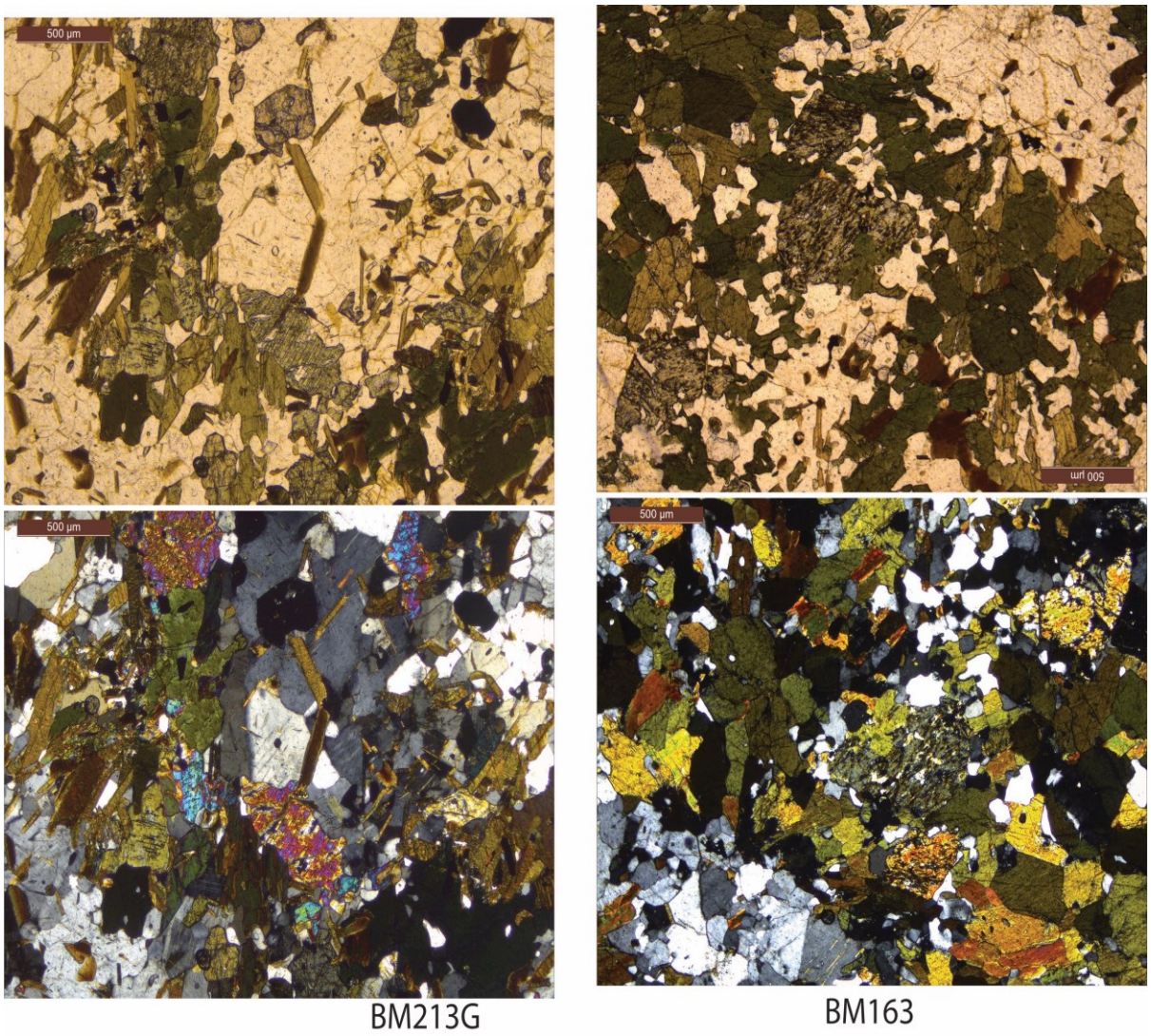

Fig. 3.11: Thin section of granite from Mwanza in southern Malawi. The top row shows the minerals in plane polarised light and the bottom row shows them in cross polarised light.

3.4.8 SYENITE/GRANITE

An older and a younger set of syenitic and granitic rocks can be recognised in the southern Malawi area. The older gneisses have been mapped in the Kirk range area, around Chiradzulu,

Blantyre and close to Zomba.
These rocks are porphyroblastic, and vary from quartz-rich granitic gneisses to quartz-poor syenitic gneisses. A thin section from Chiradzulu Hill shows 40% potassic feldspar, 36% perthitic feldspar, 5% plagioclase feldspar, 8% quartz, 5% biotite, 3% pyroxene, with accessories of unknown opaque minerals. The younger rocks belong to the Chilwa Alkaline Province (Upper Jurassic to Lower Cretaceous) (Evans, 1965) and include the highest hills in the area - Mulanje Mountain and Zomba Plateau. They are largely unfoliated, buff to pink coloured, coarsely crystalline, with biotite as the main mafic mineral and commonly contain varied mafic xenoliths (Fig. 12). The outcrops contain both syenitic and granitic rocks, possibly reflecting various intrusion phases, but no clear field contacts could be established to determine their relative age relationships.

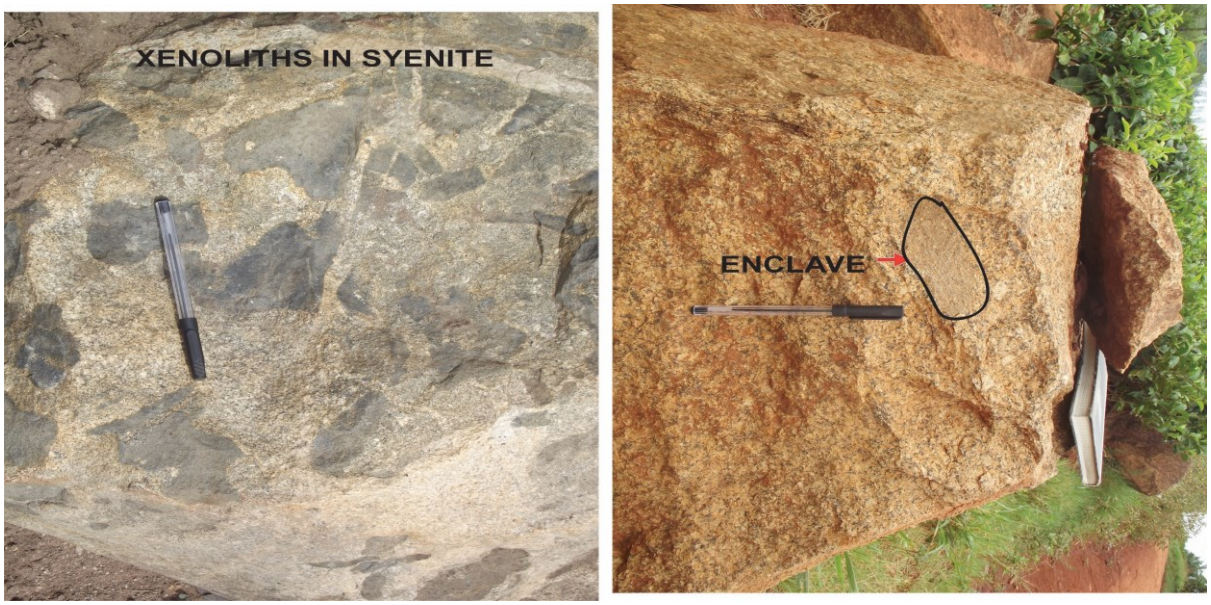

Fig. 3.12: Mulanje Mountain syenite showing mafic xenoliths and a granite with a darker enclave.

A granite thin section from the eastern side of Mulanje Mountain close to Muloza shows euhedral to subhedral K-feldspar being present in as much as 75%, and plagioclase being minor, about 2% or less. Subhedral to anhedral quartz makes up about 13%. Minor amounts of hornblende occur and are recognised by the distinctive pleochroism (in shades of green) and euhedral/subhedral crystals with typical cleavage in two directions. Pleochroic euhedral elongated biotite crystals make up c. 4% and are subordinate to hornblende. Magnetite is the predominate accessory mineral.

3.4.9 DOLERITE DYKES

A swarm of dolerite dykes, in a general east-west trending, cross cut the various gneisses. These dykes typically stand out as resistant ridges extending for as much as several kilometers. Their trend coincides with known faults and regional joint networks, which implies a structural control on their occurrence.

3.4.10 ULTRAMAFIC ROCKS

Ultramafic bodies have been mapped mainly in the Kirk Range area and include serpentinised peridotites, metapyroxenites, metagabbros, and gabbroic amphibolites. Chimwadzulu Hill forms the main ultramafic complex. The Chimwadzulu Hill has serpentinised peridotite

(harzburgite; Bloomfield 1965). Andreoli (1984) observed that relic ultramafic sequences occur in association with garnetiferous quartzite, gabbros and amphibolite and serpentinised peridotite in the Kirk Range area.

A sample collected on the southern slopes of Chimwadzulu Hill is dark, massive, and medium grained. In thin section olivine dominates (77%) and hornblende forms c. 9%, feldspar makes up c. 9% and other unknown opaques c. 4%.

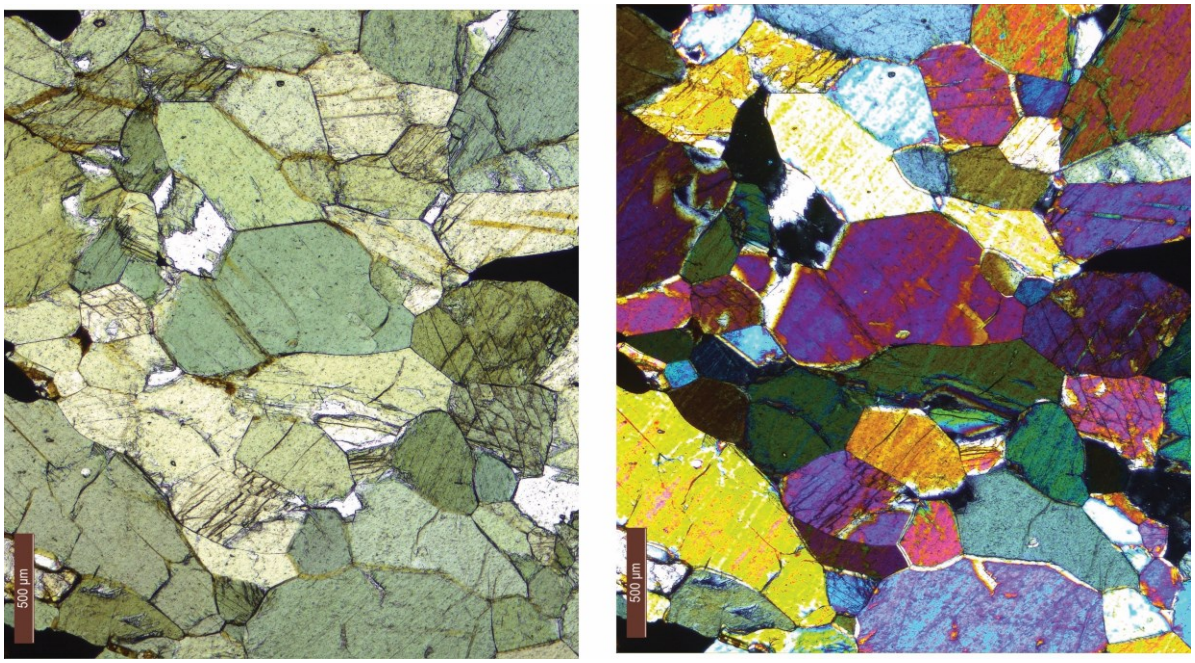

Fig. 3.13: Thin section of an ultramafic rock from Chimwadzulu Hill - Kirk Range area, southern Malawi.

3.5 STRUCTURE

Based on the remote sensing interpretation of Aster DEM data and on the field work, the foliation in the northwest of the region strikes NW-SE but swings to NE-SW creating a fold like structure around the Kirk Range area. NE-SW trends are common in the Zomba – Blantyre-Thyolo areas (Appendix 3.2). The gneisses are foliated in a general NE-SW trend with steep north-west dips. Isoclinal folding is prevalent (Figs. 3.14 and 3.15).

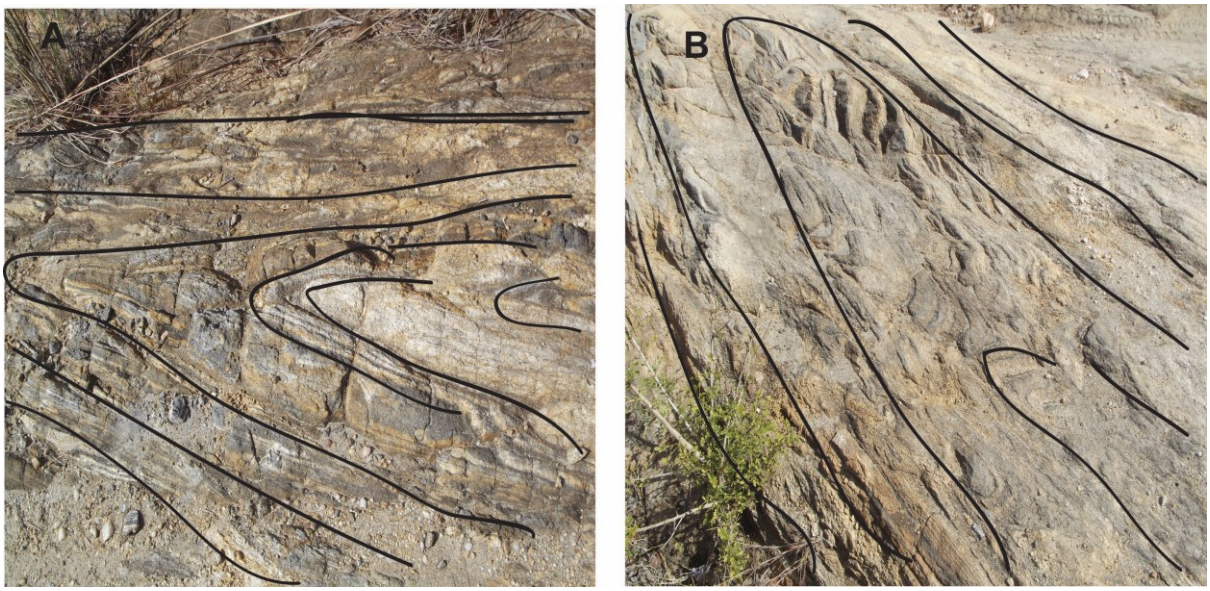

Fig. 3.14. Strongly deformed hornblende biotite gneisses showing isoclinal folding (A and B), foliation and intense shearing (B) in Mwanza - southern Malawi.

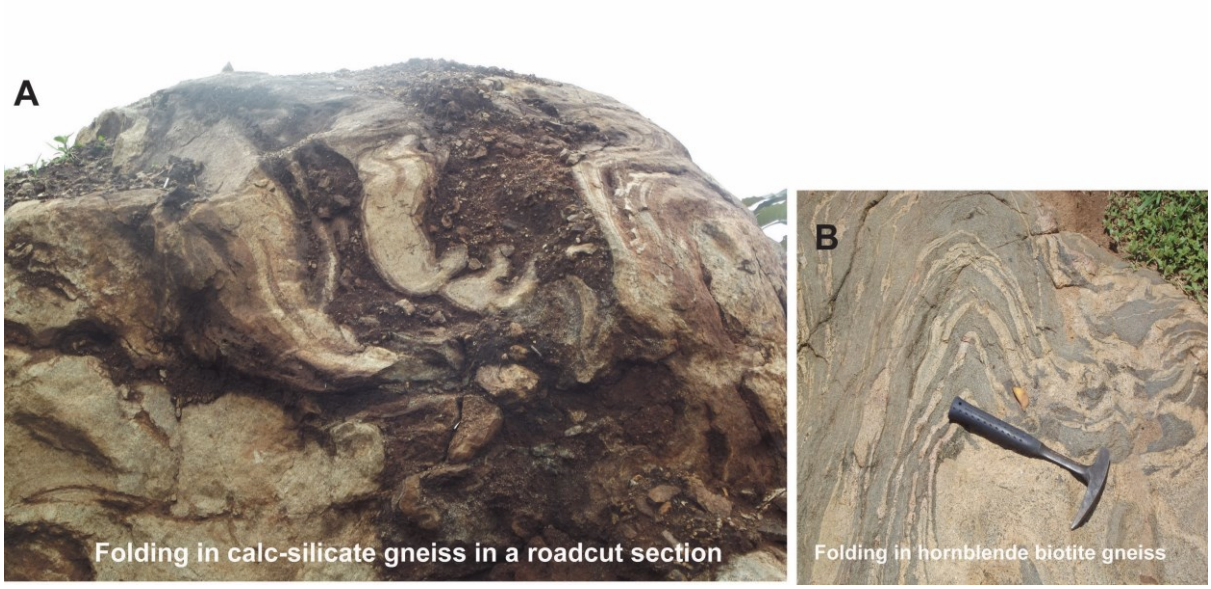

Fig. 3.15. Complexly folded calc-silicate gneiss and isoclinal folding in hornblende biotite gneiss in southern Malawi.

The structure is dominated by the NE-SW trending Rift Valley faulting (Appendix 3.1). NW-SE faulting also occurs and is similarly attributed to the rift faulting. A series of N-NE trending parallel step faults constitute the East African Rift Valley in the western part of southern Malawi and these cross-cut some NW trending, and presumably older, fault structures (Bloomfield, 1965). Both sets are, however, offset by ENE trending dextral wrench faults with lateral displacements up to 1 km and associated with a Mesozoic-age solvsbergite dyke swarm. The Shire Highlands Faults defines the eastern wall of the Rift. This is a continuation of the Great East African Rift Valley Fault from the north and has been named the Main Rift Valley Fault in Malawi (Evans, 1965; Bloomfield, 1965).

Aster DEM satellite data were processed using Image Analysis in ARCGIS 10.2. Lineaments were digitised to show the general fault trends in the southern Malawi region and adjacent areas (Appendix 3.1). From the image interpretation the regional (Great East African Rift) NE- SW trend of faulting cutting across the Malawi section is shown and the associated NW – SE trends of normal faulting are also visible and well defined. These two trends are shown being offset by some SNE – WSW faults, and most of these are associated with Upper Jurassic dolerite and Lower Cretaceous solvsbergite dykes (Bloomfield, 1974).

3.6 DISCUSSION

The aim of this chapter has been to provide an analysis of the main geological units in Southern Malawi, which formed the basis for collecting samples for geochemical and geochronological analysis, as well as providing information on tectonic relationships and on the relative ages of units and events within the area. The study area has been mapped by various authors (Bloomfield, 1960; Garson et al., 1969; Evans, 1965; Wooley, et al., 1979; Morel S, 1989) and shown to consist of paragneisses and orthogneisses, which are generally thought to be Precambrian in age. This mapping also shows the presence of calc-silicate gneisses and meta-limestones interbanded with the hornblende biotite gneisses that indicate a metasedimentary origin for some of these rocks.

The overall average mineralogy of the southern Malawi area of quartz + plagioclase + pyroxene + hornblende + biotite is consistent with amphibolite – granulite facies. High grade metamorphism of this type is akin to collisional zones. Sericitisation is evident in some feldspars as is overprinting of pyroxene by amphiboles and these alterations may be a result of later hydrothermal fluids (an absolute age for these alteration features is not known). Additional geochemistry outside the scope of this thesis may assist in identifying any role such fluids might have played in the geodynamic evolution of the area.

Bloomfield (1965) described perthitisation in this area as post-metamorphic due to partial melting of supracrustal gneisses. He argued that anatexis occurred with introduction of Al, K, and Na and later K (plus Ba) and Si, giving rise to various granites, perthitic gneisses, foliated perthosite, or anatectic perthosite. These syenitic rocks have been regarded as major diapirs and have been called infracrustal ring complexes, with a foliation concentric but later parallel gneisses (Bloomfield, 1965; Morel, 1989). Various authors (Bloomfield, 1965; Evans, 1965; Garson et al., 1965) noted that the field relationships, petrology and mineralogy of these rocks display a clear relationship of tectonism and metamorphism exemplified in an area south west of Zomba towards Blantyre where the rocks clearly associate with a faulted/shear zone.

Enclaves occur in many granitoids as cm- to m-scale bodies having various grain sizes and variable compositions (see above). These are interpreted as xenoliths and the varying contact relationships (sharp to diffuse) between them likely reflect differing degrees of melt assimilation of the xenoliths. In other places, rounded globules or trains of blebs with a different composition suggestive of new magma injection (e.g. Gill, 2011). The discovery of enclaves in several outcrops in the Mwanza area is confirmation that the paragneisses were at various stages intruded by magmatic (granitoid) bodies. The existence of several hill outcrops of granitic rocks, showing both foliated and unfoliated textures, suggests different episodes of magma intrusion, or differential preservation of flow layering by the individual intrusions. More detailed study would assist in understanding the genesis and evolution as well as the tectonic settings of the area.

Southern Malawi has undergone complex and intense regional deformation that is manifest as well-defined foliation and banding, including migmatisation indicative of high temperature metamorphism. All of these features are cut by later rift-related faults as seen in the Great Rift Valley Fault. This type of faulting is equally in phases at varied times, such as cross cutting SNE – NSW wrench faults and later jointing.

In terms of the metamorphic rocks focused on for this study, a tectonic model was proposed by Andreoli (1984) suggesting subduction of ocean crust around 1200 Ma followed by continental collisions between what he termed the Niassa craton and an island arc complex. The southern Malawi granulites were said to represent the underthrusted island arc suite with the ultramafic bodies inferred to be ophiolites and a massif of eclogitic garnet marking the suture zone. However the nature and timing of these events are poorly understood, and hitherto not well constrained. It is important to better understand these events because Malawi lies at the junction of the East African Orogen and the Kuunga Orogen and provides a key component to our understanding of Gondwana assembly as it partly has a record of collision, purported arc magmatism and subduction dynamics. Refining this understanding by establishing better geochronological constraints is the main aim of this study and constitutes much of the research undertaken.

3.7 CONCLUSION

High grade, amphibolite to granulite facies crustal rocks comprising various paragneisses, schists, calc-silicates, limestones, amphibolites, metapyroxenites and various granitoids intruded by various syenites, carbonatites, and pegmatites/quartz bodies, define the geology of southern Malawi. A swarm of NE-SW trending Mesozoic-age solvsbergite and dolerite dykes of the Chilwa Alkaline Province and NW-SE trending lamprophyre dykes cut across all the above lithologies. Deformation has occurred to various degrees, and foliation is complex but generally NW-SE trending. The foliation in the northwest of the region is NW-SE but swings to NE-SW creating a fold-like structure around the Kirk Range area. NE-SW trends are common in the Zomba – Blantyre-Thyolo areas. The youngest structures are dominated by NE-SW trending Rift Valley faulting and NW-SE faulting related to the rift faulting is also present.

To improve understanding of the geologic history of the southern Malawi area and therefore constrain tectonic models of the Mozambique Belt samples have been collected for geochemistry and isotopic dating especially from the granitoids.

3.8 REFERENCES

Andreoli, M. A. G., (1984), Petrochemistry, Tectonic Evolution and Metasomatic Mineralizations of Mozambique Belt Granulites from Southern Malawi and Tete (Mozambique), Precambrian Research, Vol. 25, Issue 1-3, pp. 161-186.

Bloomfield, K. and Garson, M. S., (1965), The geology of the Kirk Range – Lisungwe Valley Area, Bull. Geol. Survey. Malawi, 17, Malawi Government Printer, Zomba Malawi.

Bloomfield, K., (1970), The Geology of the Zomba Area, Bulletin 16, Geological Survey of Malawi, Government Printer, Zomba, Malawi.

Evans, R. K., (1965), The Geology of the Shire Highlands, Bulletin 18, Geological Survey of Malawi, Government Printer, Zomba, Malawi.

Garson, M. S. and Walshaw, R.D., (1969), The geology of the Mulanje area, Bulletin 21, Geological Survey of Malawi, Government Printer, Zomba, Malawi.

Gill, R., (2011), Igneous Rocks and Processes; A Practical Guide, John Wiley & Sons, Ltd., Publication, West Sussex, PO19 8SQ, UK

Grantham G. H., Maboko M. & Eglington B. M. (2003), A Review of the Evolution of the Mozambique Belt and Implications for the Amalgamation and Dispersal of Rodinia and Gondwana, Geological Society, London, Special Publications, Vol. 206, Issue 1, pp. 401-425.

Morel S, (1989), Chemical Mineralogy and Geothermometry of the Middle Shire Granulites, Malawi, Journal of African Earth Sciences, Vol. 9, No. 1, pp. 169 – 178.

Woolley A. R., Bevan J. C. And Elliott C. J. (1979), The Karroo Dolerites of Southern Malawi and their Regional Geochemical Implications Mineralogical Magazine, Vol. 43, Pp. 487-95.

http//:gdem.ersdac.jspacesystems.or.jp. Accessed 20-08-2015

APPENDICES

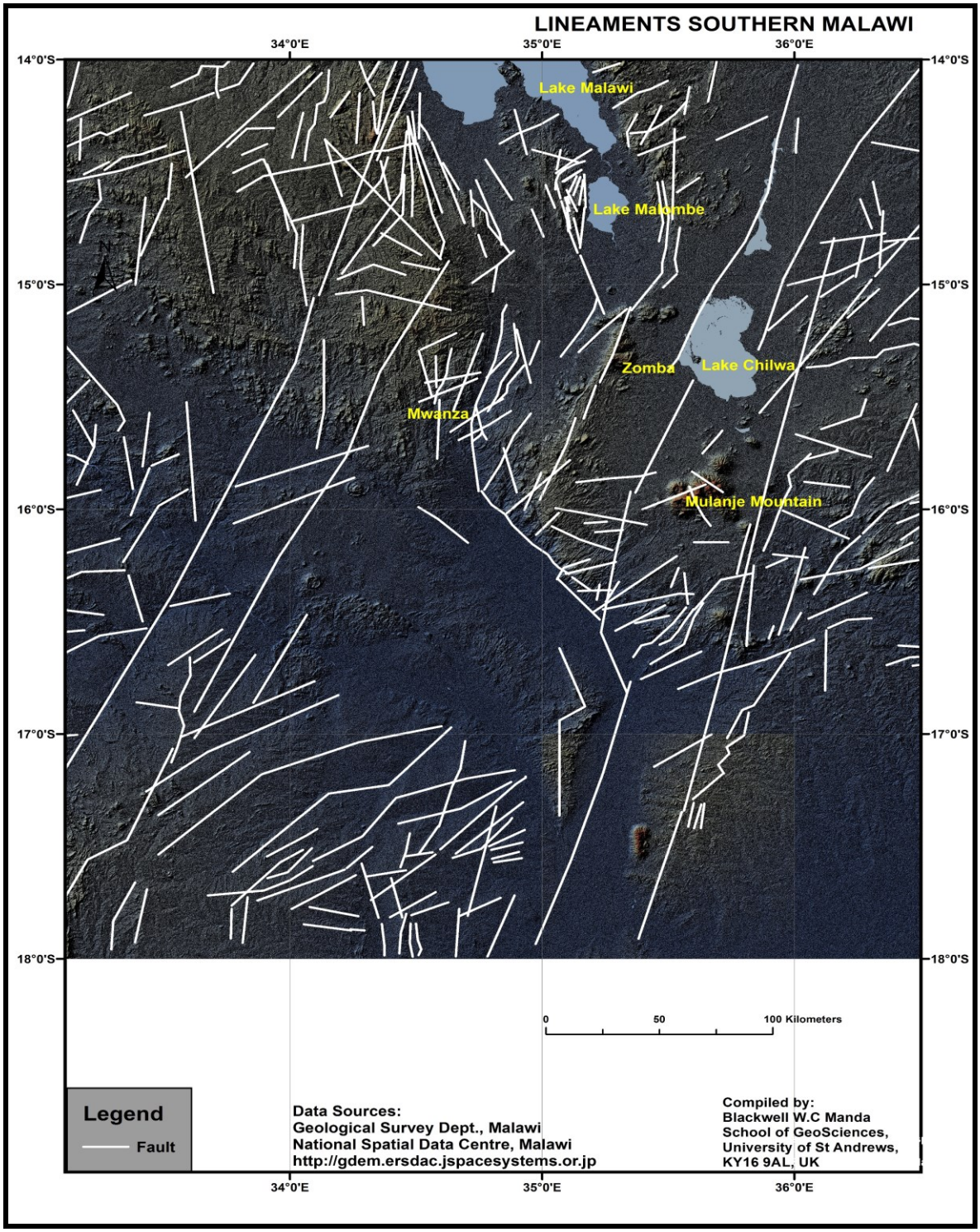

Appendix 3.1: Aster Dem satellite data interpretation showing some lineaments and faults in southern Malawi and surrounding areas (Compiled by Blackwell Manda)

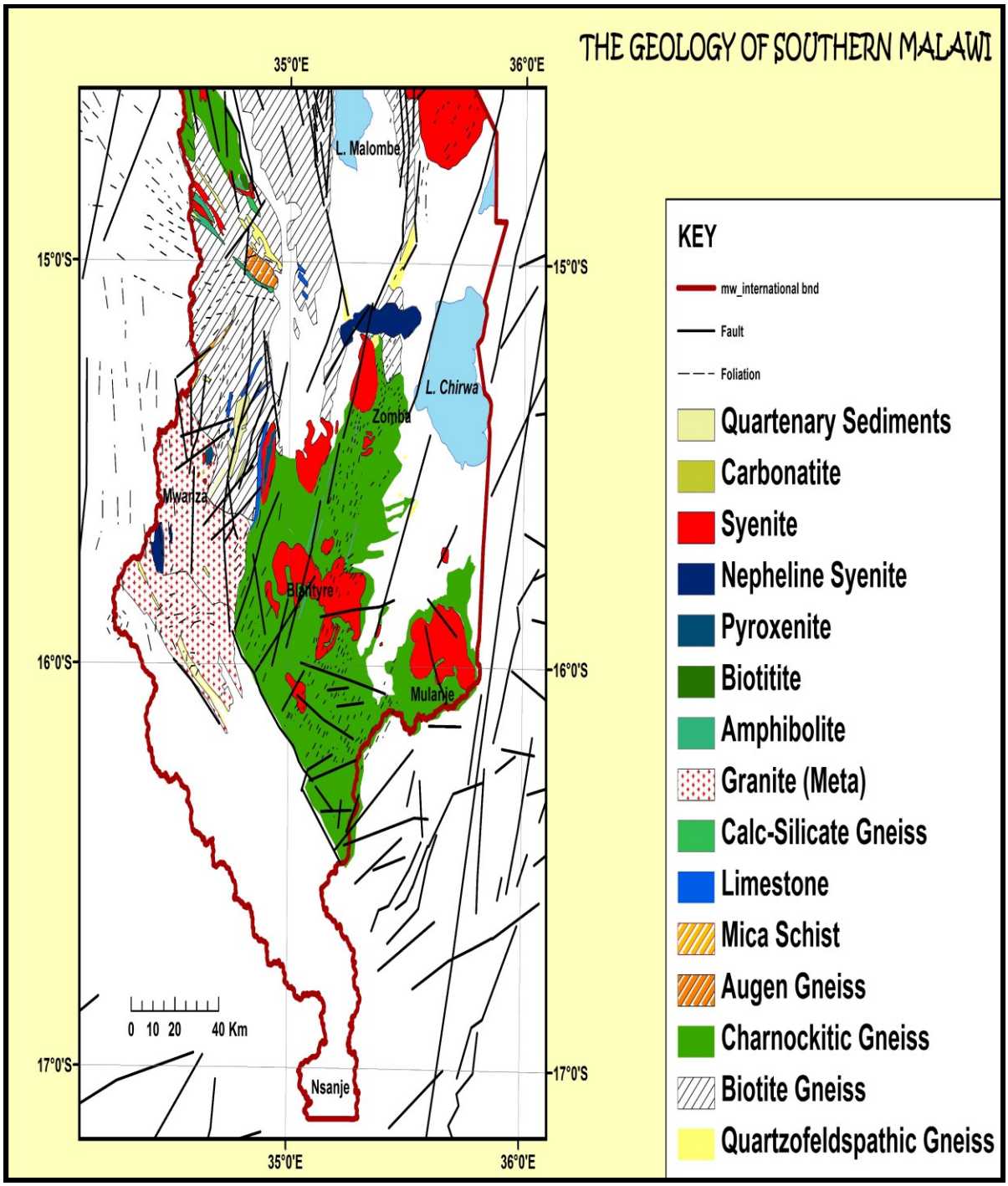

Appendix 3.2: Revised geological map of southern Malawi showing the main lithological units and structure (after Geological Survey of Malawi, 1974). Compiled by Blackwell Manda.

No	Sample No	Locality GPS	Locality Name	Description	Tentative Name	Purpose
1	BM 163	-15.6912700 +34.4177300	Thambani Rd	Leucocratic, Coarse grained, partly foliated.	Metagranite	Whole rock geochem, Petrology, U-Pb isotopes
2	BM 174	-15.7080300 +34.5266700	Envulo Road	Leucocratic, Coarse grained partly foliated.	Metagranite	Whole rock geochem, Petrology, U-Pb isotopes
3	BM 179	-15.5522500 +34.4933800	Kunenekude Rd	Leucocratic, Coarse grained partly foliated.	Metagranite	Whole rock geochem, Petrology, U-Pb isotopes
4	BM 196	-15.4758100 +34.8118800	Zalewa Road	Leucocratic, Med– coarse grained	Qtz-felds gneiss	Whole rock geochem, U-Pb isotopes
5	BM 200	-15.3636700 +34.5678000	East Dambe	Leucocratic fine grained, weak foliation	Qtz-felds gneiss	Whole rock geochem, Petrology, U-Pb isotopes
6	BM 202	-15.2504200 +34.5984600	Kweneza	Mesocratic, med – coarse grained, schictose	Schist	Whole rock geochem, Petrology, U-Pb isotopes
7	BM 205	-15.3171800 +34.8397100	Manondo	Leuco/mesocratic fine grained, foliated.	Biotite gneiss	Whole rock geochem, Petrology, U-Pb isotopes
8	BM 209	-15.7139300 +34.7369600	Mpatamanga	Leucocratic, Coarse grained, partly foliated.	Metagranite	Whole rock geochem, Petrology, U-Pb isotopes
9	BM 213X	-15.7769000 +34.4452700	Envulo	Mafic, fine with phenocrysts	Xenolith	Whole rock geochem, Petrology, U-Pb isotopes
10	BM 213G	-15.7769000 +34.4452700	Envulo	Leucocratic, Coarse grained, massive/partly foliated	Metagranite	Whole rock geochem, Petrology, U-Pb isotopes
11	BM 213GX	-15.7769000 +34.4452700	Envulo	Leucocratic, Coarse grained	Metagranite	Whole rock geochem, Petrology, U-Pb isotopes
12	BM 215	-15.0136500 +35.0446200	Chenkumbi Lafarge quarry	White, Coarse grained.	Limestone	Whole rock geochem, U-Pb isotopes
13	BM 221	-15.0201600 +35.1322900	East Nkhuku	Brown, Medium grained, weak foliation	Leucogranite	Whole rock geochem, Petrology, U-Pb isotopes
14	BM 223A	-15.0246800 +35.1206600	Nkhuku Quarry	Leucocratic, greyish, coarse grained partly foliated.	Charnockitic?/Granite	Whole rock geochem, Petrology, U-Pb isotopes
15	BM 225	-15.0490700 +35.0588100	Chenkumbi	White, Coarse grained.	Limestone	Whole rock geochem, Petrology, U-Pb isotopes
16	BM 226	-15.0386800 +34.6239800	Kirk Range Katsekera	Leucocratic, coarse grained, foliated,	Biotite gneiss	Whole rock geochem, Petrology, U-Pb isotopes
17	BM 233	-15.0852700 +34.6192100	Namiso	Leucocratic, white/buff, coarse grained	Qtz-felds gneiss/schist	Whole rock geochem, Petrology, U-Pb isotopes
18	BM 235A	-14.8937200 +34.5939600	Ndzama Mission	Leucocratic, coarse grained, graphitic, weak foliation	Qtz-felds gneiss	Whole rock geochem, Petrology, U-Pb isotopes
19	BM 235B		Matanda H/Centre	Leucocratic, coarse grained, foliated	Biotite gneiss	Whole rock geochem, Petrology,

						U-Pb isotopes
20	BM 236	-14.8638000 +34.7848700	Njereza (Balaka)	Pink, Coarse grained.	Limestone	Whole rock geochem, Petrology, U-Pb isotopes
21	BM 240	-16.0511100 +35.7783500	Mulanje Mt	Brown/pink, coarse grained, not foliated with mafic xenoliths	Syenite/granite	Whole rock geochem, Petrology, U-Pb isotopes
22	BM 249	-15.8338600 +35.5992400	Phalombe Rd	Leucocratic, banded & foliated, coarse	Charnockitic	Whole rock geochem, Petrology, U-Pb isotopes
23	BM 252	-16.1406400 +35.0914900	Sambankhuni	Leucocratic, banded & foliated, coarse	Charnockitic	Whole rock geochem, Petrology, U-Pb isotopes
24	BM 256	-16.3755300 +35.1994800	Muona Area	Leucocratic, Coarse grained	Granite	Whole rock geochem, Petrology, U-Pb isotopes
25	BM 266	-16.0000800 +35.4062700	Kapiri Quarry	Leucocratic, banded & foliated, coarse	Charnockitic	Whole rock geochem, Petrology, U-Pb isotopes
26	BM 281	-15.4565600 +35.2863100	Six Miles Zomba	Leucocratic, banded & foliated, coarse	Charnockitic	Whole rock geochem, Petrology, U-Pb isotopes
27	BM 282 A	-15.4925100 +35.2291100	Thondwe	Leucocratic, banded & foliated, coarse	Charnockitic	Whole rock geochem, Petrology, U-Pb isotopes
28	BM 282 B	-15.4925100 +35.2291100	Thondwe	Leucocratic, banded & foliated, coarse	Charnockitic	Whole rock geochem, Petrology, U-Pb isotopes
29	BM 289	-15.6907200 +35.1889900	Chiradzulu Hill	Pink, coarse grained, massive with xenoliths	Syenite	Whole rock geochem, Petrology, U-Pb isotopes

Appendix 3.3: Representative samples collected from southern Malawi for petrological, geochemical and geochronological analysis.

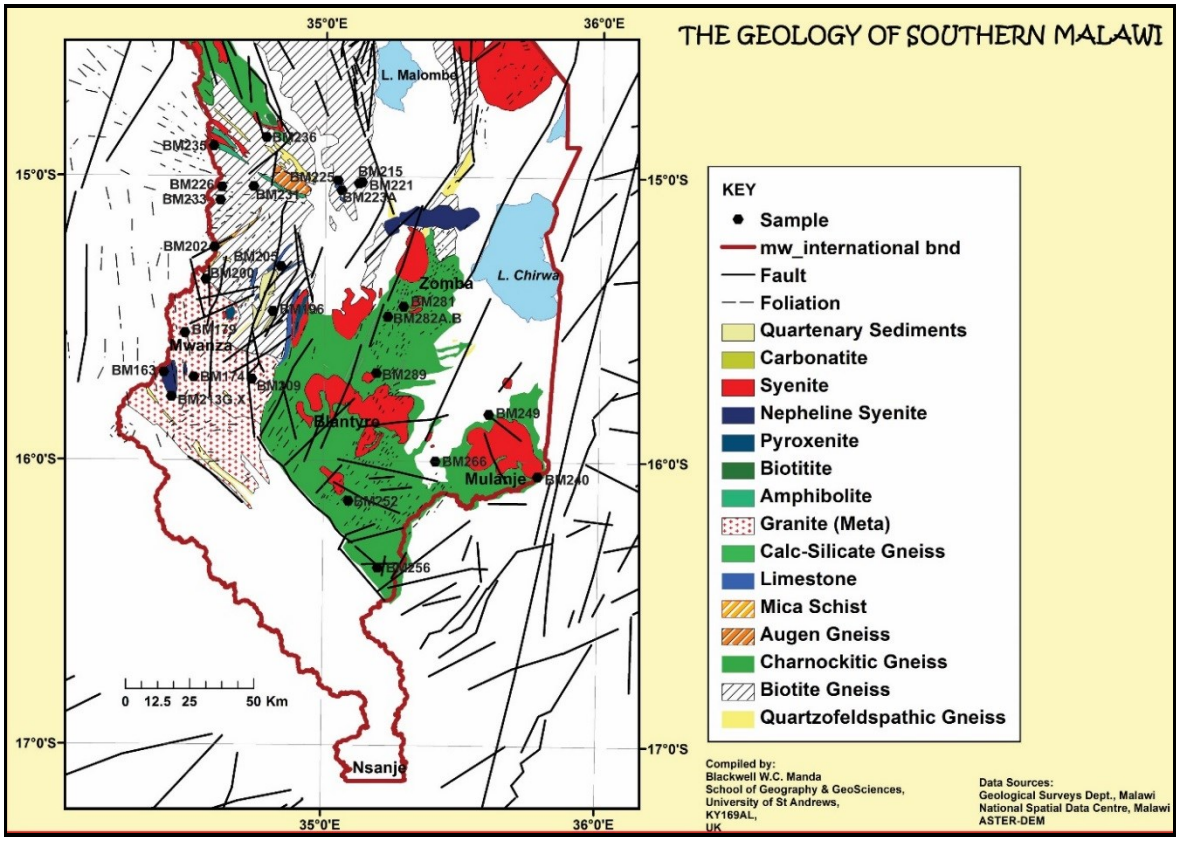

Appendix 3.4: Locality map for samples collected from southern Malawi for petrological, geochemical and geochronological analysis.

Chapter 4: Major and trace element geochemistry

4.1 INTRODUCTION

4.1.1 GEOLOGICAL SETTING

Southern Malawi consists of Precambrian peraluminous and metaluminous granitoids, biotite hornblende gneisses and migmatites, amphibolite gneisses, calc-silicates and meta-limestones (Bloomfield, 1974; Evans, 1965; Kröner et al., 2003). The granitoids are metamorphosed to amphibolite and granulite grade and are now mostly hornblende biotite and charnockitic gneisses (Fig. 4.1) ranging in composition from monzo-dioritic to granitic. Minor pyroxenites and metagabbros and mafic dykes often lie concordant to these granitoids but sometimes they cut across them. Pink perthitic syenites, granites and pegmatites are reported as resulting from anatexis or metasomatism of the older granitoids (Bloomfield, 1974; Evans, 1965; Andreolli, 1984).

Andreolli (1984) interpreted the orthogneisses as products of continental arc margin magmatism. He proposed a tectonic model for the area, specifying ocean floor subduction during the Mesoproterozoic and subsequent collision between an island arc and what he called "Niassa craton". The area now comprises of migmatitic, reworked Archaean granitoids with relics of ophiolites, ultramafics and eclogitic garnet granulites marking the suture zone (Andreolli, 1984). Intrusive anorthosite, metamorphosed monzonite, syenite and K-rich charnockitic granite were also identified (Bloomfield, 1974; Evans, 1965; Andreolli, 1984).

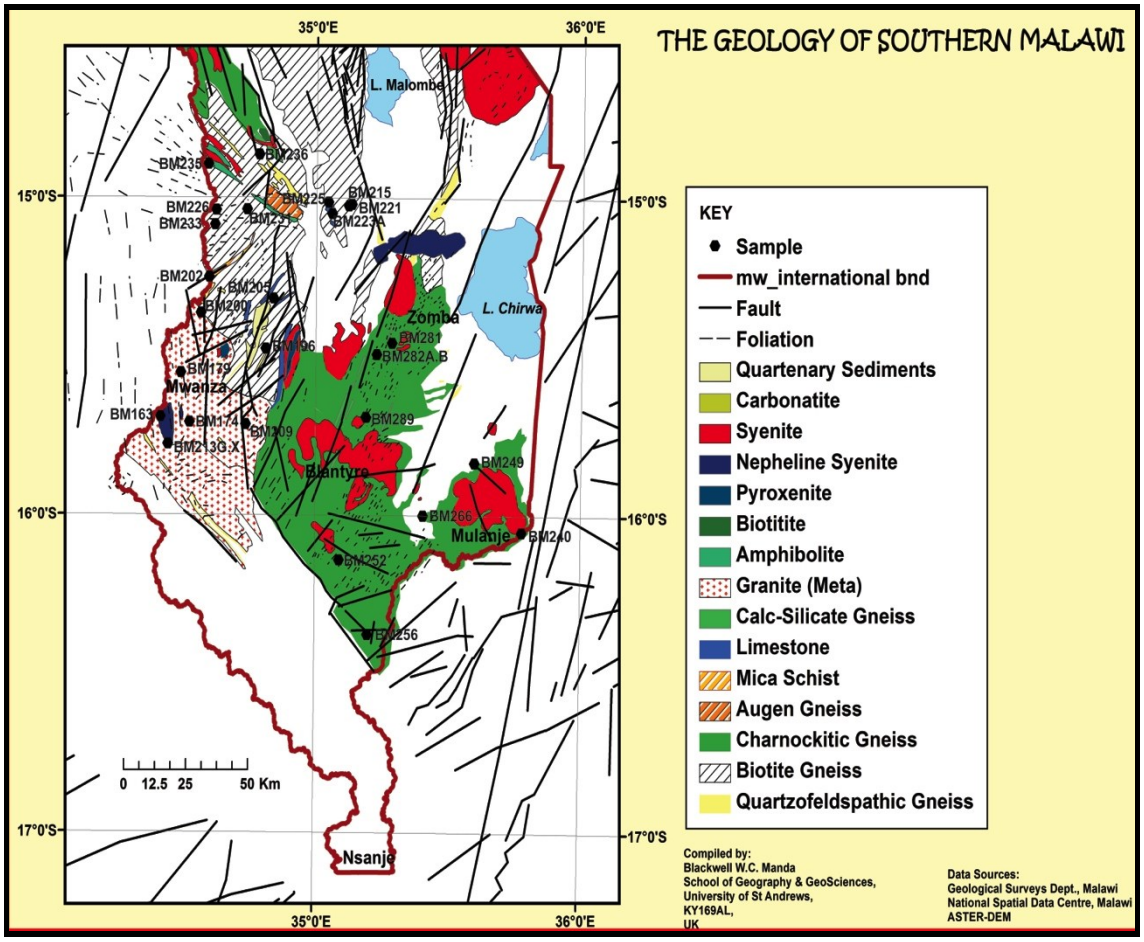

Fig. 4.1: Map of southern Malawi showing the lithological units and the sample locations

4.1.2 PREVIOUS GEOCHEMICAL STUDIES

Bloomfield (1965) mapped some granulite facies charnockitic metadolerites to the west of the study area and noted that they were low in SiO_2 (48 – 50 wt. %) with MgO concentrations of 5 – 6 wt. % and CaO at 9 wt. %, features that are consistent with tholeiitic olivine-basalts. The charnockitic granulites of southern Malawi (around Zomba – Blantyre and Mulanje) are similar in geochemistry to those in the Varberg area Sweden and indeed to those occurring elsewhere in the world which are derived from metadolerites, metagabbros, and metabasalts (Evans, 1965). Evans (1965) further observed that the charnockitic rocks of Malawi are varied (felsic –intermediate- basic) with SiO_2 ranging from 47 to 59 wt. %, and $(Na_2O + K_2O) > CaO$. Other authors notably Morel (1989) and Bloomfield (1965) shared Evans opinion of derivation of the granulites from a pre-metamorphic series of basaltic or andesitic volcanic rocks, with their erosion giving rise to greywackes. Further work by Andreolli (1984) confirmed that the granulites in southern Malawi are similar to high grade rocks widely occurring in Africa, with bulk chemistry suggestive of origins from alkali olivine to high alumina basalts and pelitic-greywacke compositions. However, he specifically noted the absence of chemical data for tonalitic, grano-dioritic orthogneisses described in the Mwanza--Blantyre area (Fig. 4.1), which are typical of Precambrian regions.

4.1.3 AIMS OF THIS CHAPTER

Controversy and questions abound as regards the geodynamic evolution of southern Malawi and surrounding areas in the Mozambique Belt during and after the Proterozoic age (Grantham

et al., 2003). This study aims to provide answers to some of the questions, including the type of orogen this area represents, i.e. collisional or accretionary. It is important to establish whether or not there is any occurrence of arc systems and to determine the timing of magmatic events during the Proterozoic in southern Malawi. On a larger scale these constraints will contribute to our understanding of the role this belt plays in the assembly of Gondwana and the implications for models of Paleoproterozoic supercontinent reconstruction.

The objectives of this chapter are to present new whole rock major and trace element geochemistry to constrain the sources and the nature of magmatism forming the granitoids in southern Malawi, and to use similar data to characterise the regional tectonic setting. The petrology and geochemistry of magmatic bodies contain information on their genesis and evolution which in turn reflects the growth of continental crust (Ghosh et al., 2005). Granitoids may, therefore, provide detailed insight into crustal/mantle composition associated with the Proterozoic Mozambique Belt and with related petrogenetic and geo-tectonic processes (Wilson, 2007). The tectono-thermal history is critical as this area falls within the East African Orogen, which comprises deformed and metamorphosed Precambrian rocks and is generally considered to be the principal collision zone during late Neoproterozoic amalgamation of Gondwana and therefore records evidence of genesis and evolution of the belt (Vogt et al., 2006; Kröner, 2001; Cawood et al., 2007). The chapter is based on geochemical results from Inductively Coupled Plasma Mass Spectrometer (ICP-MS) and from X-Ray Fluorescence (XRF) analyses of granitoid samples from southern Malawi.

4.2 ANALYTICAL METHODS

4.2.1 MAJOR ELEMENTS

Representative samples for granitoids and charnokites as well as some supracrustals from southern Malawi were selected for whole rock geochemistry from reconnaissance mapping. Approximately 1 kg of sample was collected and then crushed in a jaw crusher and pulverised in a tungsten carbide mortar at the University of St Andrews in Scotland. Approximately 2g of this fine powder was ignited for two hours in a furnace at 900°C to remove any volatile substances and to determine loss on ignition (LOI) values for each sample. 10 grams of powder was carefully mixed with 10 drops of a binder then placed in a mould and pressed into a pellet which was left overnight to dry in an oven at 60°C. Analysis of major oxides was carried out using a Spectro XLAB EDP XRF spectrometer equipped with a Rh anode X-ray tube with an excitation potential of up to 3.0kW. Detection was achieved using a Si(Li)-semiconductor with a 5 μm beryllium window cooled by liquid nitrogen and the samples were presented on a 20-position sample changer and analysed under vacuum conditions (Stephens et al., 2004). The effectiveness of the method to calibration was checked by the use of reference materials GRS1, GRS2, GRS3 GRS4, GRS6, PM-S, OU-6, and BHVO-1.

4.2.2 TRACE ELEMENTS

Glass beads were prepared for minor and trace element analyses using a Thermo Scientific XSERIES 2 Quadrupole Inductively Coupled Plasma Mass Spectrometer (ICP-MS). Samples were prepared for ICPMS analysis using the lithium metaborate fusion method. 0.25 ± 0.001 g of each powder sample was mixed with 1.25 ± 0.001 g of lithium metaborate flux (M80/T20) and a very small fraction of lubricant and placed in a platinum crucible. This mixture was fused in an oven at 1060^{O}C for twenty minutes and subsequently left to cool. The melt was poured onto a platinum crucible to create a glass bead.

The beads were placed in beakers with magnet stirrers and then dissolved for one hour in a solution of 5% HNO_3 and 60 ml deionised water. After the mixture had fully dissolved, the solution was then made up to 100 ml with deionised water. Approximately 50ml of this solution was finally reserved in a centrifuge test tube for the next stage. An aliquot of 1 ml of each solution was added to 9 ml of internal standard consisting of 5% HNO_3 + Ge (10 ppb) + Rh (10 ppb) + Re (50 ppb) providing the final solution to be run for minor and trace elements. Some of the reference materials that were used to validate the analyses were GRS1, GRS2, GRS3 GRS4 and GRS6, PM-S, OU-6, and BHVO-1.

The diagrams and graphs were plotted using the software GeoChemical Data toolkit (GCDkit) (Janoušek et al., 2006) and in Microsoft Excel.

4.3 RESULTS

Some analysed samples, such as meta-limestones and associated calc-silicates are clearly of sedimentary origin, so also are quartzo-feldspathic gneisses with graphite. These samples have been omitted from the geochemical interpretation. As a matter of convenience the remaining samples have been subdivided into two groups; charnockitic and meta-granites/granites reflecting the dominant lithologies in the area.

Table 4.1: Major oxides and trace elements data in selected meta-igneous from southern Malawi. Major oxide elements are in weight percentage (wt. %) whereas trace elements are in parts per million (ppm).

Sample Name	BM223A	BM226	BM249	BM252	BM266	BM281	BM282A	BM282B	BM289
Petrology	Horn-Biotite Gneiss	Horn-Biotite Gneiss	Charnockitic gneiss	Charnockitic gneiss	Charnockitic gneiss	Charnockitic gneiss	Charnockitic gneiss	Charnockitic gneiss	Perthitic syenite
Latitude	-15.02468	-15.03868	-15.83386	-16.14064	-16.00008	-15.45656	-15.49251	-15.49251	-15.69072
Longitude	35.12066	34.62398	35.59924	35.09149	35.40627	35.28631	35.22911	35.22911	35.18899
SiO2	60.39	57.27	57.73	63.44	59.15	57.41	56.52	67.81	67.48
TiO2	0.91	0.83	1.85	0.38	0.65	0.80	0.59	0.28	0.65
Al2O3	14.33	16.68	17.54	15.39	16.52	17.72	17.38	16.32	17.97
Fe2O3	8.26	6.91	8.75	8.30	7.03	6.62	8.18	1.44	2.31
MnO	0.14	0.17	0.13	0.15	0.21	0.12	0.15	0.03	0.06
MgO	3.32	4.58	2.32	3.32	2.39	3.98	3.00	1.27	0.72
CaO	6.60	7.47	4.69	6.58	6.39	6.85	7.02	5.25	1.24
Na2O	3.21	4.03	3.80	1.73	3.70	4.17	4.79	6.00	4.04
K2O	1.95	1.04	2.21	0.32	1.22	1.47	1.15	0.59	5.47
P2O5	0.30	0.17	0.68	0.05	0.19	0.19	0.20	0.09	0.14
BaO	0.05	0.05	0.07	0.02	0.04	0.05	0.05	0.01	0.06
SO3	0.02	0.00	0.00	0.00	0.92	0.04	0.01	0.00	0.00
LOI	0.50	0.81	0.26	0.36	1.48	0.52	0.99	0.94	-0.12
TOTAL	99.99	100.00	100.04	100.04	99.89	99.93	100.03	100.04	100.03
Sc	27.28	19.35	18.58	34.80	17.96	15.58	24.51	16.03	12.18
V	131.50	143.50	127.20	237.70	93.43	116.10	129.90	38.40	23.34
Cr	145.90	91.80	3.00	2.30	9.80	26.40	20.70	2.80	5.30
Ni	28.30	47.90	3.00	6.00	9.90	13.40	14.40	4.20	2.00
Rb	50.60	36.20	7.80	140.90	1.20	149.00	2.50	1.10	214.50
Sr	496.10	628.40	2300.00	328.60	220.60	323.80	418.80	368.90	355.70
Zr	285.40	127.00	3.00	594.60	17.10	334.70	76.80	101.10	756.90
Y	41.90	25.96	57.56	18.41	63.00	18.31	33.85	25.92	53.33
Nb	14.59	3.14	15.12	0.79	5.83	8.34	3.41	4.18	48.02
La	62.37	8.32	55.47	3.32	41.13	27.90	13.20	17.50	219.10
Ce	141.50	24.01	108.30	8.09	80.64	54.85	31.26	42.06	430.80
Pr	18.68	4.21	15.48	1.30	9.77	6.94	4.69	5.84	48.43
Nd	71.07	20.56	64.45	6.37	36.89	27.34	21.44	23.75	166.90
Sm	12.55	5.16	12.68	1.84	7.10	5.10	5.33	4.92	23.78
Eu	2.47	1.31	2.95	0.52	2.01	1.70	1.12	0.94	3.55
Gd	10.61	4.72	12.44	2.18	8.21	4.58	5.34	4.60	20.06
Tb	1.44	0.77	1.77	0.42	1.57	0.65	0.91	0.72	2.26
Dy	7.41	4.30	9.31	2.82	10.16	3.42	5.49	4.14	10.35
Ho	1.53	0.92	1.97	0.67	2.32	0.70	1.25	0.92	2.04
Er	4.10	2.61	5.20	1.98	6.33	1.86	3.54	2.60	5.42
Tm	0.58	0.39	0.70	0.32	0.94	0.27	0.54	0.38	0.74
Yb	3.82	2.75	4.42	2.24	6.28	1.80	3.77	2.55	4.83
Lu	0.58	0.43	0.67	0.36	0.93	0.27	0.58	0.37	0.72
Hf	10.95	3.59	16.75	1.13	4.65	3.64	3.15	2.90	23.44
Ta	1.51	0.38	1.30	0.18	0.49	0.61	0.34	0.75	3.81
Th	13.67	0.34	5.24	0.20	2.35	1.64	0.07	1.64	21.77
U	2.41	0.16	1.80	0.05	1.14	0.28	0.05	0.54	2.66
Fe#	0.69	0.58	0.77	0.69	0.73	0.60	0.71	0.51	0.74
Fe*	0.71	0.60	0.79	0.71	0.75	0.62	0.73	0.53	0.76
ASI	0.89	0.97	1.24	1.31	1.07	1.03	0.98	1.00	1.14

Table 4.2: Major oxide and trace elements for selected meta-granites and granites from southern Malawi. Major oxide elements are in weight percentage (wt. %) whereas trace elements are in parts per million (ppm).

Sample Name	BM163	BM174	BM179	BM209	BM213G	BM213X	BM221	BM240	BM256
Petrology	Metagranite	Metagranite	Metagranite	Metagranite	Metagranite	Metagranite enclave	Leucogranite	Granite	Metagranite
Latitude	-15.69127	-15.70803	-15.55225	-15.71393	-15.7769	-15.7769	-15.02016	-16.05111	-16.373553
Longitude	34.41773	34.52667	34.49338	34.73696	34.44527	34.44527	35.12066	35.77835	35.19948
SiO2	54.96	62.91	64.33	60.68	61.04	56.31	75.07	64.04	63.44
TiO2	1.23	0.98	1.00	0.96	1.27	1.25	0.16	0.79	1.00
Al2O3	16.25	15.73	16.04	15.47	15.69	15.33	12.98	16.07	14.66
Fe2O3	9.05	6.36	6.07	7.10	7.19	8.75	1.67	5.98	6.16
MnO	0.16	0.11	0.09	0.12	0.12	0.17	0.02	0.16	0.10
MgO	3.61	2.19	2.02	2.47	2.43	3.90	0.35	0.97	1.93
CaO	7.26	4.46	3.86	5.25	4.74	6.74	1.61	2.36	3.90
Na2O	4.15	3.38	3.10	3.79	3.79	4.14	3.47	3.90	3.66
K2O	2.07	2.93	2.50	3.33	2.98	2.33	3.86	4.62	4.01
P2O5	0.29	0.33	0.32	0.28	0.34	0.30	0.04	0.32	0.26
BaO	0.08	0.08	0.07	0.10	0.08	0.08	0.06	0.13	0.09
SO3	0.01	0.00	0.00	0.01	0.01	0.01	0.00	0.00	0.00
LOI	0.66	0.56	0.64	0.25	0.35	0.68	0.55	0.60	0.80
TOTAL	99.80	100.01	100.03	99.79	100.03	99.98	99.83	99.96	100.01
Sc	27.55	15.87	18.86	18.32	17.61	23.38	1.91	16.11	15.87
V	150.10	113.70	117.00	110.90	106.90	158.20	10.70	5.81	84.66
Cr	63.60	39.00	37.60	39.50	42.50	88.30	1.30	11.90	5.50
Ni	26.30	17.70	18.90	21.60	18.50	38.00	3.70	11.90	15.00
Rb	57.80	110.50	118.80	79.00	86.60	56.30	72.30	42.70	80.60
Sr	544.60	434.80	440.40	450.50	431.50	461.60	255.20	731.20	392.00
Zr	101.50	269.70	286.30	314.20	299.10	261.90	137.20	87.90	463.30
Y	39.21	35.81	38.48	36.07	41.16	43.25	2.79	63.22	38.09
Nb	8.37	10.52	10.78	9.22	13.45	10.40	1.62	80.40	10.96
La	26.79	32.15	33.89	27.76	33.66	28.51	11.02	132.50	24.55
Ce	57.69	67.83	72.30	58.59	72.18	61.40	17.63	237.80	70.37
Pr	8.04	8.85	9.53	7.93	9.67	8.51	1.91	26.79	7.64
Nd	34.96	35.93	38.87	33.44	40.21	36.59	6.53	97.03	31.77
Sm	8.00	7.47	8.11	7.18	8.63	8.19	1.03	16.71	7.14
Eu	2.12	1.82	1.88	1.83	2.16	2.25	1.07	3.57	1.63
Gd	7.72	7.08	7.61	6.96	8.16	8.04	0.92	15.75	7.02
Tb	1.25	1.11	1.19	1.09	1.28	1.32	0.11	2.21	1.12
Dy	6.94	6.09	6.62	6.13	7.06	7.51	0.51	11.66	6.41
Ho	1.49	1.32	1.41	1.32	1.51	1.64	0.11	2.42	1.40
Er	3.94	3.58	3.86	3.54	4.11	4.39	0.30	6.53	3.90
Tm	0.56	0.53	0.56	0.51	0.59	0.64	0.05	0.94	0.58
Yb	3.67	3.59	3.73	3.40	3.94	4.29	0.34	6.28	3.89
Lu	0.56	0.54	0.56	0.52	0.60	0.66	0.07	0.95	0.60
Hf	3.56	9.81	8.98	9.35	8.24	8.22	6.27	22.60	11.01
Ta	0.75	1.01	1.00	0.90	1.00	0.83	0.48	5.22	1.30
Th	3.51	10.50	9.40	4.06	5.43	1.07	2.55	15.64	16.95
U	1.29	2.34	2.94	1.39	2.04	0.54	1.39	1.53	4.68
Fe#	0.69	0.72	0.73	0.72	0.73	0.67	0.81	0.85	0.74
Fe*	0.71	0.74	0.75	0.74	0.75	0.69	0.83	0.86	0.76
ASI	0.88	1.06	1.23	0.90	0.99	0.84	1.00	1.04	0.90

4.3.1 HARKER DIAGRAMS

In order to examine the relationships between major and trace elements in these samples the main variables and some ratios are plotted against SiO_2 in Harker plots.

MAJOR OXIDES

Fig. 4.2: Variations in major oxides with SiO_2 (all weight %) from southern Malawi metaigneous and igneous rocks. Key to symbols is shown at the bottom of the figure.

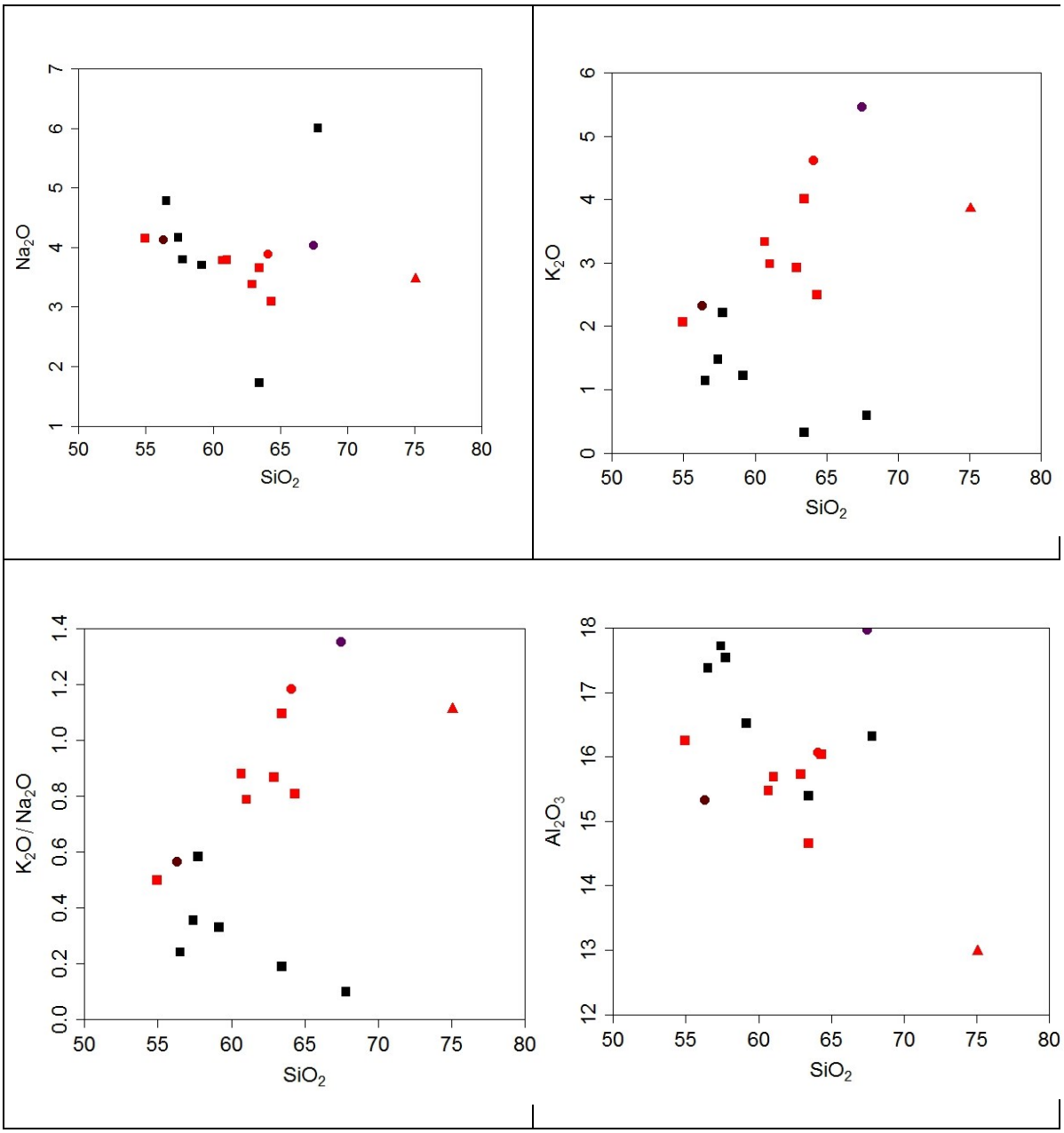

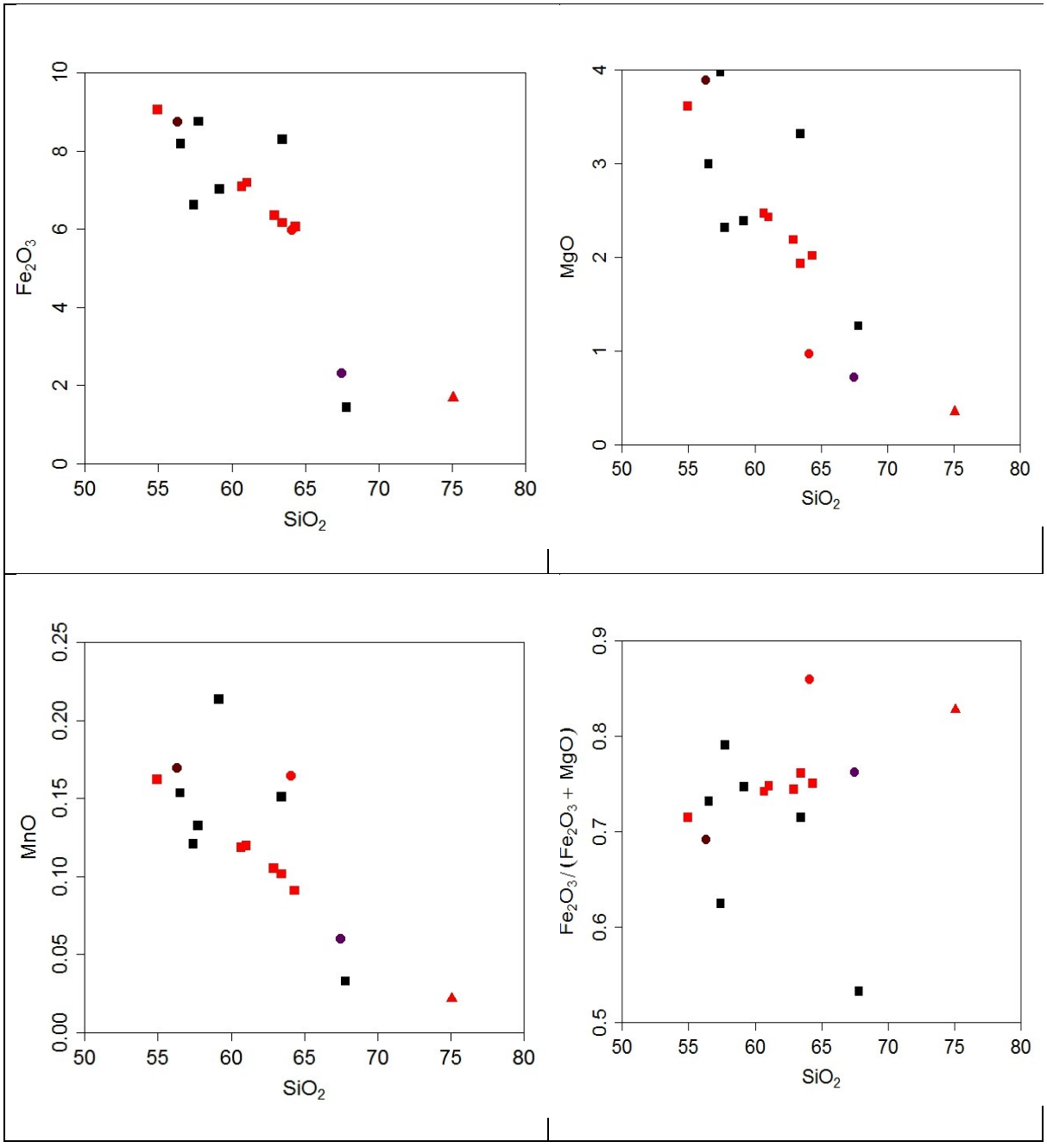

Fig. 4.2 (continued)

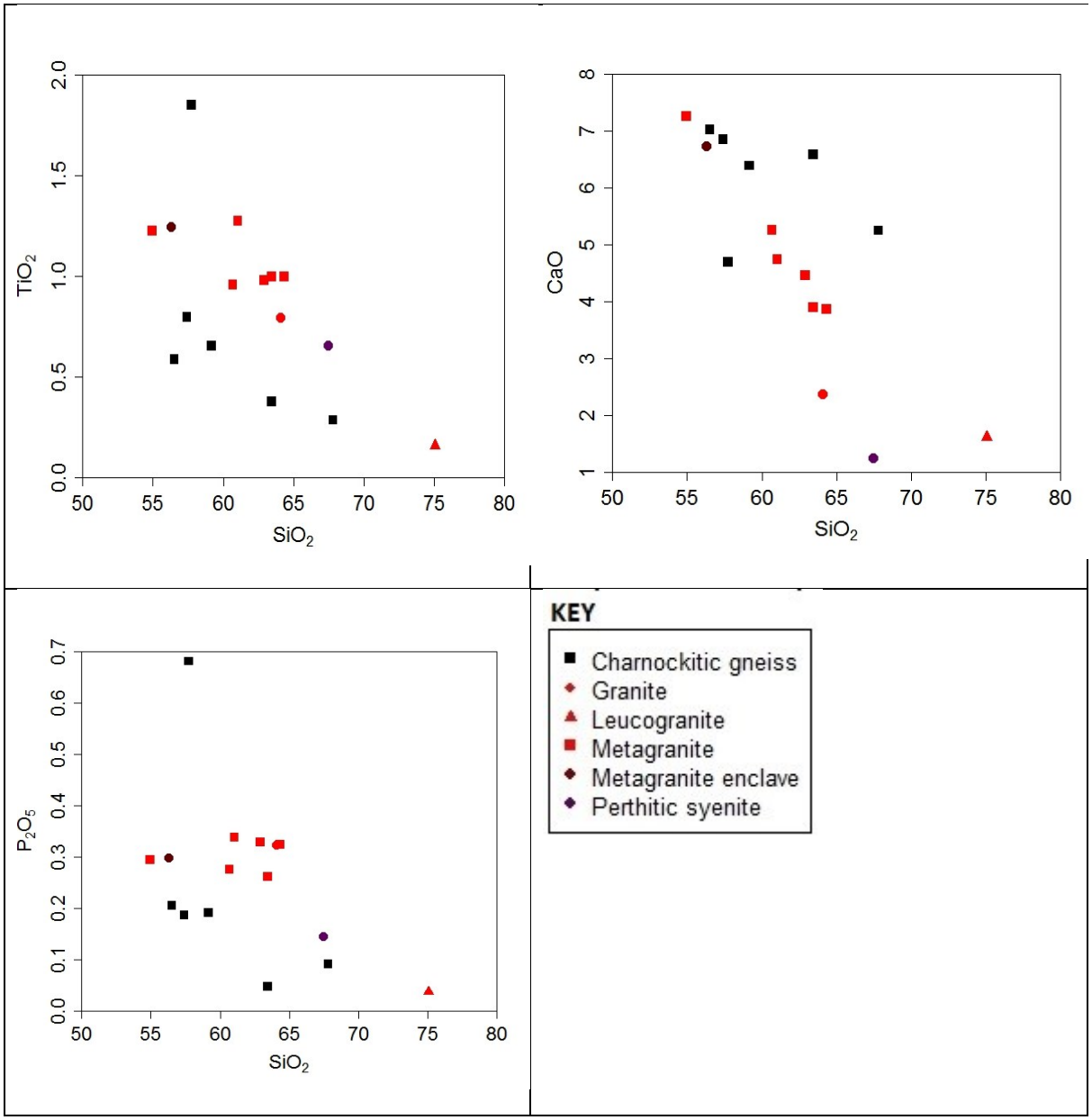

TRACE ELEMENTS

Fig. 4.3: Variation in trace elements (ppm) with SiO_2 (weight %) in metaigneous and igneous rocks from southern Malawi. Key to symbols is shown at the bottom of the figure.

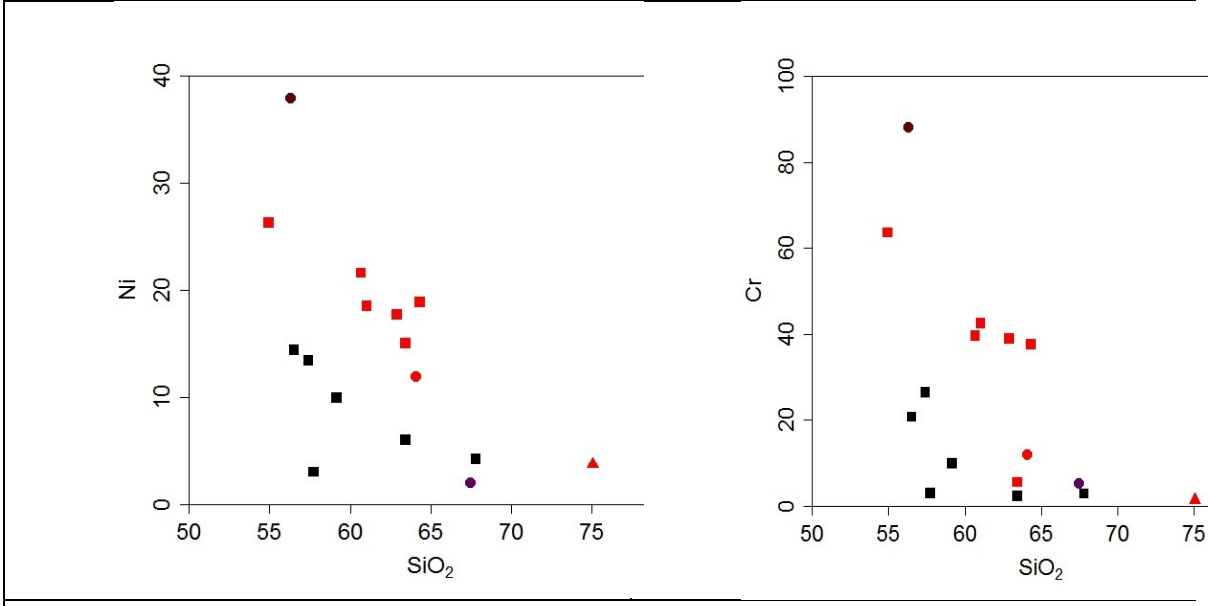
Ni
0
10
20
30
40
50
55
60
65
70
75
SiO2

Cr
0
20
40
60
80
100
50
55
60
65
70
75
SiO2

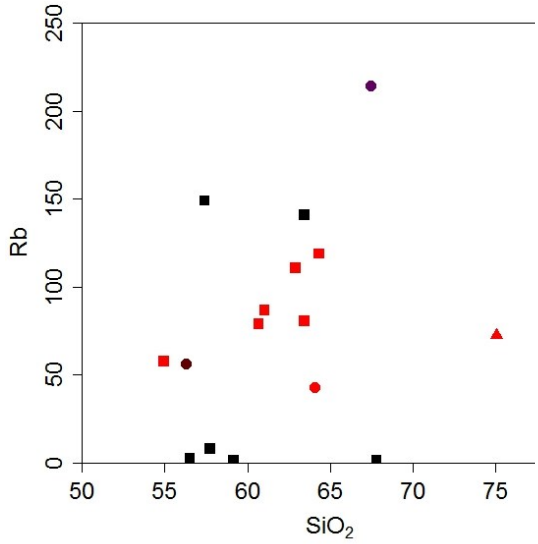
Rb
0
50
100
150
200
250
50
55
60
65
70
75
SiO2

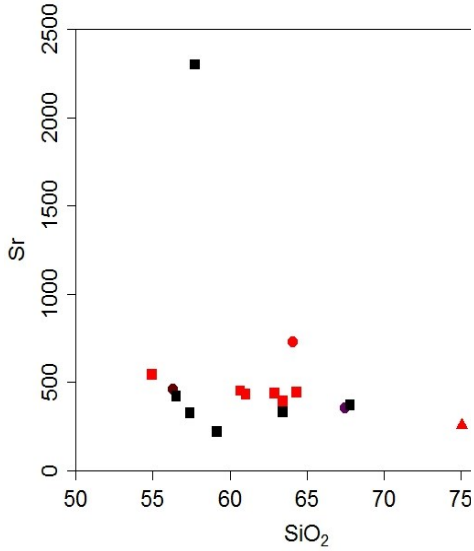
Sr
0
500
1000
1500
2000
2500
50
55
60
65
70
75
SiO2

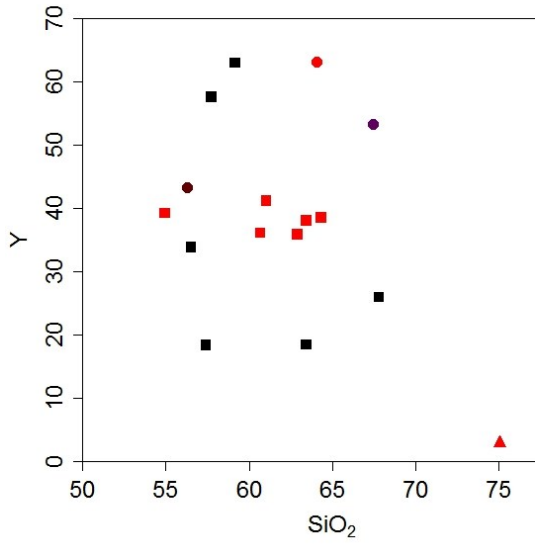
Y
0
10
20
30
40
50
60
70
50
55
60
65
70
75
SiO2

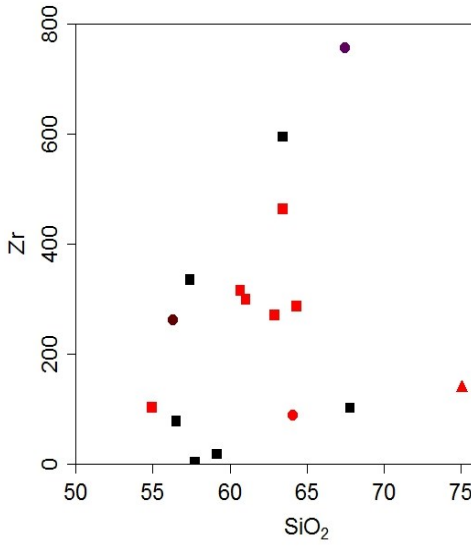
Zr
0
200
400
600
800
50
55
60
65
70
75
SiO2

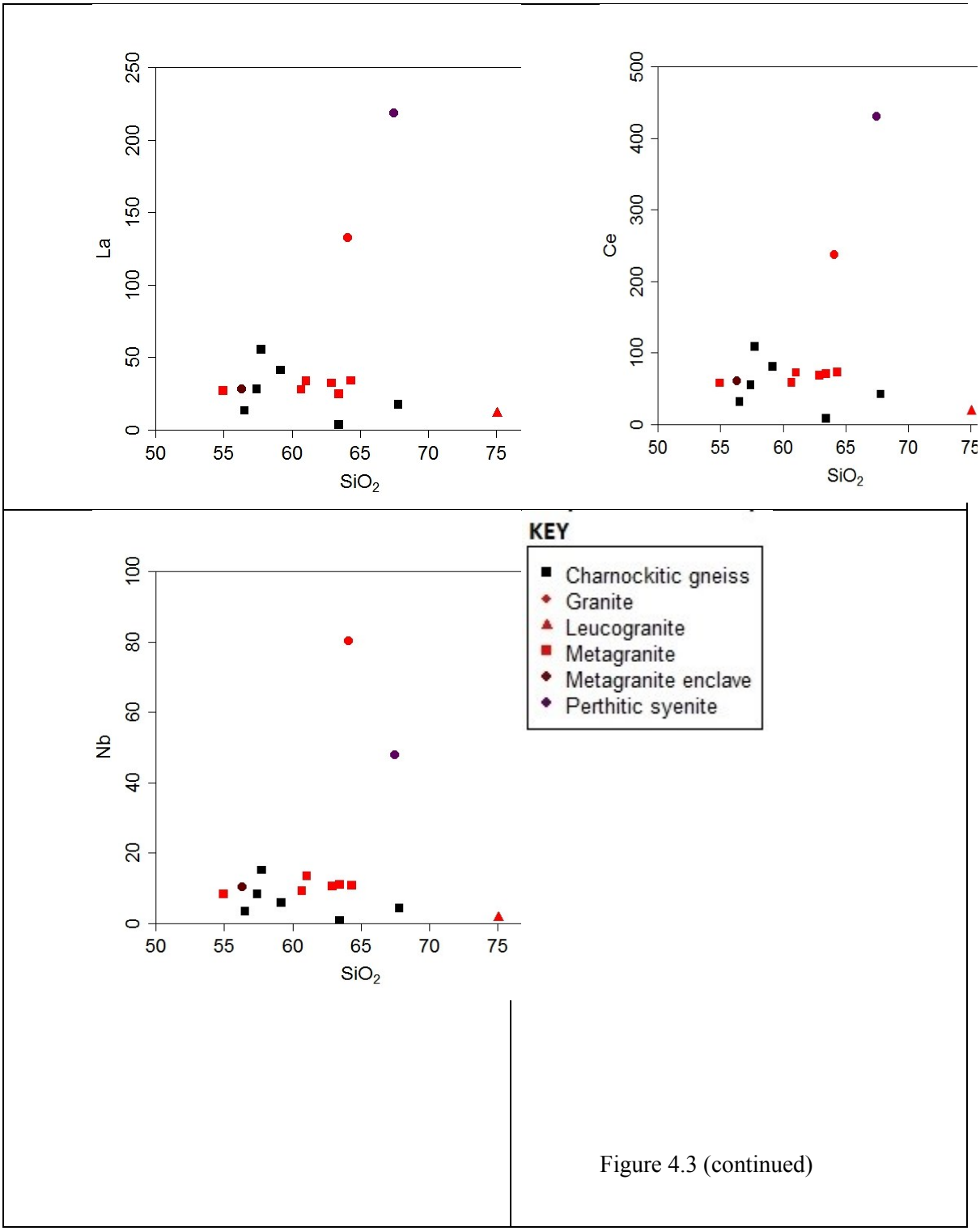

Figure 4.3 (continued)

4.3.2 CHARNOCKITIC GNEISSES

MAJOR ELEMENTS

Major oxide data (Table 4.1) for charnockitic gneisses for southern Malawi show variable compositions with moderate to high silica (SiO_2 ranging from 56.52 to 67.81 wt. %). The charnockitic gneisses from southern Malawi are intermediate to acid in igneous terms (Best, 2003). Some contain relatively high CaO (range 1.24 – 7.02 wt. %), and low MgO (0.72 - 3.98 wt. %), TiO_2 (0.28 - 1.85 wt. %), MnO (0.03 to 0.15 wt. %) and P_2O_5 (0.05 to 0.68 wt. %). The

analysed samples have high average Al_2O_3 contents of 17.05 wt. % ranging from 15.39 to 17.97 wt. % and the Fe_2O_3 % mean is 5.93 wt. %, with a range from 1.44 to 8.75 wt. %.

The alkalis are highly variable. Na_2O content ranges from 1.73 – 6.00 wt. % with the average being 4.09 wt. % whereas K_2O ranges from 0.32 – 5.47 wt. % with an average value of 1.87 wt. %. Two samples BM 249, and BM 282B have their $Na_2O + K_2O$ content higher than CaO. The other three samples have their $Na_2O + K_2O$ content lower than CaO. The average total Na_2O and K_2O content is thus slightly higher (5.96 wt. %) than that of CaO (5.27 wt. %). The K_2O/Na_2O ratio for all the samples is <1.0.

Two samples (Fig.4.4) BM 282A and BM 282B were taken from the same locality. They occur as separate charnockitic gneiss units that are interbanded. BM 282A is leucocratic-mesocratic, greyish – greenish, whilst BM 282B is leucocratic and pink. BM 282A has relatively higher contents of all the major oxides except for SiO_2 and Na_2O.

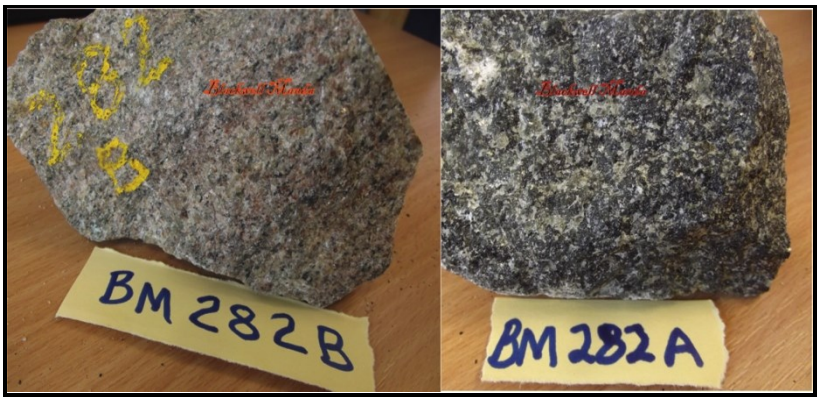

Fig. 4.4: Showing light and darker bands of charnockitic gneiss from the same locality in southern Malawi (Samples BM 282A and 282B)

Overall the charnokitic gneisses show decreasing K_2O, Al_2O_3, TiO_2, CaO, MgO, Fe_2O_3, MnO and P_2O_5 with increasing SiO_2. No oxides show a clear increase whereas trends usually attributed to magmatic differentiation typically show an increase in K_2O (Wilson, 2005; Rollinson, 1993). The analysed samples generally have very low contents of Ti (TiO_2 with range 0.16 – 1.85 wt. %) and such low contents may signify the low abundance of ilmenite and titano-magnetite phases (Best, 2003; Wilson, 2007), consistent with their absence in thin sections. The Aluminium Saturation Index (ASI) for these rocks ranges from 0.98 to 1.31 and the excess of Al_2O_3 (index ratio > 1) is accommodated in mafic or accessory minerals i.e. micas, especially Al-rich biotite, and garnet (Frost, 2001; Best, 2003). The Fe_2O_3 concentrations range from 1.4 to 9 wt. % and on average these are higher than the MgO that range from 1.3 – 4 wt. %. Based on Fe* which is equal to the ratio FeO/(FeO + MgO) most of the charnockitic gneisses would be classified as magnesian (Frost, 2001). Magnesian rocks are associated with hydrous oxidising magmatic environments typical of subduction zones (Frost, 2001). Concentrations of P_2O_5 are very low ranging from 0.02 to 0.7 wt. % and this is normally associated with accessory apatite (Wilson, 2007).

TRACE ELEMENTS

From the data in Table 4.1 the southern Malawi charnockitic gneisses display a wide range for Rb (1 – 149 ppm), a relatively narrow range for Sr (324 – 420 ppm) and a very wide range for Zr (76.80 –595 ppm). Similarly there is a wide range in Nb (0.8 – 48 ppm) and Y (18.3 – 57.6 ppm). The rocks display Th/U ratios ranging from 1.4 to 5.9, Th/Nb ratios from 0.02 to 0.40, and Sm/Nd ratios from 0.19 to 0.29.

Trace element data for these gneisses are plotted against SiO_2 in Fig. 4.3. Cr and Ni decrease with increasing SiO_2 a trend typical of magmatic differentiation in which olivine and/or pyroxene fractionate from a melt (Wilson, 2005; Rollinson, 1993). No trace elements show a consistent increase with SiO_2.

Normalised multi-element diagrams are based on groups of elements broadly incompatible with typical mantle mineralogy and were originally devised for characterising basalt geochemistry but usage has been extended to other igneous rocks (Rollinson, 1994). In the primitive-mantle normalized trace element plot (Sun and McDonough, 1989) (Fig. 4.5), the charnockitic gneisses exhibit a relatively flat pattern between about x3 and x100 enrichment over mantle but there is some enrichment in large ion lithophile elements (LILE) like Rb, and Ba, while in some samples there are negative anomalies in high field strength elements (HFSE) such as Th, Nb, P, Zr and Ti.

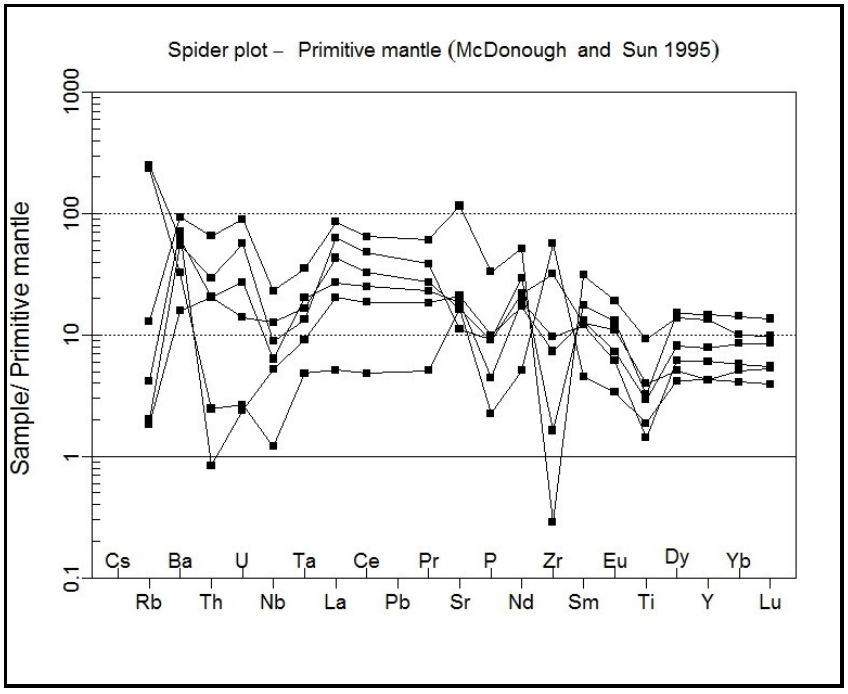

Fig. 4.5: Primitive mantle spider plot showing trace elements for charnockitic gneisses from southern Malawi.

The primitive mantle-normalised REE patterns of the charnockitic gneisses are displayed in Fig. 4.6. The samples display slight enrichment in the light rare earth elements (LREE) and depletion in the heavy rare earths elements (HREE), and most samples also show negative Eu anomalies. One sample BM252 is distinctive in having a flatter rare earth element pattern and a small negative Eu anomaly.

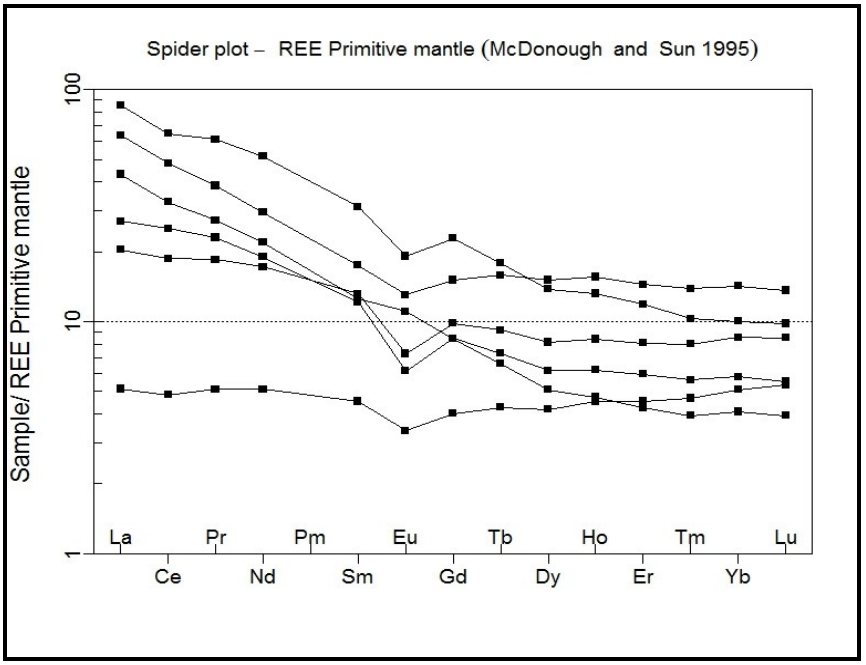

Fig. 4.6: Rare earth element plot of charnockitic gneisses from southern Malawi normalised to primitive mantle. Samples plotted are BM249, BM252, BM281, BM282A, and BM282B, BM289

.

PETROGENETIC INDICATORS

In summary, charnockitic gneisses from southern Malawi are intermediate to acidic in igneous terms with SiO_2 contents in the range 57-68 wt. %. They also display trends on Harker plots that are mostly typical of magmatic differentiation although the lack of increase in K_2O is unusual. The trace elements depict a relative enrichment in LILEs and depletion in HFSEs with moderate negative anomalies in Th, Nb, P, Zr and Ti. The REE spider plots show enrichment in the LREEs and depleted HREEs with negative Eu anomalies, a typical feature of magmatic differentiation related to the removal of plagioclase, or alternatively the retention of plagioclase in the source. The latter interpretation would imply a crustal source for precursor magmas.

4.3.3 CHARNOCKITIC GNEISSES; METAMORPHIC OR IGNEOUS ORIGIN

Charnockite, a hypersthene bearing granite, has been described as having a magmatic origin (Kilpatrick, 1992; Gill, 2011). However it has been observed as occurring mostly in granulite areas of intermediate to high pressure and it has been said that charnockitisation resulted from the influx of CO_2 leading to the breakdown of biotite and amphiboles to pyroxene (Harlov et al., 2005) in previously existing amphibolites and granulites. Debate has prevailed over the origins of charnockite; for example, orthopyroxene crystallisation directly from water-depleted magma or from post-magmatic dehydration metamorphism of hornblende granite. One view is that the former (igneous charnockites) are appropriately dissimilar in geochemistry exhibiting high TiO_2, P_2O_5, and Zr (Gill, 2011).

Kilpatrick et al., (1992) studied charnockites from Antarctica and Australia using petrology and geochemistry and showed evidence of their magmatic origin such as magmatic layering, intrusive contacts, enclave swarms, and high crystallisation temperatures, clearly distinguishing them from the metamorphic charnockites. They named them Charnockite Magma type (C-Type), having an overall range from 45 – 78 wt. % SiO_2, and characterised by high TiO_2, P_2O_5, and K_2O, lower CaO, and lower magnesium number for a given SiO_2 content in comparison with metamorphic charnockites. The coupled enrichment in TiO_2, P_2O_5, and

K_2O with lower CaO abundances were deemed unique among igneous rocks. Rocks with these distinctive geochemical characteristics intrude late Archean-Proterozoic granulite terranes in Australia, Antarctica, Africa (Limpopo Belt), North America and Scandinavia (Grantham et al., 2012; Rajesh, 2004). Grantham et al., (2012) reported the existence of both magmatic and metamorphic charnockites in the Mesoproterozoic Natal belt, Kwazulu, Natal in South Africa. In this area, the Oribi Gorge Suite is a magmatic type described as tholeiitic, with high K_2O, P_2O_5, TiO_2 and $(Na_2O + K_2O)/CaO$ ratios. In southern India, the Madurai Block charnockites based on the geochemistry and petrology have been classified as a magmatic suite with both intermediate and felsic members consistent with a basaltic source (Rajesh et al., 2004).

Comparative analysis between the charnockitic gneisses from Malawi and the C-Type charnockites from Antarctica provides a context for the Malawian rocks. Data from magmatic charnockites from Limpopo (Grantham et al., 2012) and from India (Rajesh, 2004) have also been included in this comparative analysis and data are presented in Table 4.3. In the AFM diagram (Fig. 4.7) the Malawi charnockitic gneisses generally fall in similar fields with the C-Type from Antarctica and charnockites from India and those from Limpopo, classifying close to the tholeiitic–calc-alkaline series boundary. The TAS diagram (Fig. 4.7) plots the rocks from all the localities as quartz diorites, monzodiorites tonalites and granites. At any given SiO_2 in the variation diagrams, the TiO_2 for Malawi charnockitic rocks is lower than in the C-Type charnockites. At any given SiO_2 value P_2O_5, values for the Malawi charnockitic gneisses are lower than the C-Type charnockites and the CaO is higher for the Malawi rocks than the C-Types. In the TiO_2 vs K_2O diagram (Fig. 4.7) the Malawi charnockitic rocks show lower values of K_2O than the C-Type charnockites. Overall, the charnockitic gneisses from Malawi show comparatively low TiO_2, P_2O_5, and CaO relative to SiO_2. In the K_2O vs SiO_2 diagram (Fig. 4.7) the Malawi charnockitic gneisses are also relatively lower than in the other charnockites. Thus, based on these oxides the C-Type are different from the Malawi charnockites. Using the classification scheme of Kilpatrick et al., (1992) the charnockitic rocks from Malawi fall in the field of metamorphic charnockites and are distinct from the C-Type charnockites (Fig. 4.7b). This classification scheme is an effective tool for identifying the possible origins of these charnockitic rocks.

Table 4.3: Chemical data for charnockites to distinguish origins (igneous vs metamorphic) from other areas (Antarctica, India, Limpopo). Data for charnockitic gneisses from Malawi in Table 4.1.

Sample Nan	CMT5	CMT4	CMT3	CMT2	CMT1	LimpUND4	LimpGG74	LimpGG71	LimpGG67	LimpGG75	Antarctica	INTER CM5	INTER CM4	INTER CM3	INTER CM2	INTER CM
Petrology	Charnockite	Charnockite	Charnockite	Charnockite	Charnockite	Charnockite	Charnockite	Charnockite	Charnockite	Charnockite	Charnockite	Charnockite	Charnockite	Charnockite	Charnockite	Charnockite
Locality	Antarctica	Antarctica	Antarctica	Antarctica	Antarctica	Limpopo	Limpopo	Limpopo	Limpopo	Limpopo	Antarctica	India	India	India	India	India
SiO2	77.34	70.75	66.37	62.02	56.23	55.76	55.68	55.54	53.65	52.66	64.00	56.31	55.98	55.01	54.41	53.14
TiO2	0.23	0.75	1.16	1.63	2.55	2.41	2.43	2.57	2.72	2.73	1.25	1.28	1.62	1.34	1.55	2.06
Al2O3	11.80	13.28	13.85	14.38	14.39	15.76	15.53	15.98	16.15	16.55	13.92	16.38	16.11	17.01	14.74	15.31
Fe2O3	1.27	4.25	6.47	7.99	11.01	11.07	8.84	10.85	11.04	11.80	7.63	8.36	8.97	7.98	9.01	10.14
MnO	0.02	0.09	0.09	0.16	0.20	0.17	0.17	0.17	0.18	0.18	0.15	0.13	0.15	0.17	0.15	0.17
MgO	0.19	0.82	1.44	1.89	2.28	2.53	2.60	2.71	3.10	3.08	1.19	4.01	4.41	3.78	4.86	4.88
CaO	0.69	2.46	3.67	4.89	6.55	5.95	6.00	5.80	6.57	6.53	3.59	6.24	6.42	6.41	7.98	8.01
Na2O	1.86	2.85	2.51	2.90	2.86	3.00	3.11	3.31	3.51	3.26	2.30	4.00	3.57	4.21	3.61	3.40
K2O	6.53	4.51	4.08	3.66	2.98	2.59	2.42	2.16	1.24	2.14	4.16	2.24	1.98	1.60	2.10	1.54
P2O5	0.06	0.25	0.35	0.48	0.94	0.93	0.93	1.01	1.06	1.04	0.47	0.56	0.62	0.64	0.76	0.92
BaO	NA	NA	NA	NA	NA	NA	NA	NA	NA	NA	NA	NA	NA	NA	NA	NA
SO3	NA	NA	NA	NA	NA	NA	NA	NA	NA	NA	NA	NA	NA	NA	NA	NA
LOI	NA	NA	NA	NA	NA	NA	NA	NA	NA	NA	0.78	NA	NA	NA	NA	NA
TOTAL	NA	NA	NA	NA	NA	NA	100.00	100.10	100.22	99.97	99.44	99.51	99.83	98.15	99.57	99.57

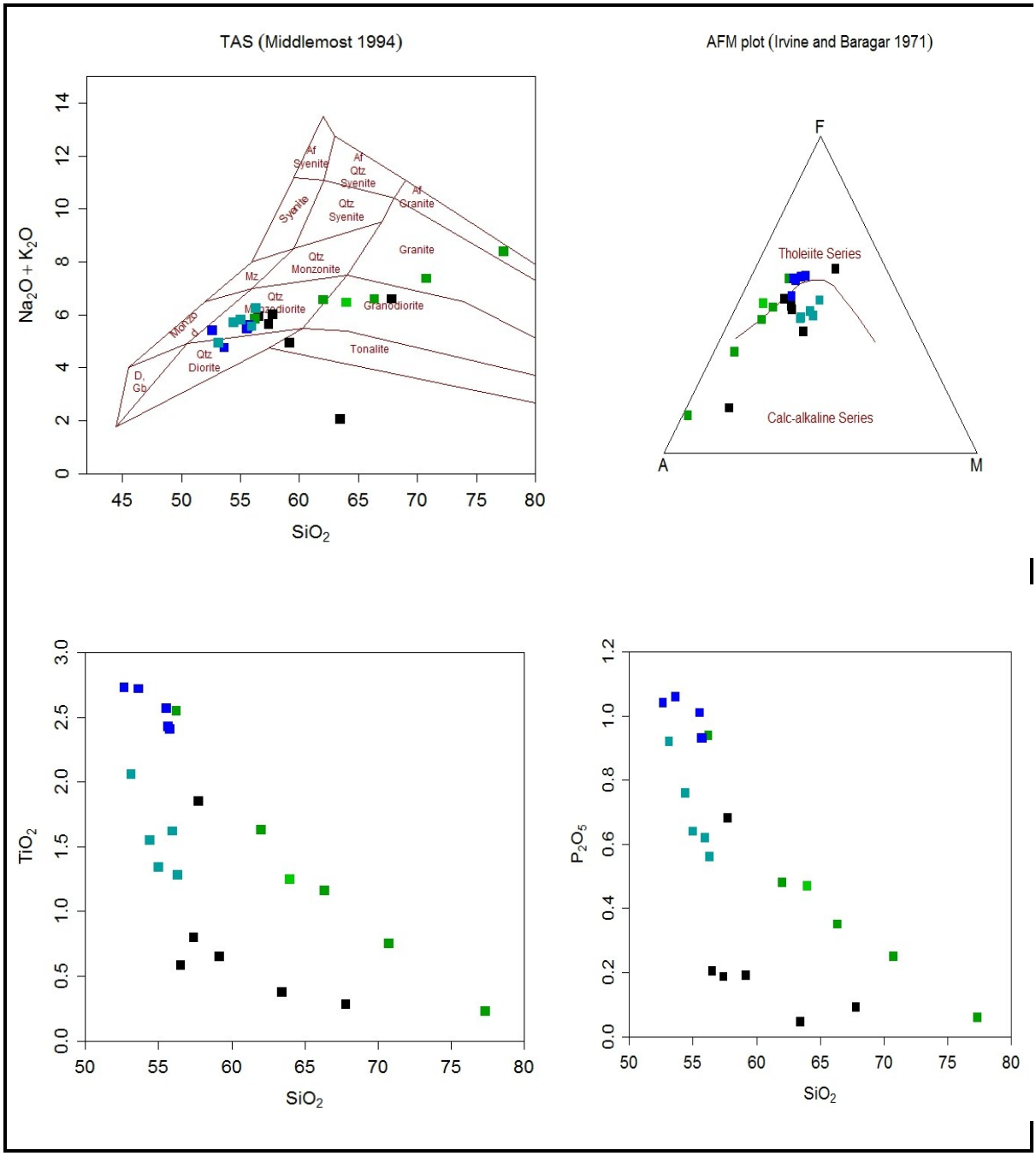
TAS (Middlemost 1994)
AFM plot (Irvine and Baragar 1971)
Af Syenite
Af Qtz Syenite
Af Granite
Syenite
Qtz Syenite
Granite
Qtz Monzonite
Mz
Qtz Diorite
Granodiorite
Monzo d.
Qtz Diorite
D. Gb.
Tonalite
Na2O + K2O
SiO2
F
Tholeiite Series
Calc-alkaline Series
A
M
TiO2
P2O5

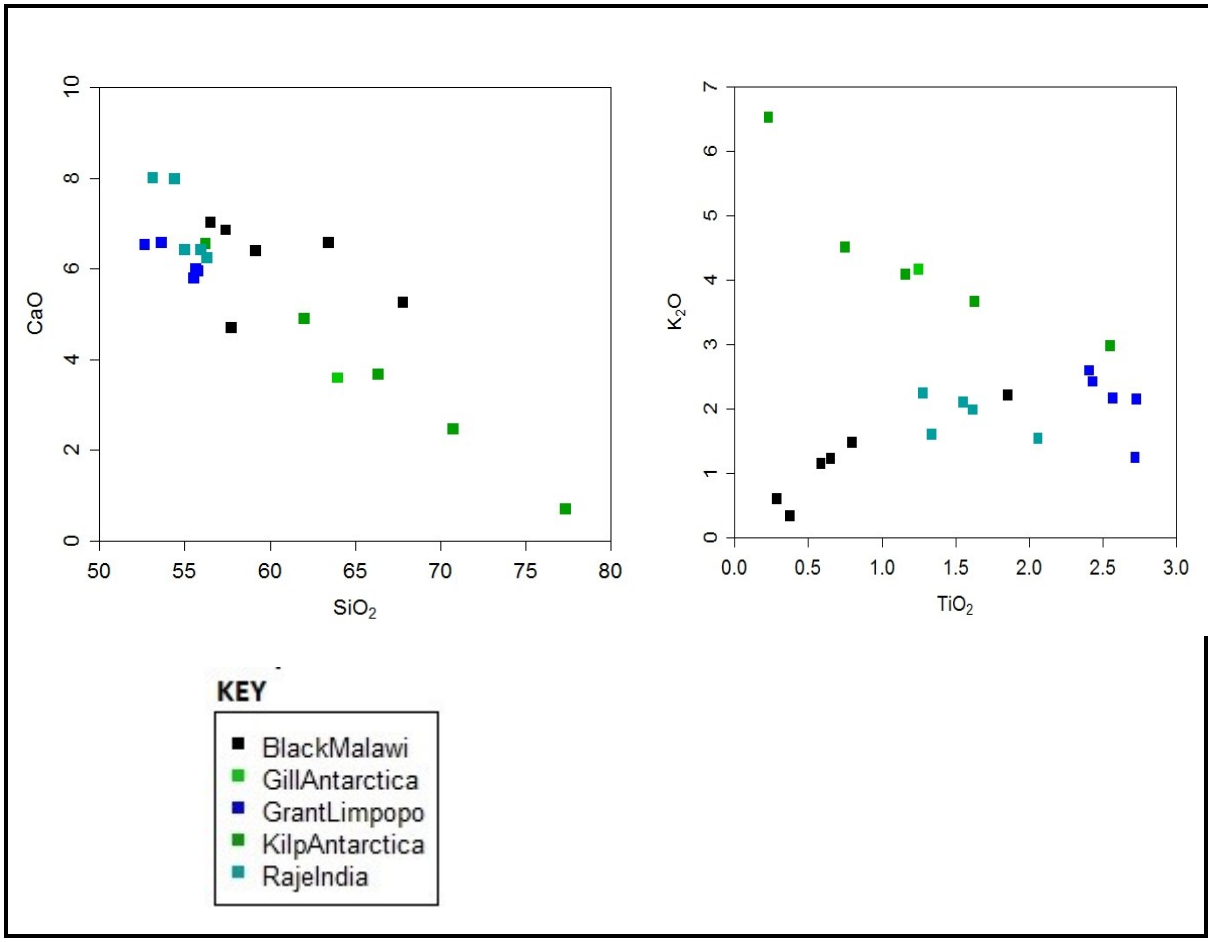

Fig. 4.7: Variation diagrams summarising some major element oxide data to separate igneous from metamorphic charnockites.

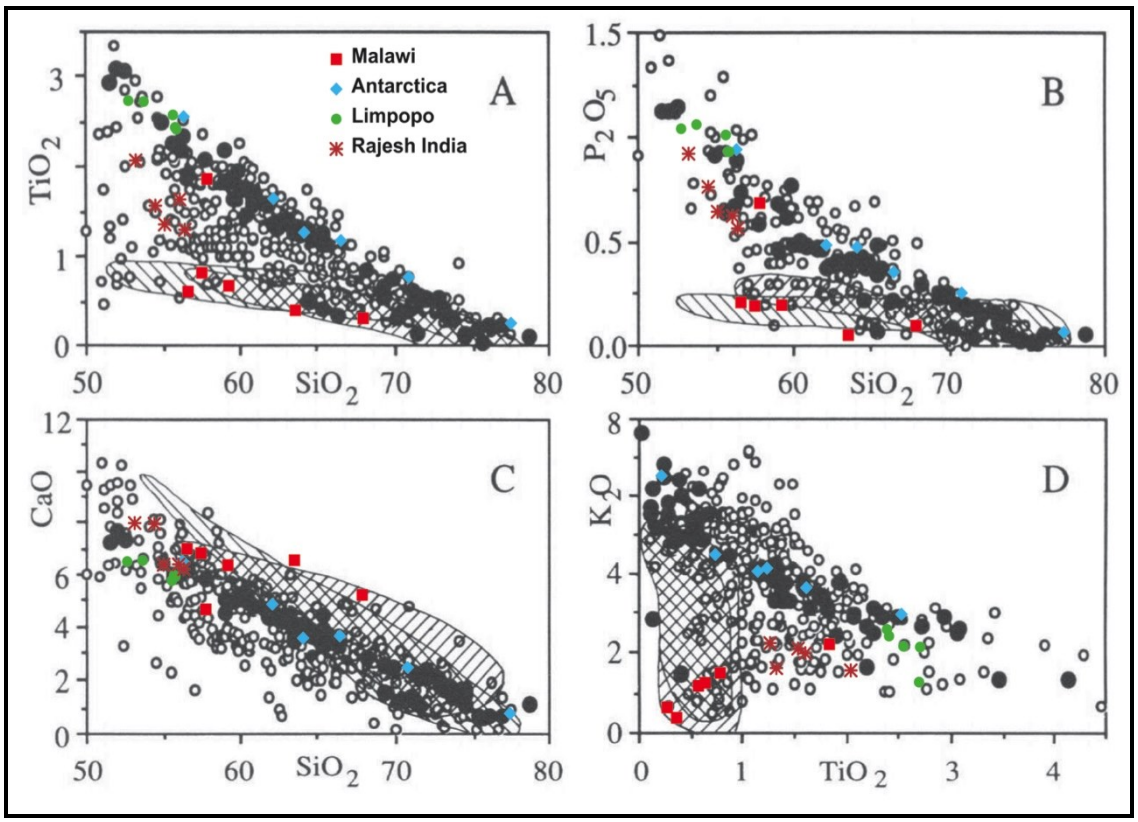

Fig. 4.7b: Charnockitic gneiss samples in this study superimposed onto Kilpatrick et el., 1992 diagrams showing differences between igneous and metamorphic charnockites. Southern Malawi charnockitic gneisses fall in metamorphic charnockite zones. Fields for metamorphic charnockites have \ \ \ \ \ shading and Lachlan Fold Belt granites / / / / / shading.

4.3.4 META-GRANITES AND GRANITES

MAJOR ELEMENTS

Geochemical data on the meta-granitic and granite rocks of southern Malawi are presented in Table 4.2 and plotted in Figs. 4.2 and 4.3. The meta-granitic rocks have intermediate to high SiO_2 (54.9 – 75.1 wt. %) and low MgO concentrations (0.35 -3.9 wt. %), with CaO contents that range between 1.6 and 7.3 wt. %, and high Al_2O_3 concentrations from 13.0 to 16.3 wt. %. The samples exhibit low contents of K_2O (1.9 – 4.6 wt. %), FeO_3 (1.6 – 9.1 wt. %), TiO_2 (0.1 – 1.2 wt. %), and P_2O_5 (0.04 – 0.34 wt. %). In samples BM 163, BM 213X and BM 223A, the $Na_2O + K_2O$ content is less than the CaO content. All other samples have higher $Na_2O + K_2O$ content relative to CaO content.

Granite sample BM 240 displays relatively high content of K_2O (4.6 wt. %) and high Na_2O (3.9 wt. %). The K_2O/Na_2O ratio (Fig. 4.2) ranges from 0.50 to 1.2 wt. & showing the rocks as slightly potassic.

Leucogranite sample (BM 221) has high at SiO_2 (75.1 wt. %) and very low TiO_2 (0.16 wt. %). It also has low concentrations of Al_2O_3 (12.98 wt. %), MnO (0.02 wt. %), MgO (0.35 wt. %), and CaO (1.61 wt. %. The Fe_2O_3 content is low (1.67 wt. %), and P_2O_5 very low at 0.04 wt. %).

A perthitic syenite sample (BM 289) displays a different chemistry with relatively higher SiO_2 (67.5 wt. %), much higher K_2O (5.47 wt. %) and much lower CaO content (1.24 wt. %), relative to the meta-granites.

The Harker plots for major oxides in the southern Malawi meta-granites and granite rocks show that TiO_2, Al_2O_3, FeO_3, MgO, CaO, Na_2O, BaO, and MnO have negative correlations with SiO_2 whereas K_2O has a positive correlation. This is a typical igneous differentiation pattern for granitoids (Wilson, 2005; Rollinson, 1993).

TRACE ELEMENTS

The data are presented in Table 4.2. Some trace elements in the meta-granites and granites have very wide concentration ranges, for example Rb varies from about 1-120 ppm, Sr from 78-777 ppm, Zr from 17 to 314 ppm, Nb from 2-80 ppm and Y from 3-63 ppm. The Th/U ratio ranges from 1.98 to 10.25, the Th/Nb ratio ranges from 0.10 to 1.57, and the Sm/Nd ratio is from 0.16 to 0.22.

The leucogranitic sample BM 221 has the highest SiO_2 and the lowest concentrations of compatible elements such as Cr, Ni, Sr, Y, Nb, La, and Ce but also surprisingly low Rb, which is normally an incompatible element. The granite sample BM 240 has similarly lower concentrations of Cr Ni, Rb and Sr but much higher contents of Y (63 ppm), Nb (80 ppm), La (132 ppm), Ce (237 ppm) and most the other trace elements.

The perthitic syenite (BM 289) has the highest Rb concentration (215 ppm) but Zr (757 ppm) and Nb (48 ppm) also appear to have behaved incompatibly. This is sometimes a feature of alkaline magmas (Wilson, 2005; Rollinson, 1993).

In Fig. 4.3 trace element data for meta-granites and granites from southern Malawi are plotted against SiO_2. Cr and Ni correlate negatively whereas the relationships with other trace elements are unclear although Sr shows a slight decrease with increasing SiO_2. These trends are associated with a marked positive correlation with K_2O/Na_2O and a strong negative correlation with MgO as SiO_2 increases. These trends are very typical of magmatic differentiation as often observed with fractional crystallisation in granitoids.

The granitoids show a highly coherent pattern in the primitive-mantle normalised trace element plot (McDonough and Sun (1995) (Fig. 4.8). The meta-granites generally display a marked enrichment in lithophile (LILE) elements like Rb, and negative anomalies in Nb, Ta, P and Ti. The mafic enclave sample BM 213X shows similar patterns and additionally has a very pronounced negative Th anomaly. The general coherence however suggests that these granitoids may derive from a common source and negative Nb and Ta anomalies are typically associated with arc-related magmas (Rollinson, 1993; Wilson, 2005).

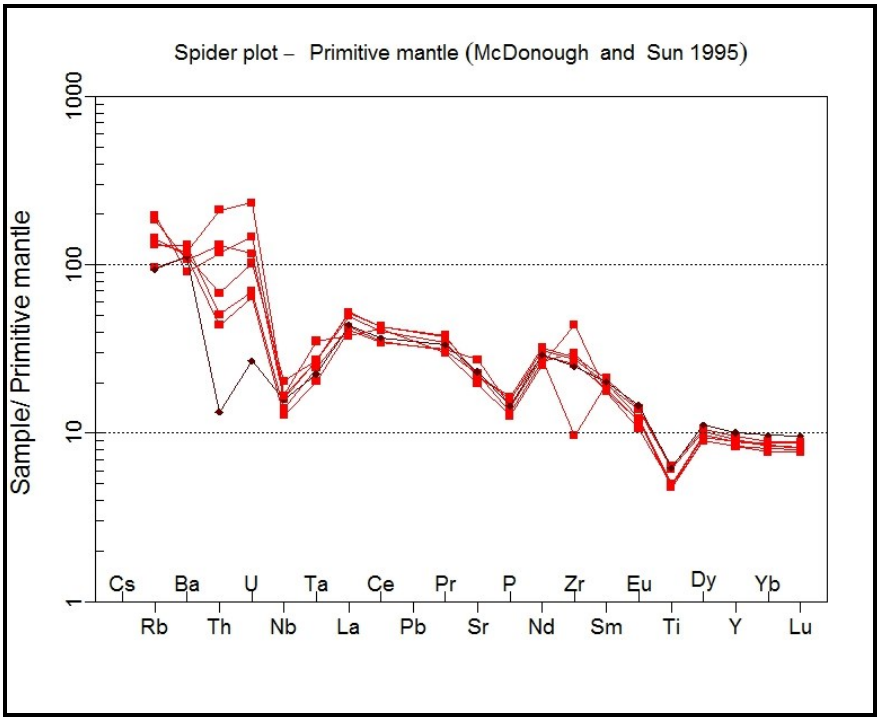

Fig. 4.8: Primitive mantle spider plot for selected meta-granite rocks and one mafic enclave from the same rocks in southern Malawi. Samples plotted are BM163, BM174, BM179, BM209, BM213G, BM213X, and BM256.

Primitive mantle-normalised rare earth patterns are shown in Fig. 4.9. There are very close similarities among the meta-granites. Typically they show enrichment in the LREEs and depleted HREEs with small but distinctive negative Eu anomalies. The meta-granites and the enclave sample BM 213X have coherent patterns suggesting co-magmatic histories.

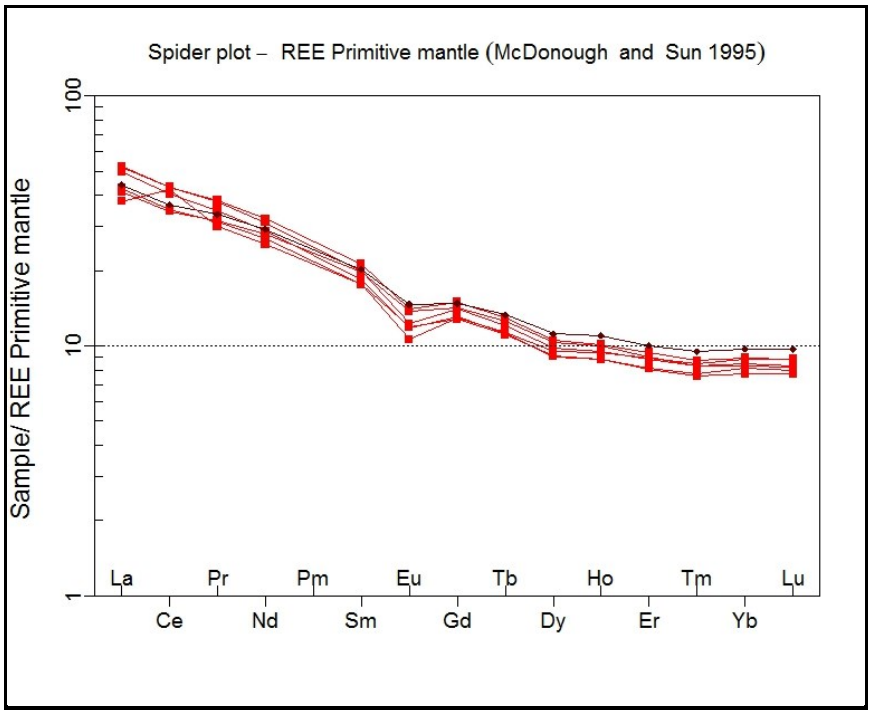

Fig. 4.9: Normalised plot for rare earth elements in selected meta-granite samples from southern Malawi. Samples plotted are BM163, BM174, BM179, BM209, BM213G, BM213X, and BM256.

.
In summary, the geochemistry of the meta-granites analyses indicates that:

a) The meta-granite samples vary from intermediate to acid with SiO_2 ranging from 54.9 to 64.3 %, and a leucogranite sample BM221 has higher values (75.1 wt. %.)
b) Compatible trace elements Ni and Cr decrease with evolving silica.
c) Most LILEs are enriched while the HFSEs (Nb, Ta, P, and Ti) are depleted.
d) The REEs have a pattern of LREE enrichment sloping down to a flat trend in the HREE. All samples show small negative EU anomalies.

4.3.5 SIGNIFICANCE OF ALTERATION

Migmatisation, sericitisation in feldspars, and mineral replacement have been observed in the granitoids from southern Malawi. The loss on ignition (LOI) ranges are small (up to about 1%). As the amount of mineral alteration may be reflected in LOI (Thirlwall, 1981) it is evident in our samples there is alteration from amphibolite-granulite metamorphism. Re-calculating the elemental quantities into a volatile free form (Best, 2003; Gill, 2011) using these rather low LOIs results in only very insignificant differences. The geochemical trends exhibited by the meta-igneous rocks described above suggest elemental distributions not significantly changed and may be assumed to be very similar to primary magmatic compositions (Dostal et al., 2001). This will apply in particular to elements that are relatively immobile in many metamorphic circumstances, including major elements, high field strength elements (HFSE) and rare earth elements (Dostal, et al., 2001). Other authors have argued that mobile elements may also be affected by weathering (Wilson, 2007, Gill, 2011). As the schemes applied on the Malawi data are strictly only applicable to unmetamorphosed fresh rocks they are treated here with due caution.

4.3.6 PETROGENETIC INDICATORS

One of the standard classification schemes for igneous rocks is the total alkali-silica diagram (TAS) (Rollinson, 1994). In the TAS diagram (Fig. 4.10), the granitoids from southern Malawi plot in the intermediate to acid fields classifying the rocks as quartz-monzodiorite, granodiorite, quartz-monzonite and granites. In the same diagram the charnockitic gneisses classify as quartz monzodiorites and tonalites with one sample (BM252) falling outside the classification. In thin section, this sample contains no biotite but has hornblende and pyroxene. It does not appear to be a pristine igneous rock and may have been significantly altered from its original state.

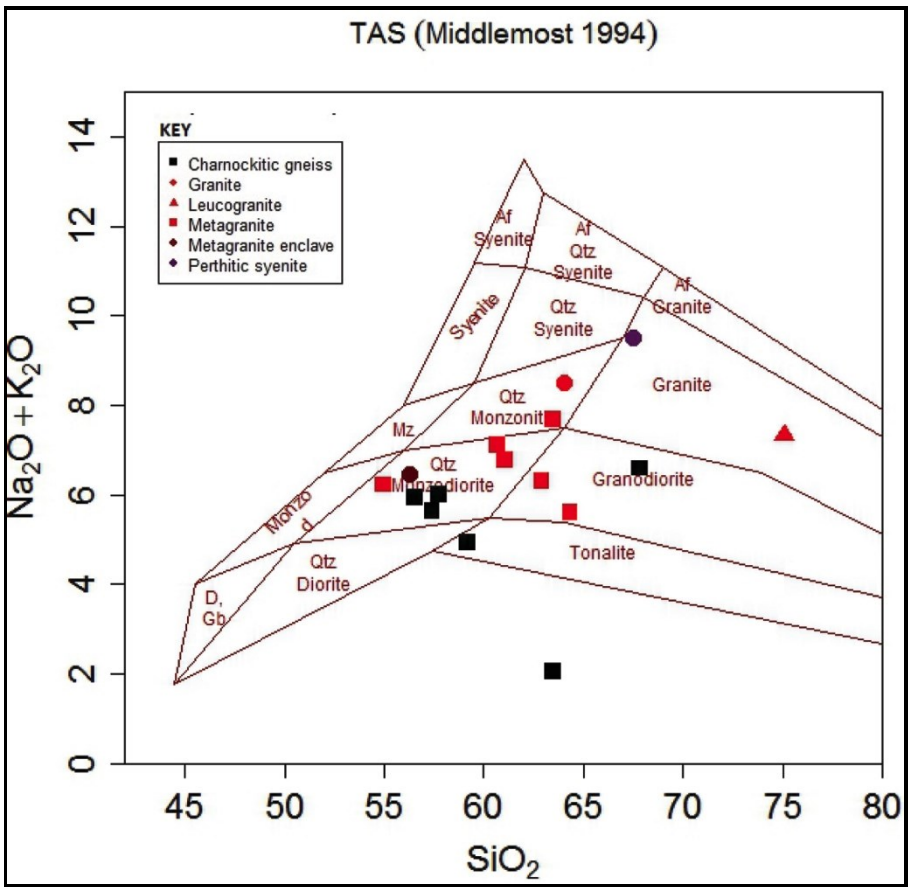

Fig. 4.10: TAS classification diagram showing southern Malawi rocks (Middlemost 1994)

The alkalis show interesting variations (Fig. 4.11). Whereas Na_2O varies widely in the charnockitic gneisses, the trend is for uniform Na_2O concentrations in the meta-granites. They tend to be more evolved with higher $Na_2O + K_2O$ values than the charnockitic gneisses (Fig. 4.2). BM282B has the highest values in Na_2O but very low K_2O. Meta-granites show higher K_2O/Na_2O ratios than the charnockitic gneisses for a given level of SiO_2 (Fig. 4.2).

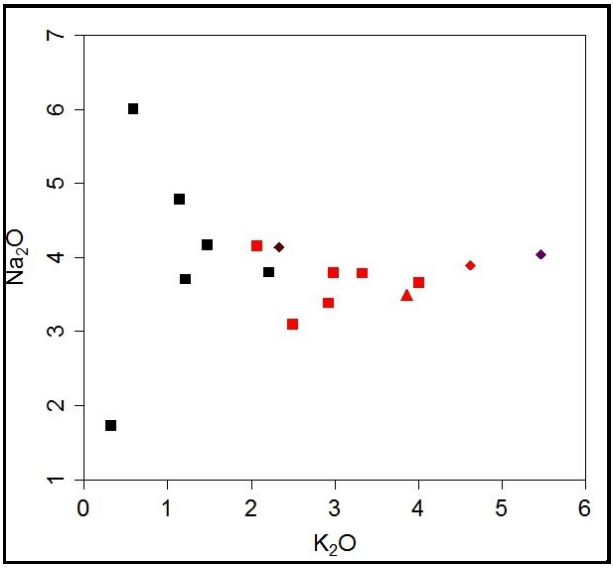

Fig. 4.11: Na_2O vs K_2O variation diagram for charnockitic gneisses and meta-granites/granites (symbols as Fig. 4.2)

In the following diagrams A=Al_2O_3, C=CaO, N=Na_2O and K=K_2O (all molar). The A/CNK vs SiO_2 diagram (Fig. 4.12) shows the charnockitic gneisses to run parallel to the meta-granites, both with increasing trends of A/CNK with increased SiO_2. The diagram shows that the meta-granites generally transition from metaluminous (A/CNK <1.0) to peraluminous (A/CNK >1.0) at about 63% SiO_2, and a similar value applies to the charnockitic gneisses. The range of metaluminous and peraluminous compositions is shown on the A/NK versus A/CNK (Shand, 1943) plot (Fig. 4.13).

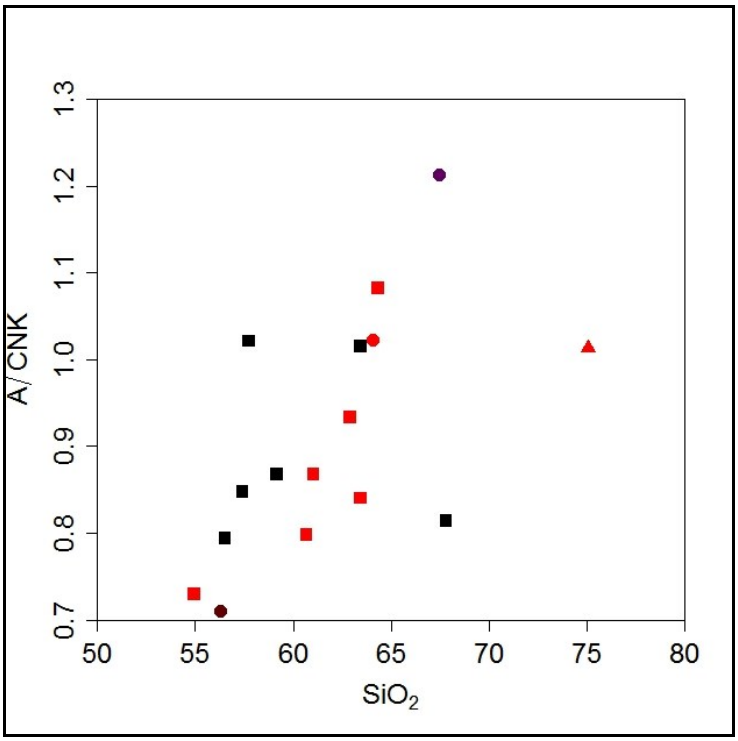

Fig. 4.12: A/CNK vs SiO_2 variation diagram for granitoids from southern Malawi (symbols as in Fig. 4.2)

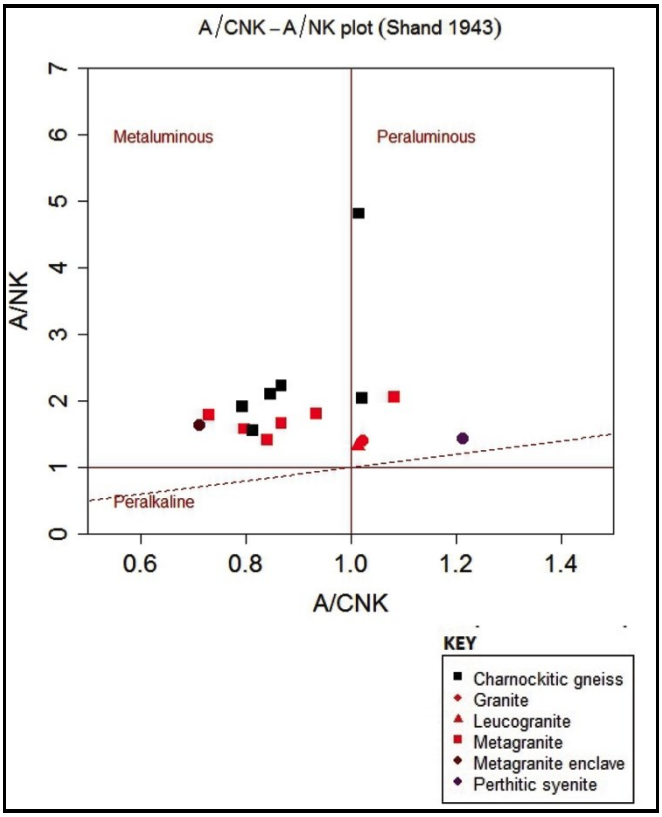

Fig. 4.13: A/CNK - A/NK PLOT (Shand 1943) of granitoids and charnockitic gneisses from southern Malawi (symbols as Fig. 4.2)

The MgO vs Fe_2O_3 diagram (Fig. 4.14) shows a very tight positive correlation among the granitoids. The charnockitic gneisses also show a positive trend in MgO vs Fe_2O_3 but the scatter is considerably greater suggesting more diverse origins for this suite of rocks.

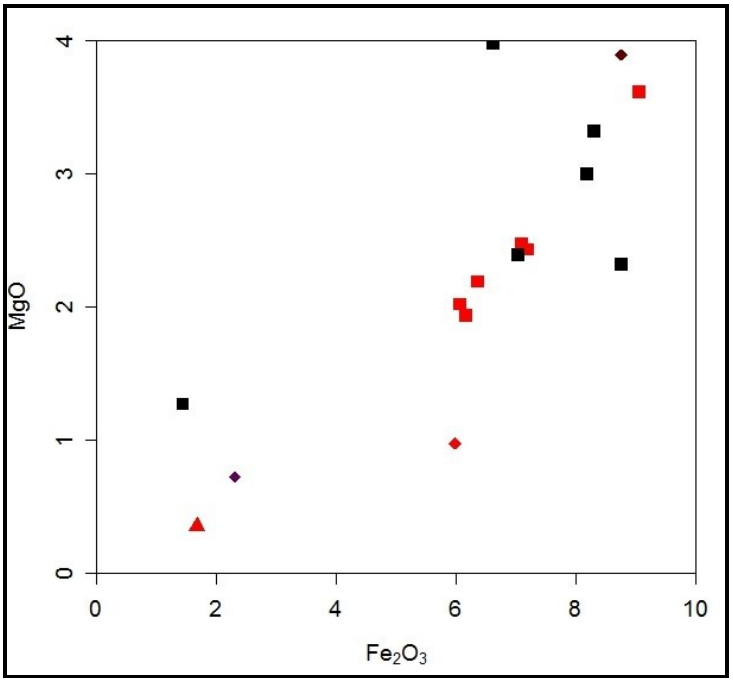

Fig. 4.14: MgO vs Fe_2O_3 variation diagram of granitoids and charnockite from southern Malawi (symbols as Fig. 4.2)

Frost et al., (2001) proposed a three-tier scheme for discriminating granitoids. The scheme involves the Fe-number or Fe* which is equal to the ratio FeO/ (FeO + MgO) (here taken to be FeO(t)/(FeO(t) + MgO)). This index differentiates ferroan granitoids with strong enrichment of iron from magnesian granitoids, which may provide constraints on the differentiation history from parent magma(s); the Modified alkali-lime index (MALI) [$(Na_2O + K_2O) – CaO$]; and the Aluminium Saturation Index (ASI) [Al/(Ca – 1.67P + Na + K)]. The three-tier scheme for southern Malawi is indicated by Figs. 4.15a, 4.15b and 4.15c. The southern Malawi granitoids show Fe* ranges from 0.39 – 0.86. The MALI variation diagram shows the two groups as distinct groups with the charnockitic gneisses having lower values for a given SiO_2 content. When plotted on the MALI diagram (Fig. 4.15b), all the meta-granites samples lie within calc-alkaline field. Charnockitic gneisses show a wide variation from alkali-calcic to calcic. Granite sample BM240 and perthitic syenite sample BM289 fall in the alkali field and the leucogranite sample BM221 is on the border at calcic. MALI is very variable ranging from -4.53 to 8.27 and the values are plotted in the MALI diagram (Fig. 4.15b). When plotted on the Fe* diagram (Fig. 4.15a) all meta-granites samples and the leucogranite classify as magnesian whilst the charnockitic samples are magnesian with one exception, which falls in the ferroan field. ASI ranges from 0.81 to 1.31 and in the variation diagram for ASI vs SiO_2 (Fig. 4.15c), the meta-granites plot near parallel to the charnockitic gneisses which would signify a different evolution path.

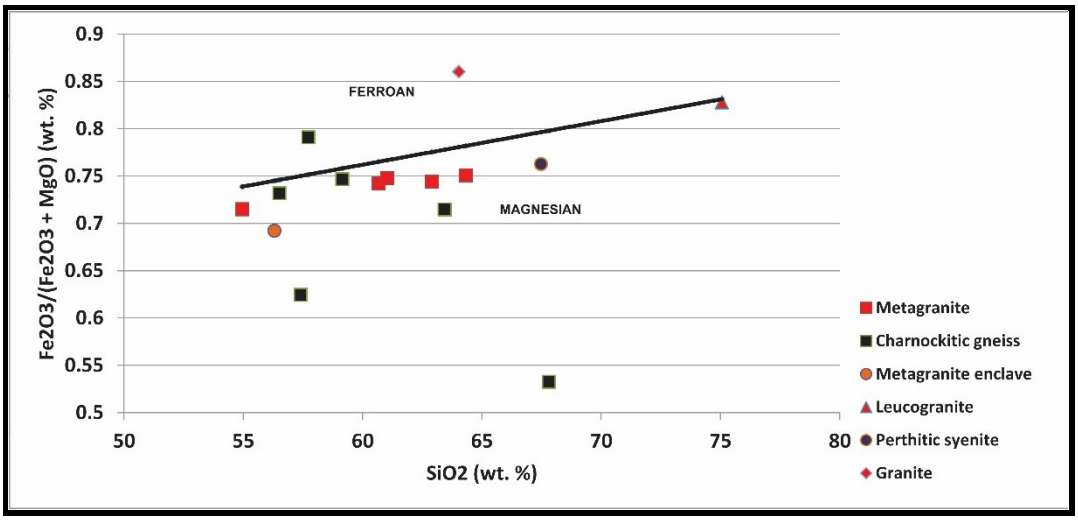

Fig. 4.15a: Fe* diagram for southern Malawi granitoids showing them as predominantly magnesian

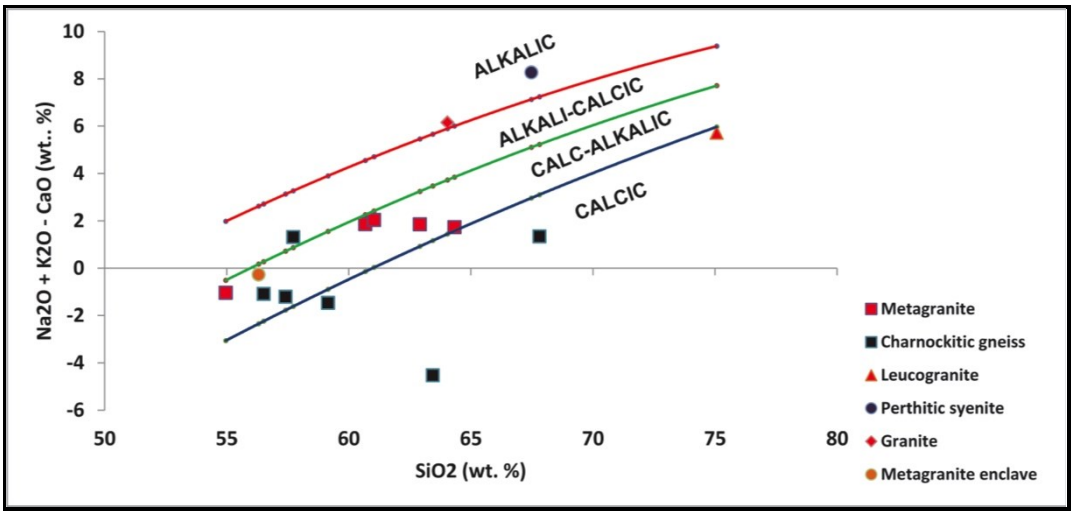

Fig. 4.15b: MALI diagram for southern Malawi granitoids showing them widely distributed from calcic to alkalic but mostly falling within calc-alkalic - alkali-calcic fields.

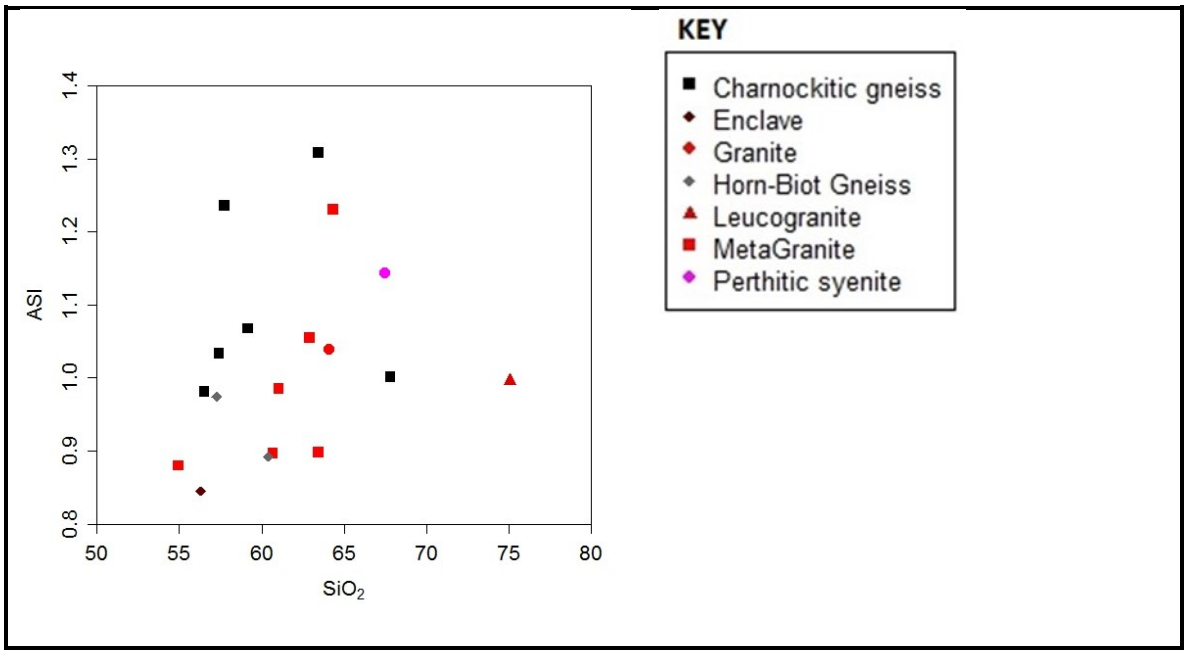

Fig. 4.15c: Showing ASI vs SiO2 for southern Malawi granitoids This diagram is used alongside Figs. 4.15a and 4.15b in Frost et al. (2001) three tier scheme for granitoids discrimination (Fe*, MALI, ASI) applied to southern Malawi granitoids.

The AFM plot (Fig. 4.16) is widely used to discriminate between two igneous series, tholeiitic and calc-alkaline (Rollinson, 1993; Wilson, 2005). The southern Malawi granitoids mostly plot in the calc-alkali series. The more evolved leucogranite and perthitic syenite plot towards the evolved A (total alkalis) apex of the diagram. A single charnockitic gneiss sample (sample BM252) plots just outside the calc-alkaline field, within the tholeiitic series. Calc-alkaline series igneous suites are typically associated with island and continental arc settings (Wilson, 2005, pp. 11, 208)).

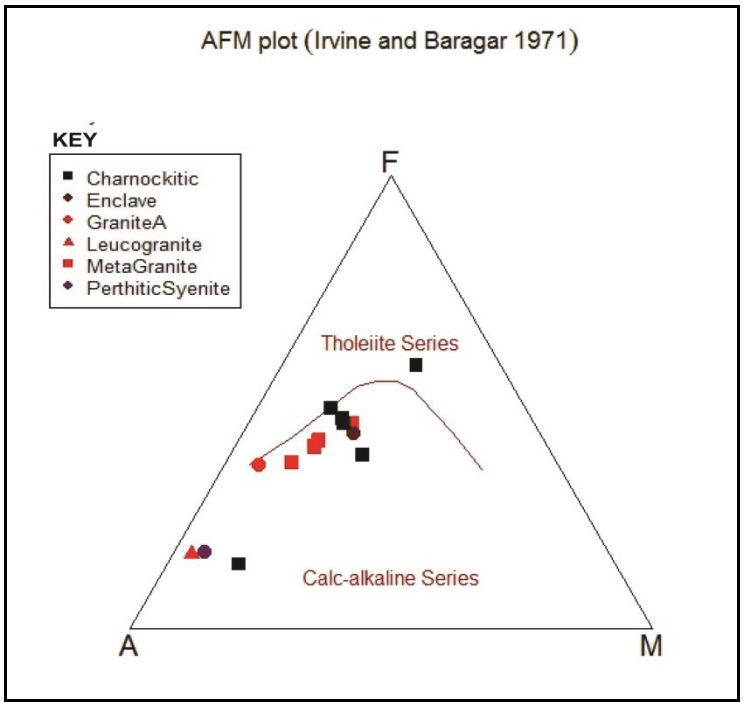

Fig. 4.16: AFM plot showing granitoids from southern Malawi (symbols as Fig. 4.2)

In the trace element plot normalised to primitive mantle (Fig. 4.17) the charnockitic gneisses are widely scattered compared with the meta-granites that are nearly homogenous (all close together in the centre of the plot). The charnockitic gneisses generally have more pronounced anomalies in HFSEs than their counterpart meta-granites. Both groups show some LILE enrichment and HFSE depletion that is often found in arc settings (Wilson, 2005). Similarly, the REE plot normalised to primitive mantle (Fig. 4.18) shows the meta-granites very closely related in the centre of the diagram suggesting a likely co-genetic association whereas the charnockitic gneisses are widely scattered. Several meta-granites have negative Eu anomalies and a single leucogranite (BM221) actually has a positive Eu anomaly, often considered to reflect feldspar accumulation (Wilson, 2005; Rollinson, 1993).

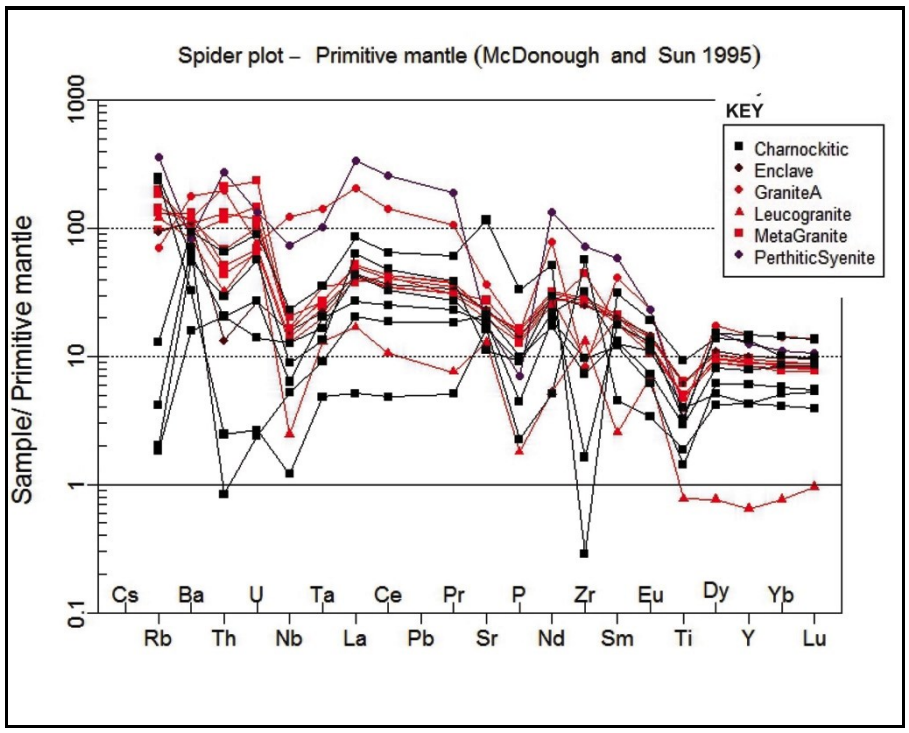

Fig. 4.17: Primitive mantle trace element spider plot selected granitoids from southern Malawi

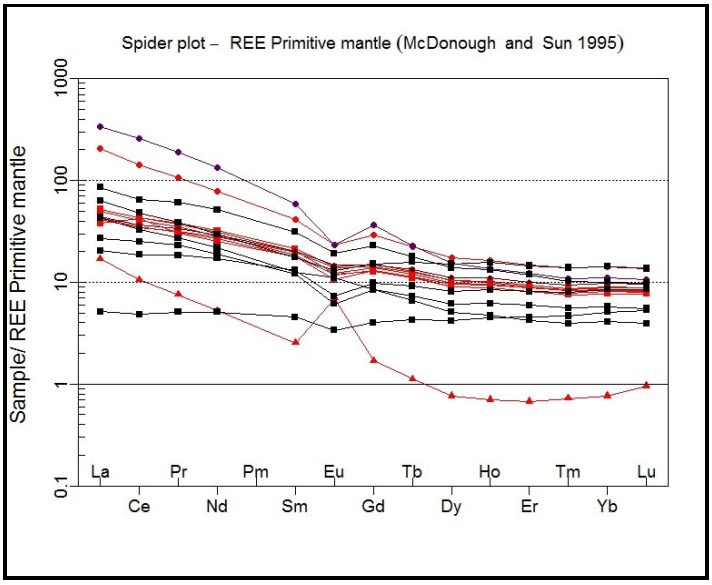

Fig. 4.18: REE patterns for selected granitoids from southern Malawi (symbols as Fig. 4.13).

4.3.7 I-TYPE OR S-TYPE GRANITES

The meta-granites have Fe* ranging from 0.69 to 0.74 and in the Fe* diagram (Frost 2001) they fall in the magnesian field (Fig. 4.19). Their MALI ranges from -0.3 to 3.8 and in the MALI diagram (Frost 2001) (Fig. 4.20) the meta-granites from southern Malawi are all in the field of calc-alkaline. ASI for these rocks range from 0.85 to 1.23, which means they are peraluminous to metaluminous.

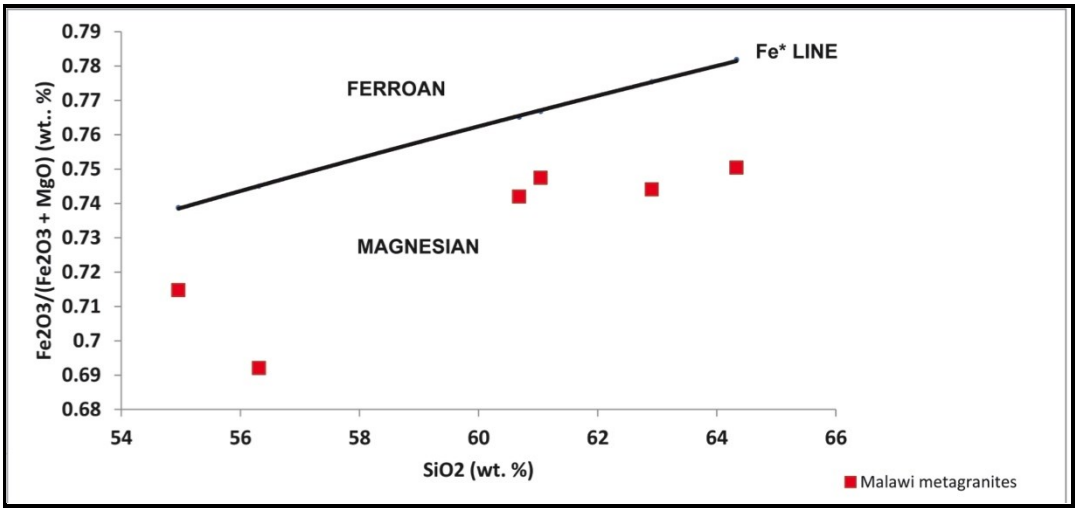

Fig. 4.19: Fe Line diagram (Frost 2001) differentiating southern Malawi meta-granites based on Fe number

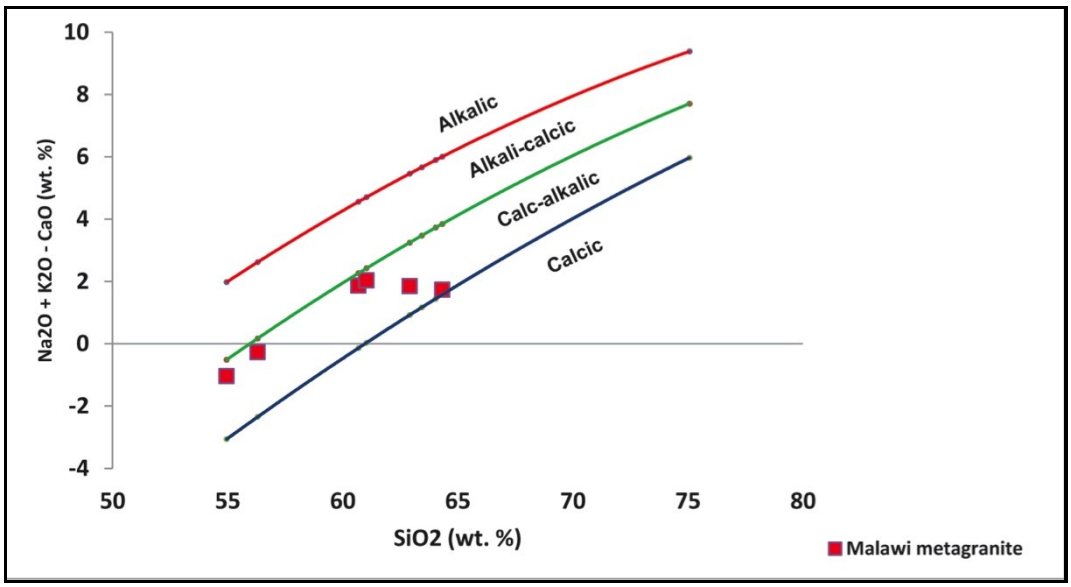

Fig. 4.20: MALI diagram (Frost, 2001) classifying southern Malawi meta-granites.

Granites can be divided into I-types and S-types (Chappell et al., 1974; Chappell et al., 2001; Frost, 2001). The I-Type are metaluminous to weakly peraluminous, intermediate to acidic and relatively sodic (Na_2O greater than 3.2 wt. %, in felsic varieties, decreasing to more than 2.2 wt. % in mafic types), and have been regarded as originating from mafic meta-igneous sources (Hine et al., 1978; Frost 2001). Hornblende is common in the more mafic I-types and is generally present in the felsic types. I-Type granites have molar $Al_2O_3/(Na_2O+K_2O+CaO)$ ratio of less than 1.1, and they also have regular inter-element variations within plutons with linear or near linear variation diagrams (Hine et al., 1978; Frost 2001). S-Type are peraluminous, acidic, and potassic, and have their sources in meta-sediments.

The meta-granites from southern Malawi have SiO_2 values below 65 wt. %, Na_2O ranging from 3.1 to 4.2 wt. %, and have molar $Al_2O_3/(Na_2O+K_2O+CaO)$ ratios ranging from 0.83 to 1.4.

Hornblende (up to 20% in thin section) is present in these samples. The meta-granite samples are plotted in the A/NK vs A/CNK diagram of Shand (1943) and A/CNK vs Fe_2O_3 after Pearce et al., (1994) (Fig. 4.21) in which the Malawi meta-granites fall within the I-Type group.

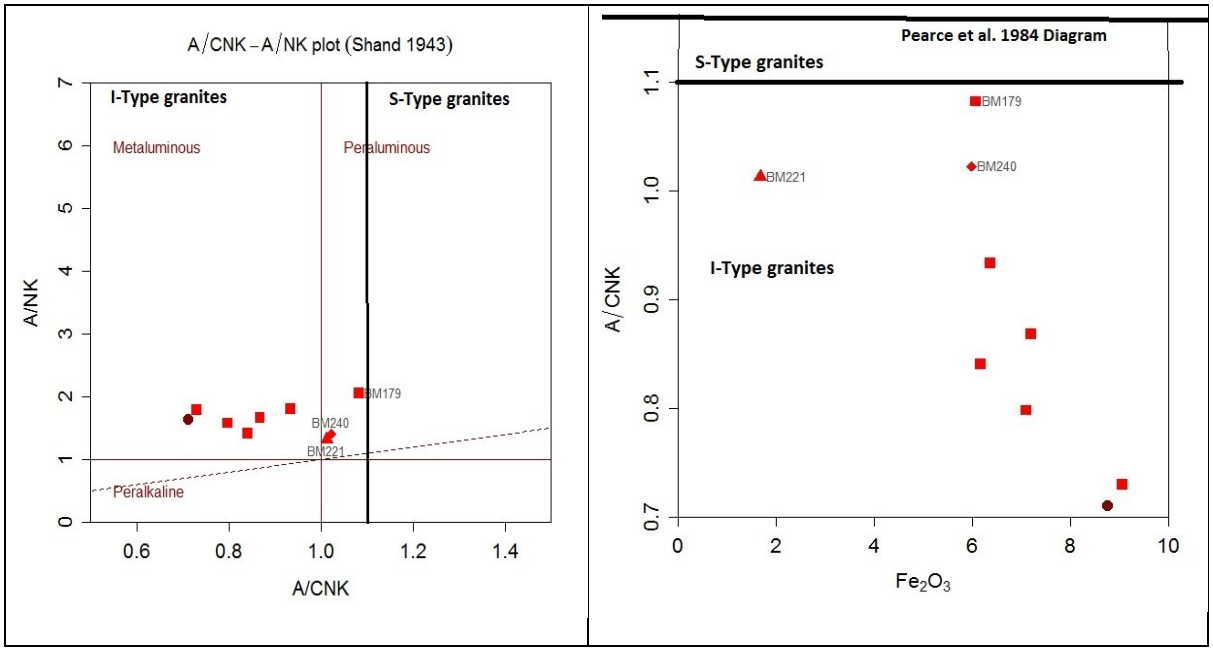

Fig. 4.21: I-Type AND S-Type diagrams (Shand, 1943; Pearce et al., 1984) for southern Malawi granitoids.

The combined evidence from the field (mafic enclaves), petrography (hornblende + biotite etc.), geochemistry (SiO_2 <65%, sodic, etc.), Fe* number, MALI, and ASI, categorise the meta-granite rocks as magnesian, metaluminous to peraluminous, I-type granitoids, all pointing to an igneous protolith for the original magmas.

4.3.8 TECTONIC DISCRIMINATION DIAGRAMS

Pearce (1984) distinguished four major tectonic environments for granites on the basis of their geochemistry in modern and recent tectonic settings, namely ocean ridge granites (ORG), volcanic arc granites (VAG), within plate granites (WPG) and collisional granites (COLG). The most effective discriminators were various trace element combinations in binary diagrams: Y-Nb, Yb-Ta, Rb-(Y + Nb) and Rb-(Yb + Ta). In the Rb vs Y + Nb and Rb vs Ta + Yb discrimination diagrams (Fig. 4.22) the southern Malawi granitoids fall in the category of Volcanic Arc Granites (VAG). Similarly the Nb vs Y and the Ta vs Yb discrimination diagrams (Fig. 4.22) identify these granitoids as VAG. The exception is sample BM240 that according to field relationships is much younger than the others, is unfoliated, and related to rifting in the area.

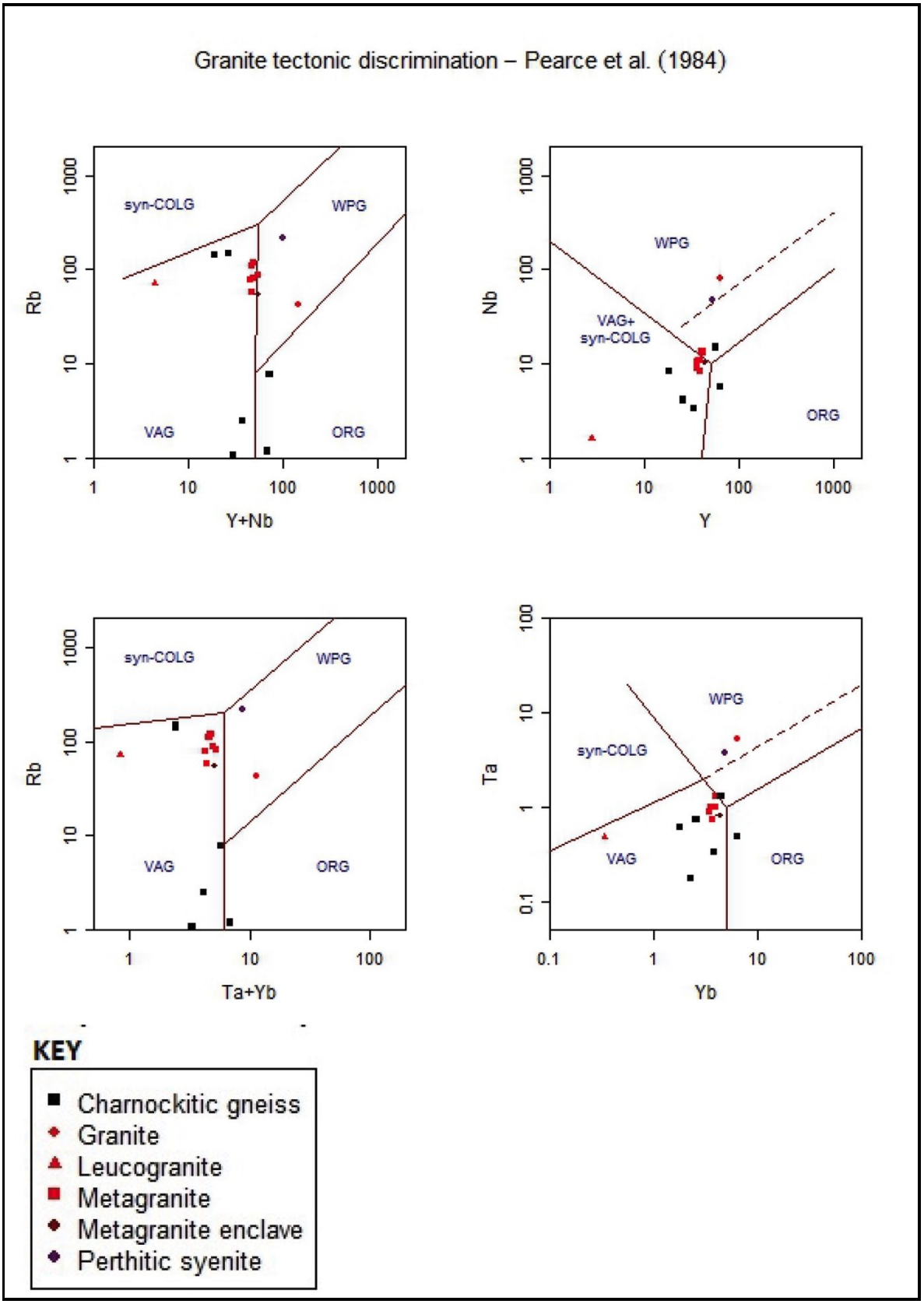

Fig. 4.22: Geotectonic discrimination diagrams (Pearce (1984) for southern Malawi granitoids.

In contrast the charnockitic gneisses do not classify consistently on most of these plots often falling in two or even three tectonic fields, but the preponderance of samples tend, like the granites, to fall within or close to the VAG field.

4.3.9 Granitoids from adjacent areas

Chemical data from published literature for Tanzania (charnockitic gneiss, Johnson et al., 2003) and Mozambique (meta-granites gneiss, Grantham et. al., (2011) and Malawi (charnockitic gneiss and meta-granites, this study) are presented in Table 4.4. The data have been plotted in variation diagrams (Fig. 4.23) to enable some regional comparisons. In the AFM diagram the granitoids from Malawi, Tanzania and Mozambique all fall within the calc-alkaline series zone with the exception of one from Malawi that falls in the tholeiitic zone, and in the TAS diagram they straddle the quartz monzo-diorite – quartz monzonite – granodiorite – granite fields, but the Tanzania samples are more siliceous. In the variation diagrams, the lithologies generally show similar compositions. In the TiO_2 and P_2O_5 diagrams, the meta-granites from Malawi indicate near constant values with increasing SiO_2 while the others tend to show declining trends. The decreasing trend for CaO with increasing SiO_2 for all the granitoids is notable, typical of differentiation in igneous granitoids. Such similarities in the data and diagrams may suggest that the Malawi granitoids have evolved through tectono-thermal processes prevailing throughout the region during the Proterozoic.

Table 4.6: Granitoids data from Tanzania and Mozambique for comparison with granitoids from Malawi. (Data for Malawi granitoids in Table 4.1 & 4.2). NA indicates that data for the element is not given in the publication. Data taken from Johnson et al., 2003 & Grantham et al., 2011.

Sample Name	MOZCVGN5	MOZCVGN4	MOZCVGN3	MOZCVGN2	MOZCVGN1	TANSJ23	TANSJ3A	TANSJ2	TAN1SJI
Petrology	MetaGranite	MetaGranite	MetaGranite	MetaGranite	MetaGranite	Charnockitic	Charnockitic	Charnockitic	Charnockitic
Locality	Mozambique	Mozambique	Mozambique	Mozambique	Mozambique	Tanzania	Tanzania	Tanzania	Tanzania
SiO2	58.69	58.9	60.89	58.65	62.43	64.98	62.66	69.05	65.17
TiO2	0.93	0.88	0.72	0.96	0.68	0.56	0.67	0.46	0.71
Al2O3	17.39	17.11	17.97	16.78	17.03	16.75	15.13	15.55	15.82
Fe2O3	7.02	7.55	5.41	7.83	5.61	3.96	5.74	2.52	5.68
MnO	0.14	0.13	0.09	0.15	0.09	0.05	0.06	0.03	0.07
MgO	2.61	2.69	2.12	2.86	2.15	1.55	3.3	0.8	3.05
CaO	5.34	5.29	4.06	5.82	4.37	4.4	5.4	2.33	3.11
Na2O	3.79	3.99	3.76	3.61	3.86	5.82	4.42	4.42	4.63
K2O	3.79	3.42	4.52	3.63	3.84	1.32	1.69	4.37	1.67
P2O5	0.36	0.38	0.31	0.38	0.32	0.1	0.18	0.11	0.05
BaO	NA	NA	NA	NA	NA	NA	NA	NA	NA
SO3	NA	NA	NA	NA	NA	NA	NA	NA	NA
LOI	NA	NA	NA	NA	NA	0.38	0.69	0.5	0.23
TOTAL	100.06	100.34	99.85	100.67	100.39	99.49	99.93	100.11	100.17
Sc	NA	NA	NA	NA	12	9	18	4	15
V	NA	NA	NA	NA	NA	71	111	38	153
Cr	NA	NA	NA	NA	NA	159	184	118	289
Ni	NA	NA	NA	NA	NA	31	34	14	48
Rb	81	95	121	78	104	30	73	86	61
Sr	881	720	820	938	871	425	342	362	475
Zr	319	720	177	243	189	124	79	179	100
Y	30	33	19	34	23	8	14	7	16
Nb	13	13	9	13	10	9	5	9	10
La	NA	NA	NA	NA	NA	7	12	36	27
Ce	NA	NA	NA	NA	NA	27	54	65	66
Pr	NA	NA	NA	NA	NA	NA	NA	NA	NA
Nd	NA	NA	NA	NA	NA	NA	NA	NA	NA
Sm	NA	NA	NA	NA	NA	NA	NA	NA	NA
Eu	NA	NA	NA	NA	NA	NA	NA	NA	NA
Gd	NA	NA	NA	NA	NA	NA	NA	NA	NA
Tb	NA	NA	NA	NA	NA	NA	NA	NA	NA
Dy	NA	NA	NA	NA	NA	NA	NA	NA	NA
Ho	NA	NA	NA	NA	NA	NA	NA	NA	NA
Er	NA	NA	NA	NA	NA	NA	NA	NA	NA
Tm	NA	NA	NA	NA	NA	NA	NA	NA	NA
Yb	NA	NA	NA	NA	NA	NA	NA	NA	NA
Lu	NA	NA	NA	NA	NA	NA	NA	NA	NA
Hf	NA	NA	NA	NA	NA	NA	NA	NA	NA
Ta	NA	NA	NA	NA	NA	NA	NA	NA	NA
Th						3	2	7	2
U						8	8	6	9

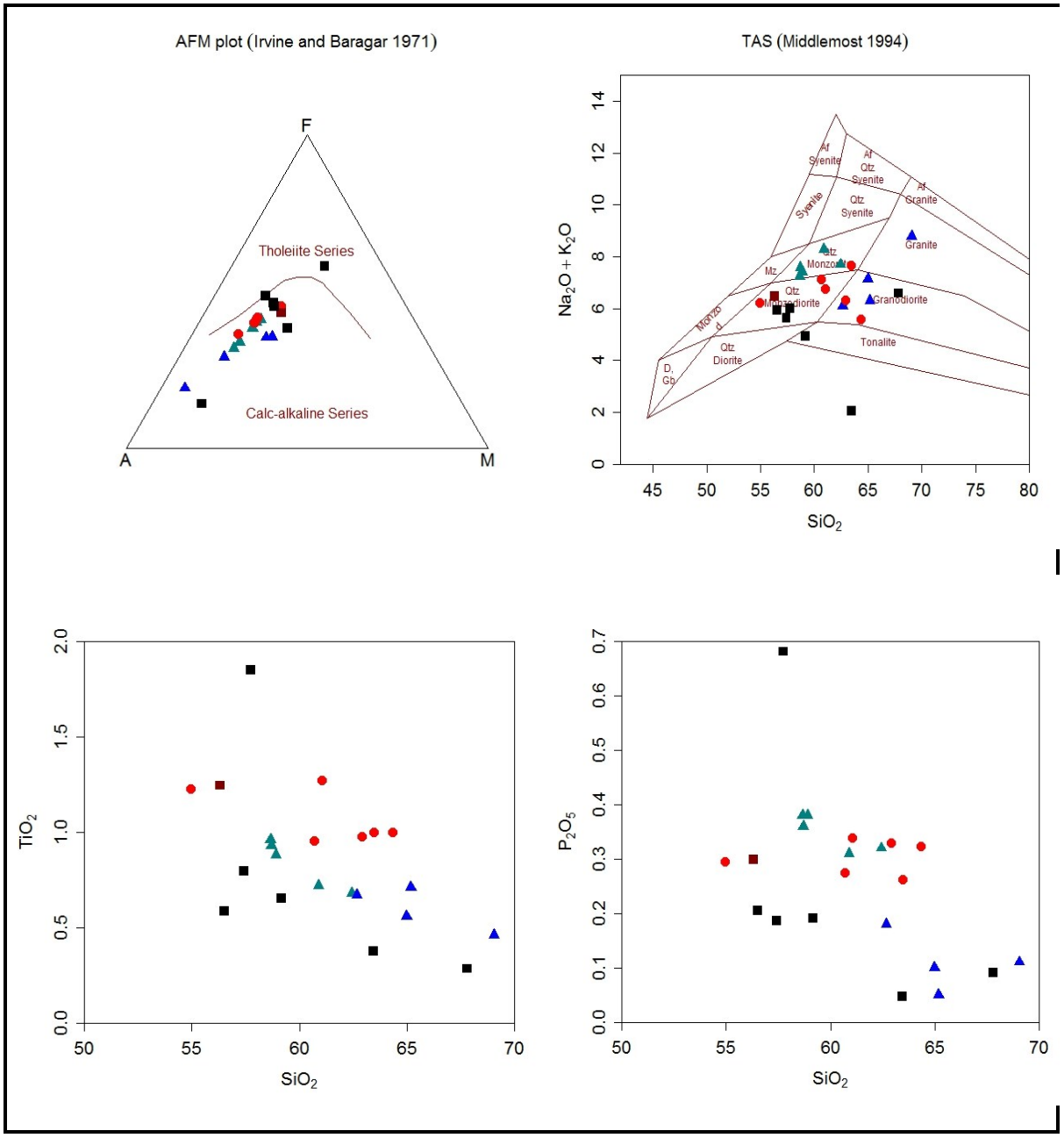
AFM plot (Irvine and Baragar 1971)
F
A
M
Tholeiite Series
Calc-alkaline Series
TAS (Middlemost 1994)
$Na_2O + K_2O$
SiO_2
Af Syenite
Af Qtz Syenite
Af Granite
Syenite
Qtz Syenite
Granite
Mz.
Monzonite
Qtz Monzodiorite
Granodiorite
Monzo d.
Qtz Diorite
Tonalite
D. Gb.
TiO_2
SiO_2
P_2O_5
SiO_2

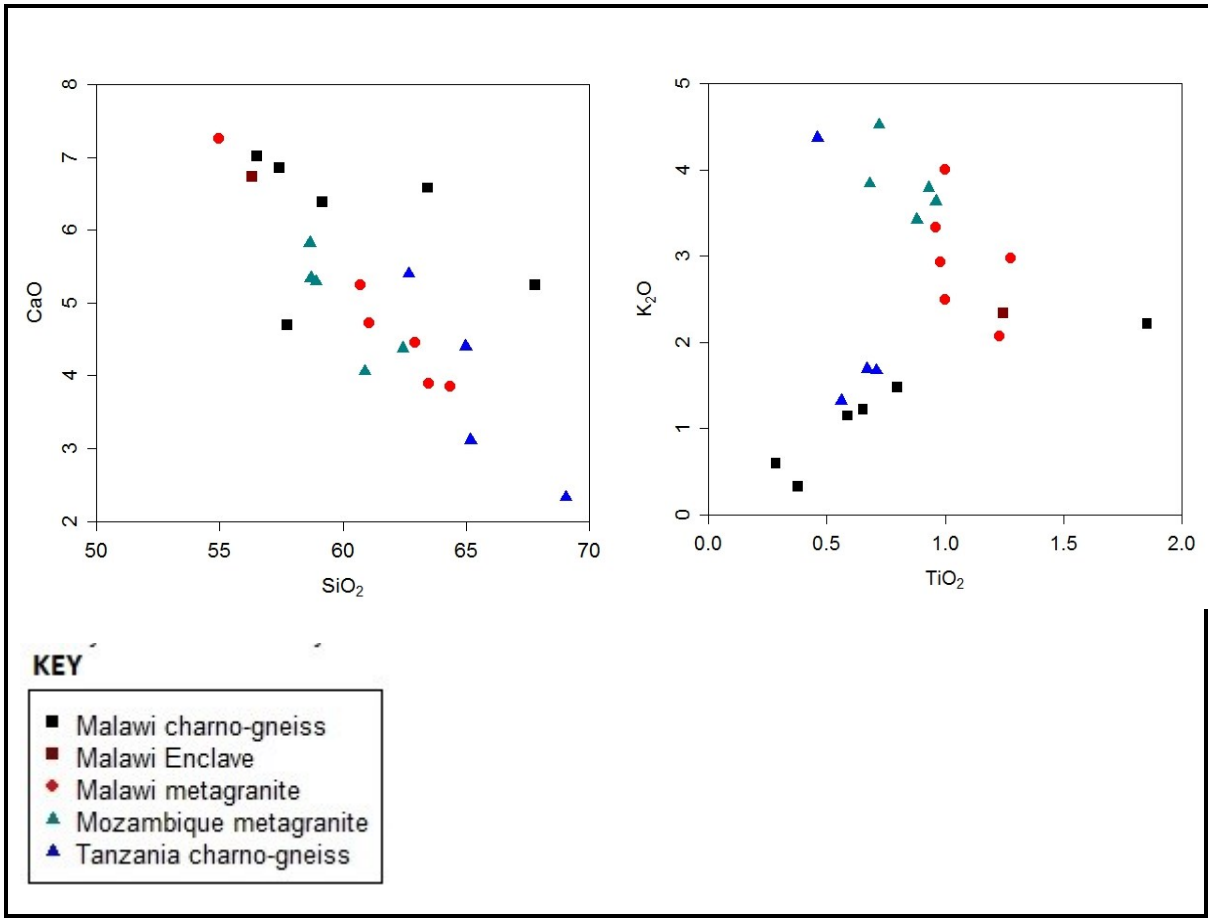

Fig. 4.23: AFM, TAS, and some Harker diagrams showing some major oxide element data for metagranitoids and charnockitic gneisses from Malawi, Mozambique and Tanzania. Data taken from Johnson et al., 2003 & Grantham et al., 2011.

4.3.10 MALAWI GRANITOIDS AND TONALITE, TRONDJHEMITE, GRANITES (TTGs)

A pertinent question related to continental crust formation is whether both Archean and modern (post-Archean) granitoids comprising the bulk of the crust formed in a subduction setting or through processes unique to the Archean and early Proterozoic (Arndt, 2013). Granitoids dominating the Archean cratons often belong to the TTG suite (tonalite, trondhjemite and granite). The TTGs have SiO_2 ~64 wt. % or above, Na_2O (3 – 7% wt. %), low K_2O/Na_2O ratios (<0.5), poor in Fe_2O_3, MgO, MnO, and TiO_2, (<5 wt. % in total) with average Ni at 14 ppm and average Cr at 29 ppm (Martin et al., 2005). The rocks are relatively sodic with a relative lack of potassium, display high concentrations of incompatible elements, are enriched in light rare earth elements (LREEs), depleted in the heavy rare earth elements (HREEs), and show negative Eu anomalies (Arndt, 2013). They are distinguished from the younger granitoids by their lower Cr and Ni values and a low magnesium number (Mg#). The geochemical signatures are consistent with being sourced in mantle wedge including subducted sediment and/or oceanic crust material (Arndt, 2013).

This study attempted to establish petrogenetic linkages between the Malawi granitoids and known TTGs from elsewhere. Geochemical data for some TTGs samples from published literature (Condie, 2005) are presented in Table 4.5 and have been plotted in diagram Fig.24. In the TAS diagram the southern Malawi granitoids plot in the fields of tonalite- quartz monzo-diorite – quartz monzonite-granodiorite-granites and the TTGs plot in the granodiorite – granite

field. In the AFM plot both fall in the fields of calc-alkaline – tholeiitic series (Fig. 4.24). Interesting to note is that the TTGs plot in the same trend line but are more evolved than meta-granites and charnockitic gneisses. In the variation diagrams for TiO_2, CaO, and P_2O_5 versus SiO_2, the southern Malawi granitoids are distinct from the TTGs, with the granitoids having higher values for the oxides at any given SiO_2 (Fig. 4.24). Whilst some overlaps are noticeable in the preceding oxide plots, the southern Malawi granitoids are clearly separate from the TTGs in the K_2O versus SiO_2 diagram (Fig. 4.24). The Cr and Ni concentrations are higher in the TTGs relative to the charnockitic gneisses but they are generally on a par with the meta-granites at the same SiO_2 values. The Mg# for the meta-granites and charnockitic gneisses range from 19 to 43 with an average of 26. The Mg# for the TTGs range from 23 to 31 with an average of 26. Based on these preceding parameters for TTGs a few of the Malawi granitoids would be described as such but otherwise the rest are not strictly TTGs. These differences may reflect a number of scenarios i.e. different age rocks with different magmatic sources, different magmatic processes, and different tectonic environments. The geochemistry here indicates geochemical techniques are insufficient without other methods to constrain the sources and processes involved in the petrogenesis of the units as well as their age.

Table 4.5: Chemical data for TTGs from published literature by Condie (2005) for comparison with granitoids from Malawi. Data for Malawi granitoids in in Table 4.1 & 4.2.

			Sample Name			
	SMIT2	SMIT1	COND4	COND3	COND2	COND1
Petrology	TTG	TTG	TTG	TTG	TTG	TTG
SiO2	68.53	70.20	65.90	67.30	68.30	70.40
TiO2	0.32	0.33	0.47	0.47	0.42	0.31
Al2O3	15.91	15.74	16.50	15.80	15.50	15.20
Fe2O3	2.49	2.84	4.11	4.04	3.42	2.79
MnO	0.04	0.04	0.09	0.08	0.08	0.06
MgO	1.41	1.09	1.67	1.48	1.39	0.96
CaO	3.36	3.17	4.36	3.42	3.26	2.74
Na2O	5.57	4.87	4.00	4.33	4.51	4.71
K2O	1.56	1.88	2.14	2.30	2.20	2.22
P2O5	0.11	0.12	0.12	0.14	0.14	0.10
BaO	N/A	N/A	N/A	N/A	N/A	N/A
SO3	N/A	N/A	N/A	N/A	N/A	N/A
LOI	N/A	N/A	N/A	N/A	N/A	N/A
TOTAL	N/A	N/A	99.36	99.36	99.21	99.49
Sc	N/A	N/A	N/A	N/A	N/A	N/A
V	N/A	N/A	N/A	N/A	N/A	N/A
Cr	32.00	36.00	1.90	55.00	35.00	45.00
Ni	23.00	19.00	12.00	23.00	22.00	17.00
Rb	30.00	50.00	716.00	63.00	67.00	76.00
Sr	586.00	495.00	493.00	473.00	515.00	362.00
Zr	95.00	149.00	122.00	152.00	154.00	152.00
Y	4.00	6.80	14.50	17.30	9.10	8.50
Nb	3.00	5.40	6.70	18.00	6.20	6.10
La	16.90	29.80	17.00	26.00	36.00	22.00
Ce	36.70	51.60	34.00	45.00	65.00	40.00
Pr	N/A	N/A	N/A	N/A	N/A	N/A
Nd	16.40	19.90	16.00	18.00	25.00	16.00
Sm	2.70	2.70	3.10	3.50	4.20	2.90
Eu	0.71	0.91	0.84	0.95	1.07	0.82
Gd		2.04	2.80	3.00	2.90	2.20
Tb	0.21	0.25	0.40	0.49	0.38	0.31
Dy	N/A	N/A	N/A	N/A	N/A	N/A
Ho	N/A	N/A	N/A	N/A	N/A	N/A
Er	N/A	N/A	N/A	N/A	N/A	N/A
Tm	N/A	N/A	N/A	N/A	N/A	N/A
Yb	0.38	0.46	1.16	1.33	0.71	0.82
Lu	0.06	0.09	0.18	0.23	0.11	0.14
Hf	N/A	N/A	3.40	4.30	4.70	3.80
Ta	N/A	N/A	0.75	0.72	0.84	0.41
Th	2.30	6.00	7.60	6.10	8.10	4.10
U	0.90	1.00	1.90	2.10	1.50	1.20
Fe#	N/A	N/A	N/A	N/A	N/A	0.72
ASI	N/A	N/A	N/A	N/A	N/A	
Mg#	32.80	24.86	25.94	24.00	25.95	22.88
Fe	1.74	1.99	2.87	2.83	2.39	1.95

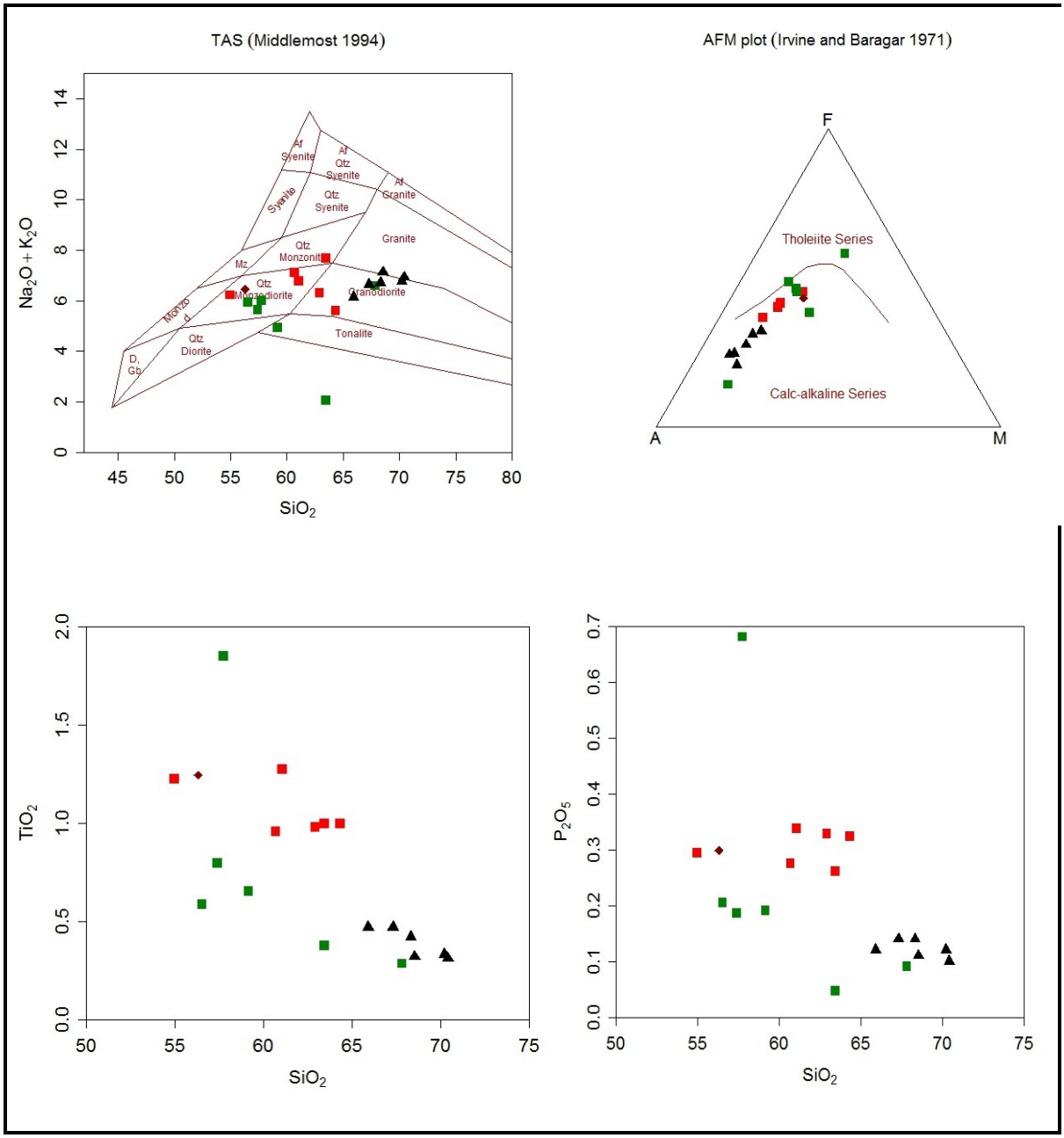
TAS (Middlemost 1994)
AFM plot (Irvine and Baragar 1971)
Af Syenite
Af Qtz Syenite
Af Granite
Syenite
Qtz Syenite
Granite
Qtz Monzonite
Mz
Qtz Monzodiorite
Granodiorite
Monzo d.
Qtz Diorite
D. Gb.
Tonalite
Na2O + K2O
SiO2
F
Tholeiite Series
Calc-alkaline Series
A
M
TiO2
P2O5

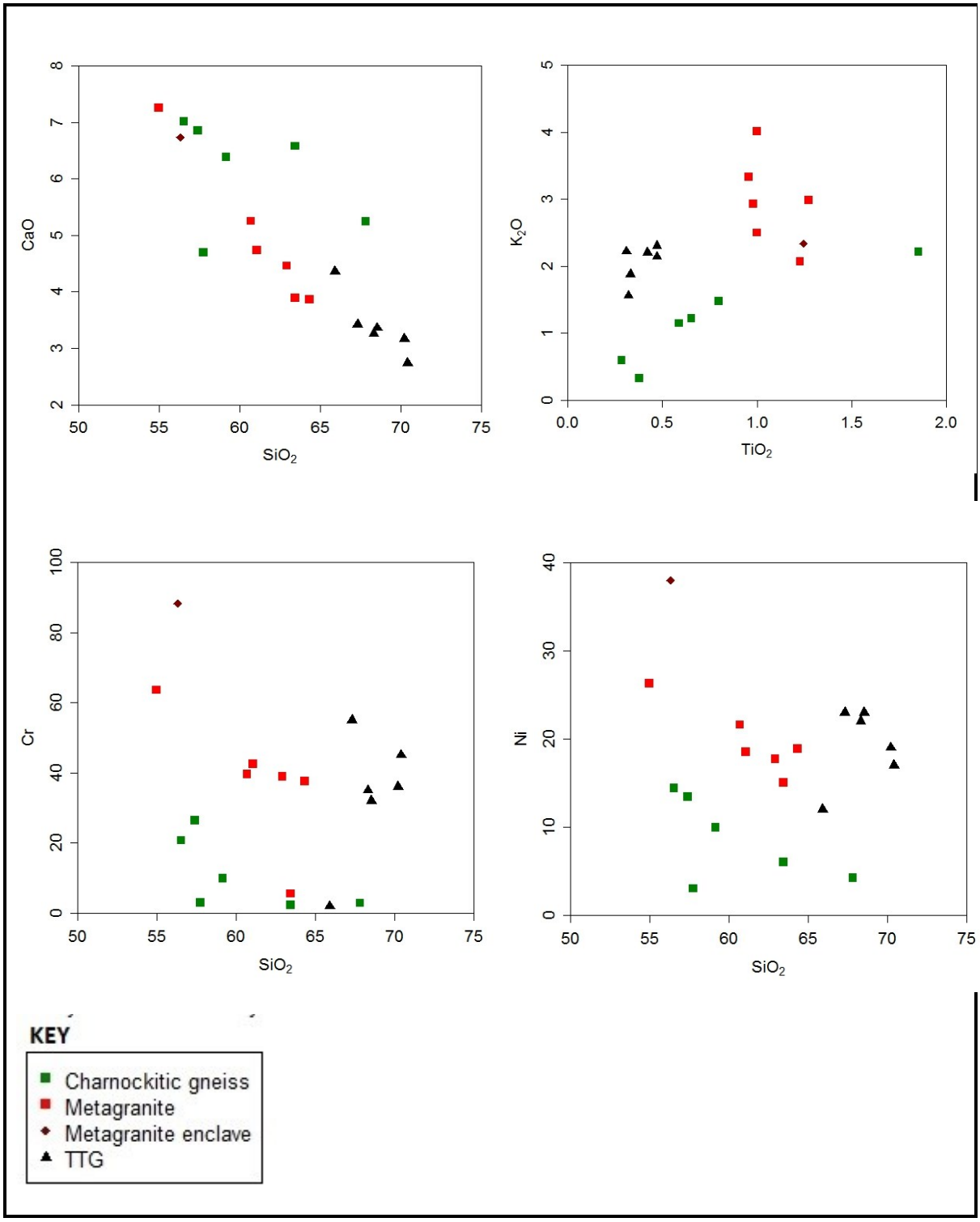

Fig. 4.24: AFM, TAS and variation diagrams showing major oxide trends in granitoids from southern Malawi in comparison with TTGs from published literature. Data for TTGs from Condie (2005)

4.4 DISCUSSION

In the study area of southern Malawi, Precambrian peraluminous and metaluminous granitoids intrude various supracrustals including biotite hornblende gneisses and migmatites and amphibolite gneisses (Bloomfield, 1974; Evans, 1965; Kröner et al., 2003). The granitoids are metamorphosed to amphibolite and granulite grade ranging in composition from monzodioritic to granitic. Andreolli (1984) interpreted the orthogneisses as products of continental arc margin

magmatism and he proposed a tectonic model for the area, specifying ocean floor subduction during the Mesoproterozoic and subsequent collision between an island arc and what he called the "Niassa craton". However, questions remain on the characteristics of source rocks, their genesis and evolution, and the tectonic environments. Geochemistry of the charnockites and granitoids of southern Malawi has been utilised in this chapter to place some constraints on the processes, sources and the tectonic environment of their formation. The tectono-thermal history of this area is important to understanding the greater Mozambique Belt which is generally considered to be the principal collision zone during the late Neoproterozoic amalgamation of Gondwana and as such records evidence of genesis and evolution of the belt (Vogt et al., 2006; Kröner, 2001).

Petrogenesis of the southern Malawi granitoids

The meta-granites from southern Malawi are magnesian, peraluminous- metaluminous, calc-alkaline I-Type granites similar to meta-granites occurring within the region as in Tanzania and Mozambique. Based on geochemical comparisons in this chapter the meta-granites are generally more evolved than the charnockitic gneisses. They most likely originate from igneous protoliths in continental arcs (e.g., Figs. 4.16 & 4.22).

Charnockitic gneisses from southern Malawi show a relative enrichment in LILEs and depletion in HFSEs with moderately negative anomalies in Th, Nb, P, Zr and Ti (Figs. 4.5). The REE plots show enrichment in the LREEs with negative Eu anomalies (Fig. 4.6), a typical feature of magmatic differentiation related to the removal of plagioclase (or alternatively the retention of plagioclase in the source) (Rollinson, 1993; Wilson, 2005). Evidence in this study shows the charnockitic gneisses are metamorphic in origin as opposed to igneous based on the review of Kilpatrick & Ellis (1992). They are geochemically similar to charnockitic gneisses in Tanzania and in Mozambique (e.g. Fig. 4.24). The compositional overlap between metamorphic charnockites and those of the Australian Lachlan Fold Belt granites supports the contention that metamorphic charnockites are derived from pre-existing "normal" granites (Kilpatrick & Ellis, 1992). It has been suggested by Condie and Allen (1984) that the compositional range found in metamorphic charnockites is related to hornblende fractionation in normal crustal magmatic rocks prior to metamorphism (See Kilpatrick et al., 1992, Section 4).

Coherent trends in the Harker plots of major oxides (Fig. 4.2) and trace elements (Fig. 4.3) may be explained in part by fractional crystallisation, however considerable scatter is probably indicative of the involvement of processes such as multiple sources, crustal contamination and/or magma mixing (Wilson, 2007; Chen et al., 2002). Plutonic rocks from active subduction margins show similar coherent trends on Harker variation diagrams that are variously suggestive of the fractional crystallisation of olivine, plagioclase, pyroxene, magnetite and amphiboles from basaltic parental magmas (Wilson, 2007). It is a feature of Andean magmas often to display scattered patterns that signify complexity due to variable impacts of assimilation on fractional crystallisation processes (Wilson, 2007). The granitoids of southern Malawi share these characteristics with Andean subduction zone plutonic granitoids.

Trace elements for the granitoids display relative enrichment in lithophile (LILE) elements such as Rb and Ba and negative anomalies in Nb, Ta, P and Ti (Figs. 4.5 & 4.8). The granitoids display fractionated REE patterns with LREE enrichment with negative Eu anomalies and relative depletion in the HREEs. This increase in the ratio of light to heavy rare earths may reflect the role of hornblende and/or garnet in the source or alternatively the role of magmatic

fractionation crystallisation of hornblende (Rollinson, 1994; Best, 2003; Wilson 2007). The negative Eu anomalies (Figs. 4.6 & 4.9) are either the result of early crystallisation of plagioclase from the melt by fractional crystallisation, or retention of the elements in feldspars at the source during partial melting (Rollinson, 1993). Either way, LREE-enriched patterns with negative Eu anomalies are said to be associated with granitoids originating from subduction zones in island arcs and continental margins (Sreejith et al 2013) with these chemical signatures being indicative of mantle melting in a supra-subduction environment (Helo et al., 2005).

The Sm/Nd ratios for the southern Malawi granitoids range from 0.143 to 0.290 with an average of 0.205 (Tables 4.1 & 4.2). This is similar to the average Sm/Nd ratio of typical continental crustal rocks (0.190) and significantly different from mantle sourced rocks such as mid-ocean ridge basalts (MORB) with a mean ratio of 0.390 (Silantyev et al., 2014). Two main processes determine Sm and Nd behaviour in magmatic systems: partial melting of mantle material and mixing of different source magmas with varied Sm/Nd ratios (Silantyev et al., 2014). This ratio for granitoids in Malawi may, therefore, suggest mixture of sources i.e. both mantle and continental crustal inputs.

The significant P and Ti anomalies and others in Ba, and Nb and Sr in the primitive mantle-normalised plot (Figs. 3.5 & 3.8), the enriched LREEs with prominent Eu anomalies and depletion in the HREEs (Figs. 3.6 & 3.9), combined with the major and trace element characteristics suggests origins of these granitoids from crustal melts (Chen et al.,2002). These are patterns typical of igneous series associated with continental arcs.

The meta-granites rocks occurring west of the area show slightly different mineralogy to the charnockitic gneisses in the east with the latter having two pyroxenes but they depict similar geochemical behaviour on variation diagrams. The primitive-mantle normalized (Sun and McDonough, 1989) trace element plot shows generally similar patterns for both groups and the chondrite-normalised REE patterns are also similar with few exceptions. Such similarities suggest co-genetic magmas.

Sample BM 221 has extremely low Cr and Ni contents precluding formation in mantle sources unless by extreme fractional crystallisation (Wilson, 2007). The rock is a leucogranite and Frost (2001) states that these have a close affinity to overthickened orogens arising from melting of crust with no additions from the mantle (Frost, 2001). Low Ni suggests olivine fractionation whereas the low Cr may suggest spinel or clinopyroxene fractionation (Wilson, 2007). The concentration of Y is also low suggesting the fractionation of accessory phases in which Y is a compatible trace element, possibly amphibole or the accessory mineral allanite. These features suggest a leucocratic melt but the data do not constrain whether it formed by crustal melting or fractional crystallisation. Regional scale leucogranites are typical of continental collisions but they are rarely accompanied by more basic igneous rocks. It seems more likely in the case of Malawi that BM221 is the product of a leucocratic melt formed by extensive fractional crystallisation from typical I-type granite magmas in a continental arc setting.

The southern Malawi granitoids and the tonalite, trondhjemite and granite (TTGs) from other regions (Table 4.5) plot as tholeiitic – calc-alkaline series although the TTGs tend to be more evolved than meta-granites and charnockitic gneisses. There are significant differences in composition and there is insufficient evidence to regard the granitoids as part of the classic TTG suites.

The magnesian nature of the meta-granites in this study is suggestive of origins of melts along an oxidizing differentiation trend (Ray et al., 2003). Petrographic characteristics (typically quartz + plagioclase + K-feldspar + hornblende + biotite ± pyroxene) coupled with geochemical parameters (intermediate (SiO_2 ~50 – 65%), sodic (Na_2O ~3.1 – 4.2%), in addition to the Fe*, MALI and ASI indicate the meta-granites in this study derive from igneous sources. The charnockitic gneisses have the same major oxide characteristics as metamorphic charnokites compiled and plotted by Kilpatrick & Ellis (1992). They are dissimilar to igneous charnokites which occur in Antarctica, India and Limpopo Belt.

As discussed above major oxides and trace elements provide constraints on the sources and differentiation paths of magmatic rocks that may have been subsequently metamorphosed. More advanced modelling would not be well constrained by these data and potentially more useful constraints provided by radiogenic isotopes and geochronology will be introduced in later chapters.

Tectonic discrimination by geochemical diagrams can suffer various problems such as modification by high grade metamorphism and hydrothermal or surface alteration of original compositions. The former is certainly a possibility in the context of the Malawi rocks but it is worth noting the consistency of the data in implying a convergent tectonic setting for these granitoids, typically in a continental arc.

4.5 SUMMARY AND CONCLUSIONS

Whole rock major and trace element geochemistry are presented in this study on southern Malawi granitoids to provide constraints on nature and sources of magmatism. The data have been compared with conventional indices for the sources and tectonic settings of igneous rocks and compared with similar Proterozoic rocks in neighbouring regions of Africa as well as further afield with the aim of improving constraints on tectono-thermal events at the time of Rodinia and Gondwana break-up and amalgamation during the Proterozoic.

Charnockitic gneisses from southern Malawi are intermediate to acidic with relative enrichment in LILEs and depletion in HFSEs with moderately negative anomalies in Th, Nb, P, Zr and Ti. The REE spider plots show enrichment in the LREEs and depleted HREEs with negative Eu anomalies indicative of plagioclase fractionation. Both the charnockitic gneisses and the meta-granites from Malawi are geochemically similar to published literature Tanzania charnockitic gneisses and Mozambique meta-granites. In broader terms the chemistry of the charnockitic gneisses is most similar to a group termed metamorphic charnokites

The meta-granites are mostly metaluminous with a few peraluminous, I-type granites belonging to the calc-alkaline series. They are enriched in LILEs while the HFSEs (Nb, Ta, P, and Ti) are depleted, in some cases anomalously. The REE patterns consistently have negative Eu anomalies. The meta-granites and the charnockitic gneisses are collectively calc-alkaline series rocks with continental arc margin signatures pointing to a volcanic arc setting.

The main conclusion of this study is that the charnokitic gneisses and meta-granites of southern Malawi bear the characteristics of an origin in a continental arc mainly by crustal melting but with the possibility of mantle inputs. They share chemical characteristics with Andean type granitoids and some aspects of the chemistry resembles tonalite-trondhjemite-granite (TTG) suites mapped in the Mozambique Belt in Kenya, Tanzania, Mozambique, and Antarctica

(Muhongo, 2003; Grantham et al., 2003; Westerhof, et al., (2007) although the data are not sufficiently compelling to assign the Malawi rocks to classic TTGs.

4.6 REFERENCES

Arndt, N. T., (2013), The Formation and Evolution of the Continental Crust, Geochemical Perspectives II, Volume 2, Number 3.

Best, M. G., (2003), Igneous and Metamorphic Petrology, 2nd Edition, Blackwell Science Ltd., Oxford, UK.

Bloomfield, K., and Garson, M. S., (1965), The Geology of the Kirk Range – Lisungwe Valley Area, Bulletin 17, Geological Survey of Malawi, Malawi Government Printer, Zomba, Malawi.

Bloomfield, K., (1970), The Geology of the Zomba Area, Bulletin 16, Geological Survey of Malawi, Government Printer, Zomba, Malawi.

Cawood P. A. & Buchan C., (2007), Linking accretionary orogenesis with supercontinent assembly, Earth-Science Reviews, Volume 82, Issues 3–4, June 2007, Pages 217–256

Chappell, B. W. & White, A. J. R. (1974), Two contrasting granite types, Pacific Geology 8, pp. 173 – 174.

Chappell, B. W. & White, A. J. R. (2001), Two contrasting granite types: 25 years later. Australian Journal of Earth Sciences (2001) 48, 489–499.

Chen B., Bor-ming J., Chunjing W., (2002), Petrogenesis of Mesozoic Granitoids in the Dabie UHP Complex, Central China: Trace Element and Nd–Sr Isotope Evidence, Lithos, Vol 60, Issue 1- 2, pp. 67 – 88.

Chen B. & Bor-Ming Jahn, (2002), Geochemical and Isotopic Studies of the Sedimentary and Granitic Rocks of the Altai Orogen of Northwest China and their Tectonic Implications, Geol. Mag. 139 (1), 2002, pp. 1–13. DOI: 10.1017/S0016756801006100.

Condie Kent C., TTGs and Adakites: Are they Both Slab Melts? Lithos 80 (2005) 33– 44.

Dostal J., Church B.N., and Hoy T., (2001) Geological and Geochemical Evidence for Variable Magmatism and Tectonics in the Southern Canadian Cordillera: Palaeozoic to Jurassic Suites, Greenwood, Southern British Columbia, Can. J. Earth Sci. 38: 75–90, DOI: 10.1139/cjes-38-1-75

Farmer, G. L., (2007), Continental Basaltic Rocks, (in Treatise in Geochemistry, Volume 3, pp 1 - 39)

Frost B.R., Barness C.G., Collins W.J., Arculus R. J., Ellis D. J., and Frost C. D., (2001), A Geochemical Classification of Granitic Rocks, Journal of Geology, Vol. 42, No. 11, pp 2011 – 2033.

Frost B. R and Frost C.D., (2008), A Geochemical Classification for Feldspathic Igneous Rocks, Journal of Geology, Vol. 49, No. 11, pp 1955 – 1969, doi:10.1093/petrology/egn054.

Garson, M. S. and Walshaw R.D., (1969), The Geology of the Mulanje Area, Bulletin 21, Geological Survey of Malawi, Government Printer, Zomba, Malawi.

Ghosh S., Fallick A. E., Paul D. K., and Potts P. J., (2005), Geochemistry and Origin of Neoproterozoic Granitoids of Meghalaya, Northeast India: Implications for Linkage with Amalgamation of Gondwana Supercontinent, Gondwana Research, V 8, No. 3, pp. 421 -432, 2005, International Association for Gondwana Research, Japan. ISSN: 1342-937X.

Gill, R., (2011), Igneous Rocks and Processes: A Practical Guide, Wiley-Blackwell, John Wiley & Sons, Ltd., West Sussex, PO19 8SQ, UK.

Grantham G. H., Maboko M., & Eglington B. M. (2003). "A Review of the Evolution of the Mozambique Belt and Implications for the Amalgamation and Dispersal of Rodinia and Gondwana." Geological Society, London, Special Publications, 2003 v.206: p 401-425.

Grantham G.H., Manhica A.D.S.T., Armstrong R.A., Kruger F.J., Loubser M., (2011), New SHRIMP, Rb/Sr and Sm/Nd Isotope and Whole Rock Chemical Data from Central Mozambique and Western Dronning Maud Land, Antarctica: Implications for the Nature of the Eastern Margin of the Kalahari Craton and the Amalgamation of Gondwana, Journal of African Earth Sciences, 59 (2011) pp. 74–100

Harlov D. E., Leif Johansson, Alfons Van Den Kerkhof and Hans-Jurgen Forster, (2005), The Role of Advective Fluid Flow and Diffusion during Localized, Solid-State Dehydration: So¨ndrum Stenhuggeriet, Halmstad, SW Sweden, Journal of Petrology Advance Access, pp.1 – 31. Doi:10.1093/Petrology/Egi062

Helo, C., Hegner, E., Kröner, A., Badarch, G., Tomurtogoo, O., Windley, B. F., Dulski, P., (2006), Geochemical Signature of Palaeozoic Accretionary Complexes of the Central Asian Orogenic Belt in South Mongolia: Constraints on Arc Environments and Crustal Growth, Chemical Geology, Volume 227, Issue 3-4, pp 236-257.

Hine R., Williams I. S., Chappell B. W. & White A. J. R. (1978) Contrasts between I- and S-type granitoids of the Kosciusko Batholith, Journal of the Geological Society of Australia, 25:3-4, 219-234, DOI: 10.1080/00167617808729029

Janoušek, V., Farrow, C. M. & Erban, V. 2006. Interpretation of whole-rock geochemical data in igneous geochemistry: introducing Geochemical Data Toolkit (GCDkit). Journal of Petrology 47(6):1255-1259

Johnson S.P., Cutten H.N.C., Muhongo S., De Waele B., (2003), Neoarchaean Magmatism and Metamorphism of the Western Granulites in the Central Domain of the Mozambique Belt, Tanzania: U–Pb Shrimp Geochronology and PT Estimates, Tectonophysics 375 (2003) 125–145

Kilpatrick J. A. and Ellis D. J., (1992), C-Type Magmas: Igneous Charnockites and their Extrusive Equivalents, Transactions of the Royal Society of Edinburgh: Earth Sciences, 83, 155-153, 1992.

Kröner A., Willner A. P., Hegner E., Jaeckel P., Nemchin A., (2001), "Single Zircon Ages, PT Evolution and Nd Isotopic Systematics of High-Grade Gneisses in Southern Malawi and their Bearing on the Evolution of the Mozambique Belt in Southeastern Africa." Precambrian Research 109(3-4): 257-291.

Martin, H., Smithies, R. H., Rapp, R., Moyen, J. F., Champion, D., (2005), An Overview of Adakite, Tonalite–Trondhjemite–Granodiorite (TTG), and Sanukitoid: Relationships and Some Implications for Crustal Evolution, Lithos 79 (2005) 1 – 24

Muhongo S., Hauzenberger C., and Sommer H., (2003), Vestiges of the Mesoproterozoic Events in the Neoproterozoic Mozambique Belt: the East African Perspective in the Rodinia Puzzle, Gondwana Research, V 6, No. 3, pp. 409-41 6.

Pearce J. A., Harris N. B. W., Tindle A. G., (1984), Trace Element Discrimination Diagrams for the Tectonic Interpretation of Granitic Rocks, Journal of Petrology , Vol. 25, Part 4, pp. 956-983.

Rajesh H. M., (2007), The Petrogenetic Characterization of Intermediate and Silicic Charnockites in High-Grade Terrains: A Case Study from Southern India, Contributions to Mineral Petrology (2007) 154:591–606

Ray J., Saha A., Ganguly S., Balaram V, Krishna A K., and Hazra S., (2011), Geochemistry and Petrogenesis of Neoproterozoic Mylliem Granitoids, Meghalaya Plateau, Northeastern India, Journal of Earth System Science, 120, No. 3, June 2011, pp. 459–473, Indian Academy of Sciences.

Rollinson H. R. (1994), Using Geochemical Data: Evaluation, Presentation, Interpretation, Longman Group UK Ltd., England.

Silantyev S. A., Portnyagin M. V., Krasnova E. A., Hauff F., Werner R., and Kuzmin D. V., (2014) Petrology and Geochemistry of Plutonic Rocks in the Northwest Pacific Ocean and Their Geodynamic Interpretation, Geochemistry International Vol. 52 No. 3 2014

Sreejith C., Kumar, G., Ravindra R., (2013), Petrogenesis of High-K Meta-granites in the Kerala Khondalite Belt, Southern India: A Possible Magmatic-Arc Link between India, Sri Lanka, and Madagascar, Journal of Geodynamics 63 (2013) 69– 82

Stephens W.E. and Calder A., Analysis of non-organic elements in plant foliage using polarised X-ray fluorescence spectrometry, Analytica Chimica Acta 527 (2004) 89–96.

Thirlwall, M. F., (1981), Implications for Caledonian Plate Tectonic Models of Chemical Data from Volcanic Rocks of the British Old Red Sandstone, J. geol. Soc. London, Vol. 138, 1981, pp. 123-138.

Vogt, M., Kroner, A., Poller, U., Sommer, H., Muhongo, S., Wingate, M.T.D., (2006) Archaean and Palaeoproterozoic Gneisses Reworked During a Neoproterozoic (Pan-African) High-Grade Event in the Mozambique Belt of East Africa: Structural Relationships and Zircon Ages from the Kidatu Area, Central Tanzania, Journal of African Earth Sciences 45, pp. 139–155.

Westerhof, A. B. Phil, Lehtonen, M. I., Mäkitie, H., Manninen, T., Pekkala, Y., Gustafsson, B. & Tahon, A. (2007), The Tete-Chipata Belt: A New Multiple Terrane Element from Western Mozambique and Southern Zambia, GTK Consortium Geological Surveys in Mozambique 2002–2007, edited by Yrjö Pekkala, Tapio Lehto & Hannu Mäkitie

Wilson M. (2007), Igneous Petrogenesis, Springer, The Netherlands

Chapter 5: LA-ICP-MS Single Zircon U-Pb Geochronology

5.1 INTRODUCTION

Of the several radioisotope dating systems that have been used to determine the age of rocks and timing of geological events, the zircon U - Pb system has provided some of the most enhanced understanding of the temporal distribution and genesis of continental crust by establishing reliable and robust age determinations (Bickford, 1988), often integrated with other isotopic systems (Hawkesworth and Kemp, 2006; Faure and Mensing, 2005). The high U-to-common –Pb ratio in zircon enables its usage in dating, as that yields highly radiogenic Pb isotope compositions over time. Apart from the U/Pb ratio, zircon suitability lies in its low Lu/Hf, producing nonradiogenic Hf, which is employed in determination of initial Hf composition of original host rock (Nebel-Jacobse et al., 2005). This system, U-Pb, is the best for rocks older than 100 m.y. and is applicable for a range of geological circumstances such as with baddeleyite in dating mafic rocks and monazite for establishing the timing of metamorphic events (Bickford, 1988). In this study, LA–ICP–MS single zircon U – Pb has been employed for selected rocks of southern Malawi. The combination of zircon morphology and associated age has provided a refined understanding of the geodynamic evolution to this part of the Mozambique Belt.

5.1.1 GEOLOGICAL SETTING

Figs. 5.1 and 5.2 show the study area in relation to the tectonic map and the outline geology of the adjacent areas in Mozambique respectively. The geologic character of the Mozambique Belt varies from north to south (Jabobs et al., 2004). The northern part of the belt (Arabian–Nubian Shield) is dominated by juvenile, mid-Neoproterozoic island arc terranes bounded by suture zones with abundant ophiolites, and marked by low to medium grade deformation (Jacobs et al., 2004). The southern part, from Kenya to its inferred extension in Dronning Maud Land (East Antarctica), is underlain by high-grade rocks (up to granulites facies) of Neoproterozoic–Cambrian age with Archean–Mesoproterozoic protoliths. Neoproterozoic plutons intrude the gneisses, and this part of the orogen is considered as resulting from continent-continent collision (e.g., Muhongo and Lenoir, 1994; Jacobs et al., 1998; Kröner, 2001; Jacobs et al., 2004). The age and distribution of carbonate and associated (meta) sedimentary rocks has also been used to characterise the Mozambique Belt. For example, Grantham et al. (2003) highlighted the occurrences of strongly deformed carbonate, quartzite, and phyllosilicate schists intruded by 1105 Ma dolerite dykes in the central Mozambique and eastern Zimbabwe areas, including 1400 Ma carbonate rocks in the Zambezi Belt, and the presence in Mozambique and eastern Zimbabwe of 1100 Ma carbonate rocks to suggest that they define the development of continental shelves and, hence, potential plate boundaries.

Southern Malawi consists of Precambrian peraluminous and metaluminous granitoids, biotite hornblende gneisses and migmatites, amphibolite gneisses, calc-silicates and meta-limestones

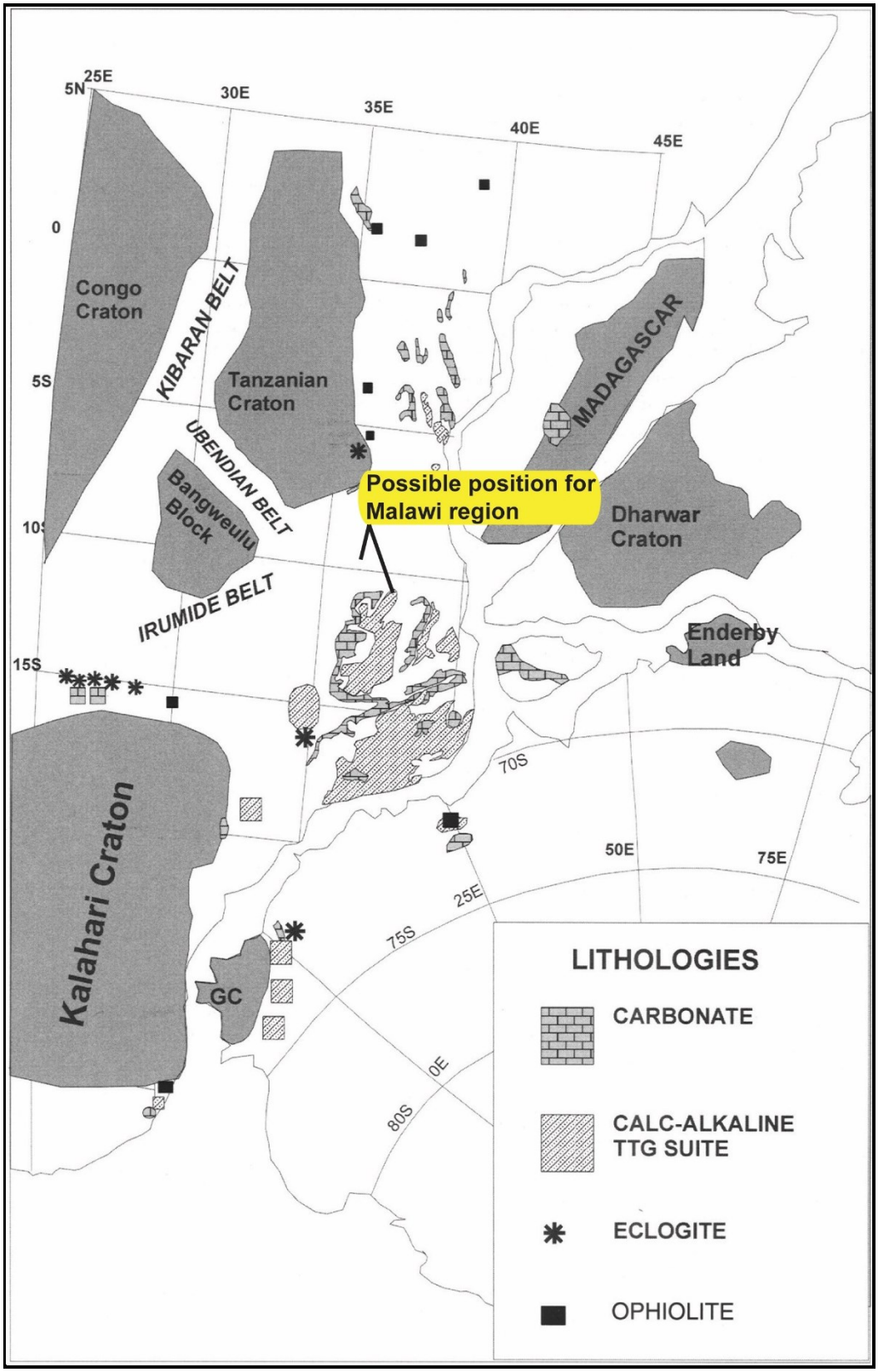

Fig. 5.1: Tectonic map showing major lithologic units of the Mozambique Belt and relationship with other belts. Possible position of Malawi in time indicated.
Adapted from: Grantham et al., 2003, Geological Society, London, Special Publications, 206, 401-425. 0305-8719/03/$15

(Bloomfield, 1974; Evans, 1965; Kröner et al., 2003). The granitoids are metamorphosed to amphibolite and granulite grade and are now mostly hornblende biotite and charnockitic gneisses ranging in composition from monzodioritic to granitic. Minor pyroxenites and metagabbros and mafic dykes commonly lie concordant to these granitoids but in places they display cross-cutting relationships. Pink perthitic syenites, granites and pegmatites are interpreted as due to anataxis or metasomatism of the granitoids (Bloomfield, 1974; Evans, 1965; Andreolli, 1984). The Precambrian geology of southern Malawi has long been considered as constituting a segment of the Pan-African Mozambique Belt (Kröner et al., 2001).

Andreolli (1984) proposed a tectonic model for the southern Malawi area, with an ocean subduction floor during the Mesoproterozoic and subsequent collision between an island arc and what he termed the "Niassa craton". This area consists of migmatitic, reworked Archean granitoids with relics of ophiolites, ultramafics and eclogitic garnet granulites identifying the suture zone (Andreolli, 1984). Intrusive anorthosite, metamorphosed monzonite, syenite and K-rich charnockitic granite were also identified (Bloomfield, 1974; Evans, 1965; Andreolli, 1984).

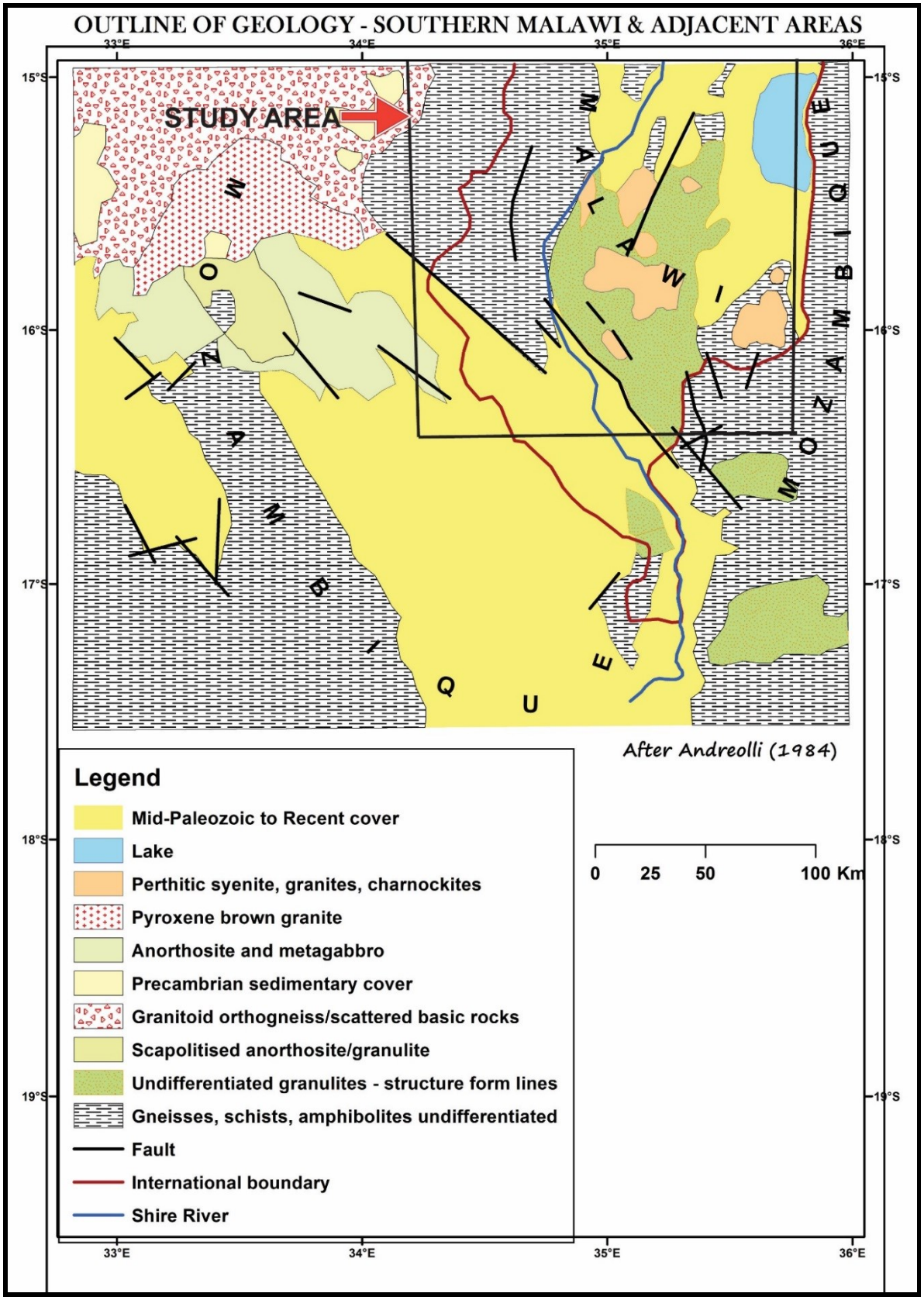

Fig. 5.2: Map showing the outline geology of study area in southern Malawi in relation to the geology in adjacent areas in Mozambique

5.1.2 PREVIOUS GEOCHRONOLOGICAL STUDIES

Age data for Malawi (Ray et al., 1974; Ring et al., 1997, 1999, 2001; Kröner et al., 2003; Ashwal et al., 2006) are limited and those that do exist are shown in Table 5.1 and illustrated in the Time Space plot diagram (Fig. 5.3). The northern part of Malawi is reported to have been affected by three tectono-thermal-metamorphic events: Paleoproterozoic, Mesoproterozoic and the Pan African (Mozambique Belt) events. Magmatism is indicated as old as Archean (3.5 Ga) on the basis of a K-Ar hornblende date (Ray et al., 1974), with subsequent magmatic events in the Mesoproterozoic and Neoproterozoic.

Table 5.1: Table showing previous geochronological for Malawi in the Mozambique Belt.

SAMPLE	ROCK TYPE AND LOCATION	DATING METHOD	AGE (MA)	INTERPRETATION	MODEL AGE (GA)	REFERENCE
Thambani	Nepheline-bearing gneisses	TIMS (Zircon)	730±4	Magmatic crystallisation		Ashwal et al., (2007)
Thambani	Nepheline-bearing gneisses	SHRIMP (Zircon)	729±7	Magmatic crystallisation		Ashwal et al., (2007)
Thambani	Nepheline-bearing gneisses	Monazite	522±17	Metamorphism		Ashwal et al., (2007)
1	Leucocratic granite	Evaporation (Zircon)	602.7±1.0	Emplacement age	1.5	Kröner et al., (2001)
2	Garnet rich granulite	Evaporation (Zircon)	644.9±0.9	Emplacement age	1.0	Kröner et al., (2001)
3	Trondhjemitic gneiss	Evaporation (Zircon)	582.9±1.0	Emplacement age	1.4	Kröner et al., (2001)
4	Leucocratic granite	Evaporation (Zircon)	577.5±1.0	Emplacement age	1.4	Kröner et al., (2001)
5	Charnockitic gneiss	Evaporation (Zircon)	590.5±1.0	Emplacement age	1.2	Kröner et al., (2001)
5	Charnockitic gneiss	Evaporation (Zircon)	928.9±0.8	Emplacement age	1.8	Kröner et al., (2001)
6	Migmatitic paragneiss	SHRIMP (Zircon)	576.0±11	Age of melt patches		Kröner et al., (2001)
6	Migmatitic paragneiss	Evaporation (Zircon)	576.7±1.0	Age of melt patches		Kröner et al., (2001)
6	Migmatitic paragneiss	SHRIMP (Zircon)	572.0±9	Peak of metamorphism		Kröner et al., (2001
6	Migmatitic paragneiss	Evaporation (Zircon)	575.0±1.0	Peak of metamorphism		Kröner et al., (2001)
7	Granodioritic gneiss	Evaporation (Zircon)	1012.5±0.8	Emplacement age	1.2	Kröner et al., (2001)
8	Migmatitic granite gneiss	Evaporation (Zircon)	998.9±0.8	Emplacement age	0.8	Kröner et al., (2001)
9	Garnetiferous metapelite	VT	547.0±10	Peak of metamorphism		Kröner et al., (2001)

9	**Garnetiferous metapelite**	**Evaporation (Zircon)**	**549.2±1.0**	**Peak of metamorphism**		**Kröner et al., (2001)**
10	**Trondhjemitic gneiss**	**SHRIMP (Zircon)**	**571.0±9**	**Emplacement age**	**1.3**	**Kröner et al., (2001)**
10	**Trondhjemitic gneiss**	**Evaporation (Zircon)**	**576.1±10**	**Emplacement age**		**Kröner et al., (2001)**
10	**Trondhjemitic gneiss**	**SHRIMP (Zircon)**	**564.0±4**	**Peak of metamorphism**		**Kröner et al., (2001)**
11	**Migmatitic granodioritic gneiss**	**SHRIMP (Zircon)**	**1040.6±0.7**	**Emplacement age**	**1.2**	**Kröner et al., (2001)**
12	**Enderbitic gneiss**	**SHRIMP (Zircon)**	**554.7±1.0**	**Emplacement age**	**1.2**	**Kröner et al., (2001)**
13	**Granite gneiss**	**SHRIMP (Zircon)**	**664.0**	**Emplacement age**	**1.3**	**Kröner et al., (2001)**
13	**Granite gneiss**	**Evaporation (Zircon)**	**667.7±0.9**	**Emplacement age**		**Kröner et al., (2001)**
14	**Retrograded granulite**	**Evaporation (Zircon)**	**710.5±0.9**	**Emplacement age**	**1.5**	**Kröner et al., (2001)**
Wililo	**Granite**	**Evaporation**	**1118 Ma**	**Protolith crystallisation**		**Ring et al., (1999)**
Lwakwa	**Granite**	**TIMS (Zircon)**	**1087±11**	**Protolith crystallisation**		**Ring et al., (1999)**
Mwenga	**Granite**	**TIMS (Zircon)**	**1119±20**	**Protolith crystallisation**		**Ring et al., (1999)**
Ka 92-57 Luromo	**Enderbite gneiss**	**Evaporation (Zircon)**	**2092.8±0.6**	**Protolith crystallisation**		**Ring et al.,(1997)**
Ka 92-57	**Enderbite gneiss**	**Evaporation (Zircon)**	**2001.6±0.3**	**Protolith crystallisation**		**Ring et al.,(1997)**
Ka 92-45 Rumphi	**Rumphi Granite**	**Evaporation (Zircon)**	**2048.4 ±0.7**	**Protolith crystallisation**		**Ring et al.,(1997)**
Ka 92-44, Chelinda	**Granitic gneiss**	**Evaporation (Zircon)**	**1988.1 ±0.6**	**Peak of Metamorphism**		**Ring et al.,(1997)**
Ka 92-46 Chelinda	**Anatectic melt in cordierite-garnet granulite**	**Evaporation (Zircon)**	**1994.8 ±0.4**	**Peak of Metamorphism**		**Ring et al.,(1997)**
	Nepheline syenite	**Rb-Sr Whole rock**	**650±40**	**Greenschist Metamorphism**		**Cannon et al., (1969)**

	Nepheline syenite	**K-Ar Biotite**	**410±20**	**Greenschist Metamorphism**		**Cannon et al., (1969)**
Luwawa	**Phyllonite**	**K-Ar Whole rock**	**415±20**	**Greenschist Metamorphism**		**Cannon et al., (1969)**
Mafingi Group	**Phyllites**	**K-Ar, whole-rock:**	**a) 350±15 b) 690±20 c) 770±25 d) 545±25**	**Greenschist Metamorphism**		**Cannon et al., (1969)**
	Lamprophyre	**K-Ar, arfvedsonite:**	**1145±60**	**Greenschist Metamorphism**		**Cannon et al., (1969)**
Nthonga	**Granite**	**K-Ar, biotite**	**1120 ± 30**	**Greenschist metamorphism**		**Cannon et al., (1969)**
Nyika	**Granite**	**Rb-Sr, whole-rock K-Ar, biotite**	**1300 ± 400 515± 25**	**Amphibolite facies**		**Cannon et al., (1969)**
	Muscovite-biotite-gneiss	**K-Ar, biotite**	**420 ± 20**	**Amphibolite facies**		**Cannon et al., (1969)**
	Amphibolite	**K-Ar, hornblende**	**1330 ± 60**	**Amphibolite facies to granulite**		**Cannon et al., (1969)**
	Metagabbros	**K-Ar, hornblende**	**3455 ± 80**	**Amphibolite facies**		**Cannon et al., (1969)**

****Evaporation = Single grain évaporation.** **VT = Single grain vapour transfer**

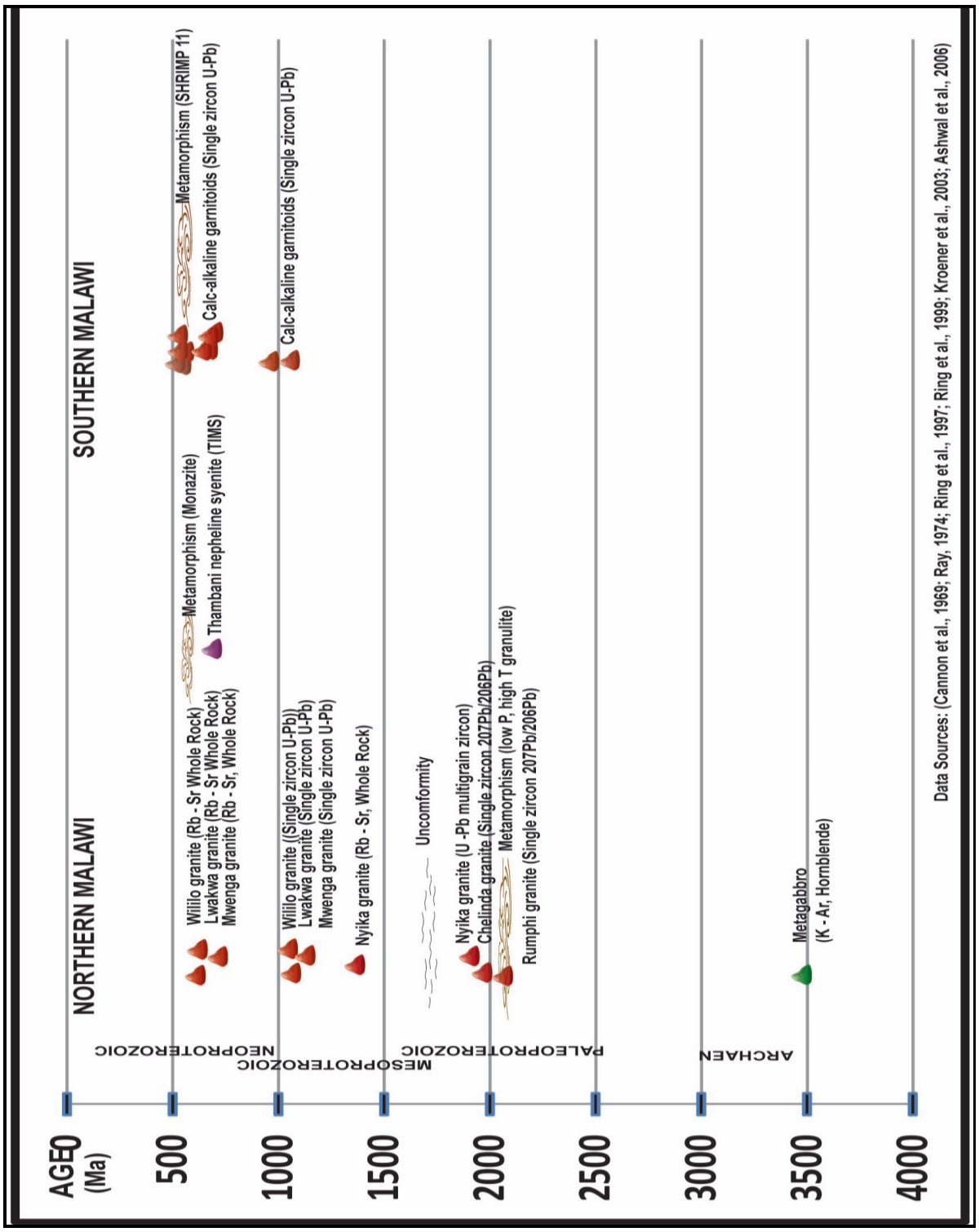

Fig. 5.3: Time space diagram for tectono-thermal events in Malawi

Sources: Cannon et al., 1969; Ray, 1974; Ring et al., 1997; Ring et al., 1999; Kröner et al., 2003; Ashwal, 2006

The region around southern Malawi is reported to have experienced a Mesoproterozoic metamorphic event which Andreolli (1984) called "Kibaran" and Johnson et al. (2005) identified as the Southern Irumide Belt (SIB), and which was subsequently overprinted by the Neoproterozoic Mozambique Belt event. No evidence for a Paleoproterozoic tectonothermal

event has been reported in southern Malawi. There is, however, a distinct area south of Malawi underlain by charnockitic gneisses that appears to record the Mozambique Belt event and that the earlier Mesoproterozoic event is absent. The gneiss assemblages of southern Malawi reached peak metamorphic conditions at 900 ± 70 °C and 9.5 ± 1.5 kbar, followed by an isobaric cooling path (Kröner et al., 2001). The first of three distinct events (all data from Kröner et al., 2001) suggested for this region is late Mesoproterozoic to early Neoproterozoic (Kibaran) in age (ca. 1040 - 929 Ma) and is represented by intrusion of calc-alkaline granitoids. Nd isotope data indicate overall juvenile compositions consistent with a magmatic arc environment, or emplacement into thinned continental crust with little involvement of older basement. The second event is a Pan-African period of intrusion of calc-alkaline granitoids around 710 - 555 Ma and the Nd isotope data show crustal residence ages of 1.0 - 1.5 Ga suggesting either re-melting of 1.0-1.5 Ga (Kibaran) protoliths or mixing of juvenile material with subordinate amounts of older crust. The last event is a thermal peak of Pan-African high grade metamorphism around 571 - 549 Ma.

The late Mesoproterozoic and Pan-African magmatic events in Malawi may be linked to granitoid magmatism of similar ages in north-western Mozambique and the central Zambezi belt of northern Zimbabwe, and therefore East Gondwana was not a coherent block colliding with West Gondwana but consisted of individual terranes before being amalgamated into the supercontinent Gondwana some 550 - 530 Ma ago (Muhongo, 2001; Kröner et al., 2001). The MORB-like chemistry of mafic rocks together with the presence of Neoproterozoic continental-margin arc magmas in southern Malawi denotes Neoproterozoic oceanic crust between the Congo and Kalahari Cratons (Johnson et al., 2005). Although the Precambrian geology of southern Malawi has long been considered as constituting a segment of the Pan-African Mozambique Belt (Kröner et al., 2001), Rb-Sr whole rock ages (Andreolli, 1984; Pinna, 1995) were interpreted as representing high-grade metamorphism thereby assigning this segment to the “Kibaran” Mesoproterozoic orogenic belt (Kröner et al., 2001). More recent high-precision zircon geochronology has failed to confirm the existence of a Mesoproterozoic event in southern Malawi or in northern Mozambique (Muhongo et al., 2003; Kröner et al., 2001).

5.1.3 OBJECTIVES

Previous geochronological work (whole-rock and mineral Rb-Sr and K-Ar, and U-Pb zircon conventional methods), indicates an Archean – Cambrian crust for Malawi for the various suites of supracrustal rocks and calc-alkaline magmatism present in this part of the Mozambique Belt. However, the nature and timing of the tectono-thermal events are poorly understood, and hitherto not well constrained, which in turn compromises our understanding of the basic regional tectono-thermal dynamics of the Mozambique Belt. Malawi, lying at the junction of the East African Orogen and the Kuunga Orogen, is critical to our understanding of Gondwana assembly as it partly has a record of collision, arc magmatism and subduction dynamics. The questions to be addressed in this study include: what is the timing of the calc-alkaline magmatism in this area? Are there multiple tectono-thermal events in this area and if so how many? The other pertinent question relates to the relevance of the geochronology to Rodinia and Gondwana fragmentation and assembly. The aim of this study therefore is to provide geochronological constraints on the calc-alkaline magmatism associated with the Proterozoic tectono-thermal events, and determine the relationship between the magmatism and that in the neighbouring/adjacent areas within the Mozambique Belt. The study attempts to characterise zircon types in the rocks of this area and by the combination of the zircon morphology and their ages help refine understanding of the geodynamic evolution to this part of the Mozambique Belt.

5.2 METHODS

Representative charnockitic gneiss, metagranites/granites/syenite, and supracrustal samples from southern Malawi were selected for LA-ICP-MS U-Pb zircon dating. Sampling locations are indicated on the map of Appendix 3.4. The granitoids were crushed in a jaw crusher and sieved to get the fraction 75µ - ≤ 250 µ. This fraction was washed with clean tap water to rid the finest portions and then dried at 500˚C for 4 – 12 hours. Zircons were further concentrated using a Franz Isodynamic magnetic separator and heavy liquid (LST 2.6g/cm) separation techniques. Distilled water followed by acetone was used to clean and dry the heavy fraction. Zircons were handpicked from the aliquots under a high-magnification binocular microscope. Grains were mounted in epoxy resin and polished to expose the grain centers and subsequently photographed. The selection of zircons for isotopic analyses was carried out based on backscatter electron (BSE) and cathodo-luminescence (CL) images which were acquired on an electron microprobe (JXA-8600 Superprobe) at the University of St Andrews.

U-Pb zircon dating was carried out at the British Geological Survey Isotope Laboratory (NIGL) in Nottingham (UK). Ages older than 900 Ma were calculated from their $^{207}Pb/^{206}Pb$ ratios, but the younger ones were based on their $^{206}Pb/^{238}U$ ratios that yield a more reliable age estimate since there are larger uncertainties in the common-Pb correction for ^{207}Pb (Cawood et al., 2001). Zircon U-Pb geochronology was carried out employing a laser ablation single collector inductively coupled plasma mass spectrometry (LA-SC-ICP-MS). The instrumentation used for U-Pb analyses comprised an Attom single-collector ICP-MS (Nu Instruments, Wrexham, UK) coupled to a UP193SS Nd:YAG laser ablation system using a low-volume ablation cell. The carrier gas through the ablation cell was Helium and Ar make-up gas was connected via a Y-piece and obtained from a Nu Instruments DSN-100 desolvating nebulizer. On the SC-ICP-MS, masses ^{202}Hg, $^{204}Pb+Hg$, ^{206}Pb, ^{207}Pb, ^{235}U were measured. The ^{238}U was calculated from ^{235}U using a $^{238}U/^{235}U$ of 137.818 (Hiess et al., 2012). Normalisations of the Pb/Pb and U/Pb ratios were carried out by bracketing primary reference material 91500, based on the average measured value of the reference material compared to the ratio determined by ID-TIMS (Wiedenbeck et al., 1995). The validation of accuracy of normalization was done by Standards GJ-1 and Plešovice (Jackson et al., 2004; Sláma et al., 2008) which also provided long-term variance statistics for uncertainty propagation (0.76%/1.7% 2s $^{207}Pb/^{206}Pb$ MC-ICP-MS/SC-ICP-MS respectively. Age interpretation used $^{207}Pb/^{206}Pb$ data in preference to U-Pb data, after assessing the data to be concordant within 2%.

Analysis uncertainties represent measurement precision propagated with the excess variance of the reference material for the respective session. Age uncertainties are propagated for systematic components by quadratic addition and include the long-term variance of the reference materials on the ICP-MS, the uncertainties of the reference values as determined by ID-TIMS, and the decay constant uncertainties (e.g. Schoene et al., 2006). Total combined age uncertainties vary between 0.5-3% (2 sigma; NB. conversion of analysis uncertainty to age uncertainty is not linear). Visualization of U-Pb concordia and zircon ages is done using Isoplot v4.15 (Ludwig, 2003). Data were interpreted mostly preferring ages derived from Pb-Pb ratios.

Results of U-Pb and Pb-Pb analyses for reference materials during nine single collector sessions and twelve multi-collector sessions spanning six months are presented in Table 5.2. Ratios for 91500 are self-normalized.

Table 5.2: Measured U–Pb data for reference materials for normalization (91500) and assessment of secondary reference materials (GJ1, Plesovice).

Standard	Measured (SC-ICP-MS)	±2s (%)	Measured (MC-ICP-MS)	±2s (%)	Preferred	n SC/MC
91500 ($^{207}Pb/^{206}Pb$)	0.07483	0.15	0.07497	0.09	0.07488	400/245
GJ1 ($^{207}Pb/^{206}Pb$)	0.05999	0.15	0.06016	0.08	0.06011	365/260
Plesovice ($^{206}Pb/^{238}U$)	0.05275	0.28	0.0546	0.16	0.05324	242/255

5.3 RESULTS

In dating zircons, consideration was given as to whether they are magmatic or metamorphic. Magmatic zircons have large crystal faces, in most cases euhedral and pyramidal or prismatic (Corfu et al., 2003; Merger et al., 1997; Wu et al., 2004). They are characterised in CL image by growth zoning, often oscillatory zoning, which is a reflection of compositional variation in Zr and Si, Hf, P, Y, the REE, U and Th (Corfu et al., 2003). In general, magmatic zircons show comparatively higher thorium (Th) and uranium (U) values and Th/U ratios. The uranium (U) concentrations are high ranging from 100 to several 1000 ppm (Merger et al., 1997) and their Th/U ratios are ca. 1 (Wu et al., 2004). Metamorphic zircons have rounded terminations due to dissolution by recrystallisation and they lack growth zoning (although sometimes euhedral shapes are possible in amphibolite facies metamorphism (Corfu et al., 2003; Merger et al., 1997; Wu et al., 2004). Metamorphic zircons have lower U concentrations (< 100 ppm) than the magmatic ones (Merger et al., 1997) and they are usually distinguished by a Th/U ratio of less than 0.1 (Wu et al., 2004). Exceptions abound where metamorphic zircons have Th/U ratios >0.1 and magmatic zircons have Th/U ratios <0.1 and causes of such anomalies are highly contested (Xiang et al., 2011). Corfu et al., 2003 suggested that zircons with high U concentrations in the core generated radiation damage responsible for the fracturing of the rim. High U concentrations may result in radiation damage to the crystal lattice of the zircon in turn leading to Pb.

5.3.1 CHARNOCKITIC GNEISSES

SAMPLE BM 249 (Refer to Table 5.3 & Figs. 5.4 and 5.5).

Sample BM 249 is a mesocratic to leucocratic, coarse grained, charnockitic gneiss with perthitised plagioclase feldspar (14%), quartz showing wavy extinction (54%), clino and ortho-pyroxenes (12%) and biotite (20%). Accessory minerals include zircon, ilmenite and magnetite. CL images reveal several varieties of zircons. The first group are euhedral with oscillatory zoning and dark inclusions indicative of magmatic zircons (Fig. 5.4A). The second group displays a featureless darker core, a brighter mantle which has oscillatory zoning, and a bright thin rim. These are magmatic but with inherited cores (Fig. 5. 4B). The last group are dark and featureless showing no cores nor mantles. These are euhedral to subhedral in shape, sometimes pyramidal with rounded edges and are interpreted as metamorphic zircon (Fig. 5.4C). All the zircons have suffered radiation damage and contain dark inclusions. Some crystals display variable overgrowths. In width, the zircons range from 250 μ to ~400 μ and in length they are up to 600μ.

Uranium concentrations range from 97 – 332 ppm and thorium ranges from 39 – 266 ppm and the Th/U ratios range from 0.33 – 0.80 and these figures are suggestive of magmatic zircons. Twenty six analyses were obtained from these zircons with fourteen concordant. The concordant grains have U concentrations above 100 ppm except for two grains #249-25 and 249-26 both with 97 ppm but they have Th/U less than 1. The weighted average $^{207}Pb/^{235}U$ for the fourteen concordant grains is 1027 ± 11 (MSWD = 4.8, 2 sigma). The analyses yield an upper intercept $^{206}Pb/^{238}U$ age of 1036 ± 15 Ma (MSWD = 2.0, 2 sigma) (Fig. 5.5) and this is indistinguishable from the weighted average age within errors and is therefore interpreted as the crystallisation age of the charnockitic gneiss.

Table 5.3: Isotopic analyses for Charnockitic gneiss Sample BM249

		CONCENTRATIONS (ppm)					ISOTOPIC RATIOS						ISOTOPIC AGES			
	Th/U	Pb	Th	U	$^{207}Pb/^{206}Pb$	1s %	$^{207}Pb/^{235}U$	1s %	$^{206}Pb/^{238}U$	1s %	$^{207}Pb/^{206}Pb$	2s abs	$^{206}Pb/^{238}U$	2s abs	$^{207}Pb/^{235}U$	2s abs
SAMPLE SPOT		ppm	ppm	ppm							age		age		age	
249_13	0.72	48	205	286	0.0744	0.75	1.706	1.68	0.1664	1.50	1052	15	992	27	1011	21
249_14	0.75	46	195	262	0.0741	0.83	1.775	1.69	0.1738	1.48	1044	17	1033	28	1036	22
249_15	0.54	22	71	131	0.0729	0.98	1.649	1.64	0.1640	1.31	1012	20	979	24	989	20
249_17	0.70	45	171	243	0.0730	0.88	1.803	1.68	0.1792	1.43	1015	18	1062	28	1047	22
249_19	0.63	31	108	171	0.0747	0.84	1.796	1.64	0.1745	1.41	1060	17	1037	27	1044	21
249_20	0.68	41	161	236	0.0736	0.91	1.738	1.74	0.1713	1.48	1032	18	1019	28	1023	22
249_21	0.67	41	156	232	0.0730	0.75	1.718	1.52	0.1707	1.32	1015	15	1016	25	1015	19
249_22	0.52	22	63	122	0.0735	1.05	1.776	1.88	0.1752	1.56	1029	21	1041	30	1037	24
249_23	0.53	26	77	145	0.0750	0.82	1.821	1.78	0.1762	1.58	1068	16	1046	30	1053	23
249_24	0.80	58	266	332	0.0737	0.90	1.738	1.52	0.1710	1.23	1035	18	1018	23	1023	19
249_25	0.42	17	41	97	0.0732	0.92	1.717	1.73	0.1701	1.46	1021	19	1013	27	1015	22
249_26	0.41	17	39	97	0.0725	1.07	1.669	1.74	0.1670	1.38	1001	22	996	25	997	22
249_27	0.41	17	41	100	0.0737	1.00	1.669	1.76	0.1644	1.45	1033	20	981	26	997	22
249_28	0.50	19	57	114	0.0744	0.96	1.684	1.74	0.1642	1.45	1052	19	980	26	1002	22
249_29	0.67	41	160	240	0.0733	0.88	1.715	1.52	0.1698	1.24	1022	18	1011	23	1014	19
249_33	0.60	35	127	211	0.0735	0.89	1.657	1.57	0.1634	1.29	1029	18	976	23	992	20
249_34	0.62	53	201	325	0.0762	0.95	1.673	1.76	0.1593	1.48	1101	19	953	26	999	22
249_35	0.33	35	66	202	0.0725	0.84	1.713	1.47	0.1714	1.21	1001	17	1020	23	1013	19
249_36	0.48	22	62	129	0.0726	1.07	1.651	1.71	0.1651	1.33	1002	22	985	24	990	21
249_37	0.40	17	40	100	0.0729	1.11	1.681	2.02	0.1673	1.68	1012	23	997	31	1002	25
249_38	0.45	18	46	103	0.0736	1.00	1.725	1.72	0.1701	1.40	1030	20	1013	26	1018	22
249_39	0.67	37	147	218	0.0760	0.83	1.725	1.62	0.1647	1.39	1095	17	983	25	1018	21
249_40	0.72	45	177	246	0.0740	0.76	1.793	1.58	0.1758	1.38	1042	15	1044	27	1043	20
249_41	0.45	19	49	108	0.0751	1.08	1.752	1.89	0.1694	1.55	1070	22	1009	29	1028	24
249_42	0.69	35	131	188	0.0730	0.95	1.797	1.63	0.1786	1.32	1014	19	1060	26	1044	21

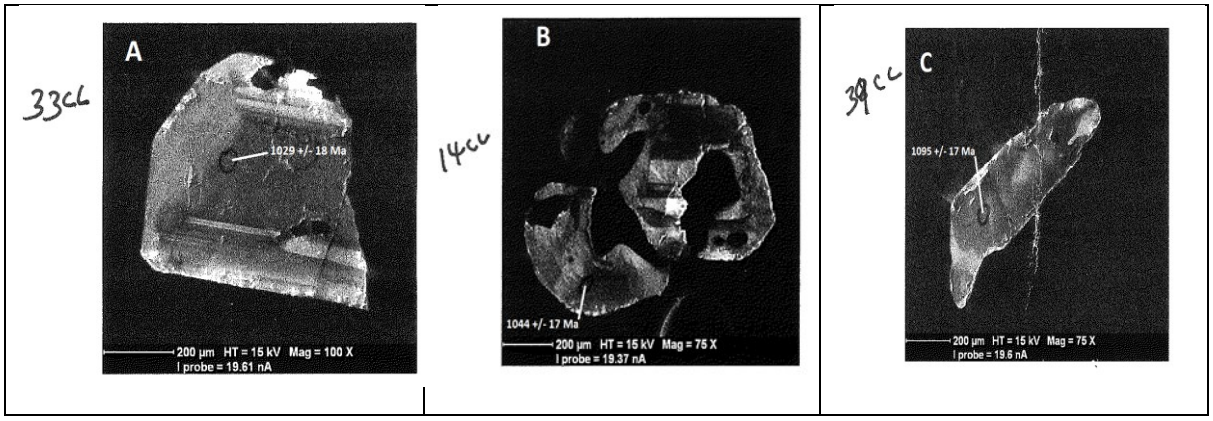

Fig. 5. 4: Showng representative samples of zircons from Sample BM249. A = Magmatic, B = Inherited, C = Metamorphic.

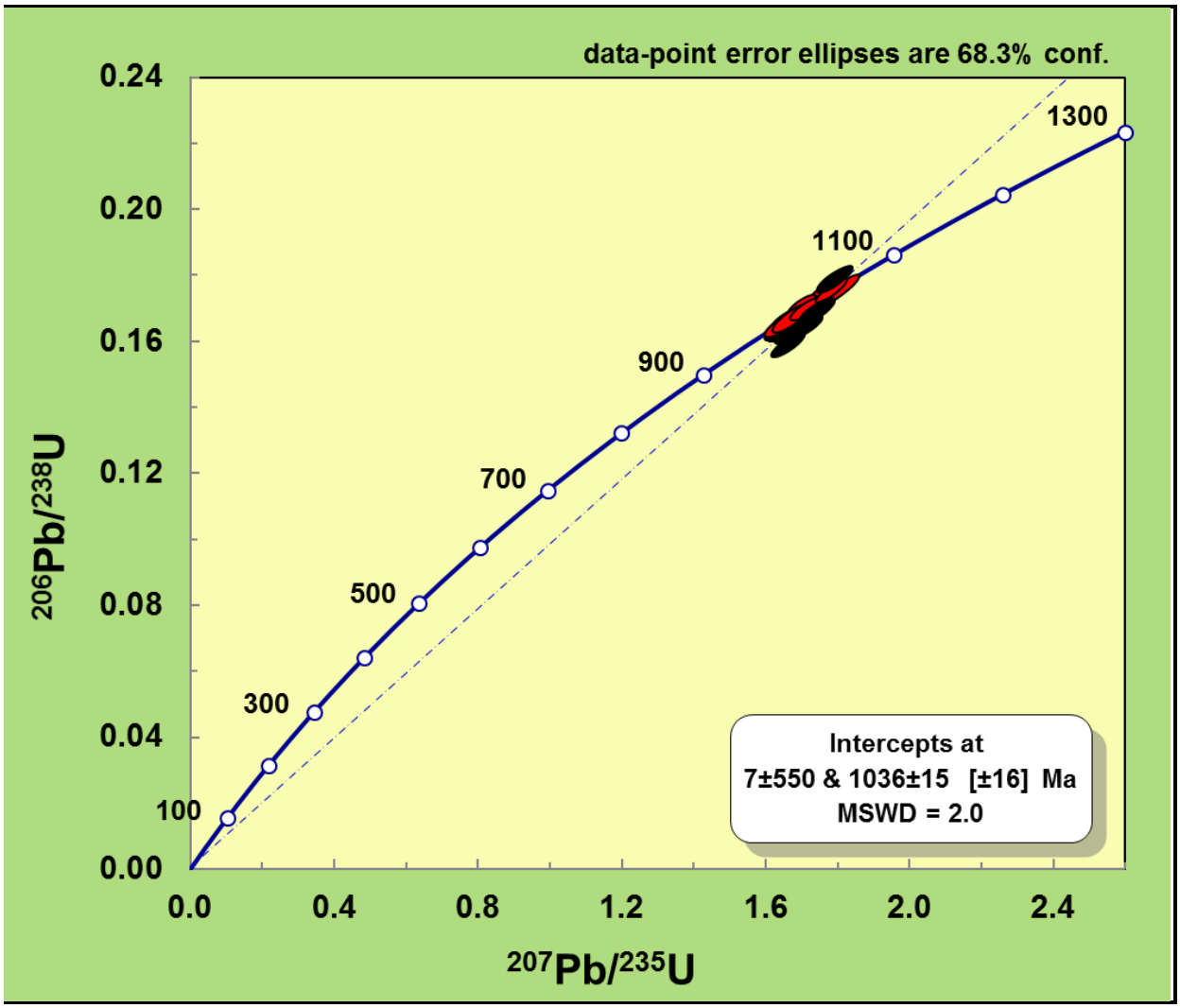

Fig. 5.5: Concordia plot for charnockitic gneiss Sample BM 249. Red colour in ellipses stands for concordant zircons. Black colour are discordant.

SAMPLE BM 252 (Refer to Table 5.4 & Fig.5.6 & 5.7)

Sample BM 252 is a leucocratic, coarse grained, foliated charnockitic gneiss. The rock comprises of quartz (43%), plagioclase feldspar (34%), pyroxenes (14%), hornblende (5%), and accessory zircons and magnetite. Three zircons were separated from this rock. In CL images the zircons are euhedral and prismatic in shape with some dark inclusions. One zircon displays a featureless core, surrounded by a mantle with oscillatory zoning, and a finally a thin rim. This is interpreted as a magmatic zircon (Fig. 5.4A). The other two zircons are bright, featureless with some dark inclusions, rounded edges, and are considered metamorphic (Fig. 5.4B & C). The zircons range from 250 μ - 400 μ in width, and 800μ in length. Eight spots were analysed from the grain that is magmatic (#252-2a, 2b, 2c, 2d, 2e, 2f, 2g, 2h) and the uranium concentrations range from range from 4 – 150 ppm and thorium from 2 – 27 ppm. The Th/U ratios range from 0.32 – 0.44. The spots yielded dates > 950 Ma. Six spots yielded discordant ages and have been omitted in the calculation. The two concordant spots (#252-2a and #252-2c) yielded a weighted average $^{207}Pb/^{206}Pb$ age of 1089 ± 160 (MSWD = 2.9, 2 sigma). This is interpreted as the age of emplacement of the charnockite. From the other two zircons twenty one spots were analysed and the U concentrations range from 15 - 33 ppm, Th ranges from 0 – 12 ppm and the Th/U ratio ranges from 0.01 to 0.37, values characteristic of metamorphic zircon. The spots analyses yielded dates < 600 Ma. Eight of the twenty-one analyses were concordant and yielded a weighted average $^{206}Pb/^{238}U$ age of 535.9 ± 6.7 (MSWD = 0.57, 2 sigma). It is suggested that this is the age for recrystallisation due to high grade metamorphism.

The upper intercept $^{206}Pb/^{238}U$ age is 1128 ± 30 Ma and the lower intercept age is 515 ± 18 Ma (MSWD = 1.10, 2 sigma) (Fig 5.7). The upper intercept date is interpreted as the age of inheritance and the lower intercept is the age of metamorphism.

Table 5. 4: Isotopic analyses for charnockitic gneiss Sample BM252

	CONCENTRATIONS (ppm)				ISOTOPIC RATIOS					ISOTOPIC AGES				
	Th/U	Pb	Th	U	$^{207}Pb/^{206}Pb$	1s %	$^{207}Pb/^{235}U$	1s %	$^{206}Pb/^{238}U$	1s %	$^{207}Pb/^{206}Pb$	2s abs	$^{206}Pb/^{238}U$	2s abs	$^{207}Pb/^{235}U$	2s abs
SAMPLE SPOT		ppm	ppm	ppm							age		age		age	
252_01d	0.28	2	7	25	0.0562	2.32	0.673	2.98	0.0868	1.86	462	52	536	19	522	24
252_01e	0.37	3	12	33	0.0597	1.81	0.701	2.43	0.0852	1.62	593	39	527	16	539	20
252_02g	0.44	1	2	4	0.0707	3.48	1.436	4.67	0.1473	3.11	950	71	886	51	904	54
252_02h	0.33	6	14	42	0.0749	1.19	1.581	2.02	0.1531	1.64	1067	24	918	28	963	25
252_03e	0.02	1	0	15	0.0581	2.38	0.692	3.33	0.0865	2.32	532	52	535	24	534	27
252_03f	0.12	2	2	18	0.0589	2.42	0.696	3.18	0.0858	2.07	562	53	531	21	537	26
252_03g	0.01	2	0	24	0.0602	2.58	0.719	3.25	0.0866	1.98	612	56	536	20	550	27
252_03h	0.02	3	1	30	0.0594	1.97	0.711	2.65	0.0869	1.77	582	43	537	18	546	22
252_1a	0.28	3	9	32	0.0583	1.71	0.686	2.42	0.0854	1.72	540	37	528	17	530	20
252_1b	0.40	3	12	30	0.0596	1.89	0.688	2.42	0.0837	1.52	590	41	518	15	532	20
252_1c	0.31	2	9	28	0.0587	1.89	0.711	2.75	0.0878	2.00	557	41	543	21	545	23
252_2a	0.35	27	52	150	0.0753	1.02	1.861	1.72	0.1793	1.39	1077	20	1063	27	1067	22
252_2b	0.35	23	50	141	0.0757	1.12	1.728	1.77	0.1657	1.37	1087	22	988	25	1019	23
252_2c	0.34	23	43	124	0.0763	1.03	1.945	1.66	0.1851	1.30	1102	21	1095	26	1097	22
252_2d	0.36	16	36	98	0.0753	1.06	1.707	1.68	0.1644	1.30	1077	21	981	24	1011	21
252_2e	0.39	14	37	93	0.0729	1.17	1.465	1.78	0.1458	1.34	1012	24	877	22	916	21
252_2f	0.32	16	32	101	0.0738	1.18	1.623	1.78	0.1597	1.34	1035	24	955	24	979	22
252_3a	0.01	1	0	15	0.0604	2.38	0.691	3.07	0.0830	1.94	617	51	514	19	533	25
252_3b	0.18	2	3	20	0.0568	2.56	0.675	3.01	0.0862	1.58	482	56	533	16	523	24
252_3c	0.02	1	0	17	0.0586	2.30	0.723	3.09	0.0895	2.07	553	50	553	22	553	26
252_3d	0.01	3	0	30	0.0582	1.85	0.693	2.56	0.0864	1.77	537	40	534	18	535	21

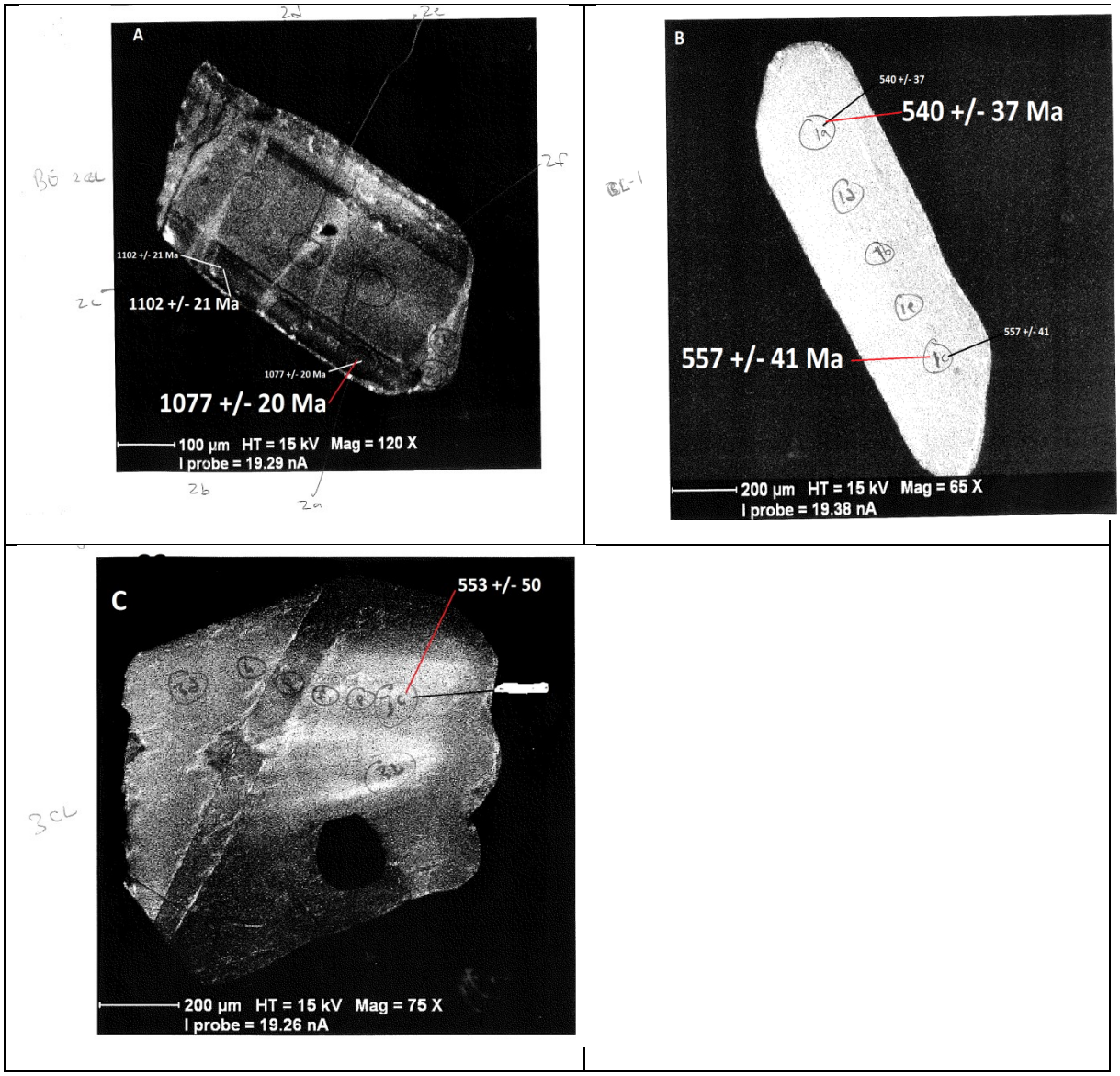

Fig. 5.6: Representative zircons and spots analysed for Sample BM252. A = magmatic zircon. B & C are metamorphic.

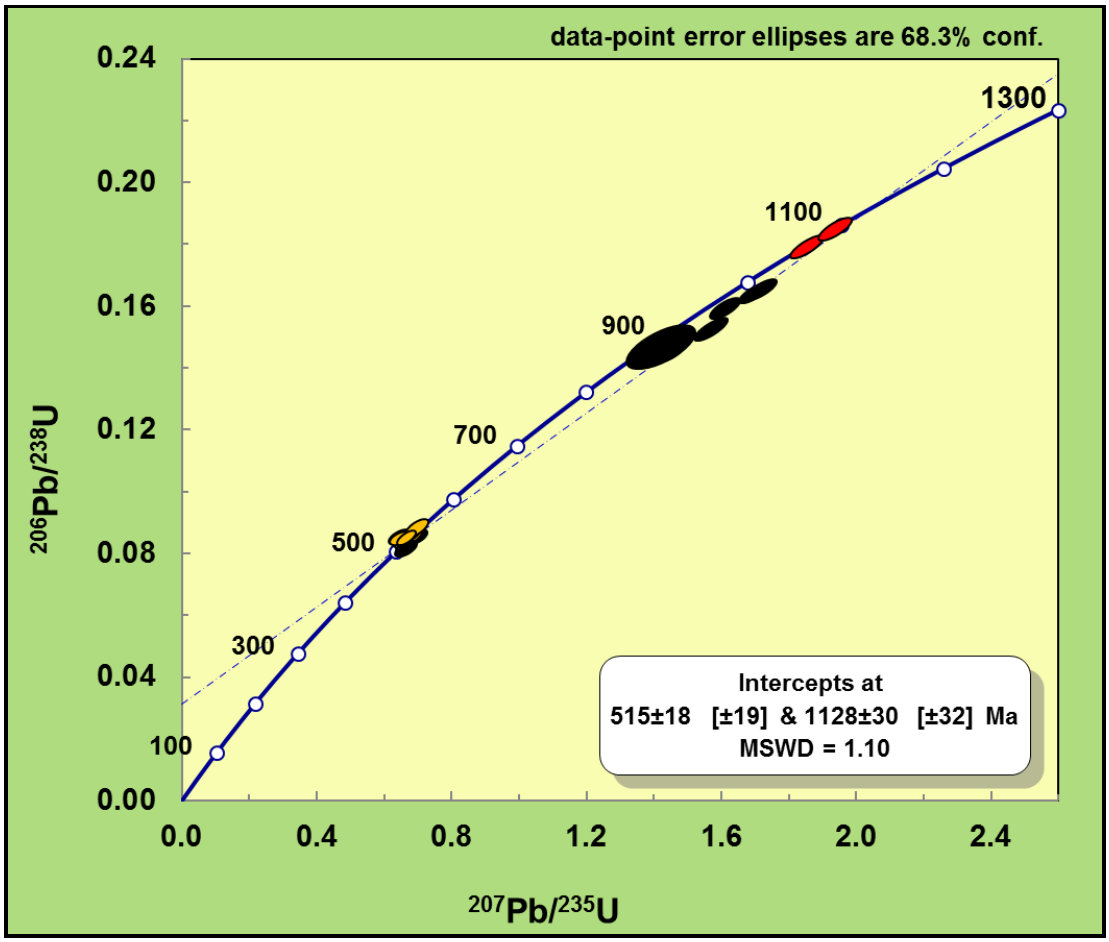

Fig. 5.7: Concordia plot of zircons from charnockitic gneiss Sample BM 252. Red and yellow eclipses stand for two populations of concordant grain analyses. Red ellipses = Magmatic. Yellow ellipses = metamorphic. Black ellipses are discordant.

SAMPLE 281(Refer to Table 5.5 & Figs.5.8 & 5.9)

Sample 281 is a mesocratic, coarse grained charnockitic gneiss composed of plagioclase feldspar (42%), quartz (12.0%), k-feldspar (9%), and ortho and clinopyroxenes (28%), biotite (8%). Accessories include zircon and apatite. Seven zircons were separated from this rock and are anhedral/subhedral and somewhat prismatic with dark inclusions. Three are not luminescing and are therefore dark in CL (Fig. 5. 8C). Some show a dark core and a mantle with alternating bright and dark phases with oscillatory zoning (Fig. 5. 8D). They show euhedral pyramidal shapes and are therefore magmatic (Fig. 5. 8A and D). The other one is a complex combination of dark inclusions in the core with a mantle displaying oscillatory zoning and some bright overgrowth and thin brighter rims (Fig. 5. 8B), which are interpreted as inherited zircons. The zircons range from 250 µ - 400 µ in width and from 300 µ to 600 µ length. U concentrations range from 117 to 2379 ppm, and are recorded with thorium concentrations ranging from 3 to 216 ppm. In three analyses the U concentrations were as high as 600 – 2379 ppm. The Th/U ratios range from 0.02 – 0.84. The weighted average $^{206}Pb/^{238}U$ is 516 ± 23 Ma, (MSWD = 32, 2 Sigma). For this group of zircons an upper intercept $^{206}Pb/^{238}U$ age of 594 ± 65 Ma (MSWD = 1.4, 2 sigma) was obtained (Fig. 5.9), which is interpreted as the age of inheritance. The uncertainty margin in the $^{206}Pb/^{238}U$ weighted average is too high to provide a meaningful date of emplacement.

Table 5.5: Isotopic analyses for charnockitic gneiss Sample BM281

		CONCENTRATIONS (ppm)					ISOTOPIC RATIOS					ISOTOPIC AGES				
	Th/U	Pb	Th	U	$^{207}Pb/^{206}Pb$	1s %	$^{207}Pb/^{235}U$	1s %	$^{206}Pb/^{238}U$	1s %	$^{207}Pb/^{206}Pb$	2s abs	$^{206}Pb/^{238}U$	2s abs	$^{207}Pb/^{235}U$	2s abs
SAMPLE SPOT		ppm	ppm	ppm							age		age		age	
281_01	0.84	20	216	258	0.0581	0.91	0.621	1.61	0.0775	1.33	532	20	481	12	490	12
281_01b	0.54	10	63	117	0.0578	1.24	0.660	2.05	0.0828	1.63	524	27	513	16	515	16
281_02a	0.87	12	138	159	0.0567	1.19	0.612	1.85	0.0784	1.42	478	26	487	13	485	14
281_02b	0.81	15	154	190	0.0589	1.02	0.648	1.71	0.0798	1.37	564	22	495	13	507	14
281_02c	0.96	15	181	189	0.0574	0.88	0.628	1.62	0.0794	1.36	506	19	492	13	495	13
281_04a	0.49	16	96	195	0.0578	0.91	0.637	1.63	0.0800	1.36	524	20	496	13	501	13
281_04a	0.55	13	87	159	0.0589	1.21	0.639	1.86	0.0787	1.41	564	26	488	13	501	15
281_04a	0.63	15	115	183	0.0570	1.19	0.616	1.75	0.0785	1.28	490	26	487	12	487	13
281_04b	0.69	13	114	165	0.0581	1.20	0.623	1.81	0.0778	1.35	533	26	483	13	492	14
281_06a	n/a	200	n/a	2379	0.0584	0.78	0.665	1.59	0.0825	1.38	546	17	511	14	517	13
281_06b	n/a	190	n/a	2258	0.0574	1.00	0.647	1.79	0.0817	1.48	508	22	506	14	506	14
281_06c	n/a	52	n/a	600	0.0606	2.43	0.699	2.87	0.0838	1.53	624	52	519	15	538	24
281_07a	0.04	13	6	140	0.0591	1.78	0.756	2.37	0.0928	1.58	572	39	572	17	572	21
281_07b	0.02	19	3	207	0.0593	1.68	0.760	2.15	0.0930	1.35	576	36	573	15	574	19
281_07c	0.02	22	4	230	0.0609	1.36	0.798	2.13	0.0951	1.63	636	29	586	18	596	19
281_07d	0.02	34	6	365	0.0600	1.15	0.759	1.85	0.0919	1.44	602	25	567	16	573	16
281_07e	0.03	95	26	1014	0.0585	1.04	0.768	1.71	0.0952	1.35	550	23	586	15	579	15

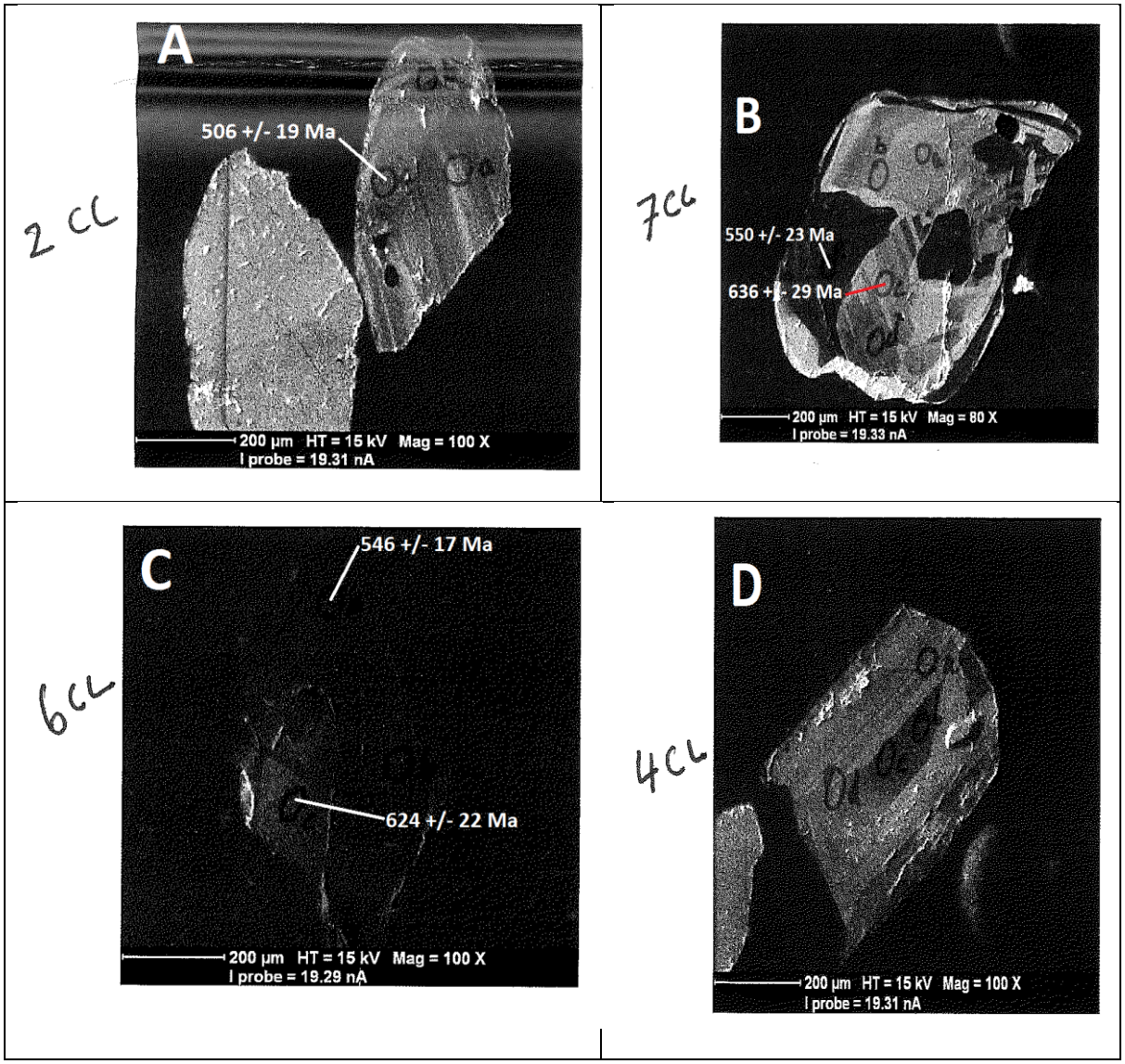

Fig. 5. 8: Showing representative zircon grains from charnockitic gneiss Sample BM281 from southern Malawi

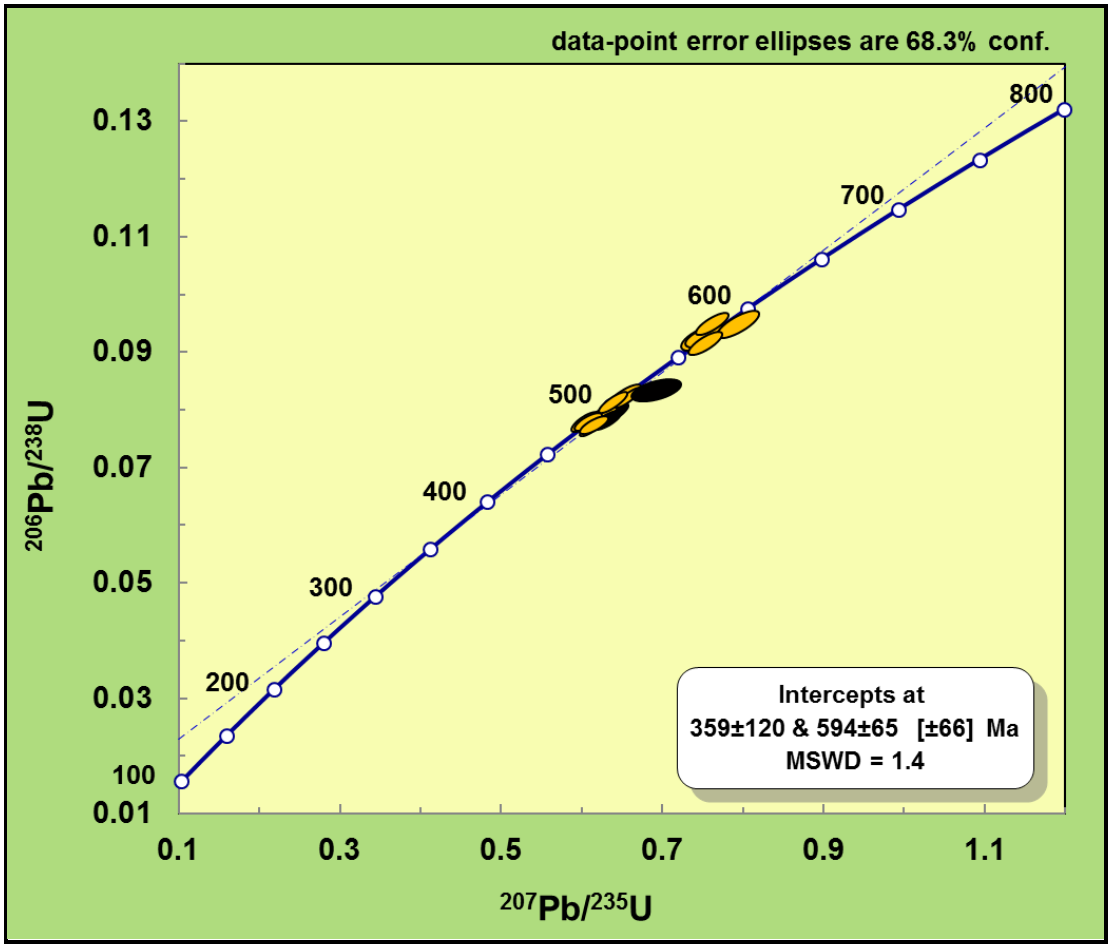

Fig. 5.9: Concordia plot for zircon grains from charnockitic gneiss Sample BM 281. The yellow ellipses are concordant grain spots and the black are discordant.

SAMPLE BM 282A (Refer to Table 5.6 & Figs.5.10 & 5.11)
This sample is a leucocratic to mesocratic, medium to coarse grained charnockitic gneiss that shows a banded foliation in outcrop. It has plagioclase feldspar (39%), quartz (19%), k-feldspar (20.0%) hornblende (10%), diopside (5%), orthopyroxene (3%), and biotite (1%). Accessory minerals include zircon, ilmenite, apatite and magnetite.

In CL images two zircons display oval, spherical shapes (Fig 5.10B & C) and one is pyramidal but fractured (Fig. 5. 10A). One oval zircon shows a bright core which itself shows three phases (bright small core, a darker mantle and then a bright rim). This complex core is then mantled by a featureless dark phase. Finally a bright rim completes the morphology (Fig. 5. 10C). The second oval zircon shows a bright oval core with a thin dark rim, encircled by a somewhat pyramidal outer region with some oscillatory zoning, which in turn is enclosed in another bright phase, then another slightly darker phase, and finally a brighter thin rim (Fig. 5. 10B). These zircons are interpreted as inherited zircons that have undergone complex deformational events. The third zircon displays alternating phases of darker and slightly bright with a thin bright rim (Fig. 5. 10A).

The uranium concentrations range from 40 – 1276 ppm and thorium ranges from 12 – 38 ppm. The Th/U ratios range from 0.03 – 0.55. Thirty one analyses were obtained and of these six yielded ages that were >1000 Ma, fifteen gave ages < 745 Ma, and fifteen were discordant. Of the six with ages >1000 Ma five are from the core and one from the mantle of grain #282A_3, and they all have low U values ranging from 40 – 68 ppm, Th ranging from 14 – 38 and the

Th/U ratios from 0.35 – 0.55. Analysis spot #282A-32 from these six is concordant and yielded a $^{207}Pb/^{206}Pb$ age 1075 ± 27 Ma and this is interpreted as the age of protolith emplacement. Fifteen spots with ages <745 Ma were concordant and yielded a $^{206}Pb/^{238}U$ weighted average age of 581 ± 20 Ma (MSWD = 14, 2 sigma). This is interpreted as the age of recrystallisation possibly from a metamorphic event. The upper intercept $^{206}U/^{238}U$ age is 1187 ± 53 Ma and the lower intercept is 536 ± 24 Ma (MSWD = 3.7, 2 sigma) (Fig. 5.11). The upper intercept is interpreted as the protolith age whilst the lower age is the age of metamorphism.

Table 5.6: Isotopic analyses for charnockitic gneiss sample BM282A

	CONCENTRATIONS (ppm)					ISOTOPIC RATIOS						ISOTOPIC AGES					
	Th/U	Pb	Th	U	$^{207}Pb/^{206}Pb$	1s %	$^{207}Pb/^{235}U$	1s %	$^{206}Pb/^{238}U$	1s %	$^{207}Pb/^{206}Pb$	2s abs	$^{206}Pb/^{238}U$	2s abs	$^{207}Pb/^{235}U$	2s abs
SAMPLE SPOT		ppm	ppm	ppm							age		age		age	
282A_2	0.25	4	12	49	0.0607	2.73	0.703	3.32	0.0841	1.90	628	59	520	19	541	27
282A_3	0.24	5	13	55	0.0594	2.52	0.689	3.24	0.0841	2.02	582	55	520	20	532	26
282A_8	0.28	6	18	65	0.0574	2.15	0.667	3.00	0.0843	2.10	506	47	522	21	519	24
282A_5	0.25	7	21	83	0.0605	1.70	0.718	2.59	0.0861	1.94	622	37	533	20	550	22
282A_4	0.25	5	14	58	0.0594	1.95	0.707	2.89	0.0864	2.13	583	42	534	22	543	24
282A_7	0.24	6	16	65	0.0604	2.45	0.719	3.14	0.0864	1.97	617	53	534	20	550	26
282A_18	0.24	6	17	71	0.0602	2.16	0.718	2.95	0.0865	2.02	612	47	535	21	549	25
282A_6	0.24	6	17	73	0.0575	2.19	0.687	2.93	0.0868	1.95	510	48	536	20	531	24
282A_19	0.26	6	17	67	0.0600	1.89	0.718	2.83	0.0868	2.11	605	41	537	22	549	24
282A_20	0.29	7	23	79	0.0581	1.98	0.696	2.67	0.0869	1.80	534	43	537	19	536	22
282A_10	0.29	5	16	54	0.0588	2.39	0.704	3.21	0.0870	2.14	558	52	538	22	541	27
282A_16	0.27	5	17	60	0.0578	2.02	0.709	2.82	0.0889	1.97	523	44	549	21	544	23
282A_17	0.24	5	15	63	0.0614	1.84	0.755	2.59	0.0892	1.82	654	40	551	19	571	22
282A_21	0.34	4	17	49	0.0608	2.04	0.759	2.78	0.0905	1.89	633	44	559	20	573	24
282A_24	0.31	5	16	54	0.0613	2.51	0.797	3.32	0.0943	2.18	650	54	581	24	595	30
282A_25	0.30	5	15	50	0.0585	2.61	0.762	3.46	0.0945	2.27	549	57	582	25	575	30
282A_22	0.32	5	17	54	0.0607	1.83	0.803	3.10	0.0959	2.50	630	40	590	28	598	28
282A_23	0.30	5	16	53	0.0602	2.26	0.798	3.22	0.0962	2.30	610	49	592	26	596	29
282A_12	0.03	123	37	1278	0.0603	0.94	0.802	1.66	0.0966	1.37	613	20	594	16	598	15
282A_26	0.07	30	23	321	0.0599	1.39	0.805	2.06	0.0975	1.53	600	30	600	17	600	19
282A_28	0.03	121	38	1260	0.0598	0.89	0.807	1.50	0.0980	1.21	595	19	603	14	601	13
282A_11	0.03	96	28	985	0.0588	0.79	0.801	1.62	0.0988	1.41	560	17	608	16	598	15
282A_9	0.20	8	17	84	0.0640	2.04	0.876	3.02	0.0994	2.22	741	43	611	26	639	28
282A_27	0.09	23	20	225	0.0608	1.44	0.846	2.12	0.1010	1.55	632	31	620	18	623	20
282A_31	0.06	35	22	345	0.0606	1.23	0.856	1.85	0.1025	1.38	625	27	629	16	628	17
282A_30	0.44	6	18	41	0.0736	2.05	1.532	3.02	0.1511	2.22	1030	41	907	37	943	36
282A_29	0.35	6	14	40	0.0787	2.23	1.742	3.12	0.1607	2.18	1164	44	960	39	1024	39
282A_14	0.36	7	16	44	0.0762	1.93	1.787	2.49	0.1702	1.57	1100	39	1013	29	1041	32
282A_13	0.37	8	17	45	0.0774	1.62	1.900	2.88	0.1781	2.39	1132	32	1056	46	1081	38
282A_32	0.50	8	23	46	0.0752	1.37	1.851	2.55	0.1786	2.15	1075	27	1059	42	1064	33
282A_15	0.55	12	38	68	0.0793	1.26	1.953	2.25	0.1787	1.87	1179	25	1060	36	1099	30

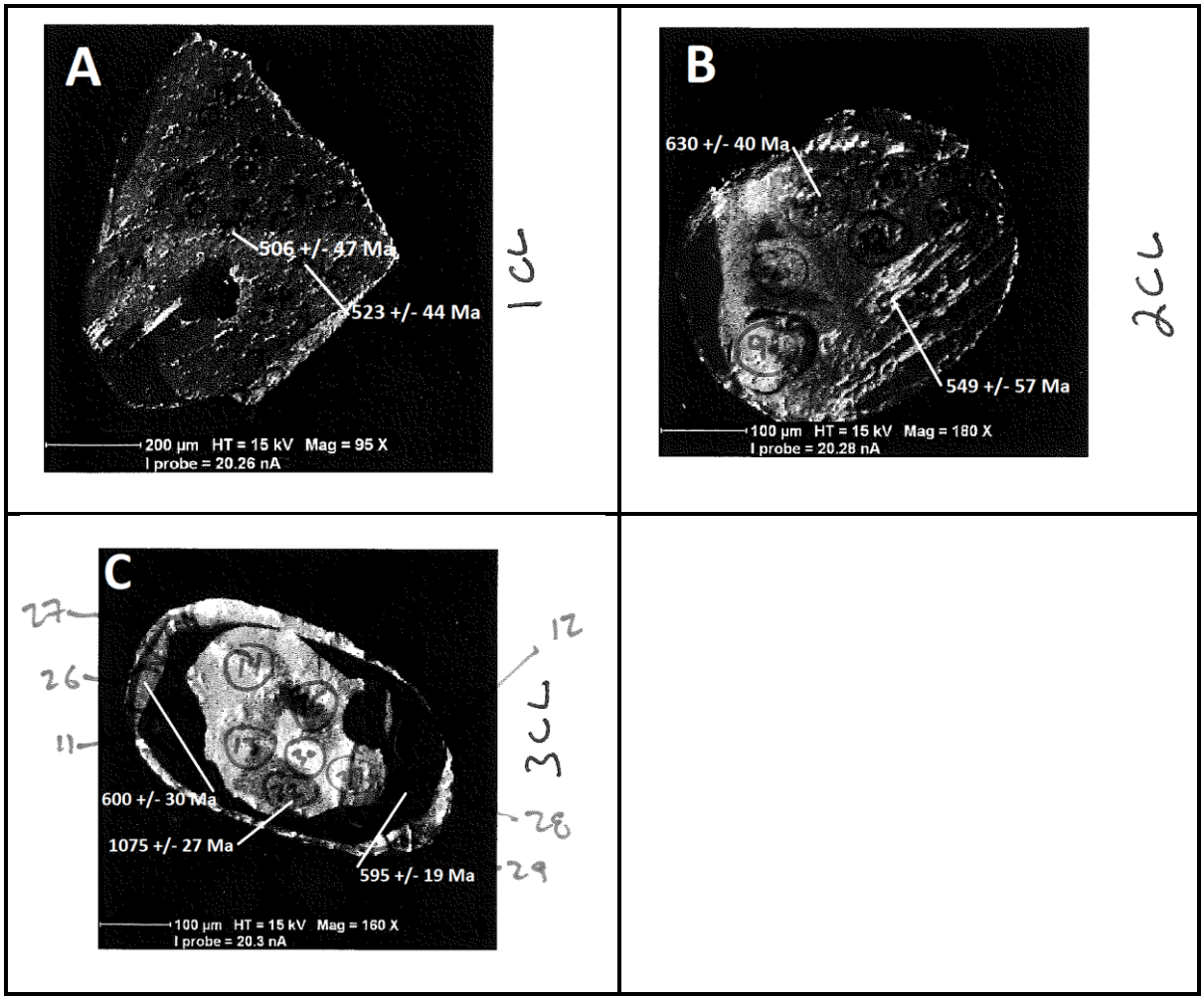

Fig. 5.10: Showing zircon grains from charnockitic gneiss Sample BM282A from southern Malawi.

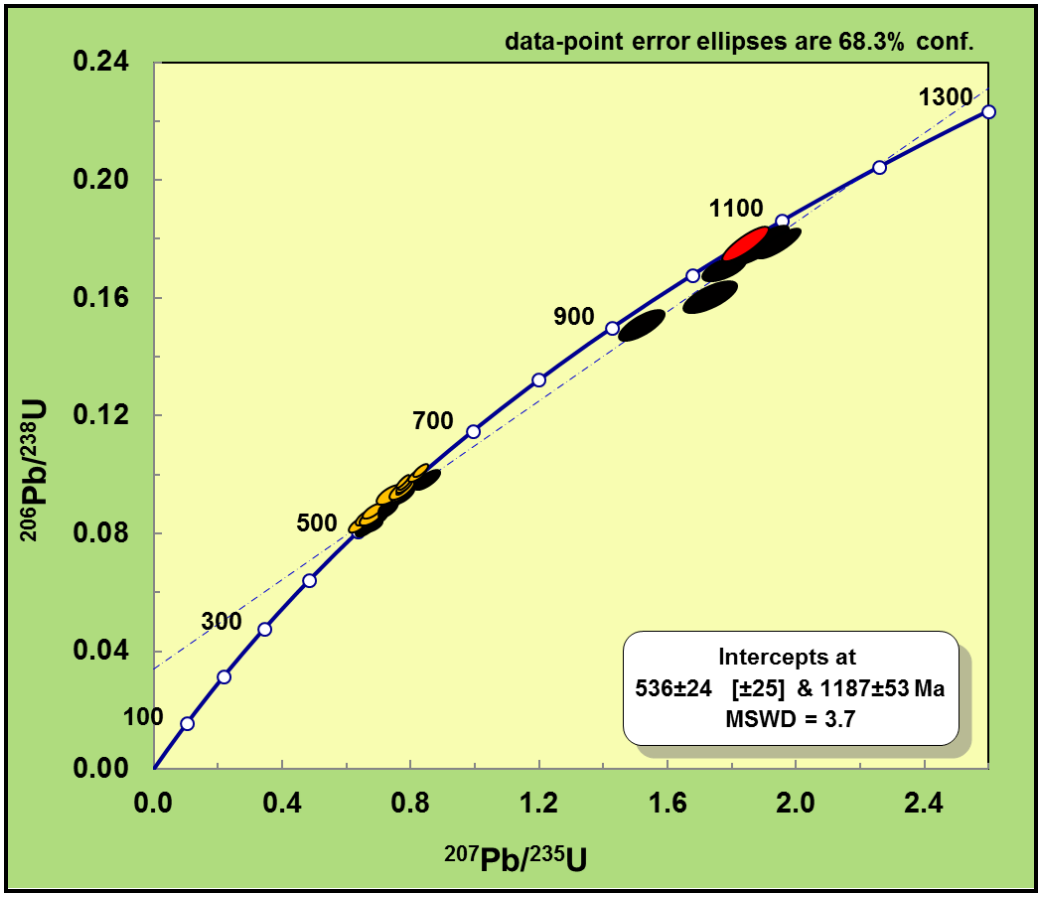

Fig. 5. 11: Concordia plot for zircon grains in charnockitic gneiss Sample BM282A. The red coloured ellipse represents the older concordant population and the yellow ellipses stand for the younger concordant population.

SAMPLE 282B (Refer to Table 5.7 & Figs.5.12 & 5.13)

Sample BM 282B is a leucocratic, medium to coarse grained, well foliated charnockitic granulite. It occurs interbanded with mesocratic charnockitic gneiss and comprised of plagioclase feldspar (50%), quartz (32%), pyroxene (7%), and accessory magnetite and zircon. Three groups of zircons are identified in this sample in BSE and CL images (Fig. 8). In CL images the zircons show variable oval shapes. The first group shows a bright oval core, mantled by a darker phase (Fig. 5.12C). The second type shows a complex core which is composed of a small oval core mantled by brighter phases and a thin dark rim. This complex core has a mantle around with regular oscillatory zoning and then finally a very thin bright rim (Fig. 5.12B). Both groups of zircon are complex xenocrystic. The last group exhibit alternating darker and brighter phases (Fig. 5.12A). Uranium concentrations range from 159 – 2998 ppm. The thorium concentrations range from 22 – 1114 ppm. The Th/U ratios range from 0.12 – 0.52. The zircons are offering conflicting characteristics i.e. rounded edges versus high U concentrations, and therefore not easy to categorise them as magmatic or metamorphic. Eighteen analyses were obtained from these zircons and fourteen were concordant yielding ages <717 Ma. The fourteen concordant analyses yielded a $^{206}Pb/^{238}U$ weighted average age of 573 ± 22 Ma (MSWD = 26, 2 sigma). All analyses yielded disappointing and largely meaningless ages: a $^{206}Pb/^{238}U$ upper intercept age of 700 ± 300 Ma and lower intercept age of 580 ± 99 Ma (MSWD = 3.5, 2 sigma) (Fig. 5.13). The uncertainty and error margins make it impossible to make meaningful interpretation of the ages. However, the $^{206}Pb/^{238}U$ weighted average age and the lower intercept fall within geologically known tectonothermal event of the Mozambique Belt.

Table 5.7: Isotopic analyses for charnockitic gneiss Sample BM282B

		CONCENTRATIONS (ppm)				ISOTOPIC RATIOS					ISOTOPIC AGES				
	Th/U	Pb	Th	U	$^{207}Pb/^{206}Pb$	1s %	$^{207}Pb/^{235}U$	1s %	$^{206}Pb/^{238}U$	1s %	$^{207}Pb/^{206}Pb$	2s abs	$^{206}Pb/^{238}U$	2s abs	$^{207}Pb/^{235}U$	2s abs
SAMPLE SPOT		ppm	ppm	ppm							age		age		age	
282b_01a	0.23	14	36	159	0.0605	1.51	0.727	2.20	0.0872	1.59	621	33	539	16	555	19
282b_01b	0.19	37	81	432	0.0595	1.05	0.684	1.84	0.0834	1.51	586	23	516	15	529	15
282b_02b	0.48	200	824	1700	0.0645	1.09	1.042	1.72	0.1172	1.33	758	23	715	18	725	18
282b_02c	0.52	201	1114	2152	0.0587	0.96	0.743	1.70	0.0919	1.40	554	21	567	15	564	15
282b_03a	0.28	276	829	2996	0.0593	0.95	0.752	1.67	0.0919	1.37	580	21	567	15	569	14
282b_04a	0.12	15	22	178	0.0576	1.22	0.661	1.97	0.0833	1.55	513	27	516	15	515	16
282b_04c	0.18	16	32	176	0.0581	1.23	0.707	1.93	0.0883	1.49	534	27	545	16	543	16
282b_04d	n/a	29	n/a	315	0.0588	1.34	0.742	1.95	0.0915	1.41	560	29	565	15	564	17
282b_04e	n/a	25	n/a	264	0.0582	1.31	0.762	1.97	0.0950	1.47	536	29	585	16	575	17
282b_04f	n/a	27	n/a	280	0.0594	1.07	0.782	1.81	0.0956	1.46	581	23	588	16	587	16
282b_05a	0.32	211	714	2222	0.0583	1.05	0.758	1.80	0.0944	1.46	542	23	581	16	573	16
282b_05b	0.16	230	380	2390	0.0575	1.07	0.760	1.85	0.0958	1.51	512	23	590	17	574	16
282b_05c	n/a	202	n/a	2143	0.0603	0.94	0.777	1.60	0.0935	1.30	614	20	576	14	584	14
282b_06a	0.39	235	972	2495	0.0587	1.00	0.749	1.60	0.0926	1.25	556	22	571	14	568	14
282b_06b	0.33	227	811	2427	0.0581	1.05	0.739	1.67	0.0924	1.30	532	23	570	14	562	14
282b_06b	0.20	180	409	2010	0.0591	0.96	0.734	1.58	0.0901	1.26	572	21	556	13	559	14
282b_07a	0.25	144	369	1492	0.0578	1.08	0.766	1.79	0.0962	1.43	522	24	592	16	578	16
282b_07b	0.31	218	716	2293	0.0587	1.04	0.749	1.69	0.0925	1.33	557	23	570	15	567	15

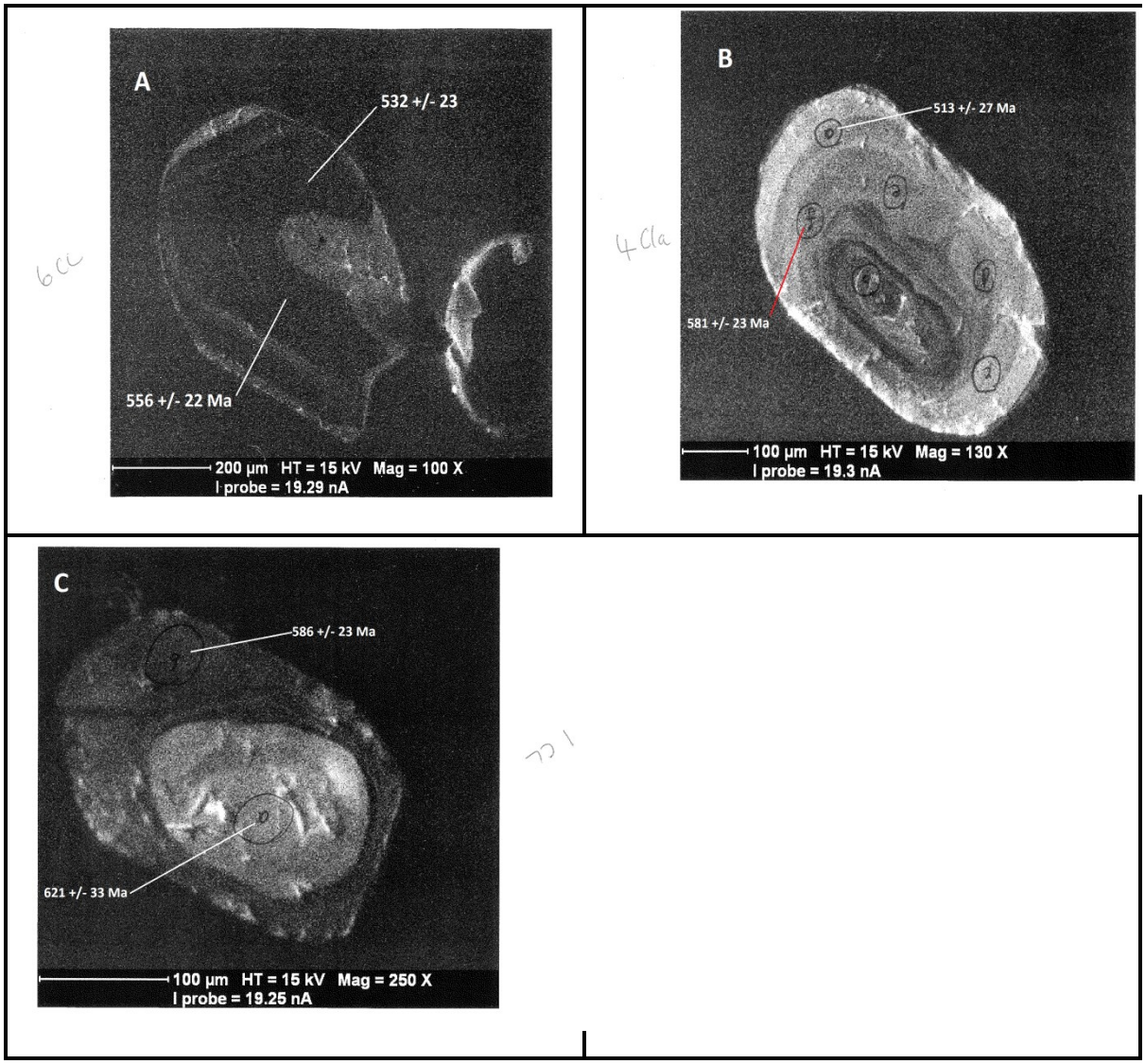

Fig. 5. 12: Representative zircons from charnockitic gneiss Sample BM282B from southern Malawi

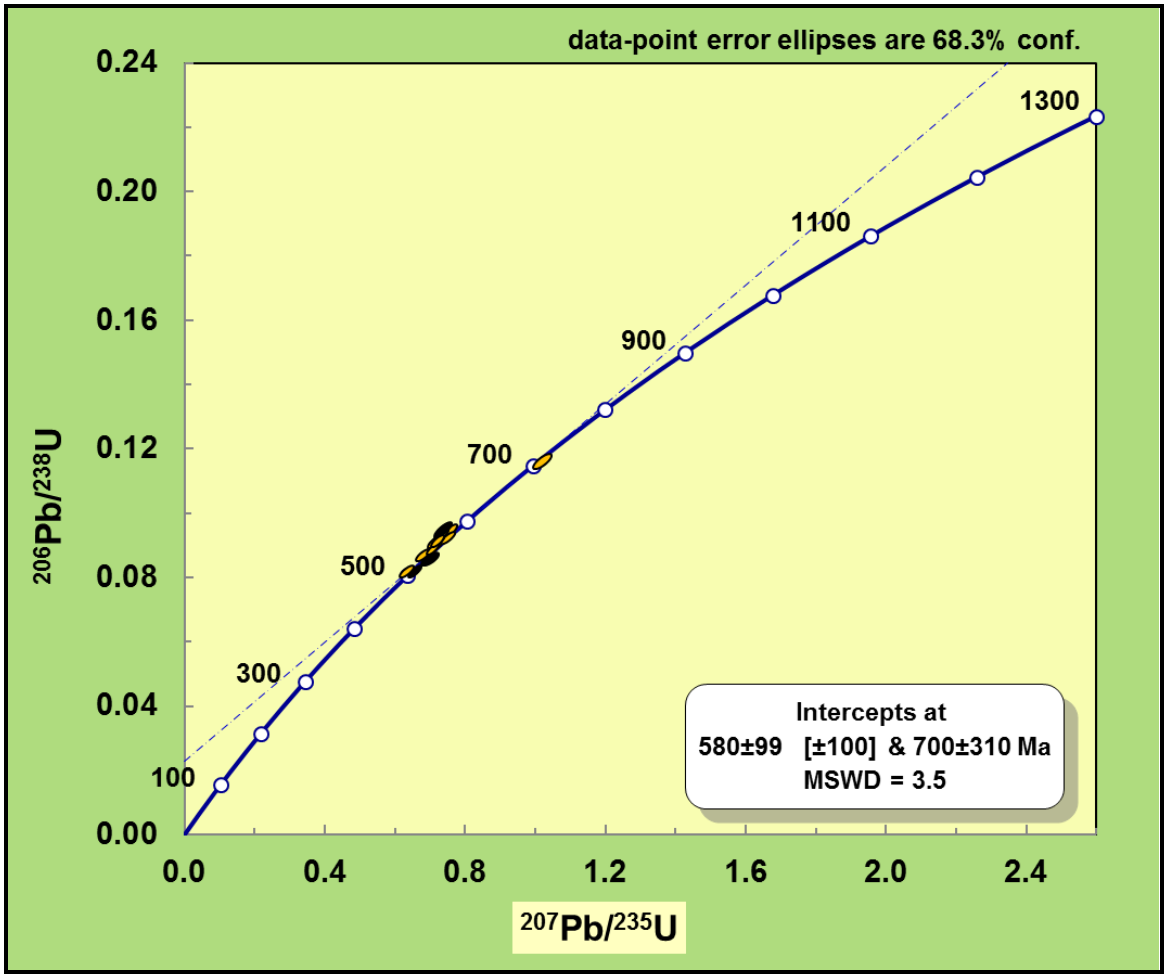

Fig. 5. 13: Concordia plot for zircon grains from charnockitic gneiss Sample BM282B form southern Malawi. The yellow ellipses stand for concordant grain analyses. The black ones are discordant grain analyses.

5.3.2 METAGRANITIC GNEISSES

SAMPLE BM 163 (Refer to Table 5.8 & Figs.5.14 & 5.15)

Sample BM 163 is a coarse grained meta-granodiorite composed of plagioclase feldspar (12%), K-feldspar (19%), quartz (29%), hornblende (20%) biotite (12%) and diopside (5%), with accessory zircon and magnetite. The zircons are transparent and some are yellowish, euhedral and prismatic. They display oscillatory zoning and no inherited cores. Some grains display alternating darker and brighter phases and these are magmatic zircons (Fig. 5.14A & B). The zircons have dark inclusions and overgrowths are seen in some grains. Some are darker and featureless with no oscillatory zoning and these are metamorphic (Fig. 5.14C). The crystals are generally large, greater than 500µ in length and 400µ in width. They have uranium (U) concentrations ranging from 17 to 284 ppm and Th concentrations ranging from 17 – 389 ppm. Th/U ratios range from 1.17 to 2.08. Seventeen spots have U concentrations <100 ppm and seven have >100 ppm. All the twenty four spots have Th/U ratios > 1. Of the 24 analyses obtained eight are concordant. The $^{207}Pb/^{206}Pb$ weighted average for the eight concordant grains is 1039 ± 12 (MSWD = 3.0, 2 sigma). The upper intercept $^{206}Pb/^{238}U$ is 1038 ± 6.8 Ma (MSWD = 1.18, 2 sigma) (Fig. 5.15) and the lower intercept age is – 67 ± 350 Ma. The upper intercept $^{206}Pb/^{238}U$ age which is indistinguishable from the weighted average $^{207}Pb/^{206}Pb$ age is interpreted as the age of emplacement of the metagranite.

Table 5.8: Isotopic analyses for metagranite Sample BM163

	CONCENTRATIONS (ppm)				ISOTOPIC RATIOS						ISOTOPIC AGES (Ma)					
SAMPLE SPOT	Th/U	Pb	Th	U	$^{207}Pb/^{206}Pb$	1s %	$^{207}Pb/^{235}U$	1s %	$^{206}Pb/^{238}U$	1s %	$^{207}Pb/^{206}Pb$	2s abs	$^{206}Pb/^{238}U$	2s abs	$^{207}Pb/^{235}U$	2s abs
		ppm	ppm	ppm							age		age		age	
163_02	1.17	8	20	17	0.0736	1.29	1.805	2.01	0.1779	1.54	1031	26	1055	30	1047	26
163_03	1.27	19	49	39	0.0739	1.01	1.782	1.78	0.1750	1.47	1038	20	1040	28	1039	23
163_04	1.58	16	53	34	0.0751	0.95	1.738	1.58	0.1680	1.26	1070	19	1001	23	1023	20
163_05	1.18	14	32	28	0.0728	1.19	1.770	2.02	0.1765	1.63	1007	24	1048	32	1034	26
163_06	2.08	17	73	35	0.0750	0.89	1.782	1.67	0.1725	1.41	1067	18	1026	27	1039	21
163_07	1.72	15	51	30	0.0739	0.94	1.833	1.64	0.1798	1.35	1040	19	1066	26	1057	21
163_08	1.30	37	98	76	0.0734	0.83	1.791	1.68	0.1770	1.46	1025	17	1051	28	1042	22
163_09	1.44	16	46	32	0.0742	1.02	1.798	1.82	0.1759	1.50	1046	21	1045	29	1045	23
163_10	1.60	105	337	210	0.0736	0.83	1.855	1.52	0.1829	1.28	1030	17	1083	25	1065	20
163_11	1.30	143	369	284	0.0732	0.83	1.802	1.43	0.1786	1.17	1020	17	1059	23	1046	19
163_12	1.35	58	158	117	0.0742	0.64	1.817	1.36	0.1776	1.20	1047	13	1054	23	1051	18
163_13	1.03	78	163	158	0.0731	0.69	1.811	1.44	0.1797	1.26	1017	14	1065	25	1049	19
163_14	1.15	35	82	71	0.0749	0.86	1.812	1.66	0.1756	1.42	1066	17	1043	27	1050	22
163_15	1.25	13	34	27	0.0737	1.23	1.756	1.96	0.1728	1.52	1034	25	1028	29	1029	25
163_16	1.25	36	94	75	0.0745	0.69	1.790	1.50	0.1743	1.33	1055	14	1036	25	1042	19
163_17	2.07	18	85	41	0.0729	0.95	1.604	1.79	0.1597	1.52	1011	19	955	27	972	22
163_18	1.62	12	40	25	0.0743	0.94	1.824	1.87	0.1783	1.62	1048	19	1058	31	1054	24
163_19	1.68	63	219	130	0.0733	0.77	1.763	1.51	0.1745	1.30	1023	16	1037	25	1032	19
163_21	1.89	12	49	26	0.0752	1.13	1.699	1.75	0.1638	1.34	1074	23	978	24	1008	22
163_22	1.21	18	45	37	0.0747	1.05	1.784	1.87	0.1734	1.54	1060	21	1031	29	1040	24
163_23	1.35	29	84	62	0.0735	1.06	1.708	1.66	0.1685	1.27	1028	21	1004	24	1011	21
163_24	1.37	106	294	214	0.0741	0.66	1.839	1.44	0.1801	1.29	1044	13	1068	25	1060	19
163_25	1.38	57	171	124	0.0731	0.80	1.681	1.50	0.1669	1.27	1016	16	995	23	1001	19
163_26	1.38	15	43	31	0.0746	1.09	1.745	1.91	0.1697	1.56	1058	22	1010	29	1025	24

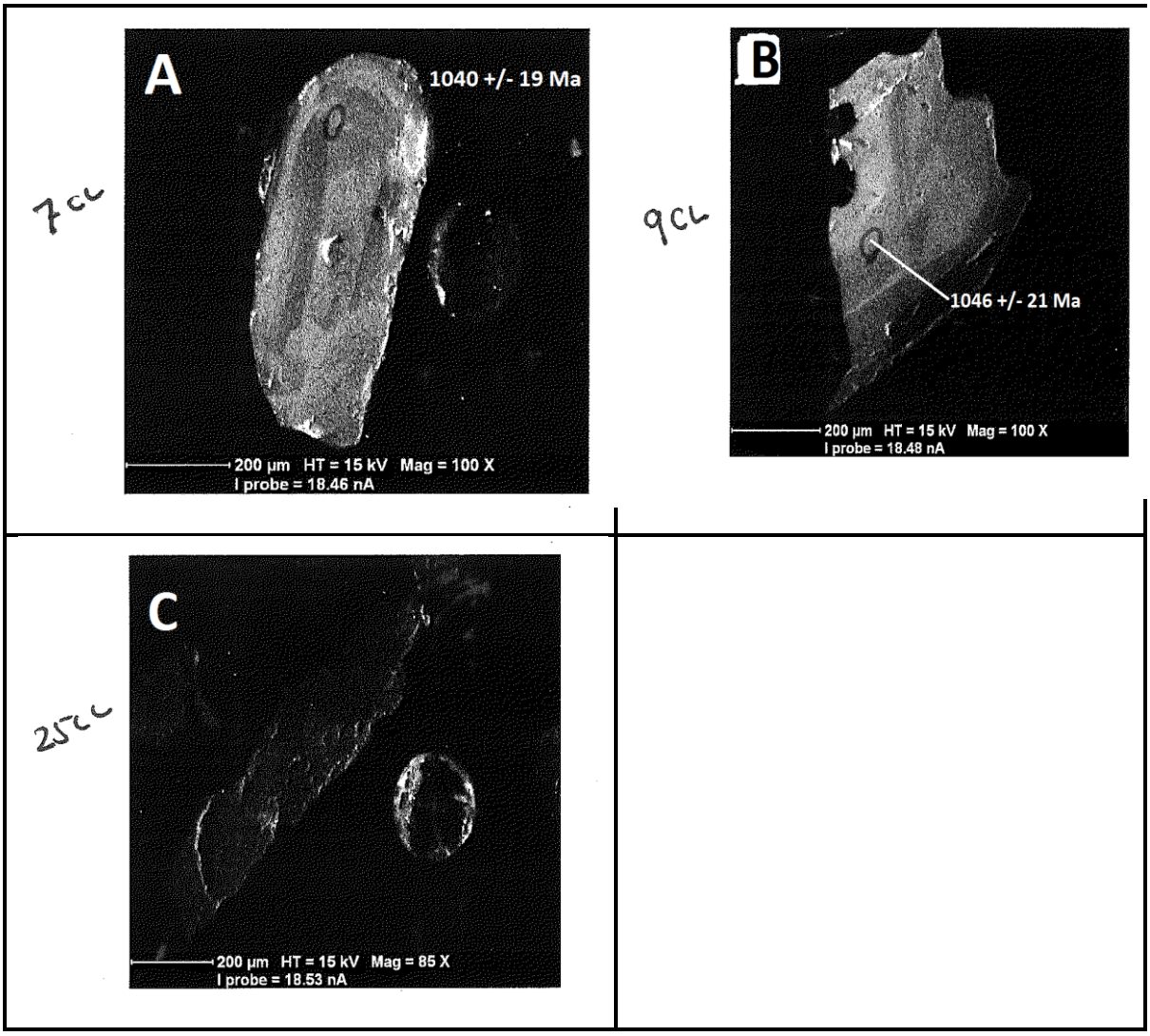

Fig.5.14: Representative zircons from metagranite Sample BM163.

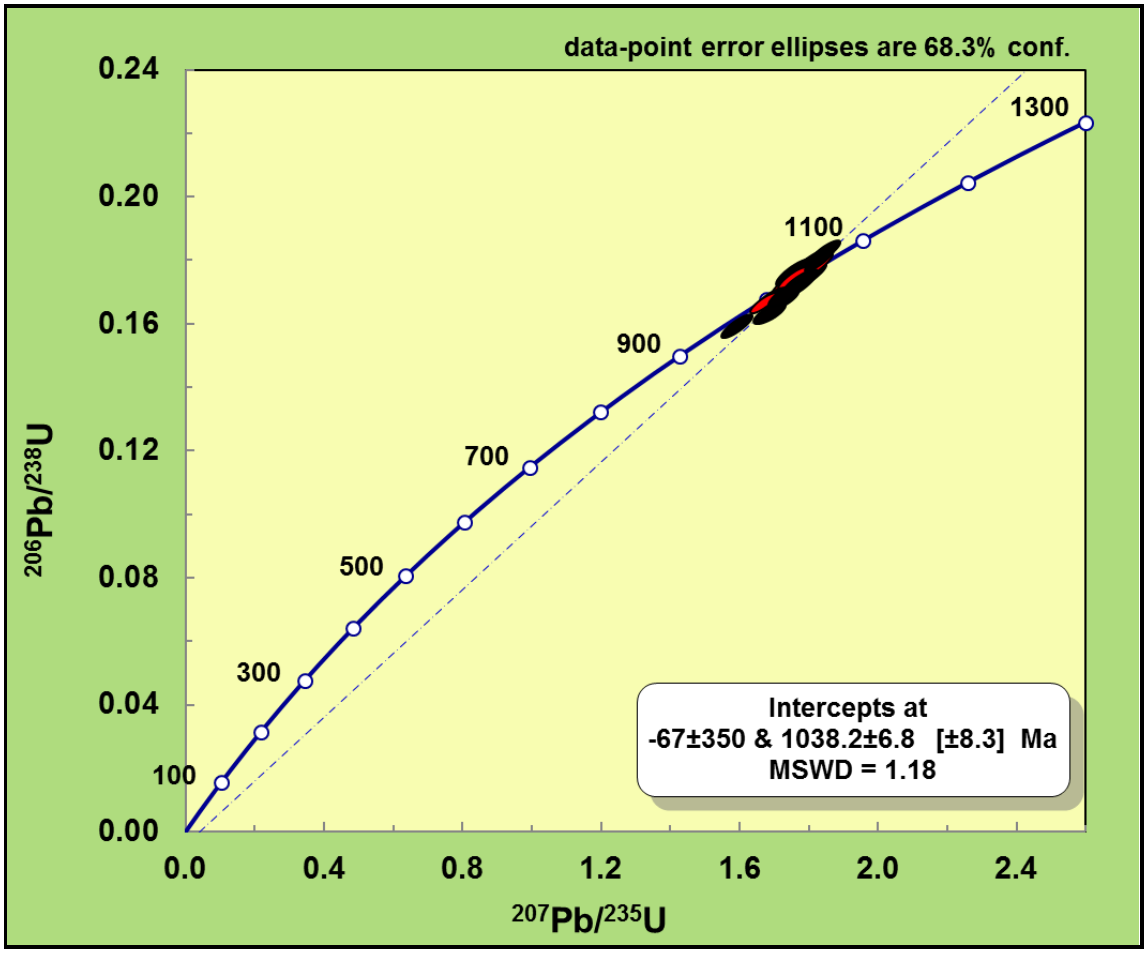

Fig. 5.15: Concordia Plot for analyses obtained from metagranite Sample BM163. Red ellipses represent concordant analyses whilst black ellipses stand for discordant ones.

SAMPLE BM 174 (Refer to Table 5.9 & Figs.5.16 & 5.17)

Sample BM 174 is a leucocratic, coarse grained, foliated metagranite, composed of anhedral quartz (51%), subhedral crystals of plagioclase feldspars(25%) appearing sericitised, hornblende (16%) and brown biotite (6%). Zircons and magnetite occur as accessories. The zircons are a mixture of colourless and yellowish. In CL images zircons in this rock are euhedral and pyramidal and elongate in shape and display typical oscillatory zoning (Fig. 5.16A). Some have dark homogeneous cores enveloped by oscillatory-zoned brighter rims (Fig. 5.16B). They are transparent and commonly showing dark inclusions and generally >250µ in width and up to 600µ in length. Oscillatory zoning is interrupted in places by overgrowths and some zircons have suffered radiation damage. The U concentrations range from 37 – 526 ppm. The thorium concentrations range from 40 – 380 ppm. The Th/U ratios range from 0.52 to 2.92. The oscillatory zoning and Th/U ratios indicate that these zircon grains are magmatogenic. Of the thirty two analyses obtained twelve were concordant and these yielded a $^{207}Pb/^{206}Pb$ weighted mean average of 1029.3 ± 8.0 Ma (MSWD = 3.2, 2 sigma) which is interpreted as the age of emplacement of the metagranite. The analyses yielded an upper intercept $^{206}Pb/^{238}U$ age of 1035.6 ± 8.3 Ma (MSWD 1.2, 2 sigma) (Fig. 5.17) that is indistinguishable from the weighted average $^{207}Pb/^{238}U$ age.

Table 5.9: Isotopic analyses for metagranite Sample BM174

		CONCENTRATIONS (ppm)					ISOTOPIC RATIOS						ISOTOPIC AGES			
	Th/U	Pb	Th	U	$^{207}Pb/^{206}Pb$	1s %	$^{207}Pb/^{235}U$	1s %	$^{206}Pb/^{238}U$	1s %	$^{207}Pb/^{206}Pb$	2s abs	$^{206}Pb/^{238}U$	2s abs	$^{207}Pb/^{235}U$	2s abs
SAMPLE SPOT		ppm	ppm	ppm							age		age		age	
174_01	1.01	40	247	244	0.0731	0.69	1.642	1.32	0.1631	1.13	1016	14	974	20	987	17
174_02	0.52	69	205	397	0.0732	0.60	1.750	1.24	0.1734	1.08	1020	12	1031	21	1027	16
174_04	1.00	28	166	166	0.0738	0.73	1.713	1.47	0.1683	1.28	1037	15	1003	24	1013	19
174_05	0.59	36	125	211	0.0739	0.74	1.740	1.35	0.1709	1.13	1038	15	1017	21	1024	17
174_06	0.58	16	61	104	0.0733	0.78	1.604	1.52	0.1587	1.30	1023	16	950	23	972	19
174_08	0.53	64	198	373	0.0738	0.63	1.747	1.27	0.1717	1.10	1037	13	1022	21	1026	16
174_09	0.97	25	142	147	0.0743	0.85	1.711	1.51	0.1671	1.25	1050	17	996	23	1013	19
174_11	0.74	23	102	138	0.0737	0.81	1.693	1.55	0.1667	1.32	1032	16	994	24	1006	20
174_12	0.54	14	46	85	0.0742	0.99	1.670	1.57	0.1634	1.22	1046	20	976	22	997	20
174_13	0.56	12	40	72	0.0739	0.94	1.691	1.57	0.1660	1.26	1039	19	990	23	1005	20
174_14	1.10	55	357	325	0.0740	0.66	1.748	1.30	0.1713	1.12	1043	13	1019	21	1026	17
174_15	1.06	30	186	175	0.0733	0.66	1.729	1.25	0.1712	1.06	1022	13	1019	20	1020	16
174_17	0.71	23	96	136	0.0736	0.87	1.711	1.43	0.1686	1.14	1031	18	1005	21	1013	18
174_18a	0.56	16	52	93	0.0733	0.88	1.737	1.60	0.1719	1.34	1023	18	1022	25	1022	20
174_18b	0.61	16	66	109	0.0727	0.81	1.450	1.49	0.1447	1.25	1005	16	871	20	910	18
174_19	1.03	29	175	169	0.0746	0.67	1.777	1.45	0.1729	1.29	1057	13	1028	24	1037	19
174_20	0.63	48	174	274	0.0743	0.74	1.800	1.39	0.1758	1.18	1049	15	1044	23	1045	18
174_22	0.53	15	45	86	0.0749	0.80	1.741	1.52	0.1687	1.29	1065	16	1005	24	1024	19
174_23	0.69	16	62	90	0.0729	0.86	1.761	1.58	0.1754	1.33	1010	17	1042	26	1031	20
174_24	0.55	92	289	526	0.0739	0.57	1.775	1.17	0.1743	1.02	1039	12	1036	19	1036	15
174_25	0.67	19	76	113	0.0725	0.69	1.705	1.36	0.1705	1.17	1001	14	1015	22	1010	17
174_26	0.58	13	55	94	0.0730	0.97	1.425	1.69	0.1417	1.39	1013	20	855	22	900	20
174_27	0.66	30	111	169	0.0736	0.72	1.814	1.52	0.1789	1.34	1030	15	1061	26	1051	20
174_28	0.86	22	111	128	0.0734	0.68	1.734	1.36	0.1714	1.18	1026	14	1020	22	1021	17
174_29	0.58	18	59	101	0.0738	0.86	1.766	1.53	0.1736	1.27	1037	17	1032	24	1033	20
174_30	0.75	23	102	135	0.0744	0.73	1.733	1.54	0.1689	1.35	1053	15	1006	25	1021	20
174_31	1.48	111	380	257	0.0715	0.71	1.535	1.38	0.1558	1.18	971	15	934	21	944	17
174_32	2.68	32	185	69	0.0737	0.74	1.687	1.44	0.1661	1.24	1033	15	990	23	1003	18
174_33	1.43	50	162	113	0.0727	0.65	1.574	1.36	0.1570	1.20	1007	13	940	21	960	17
174_34	1.67	17	62	37	0.0729	0.93	1.586	1.60	0.1578	1.30	1012	19	945	23	965	20
174_35	2.92	42	255	87	0.0739	0.77	1.745	1.35	0.1714	1.10	1038	16	1020	21	1025	17
174_36	1.64	30	101	62	0.0734	0.76	1.746	1.39	0.1726	1.16	1025	15	1026	22	1026	18

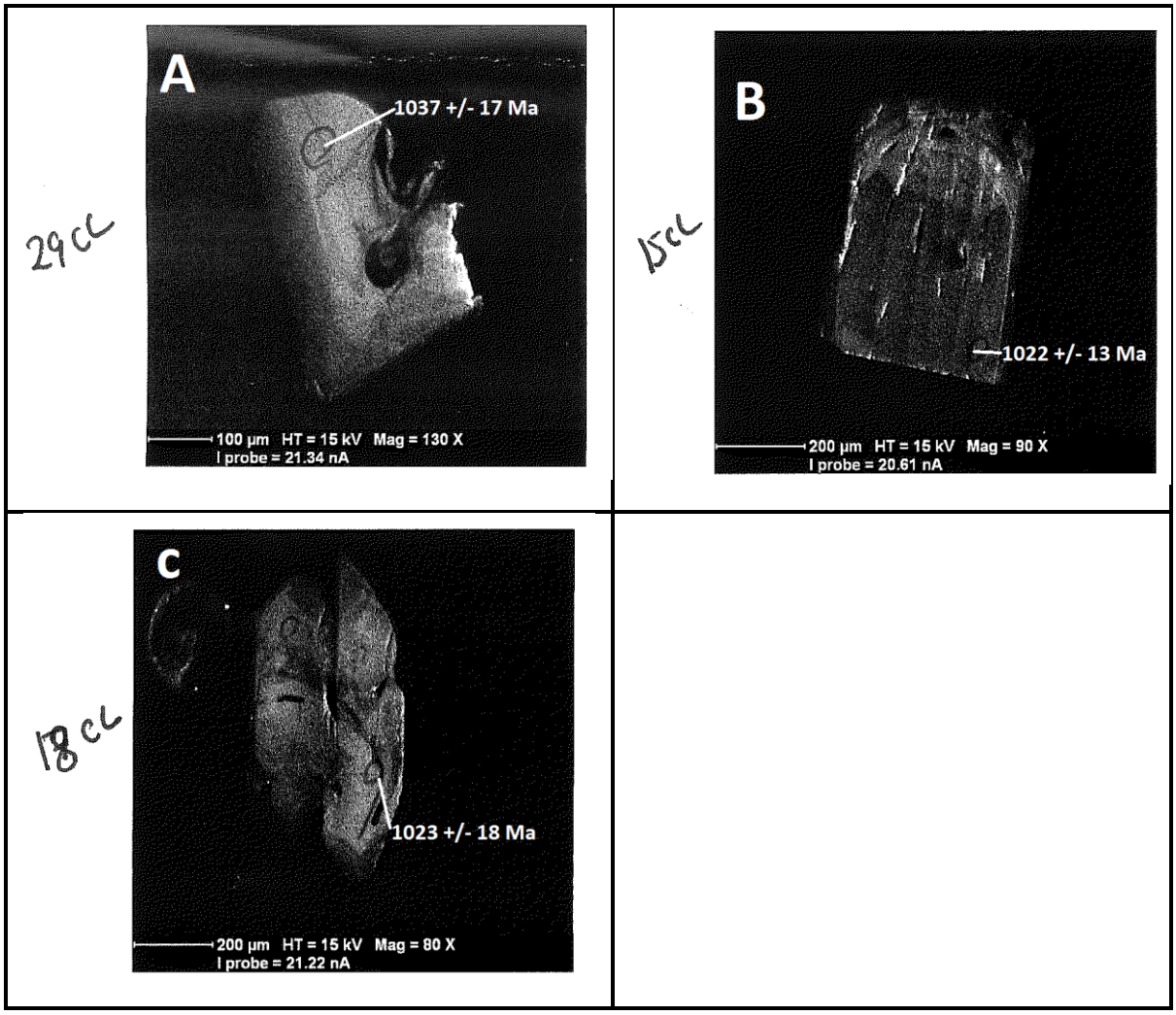

Fig. 5. 16: Showing representative zircon grains from metagranite Sample BM174 from southern Malawi.

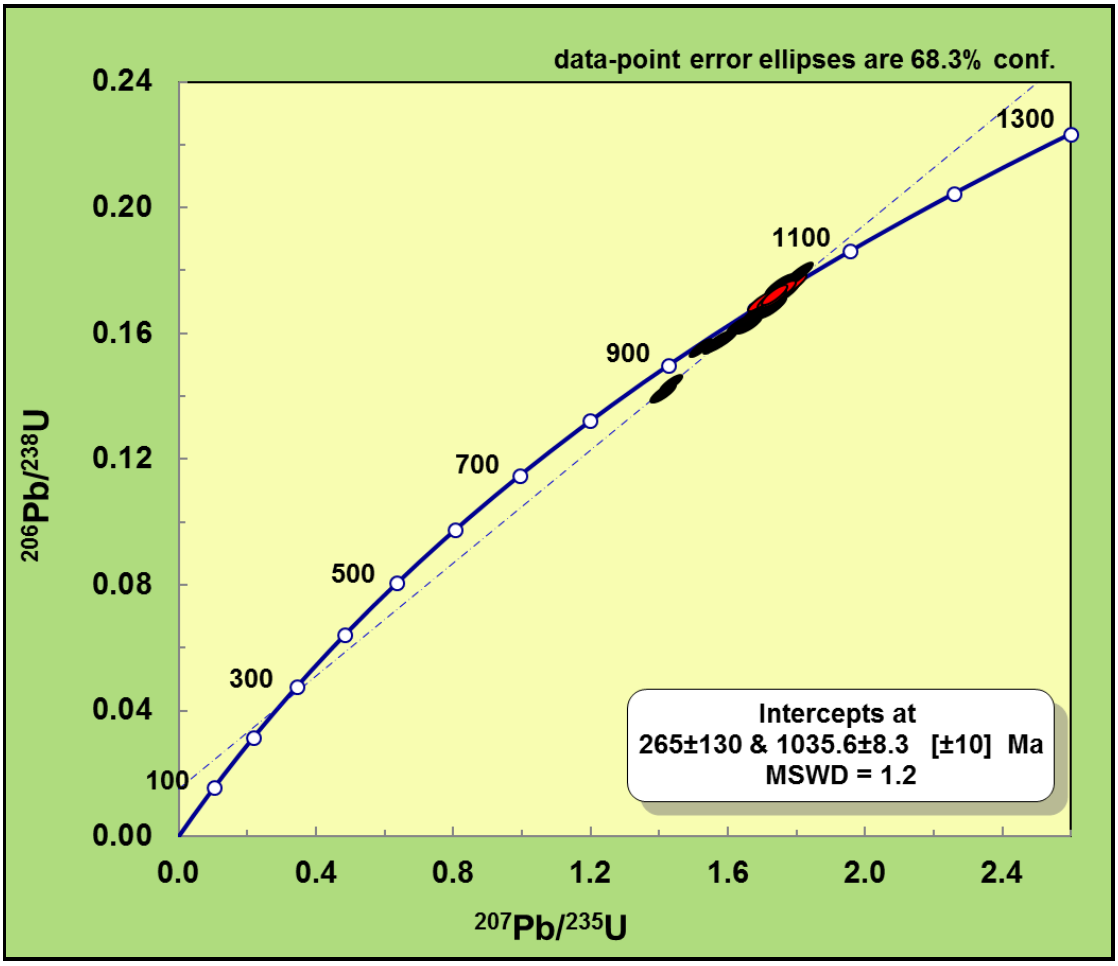

Fig. 5.17: Concordia plot for zircon grain analyses from metagranite Sample BM 174. Red ellipses = Concordant analyses. Black ellipses = Discordant analyses.

SAMPLE BM 179 (Refer to Table 5.10 & Figs. 5.18 & 5.19)

A leucocratic, coarse grained and foliated rock with lamellae twinned plagioclase feldspar (9%), orthoclase (26%), wavy extinction quartz (31%), hornblende (13%) and biotite (12%). Accessory minerals include zircon and magnetite. Zircons separated from this sample are clear and colourless. In CL images they are relatively large (>200µ wide and >600µ in length). They show some dark inclusions, and are euhedral and prismatic in shape. The CL images also show oscillatory zoning (Fig. 5.18). Some of the zircons have a featureless darker core which is inherited and then mantled by an oscillatory zoned phase (Fig. 5.18C). Twenty four analyses were carried out, eight being concordant. Of the eight concordant spots U concentrations range from 76 – 187 ppm and Th ranges from 33 – 86 ppm. Th/U ratios range from 0.44 to 0.57. One of these concordant spots #179_22a has higher uranium and thorium counts than the others and yields a much lower age which would suggest Pb loss and we omit it in the calculation. The $^{207}Pb/^{206}Pb$ weighted average for the other seven grains is 1047 ± 12 Ma, MSWD = 1.4, 2 sigma). This is interpreted as the age of crystallization of the metagranite. An upper intercept $^{206}Pb/^{238}U$ age of 1047 ± 13 Ma (MSWD = 1.01, 2 sigma) (Fig. 5.19) was obtained from the analyses interpreted as the crystallisation age of the metagranite.

Table 5.10: Isotopic analyses for metagranite Sample BM179

		CONCENTRATIONS (ppm)					ISOTOPIC RATIOS						ISOTOPIC AGES			
	Th/U	Pb	Th	U	$^{207}Pb/^{206}Pb$	1s %	$^{207}Pb/^{235}U$	1s %	$^{206}Pb/^{238}U$	1s %	$^{207}Pb/^{206}Pb$	2s abs	$^{206}Pb/^{238}U$	2s abs	$^{207}Pb/^{235}U$	2s abs
SAMPLE SPOT		ppm	ppm	ppm							age		age		age	
179_1	0.60	18	63	105	0.0740	0.94	1.677	1.68	0.1644	1.39	1042	19	981	25	1000	21
179_10	0.55	20	70	128	0.0735	1.05	1.613	1.79	0.1593	1.45	1027	21	953	26	975	22
179_11	0.49	19	55	112	0.0737	0.99	1.695	1.69	0.1668	1.36	1034	20	994	25	1007	21
179_12	0.70	17	72	102	0.0735	1.05	1.681	1.72	0.1660	1.37	1027	21	990	25	1001	22
179_13	0.58	16	56	96	0.0744	1.04	1.695	1.72	0.1652	1.37	1053	21	986	25	1007	22
179_14	0.47	25	66	140	0.0735	0.86	1.808	1.65	0.1785	1.40	1027	17	1059	27	1048	21
179_15	0.43	11	27	62	0.0734	1.47	1.813	2.21	0.1793	1.65	1025	30	1063	32	1050	29
179_19	0.52	20	56	108	0.0743	0.91	1.831	1.76	0.1788	1.51	1050	18	1060	29	1057	23
179_2	0.48	24	67	138	0.0752	0.83	1.729	1.46	0.1668	1.20	1074	17	994	22	1019	19
179_21	0.51	21	60	118	0.0745	1.02	1.823	1.75	0.1774	1.42	1056	20	1053	28	1054	23
179_22a	0.46	31	86	187	0.0717	1.00	1.617	1.89	0.1637	1.61	977	20	977	29	977	23
179_22b	0.44	14	33	76	0.0736	1.08	1.766	1.96	0.1741	1.64	1030	22	1035	31	1033	25
179_23	0.57	14	46	81	0.0741	1.11	1.760	1.93	0.1724	1.58	1044	22	1025	30	1031	25
179_24	0.46	17	45	97	0.0736	1.00	1.767	1.94	0.1741	1.67	1031	20	1035	32	1033	25
179_25	0.53	14	41	77	0.0744	1.25	1.848	2.22	0.1802	1.83	1053	25	1068	36	1063	29
179_26	0.56	14	42	74	0.0748	1.09	1.869	2.29	0.1812	2.01	1064	22	1073	40	1070	30
179_27	0.47	27	67	144	0.0742	0.92	1.844	1.62	0.1804	1.33	1046	19	1069	26	1061	21
179_3	0.50	18	56	111	0.0734	0.96	1.631	1.63	0.1611	1.32	1026	19	963	23	982	20
179_4	0.55	16	61	112	0.0715	1.19	1.369	1.75	0.1389	1.29	972	24	839	20	876	20
179_5	0.60	18	70	117	0.0735	1.06	1.514	1.65	0.1495	1.26	1028	21	898	21	936	20
179_6	0.44	18	47	107	0.0749	0.90	1.725	1.70	0.1671	1.44	1067	18	996	27	1018	22
179_7	0.41	17	46	111	0.0735	1.01	1.528	1.76	0.1510	1.44	1027	21	906	24	942	21
179_8	0.52	21	63	119	0.0744	0.85	1.765	1.65	0.1721	1.41	1052	17	1024	27	1033	21
179_9	0.46	54	148	320	0.0741	0.74	1.699	1.38	0.1665	1.16	1043	15	993	21	1008	17

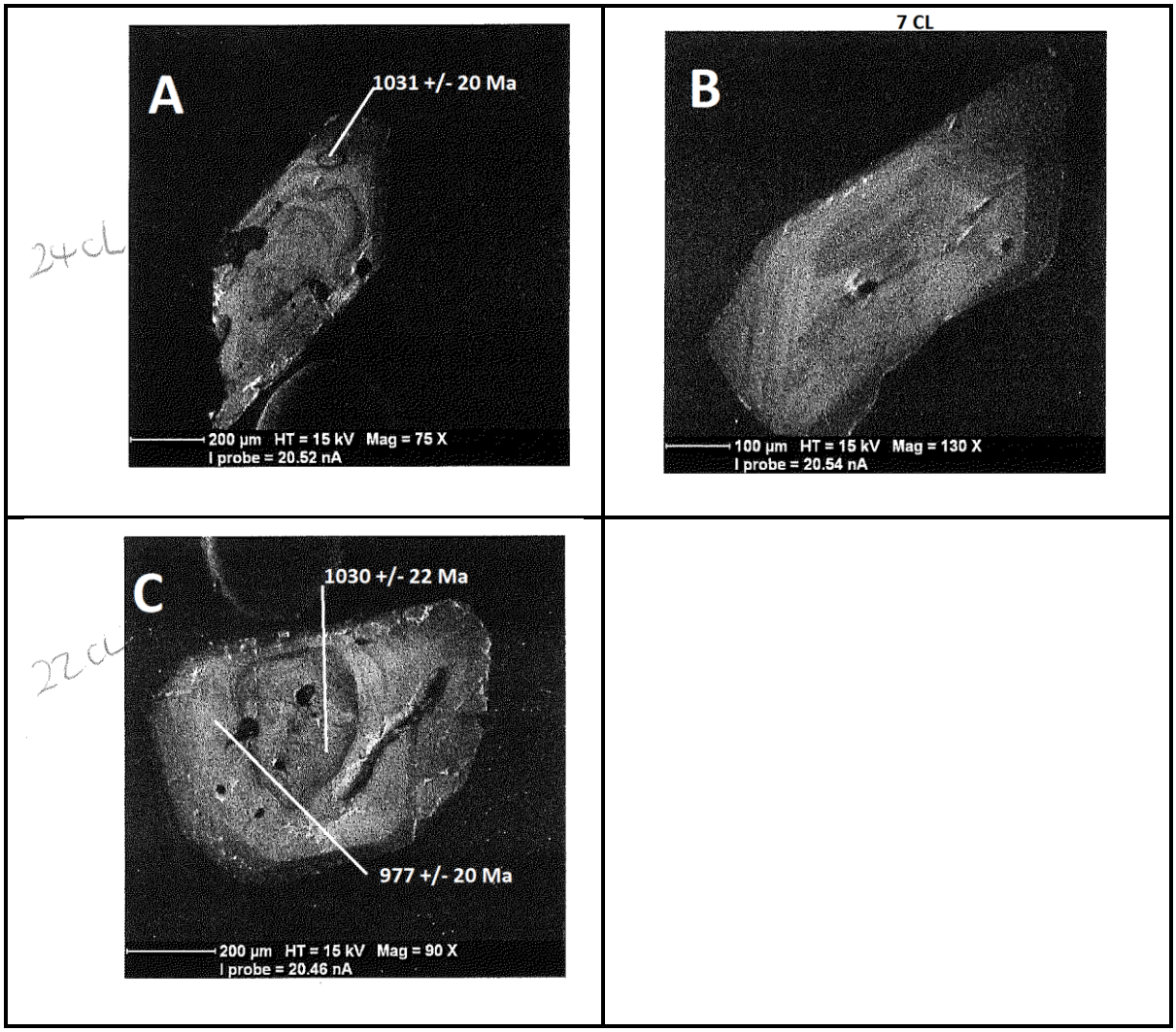

Fig. 5. 18: Representative zircon grains from metagranite Sample BM179 from southern Malawi

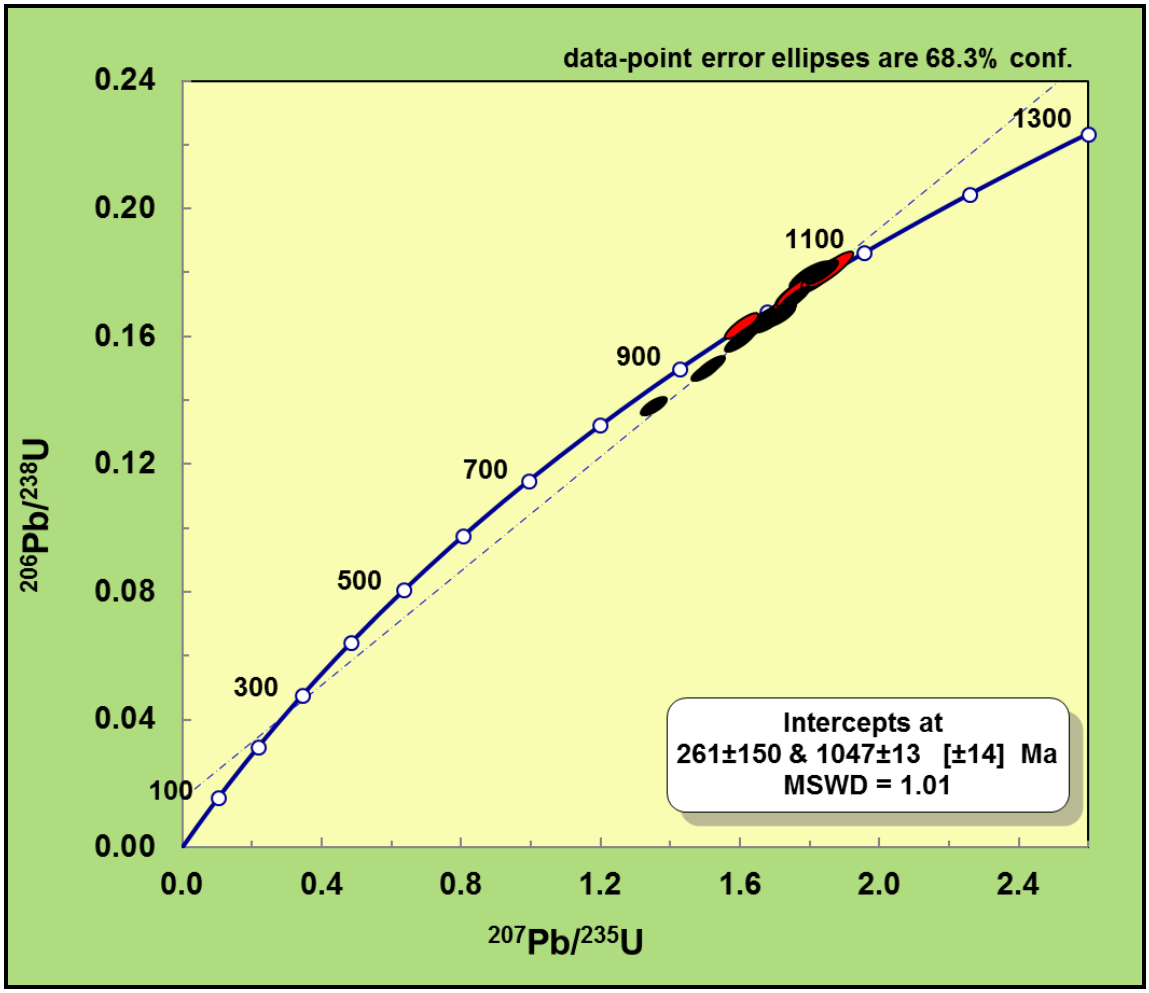

Fig. 5.19: Concordia plot for zircon grain spots from metagranite Sample BM179. Red ellipses = Concordant analyses. Black ellipses = Discordant analyses.

SAMPLE BM 209 (Refer to Table 5.11 & Figs. 5.20 & 5.21)

This is a leucocratic, coarse grained, weakly foliated, metagranite with quartz (33%), plagioclase feldspar (28%), K-feldspar (16%) hornblende (16%), and biotite (7%). Accessories include zircon and magnetite. Zircons separated from the rock are transparent in colour sometimes dirty brown. In CL image (Fig. 5.20) they are >200µ - 250µ in width and >250 µ - 600 µ in length, show euhedral and pyramidal shapes and display oscillatory zoning. They have dark inclusions and some crystals show radiation damage. The zircons are magmatic. Twenty four analyses were obtained and eight were concordant. The U concentrations for the concordant spots range from 74 – 151 ppm whilst Th ranges from 32 – 107 ppm. The Th/U ratios are from 0.39 – 0.71. The eight concordant grains yielded a $^{207}Pb/^{206}Pb$ weighted average age of 1023 ± 21 Ma, MSWD = 5.5, 2 sigma). The analyses yielded an upper intercept $^{206}Pb/^{238}U$ age of 1040 ± 5 Ma (MSWD = 2.1, 2 sigma) (Fig. 5.21) and this is interpreted as the crystallisation age for the metagranite.

Table 5.11: Isotopic analyses for metagranite Sample BM209

		CONCENTRATIONS (ppm)					ISOTOPIC RATIOS						ISOTOPIC AGES			
	Th/U	Pb	Th	U	$^{207}Pb/^{206}Pb$	1s %	$^{207}Pb/^{235}U$	1s %	$^{206}Pb/^{238}U$	1s %	$^{207}Pb/^{206}Pb$	2s abs	$^{206}Pb/^{238}U$	2s abs	$^{207}Pb/^{235}U$	2s abs
SAMPLE SPOT		ppm	ppm	ppm							age		age		age	
209_03	0.44	13	38	87	0.0717	1.10	1.454	1.98	0.1470	1.65	979	22	884	27	911	24
209_04	0.57	14	59	103	0.0714	1.06	1.321	2.17	0.1343	1.89	969	22	812	29	855	25
209_05	0.42	16	38	92	0.0747	0.98	1.764	1.70	0.1712	1.39	1062	20	1019	26	1032	22
209_06a	0.45	15	38	85	0.0751	0.92	1.795	1.73	0.1735	1.47	1071	18	1031	28	1044	22
209_06b	0.57	15	50	88	0.0733	0.99	1.704	1.74	0.1687	1.43	1022	20	1005	27	1010	22
209_06c	0.35	24	48	137	0.0738	0.96	1.689	1.72	0.1662	1.43	1035	19	991	26	1004	22
209_07	0.47	18	52	110	0.0733	1.04	1.623	1.72	0.1606	1.37	1023	21	960	24	979	21
209_08a	0.49	15	49	101	0.0715	1.28	1.466	1.88	0.1488	1.38	971	26	894	23	916	22
209_08b	0.43	13	32	74	0.0728	1.23	1.696	1.90	0.1691	1.45	1008	25	1007	27	1007	24
209_09	0.42	13	41	97	0.0752	1.52	1.409	2.12	0.1358	1.48	1075	31	821	23	893	25
209_10	0.71	27	107	151	0.0740	0.95	1.762	1.57	0.1728	1.25	1041	19	1027	24	1031	20
209_11	0.39	17	38	97	0.0725	1.05	1.682	1.66	0.1684	1.29	999	21	1003	24	1002	21
209_12	0.44	13	32	72	0.0743	1.11	1.786	1.81	0.1744	1.43	1050	22	1036	27	1040	23
209_13a	0.60	11	55	93	0.0665	1.08	1.088	1.91	0.1187	1.58	821	23	723	22	747	20
209_13b	0.52	12	35	68	0.0751	1.14	1.796	1.92	0.1736	1.55	1070	23	1032	29	1044	25
209_14	0.37	16	36	98	0.0718	1.10	1.513	1.81	0.1529	1.44	980	22	917	25	936	22
209_15	0.44	15	37	86	0.0732	1.13	1.693	1.84	0.1678	1.46	1020	23	1000	27	1006	23
209_16	0.60	17	64	106	0.0733	0.94	1.561	1.78	0.1545	1.51	1023	19	926	26	955	22
209_17	0.47	14	35	75	0.0729	1.15	1.806	1.86	0.1797	1.46	1012	23	1066	29	1048	24
209_18	0.46	15	41	89	0.0716	1.17	1.577	2.00	0.1599	1.63	974	24	956	29	961	25
209_20a	0.69	16	60	87	0.0728	1.06	1.806	1.69	0.1799	1.32	1010	21	1066	26	1048	22
209_20b	0.54	14	42	78	0.0742	0.97	1.792	1.78	0.1753	1.49	1046	20	1041	29	1042	23
209_21	0.42	15	38	89	0.0724	0.93	1.610	1.80	0.1614	1.54	997	19	965	27	974	22
209_22	0.44	14	36	82	0.0744	1.09	1.681	1.74	0.1639	1.36	1052	22	979	25	1001	22

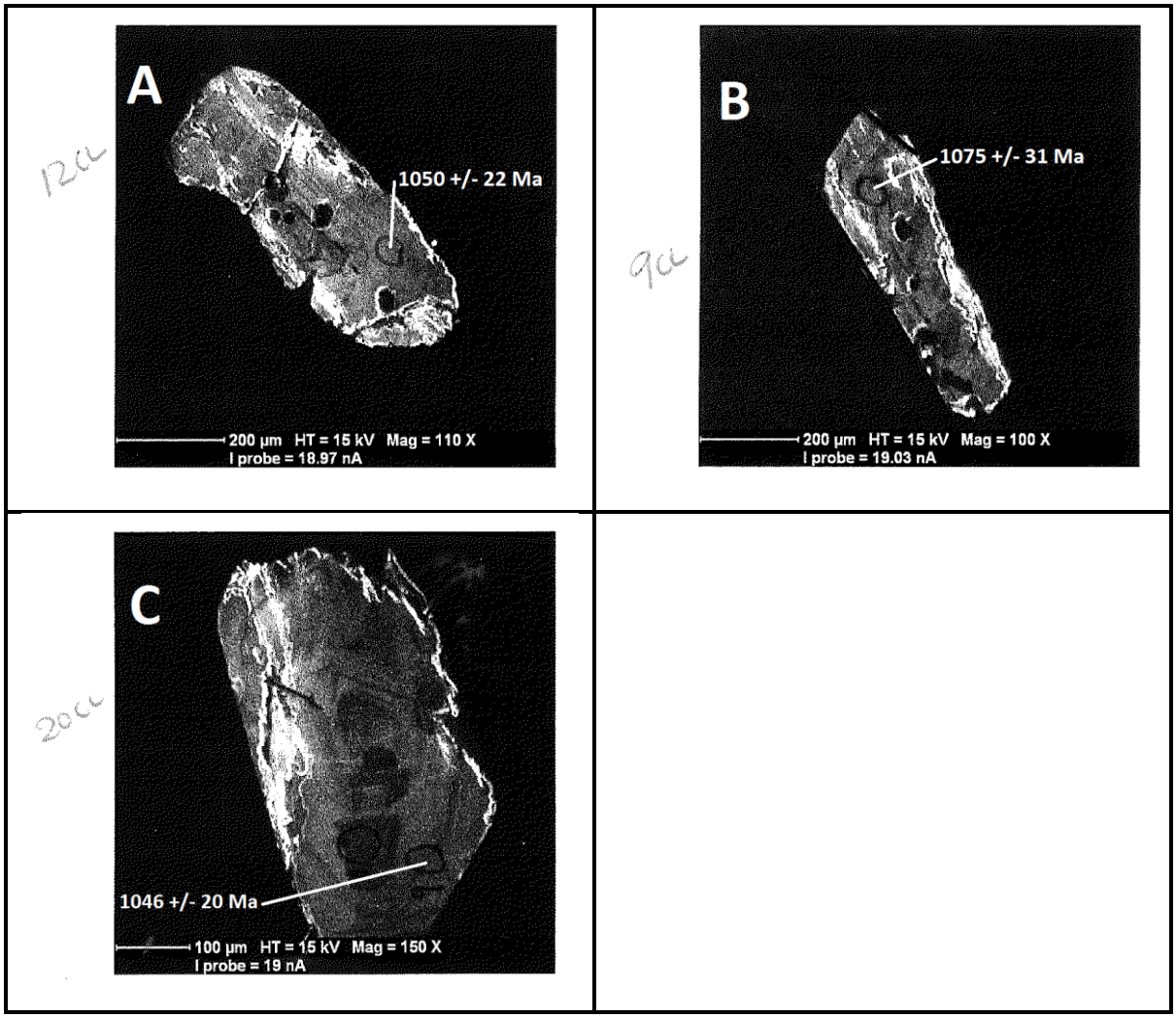

Fig. 5.20: Representative zircon grains for metagranite Sample BM209 from southern Malawi

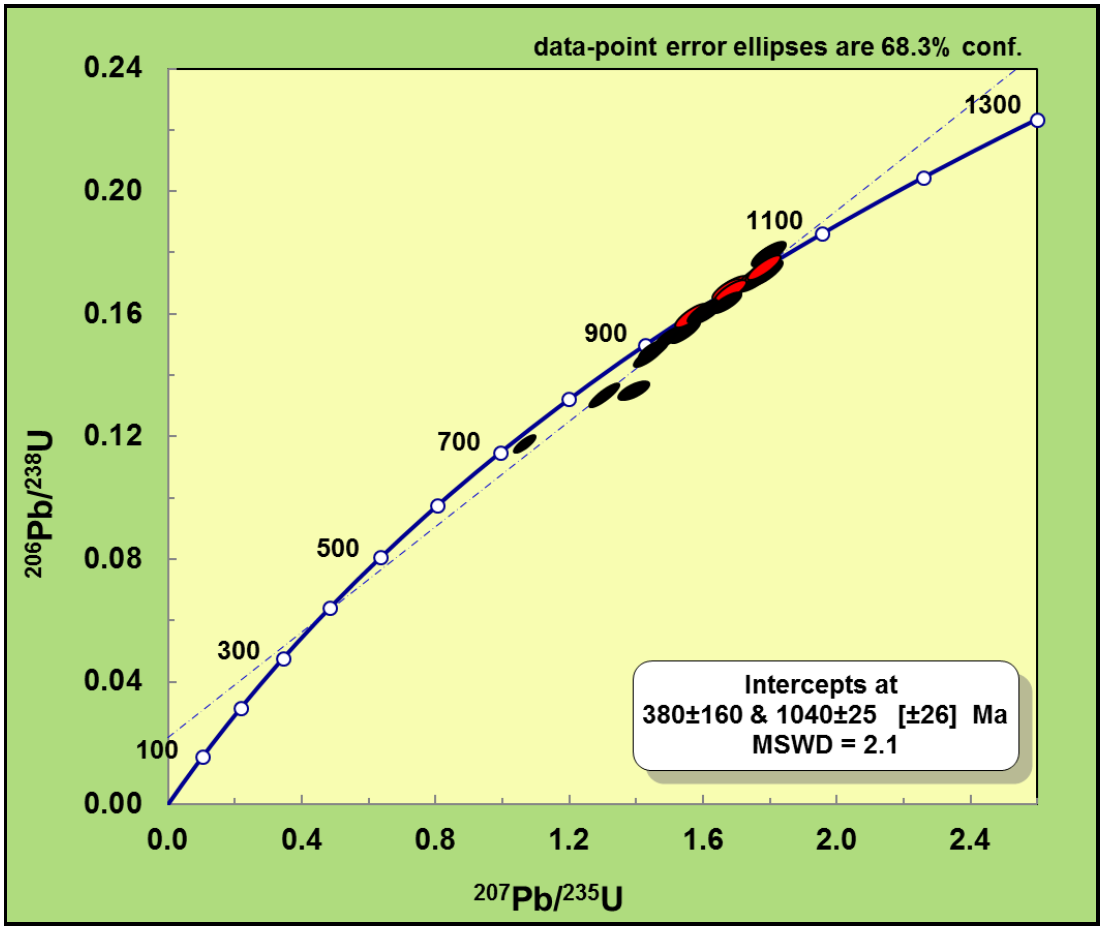

Fig. 5. 21: Concordia plot for zircon grain analyses for metagranite Sample BM209 from southern Malawi. Red ellipses = Concordant grain analyses. Black ellipses = Discordant analyses.

SAMPLE BM 213G (Refer to Table 5.12 & Figs. 5.22 & 5.23)

Sample BM 213G is coarse grained, leucocratic, weakly foliated metagranite. It comprises of anhedral quartz crystals with undulose extinction (30%), plagioclase feldspar with typical lamellae twinning (27%), hornblende (18%) biotite (13%) and accessory zircon, magnetite and ilmenite. Colourless zircons with black inclusions were separated from this sample. In CL images the zircons are euhedral and pyramidal in shape some with widths >250µ - 400µ and the lengths are typically >250 µ - 600 µ. They show oscillatory zoning and some display inherited cores (Fig. 5.22A). Dark inclusions are present and some grains show evidence of radiation damage. U concentrations range from 73 – 393 ppm whilst Th ranges from 32 to 187 ppm. The Th/U ratios range from 0.36 – 0.69. Twenty five analyses were obtained, with one concordant (#213G_23). The concordant grain yielded a $^{207}Pb/^{206}Pb$ age of 1035 ± 21 Ma. This age is interpreted as the age of emplacement of the meta-granite. The analyses yielded an upper intercept $^{206}Pb/^{238}U$ age of 1088 ± 23 Ma (MSWD = 1.5, 2 sigma) (Fig. 5.23) that is interpreted as the age of inheritance.

Table 5.12: Isotopic analyses for metagranite Sample BM213G

	CONCENTRATIONS (ppm)				ISOTOPIC RATIOS						ISOTOPIC AGES					
	Th/U	Pb	Th	U	$^{207}Pb/^{206}Pb$	1s %	$^{207}Pb/^{235}U$	1s %	$^{206}Pb/^{238}U$	1s %	$^{207}Pb/^{206}Pb$	2s abs	$^{206}Pb/^{238}U$	2s abs	$^{207}Pb/^{235}U$	2s abs
SAMPLE SPOT		ppm	ppm	ppm							age		age		age	
213G_02	0.48	15	41	87	0.0750	0.89	1.713	1.68	0.1656	1.43	1070	18	988	26	1013	21
213G_03	0.55	19	67	123	0.0743	0.87	1.593	1.54	0.1556	1.27	1049	17	932	22	967	19
213G_04	0.46	13	34	73	0.0743	0.94	1.735	1.72	0.1694	1.43	1051	19	1009	27	1022	22
213G_05	0.55	15	52	95	0.0733	1.21	1.571	1.88	0.1555	1.43	1023	25	932	25	959	23
213G_07	0.48	68	187	393	0.0747	0.76	1.742	1.46	0.1692	1.24	1061	15	1008	23	1024	19
213G_08	0.42	16	39	92	0.0740	0.98	1.728	1.76	0.1694	1.46	1041	20	1009	27	1019	22
213G_09	0.58	26	85	147	0.0749	0.85	1.776	1.46	0.1719	1.18	1067	17	1023	22	1037	19
213G_10	0.69	15	75	107	0.0723	0.99	1.404	1.73	0.1409	1.42	996	20	849	23	891	20
213G_11	0.47	18	48	101	0.0752	1.51	1.796	2.29	0.1733	1.72	1074	30	1030	33	1044	29
213G_12	0.54	14	47	87	0.0744	1.16	1.658	1.79	0.1618	1.37	1052	23	967	25	993	22
213G_13	0.56	18	58	103	0.0751	0.85	1.762	1.62	0.1701	1.38	1072	17	1013	26	1032	21
213G_14	0.43	12	32	75	0.0728	1.10	1.627	1.73	0.1623	1.34	1007	22	969	24	981	22
213G_15	0.60	21	74	122	0.0752	0.84	1.777	1.51	0.1716	1.25	1073	17	1021	24	1037	19
213G_16	0.48	21	63	130	0.0746	1.05	1.654	1.60	0.1608	1.20	1059	21	961	21	991	20
213G_18	0.58	20	69	119	0.0733	0.90	1.648	1.61	0.1631	1.34	1022	18	974	24	989	20
213G_19	0.36	27	72	200	0.0713	0.80	1.316	1.36	0.1339	1.10	967	16	810	17	853	16
213G_20	0.42	14	35	83	0.0743	1.14	1.712	1.98	0.1671	1.61	1050	23	996	30	1013	25
213G_21	0.49	16	49	99	0.0735	1.00	1.574	1.64	0.1554	1.29	1028	20	931	22	960	20
213G_22	0.45	15	42	94	0.0722	0.95	1.609	1.71	0.1618	1.42	991	19	967	26	974	21
213G_23	0.53	16	47	88	0.0738	1.04	1.791	1.63	0.1761	1.26	1035	21	1046	24	1042	21
213G_24	0.53	20	62	116	0.0743	0.95	1.744	1.59	0.1703	1.28	1051	19	1014	24	1025	20
213G_25	0.60	21	73	120	0.0742	0.86	1.738	1.53	0.1699	1.26	1048	17	1011	24	1023	19
213G_27	0.67	12	56	84	0.0703	1.02	1.416	1.61	0.1462	1.24	937	21	879	20	896	19
213G_31	0.47	15	42	89	0.0752	0.91	1.710	1.71	0.1650	1.45	1074	18	984	26	1012	22

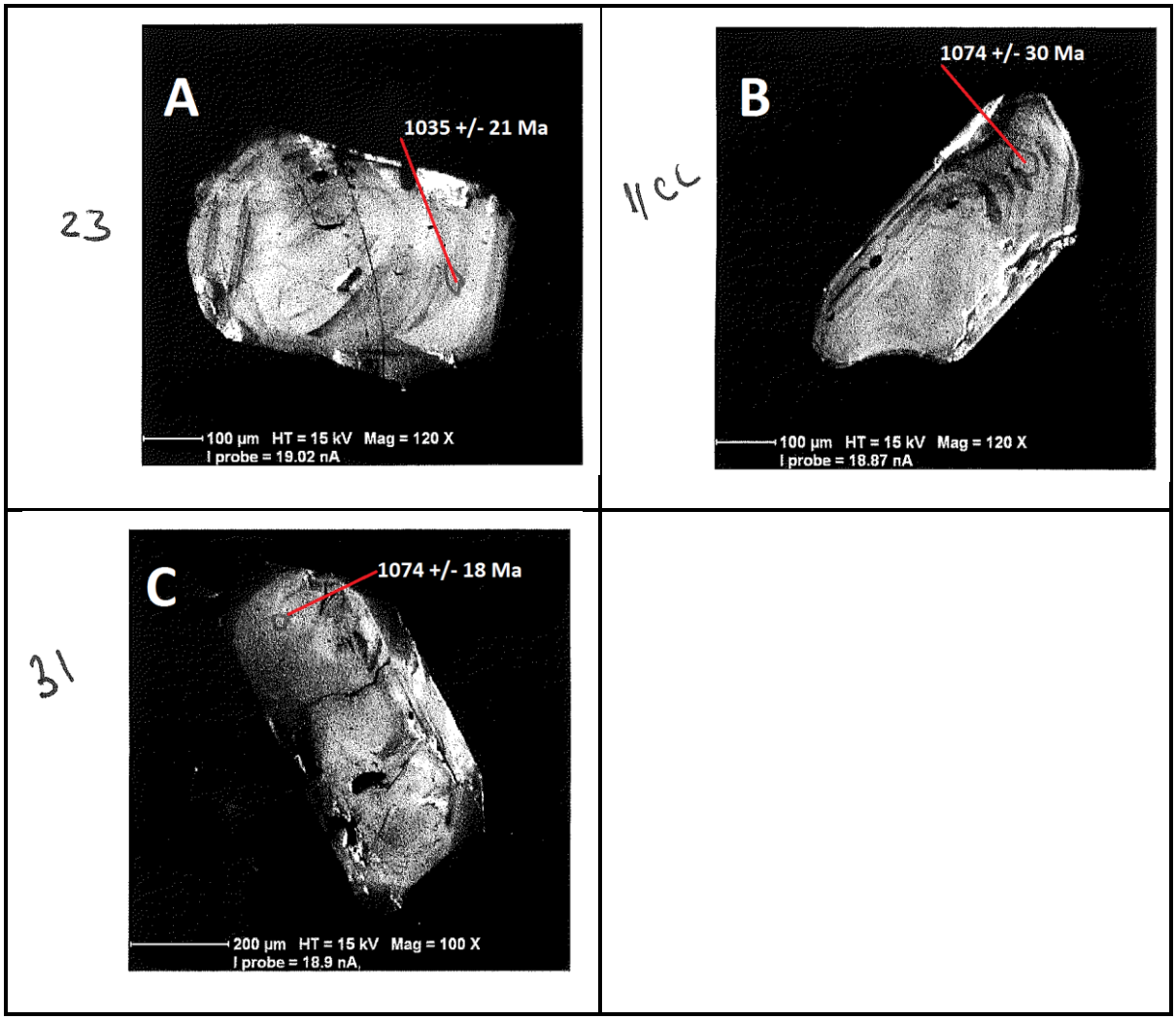

Fig. 5.22: Representative zircons from metagranite Sample BM215G showing inherited grain (A) and oscillatory zoning in magmatic zircons (B & C)

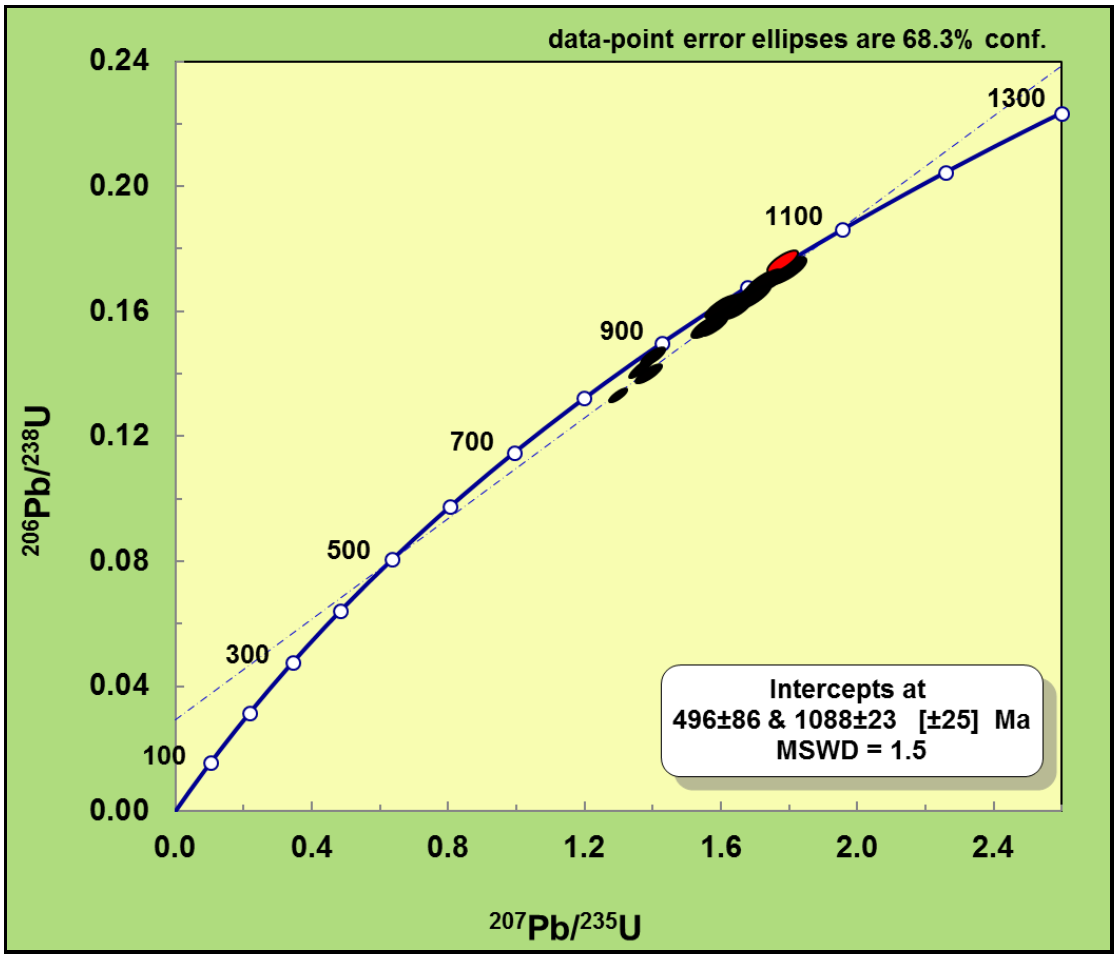

Fig. 5. 23: Concordia plot for zircon grain analyses from metagranite Sample BM213G. Red ellipses = Concordant analyses. Black ellipses = Discordant analyses.

SAMPLE BM 213X (Refer to Table 5.13 & Figs.5.24 & 5.25)

Sample BM 213X is a fine to medium grained, mesocratic mafic enclave with some foliation. It is an enclave in metagranite (sample BM213G) and comprise of plagioclase feldspar (14%), quartz crystals with undulose extinction (39%), K-feldspar (7%), hornblende (7%), biotite (18%), pyroxene (14%) and accessory zircon, magnetite and ilmenite. In CL images the zircons are subhedral and somewhat pyramidal, some with widths of 200 µ and lengths typically >250 µ - 400 µ. They show dark inclusions and appear damaged. Some crystals show inherited cores with oscillatory zoning. Twenty four analyses were obtained of which twelve were concordant. U concentrations for the concordant spots range from 86 – 430 ppm whilst Th ranges from 39 to 315 ppm. The Th/U ratios range from 0.42 – 0.79. The $^{207}Pb/^{206}Pb$ weighted average for the concordant grains is 1023 ± 15 Ma, (MSWD = 5.5, 2 sigma), interpreted as the crystallization age. The analyses yielded an upper intercept $^{206}Pb/^{238}U$ age of 1034 ± 17 Ma (MSWD = 1.08, 2 sigma) (Fig 5.25) which is interpreted as the inheritance age.

Table 5.13: Isotopic analyses for metagranite enclave Sample BM213X

		CONCENTRATIONS (ppm)				ISOTOPIC RATIOS						ISOTOPIC AGES				
	Th/U	Pb	Th	U	$^{207}Pb/^{206}Pb$	1s %	$^{207}Pb/^{235}U$	1s %	$^{206}Pb/^{238}U$	1s %	$^{207}Pb/^{206}Pb$	2s abs	$^{206}Pb/^{238}U$ age	2s abs	$^{207}Pb/^{235}U$ age	2s abs
SAMPLE SPOT		ppm	ppm	ppm							age					
213X_01	0.52	23	67	127	0.0739	0.86	1.789	1.38	0.1757	1.08	1038	17	1043	21	1041	18
213X_02	0.51	18	49	97	0.0746	1.08	1.803	1.81	0.1755	1.45	1057	22	1042	28	1046	23
213X_03	0.50	15	46	91	0.0735	0.98	1.664	1.66	0.1643	1.34	1027	20	981	24	995	21
213X_04	0.59	27	90	151	0.0744	1.03	1.777	1.64	0.1732	1.27	1053	21	1030	24	1037	21
213X_05a	0.44	18	46	105	0.0729	1.07	1.739	1.83	0.1731	1.49	1011	22	1029	28	1023	23
213X_05b	0.46	14	40	86	0.0726	1.02	1.672	1.71	0.1671	1.37	1004	21	996	25	998	21
213X_06	0.73	76	315	430	0.0731	1.01	1.731	1.68	0.1718	1.35	1017	20	1022	25	1020	21
213X_07a	0.69	65	257	372	0.0741	0.86	1.745	1.48	0.1709	1.21	1044	17	1017	23	1025	19
213X_07b	0.55	37	115	207	0.0745	1.02	1.806	1.69	0.1759	1.35	1056	20	1044	26	1048	22
213X_08	0.56	43	141	251	0.0721	0.88	1.691	1.57	0.1703	1.30	987	18	1014	24	1005	20
213X_09	0.42	17	39	92	0.0739	1.10	1.807	1.75	0.1774	1.36	1040	22	1053	26	1048	23
213X_10a	0.85	165	792	928	0.0733	1.05	1.778	1.62	0.1761	1.23	1021	21	1046	24	1037	21
213X_10b	0.79	46	208	263	0.0727	1.21	1.731	1.81	0.1727	1.34	1007	25	1027	25	1020	23
213X_12	0.57	59	187	329	0.0737	0.75	1.784	1.39	0.1756	1.16	1034	15	1043	22	1040	18
213X_13a	0.51	22	65	127	0.0731	0.99	1.709	1.66	0.1697	1.33	1016	20	1010	25	1012	21
213X_13b	0.42	17	44	106	0.0737	0.96	1.609	1.61	0.1584	1.29	1033	19	948	23	974	20
213X_14a	0.74	19	83	112	0.0739	1.02	1.698	1.75	0.1668	1.43	1038	20	994	26	1008	22
213X_14b	0.49	13	38	78	0.0734	1.27	1.615	1.75	0.1596	1.21	1026	26	955	21	976	22
213X_15a	0.60	40	142	235	0.0732	0.96	1.724	1.61	0.1708	1.30	1021	19	1017	24	1018	21
213X_15b	0.45	16	43	94	0.0751	1.17	1.760	1.83	0.1701	1.41	1070	24	1013	26	1031	23
213X_16a	0.66	28	111	168	0.0715	0.97	1.597	1.62	0.1620	1.30	972	20	968	23	969	20
213X_16b	0.45	19	52	116	0.0720	1.14	1.593	1.70	0.1604	1.26	987	23	959	22	967	21
213X_18a	0.62	17	72	116	0.0703	1.31	1.377	1.89	0.1421	1.37	938	27	856	22	879	22
213X_28b	0.52	15	46	88	0.0738	0.98	1.716	1.78	0.1687	1.48	1036	20	1005	27	1015	23

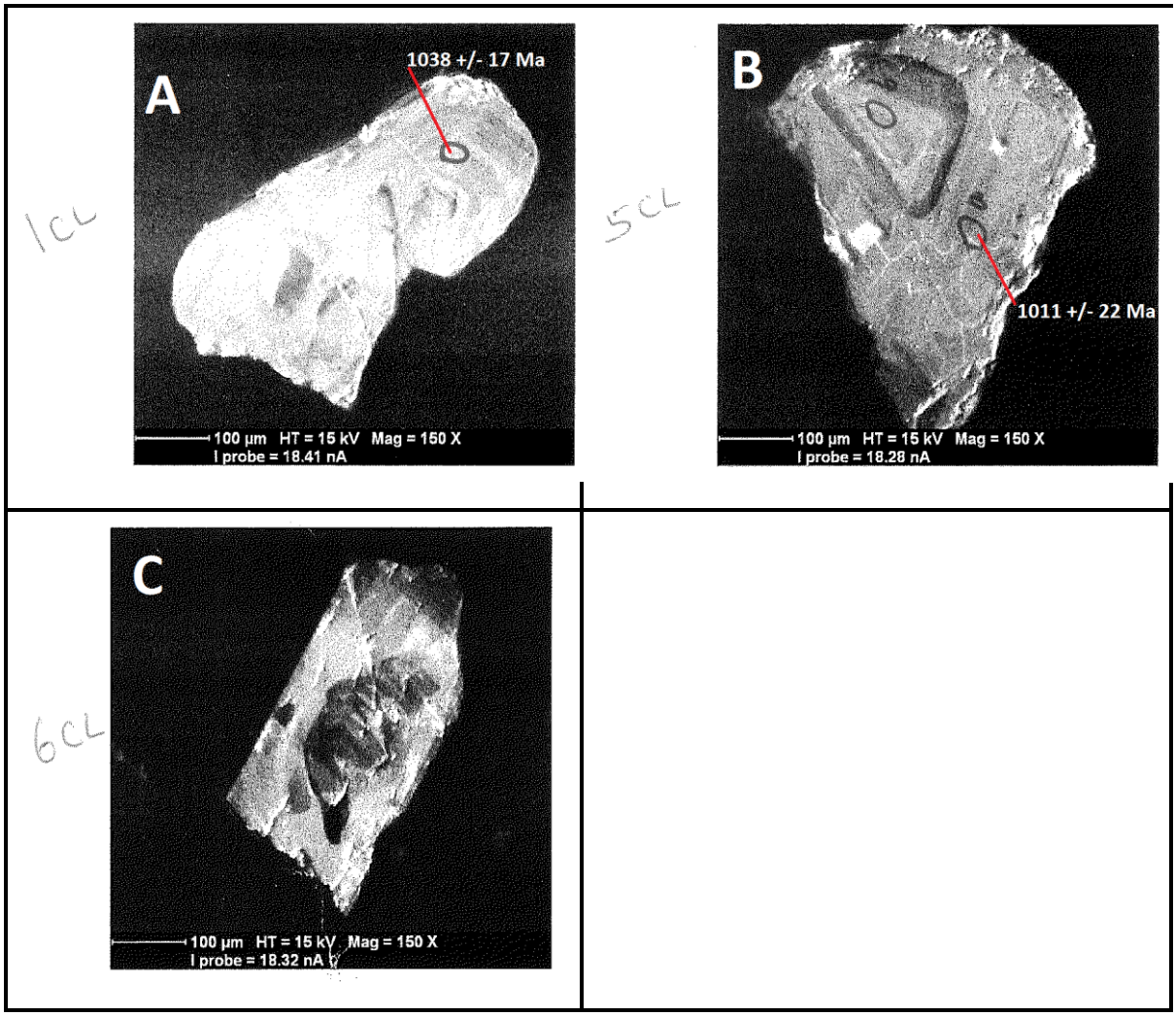

Fig. 5.24: Representative zircon grains from enclave Sample BM213X.

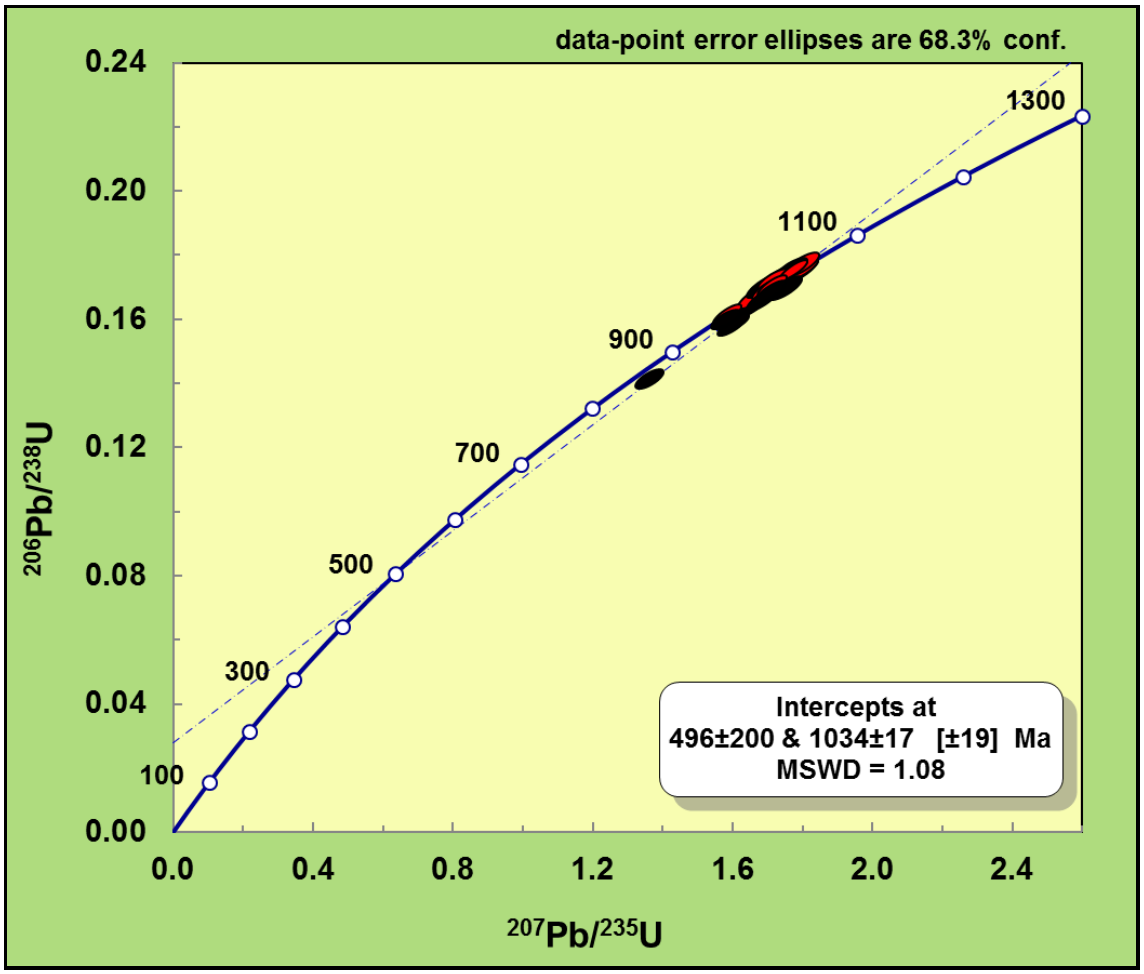

Fig. 5.25: Concordia plot for zircon grain analyses from enclave Sample 213X. Red ellipses = Concordant analyses. Black ellipses = Discordant analyses.

SAMPLE BM 256 (Refer to Table 5.14 & Figs. 5.26 & 5.27)

Sample BM 256 is a leucocratic, coarse grained foliated meta-granite with plagioclase feldspar (12%), quartz (26%), K-feldspar (30%), hornblende (11%), biotite (19%), and diopside (2%) Accessory minerals include zircon and magnetite. Brownish-smoky and colourless zircons were separated from this rock. In CL images (Fig. 5.26) the zircons are euhedral and pyramidal in shape, in width ranging between 300 µ - 400 µ and up to 600 µ in length. They show oscillatory zoning and some of the crystals display darker overgrowths. Radiation damage is seen in some grains and some have dark inclusions. U concentrations range from 106 to 1649 ppm and Th ranges from 52 to 2297 ppm. The Th/U ratios range from 0.37 to 1.39. Of the seventeen analyses obtained only four were concordant and yielded a $^{207}Pb/^{206}Pb$ weighted average age of 1033 ± 40 (MSWD = 7.5, 2 sigma). The analyses yielded an upper intercept $^{206}Pb/^{238}U$ age of 1070 ± 16 Ma (MSWD = 0.97, 2 sigma) interpreted as the crystallisation age of the metagranite.

Table 5.14: Isotopic analyses for metagranite Sample BM256

		CONCENTRATIONS (ppm)					ISOTOPIC RATIOS					ISOTOPIC AGES				
	Th/U	Pb	Th	U	$^{207}Pb/^{206}Pb$	1s %	$^{207}Pb/^{235}U$	1s %	$^{206}Pb/^{238}U$	1s %	$^{207}Pb/^{206}Pb$	2s abs	$^{206}Pb/^{238}U$	2s abs	$^{207}Pb/^{235}U$	2s abs
SAMPLE SPOT		ppm	ppm	ppm							age		age		age	
256_01b	0.44	31	78	176	0.0741	0.90	1.766	1.67	0.1729	1.40	1046	18	1028	27	1033	21
256_02a	0.69	32	129	188	0.0744	0.87	1.715	1.54	0.1673	1.27	1052	17	997	23	1014	20
256_02b	0.42	35	86	205	0.0737	0.90	1.701	1.70	0.1676	1.44	1032	18	999	27	1009	22
256_03	0.37	24	52	141	0.0745	0.90	1.720	1.58	0.1675	1.30	1055	18	998	24	1016	20
256_04a	0.65	52	204	313	0.0737	0.79	1.683	1.45	0.1656	1.21	1034	16	988	22	1002	18
256_04b	0.46	23	62	135	0.0745	0.95	1.719	1.68	0.1675	1.38	1054	19	998	26	1016	21
256_05a	0.64	28	106	165	0.0751	0.90	1.738	1.72	0.1680	1.47	1071	18	1001	27	1023	22
256_05b	0.52	20	57	111	0.0742	0.95	1.799	1.83	0.1758	1.56	1048	19	1044	30	1045	24
256_06a	0.82	23	109	133	0.0741	0.90	1.754	1.72	0.1718	1.47	1044	18	1022	28	1029	22
256_06b	0.75	20	88	116	0.0747	0.98	1.763	1.75	0.1712	1.45	1062	20	1019	27	1032	22
256_07a	0.50	32	92	185	0.0752	0.86	1.770	1.56	0.1709	1.30	1073	17	1017	24	1035	20
256_07b	0.50	21	58	117	0.0742	1.00	1.773	1.75	0.1733	1.43	1048	20	1030	27	1036	22
256_07c	0.66	23	88	134	0.0742	1.05	1.692	1.76	0.1655	1.41	1047	21	987	26	1006	22
256_08a	0.44	21	53	119	0.0747	0.90	1.802	1.78	0.1749	1.53	1061	18	1039	29	1046	23
256_08b	0.42	70	176	415	0.0725	0.84	1.684	1.57	0.1686	1.32	999	17	1005	25	1002	20
256_08c	1.39	182	2297	1649	0.0664	0.82	0.981	1.57	0.1072	1.34	819	17	657	17	694	16

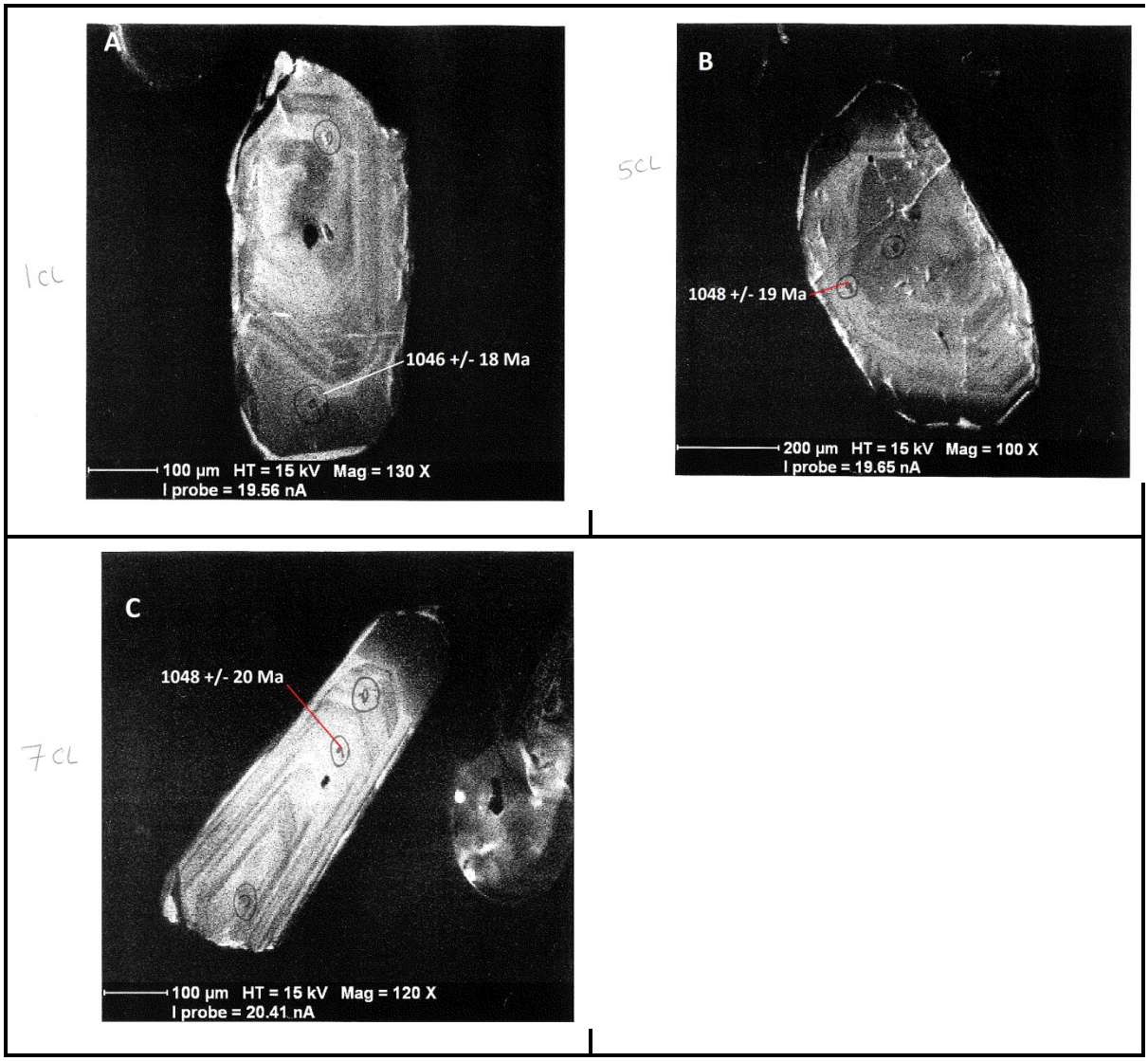

Fig. 5.26: Representative zircons from metagranite Sample BM256 from southern Malawi

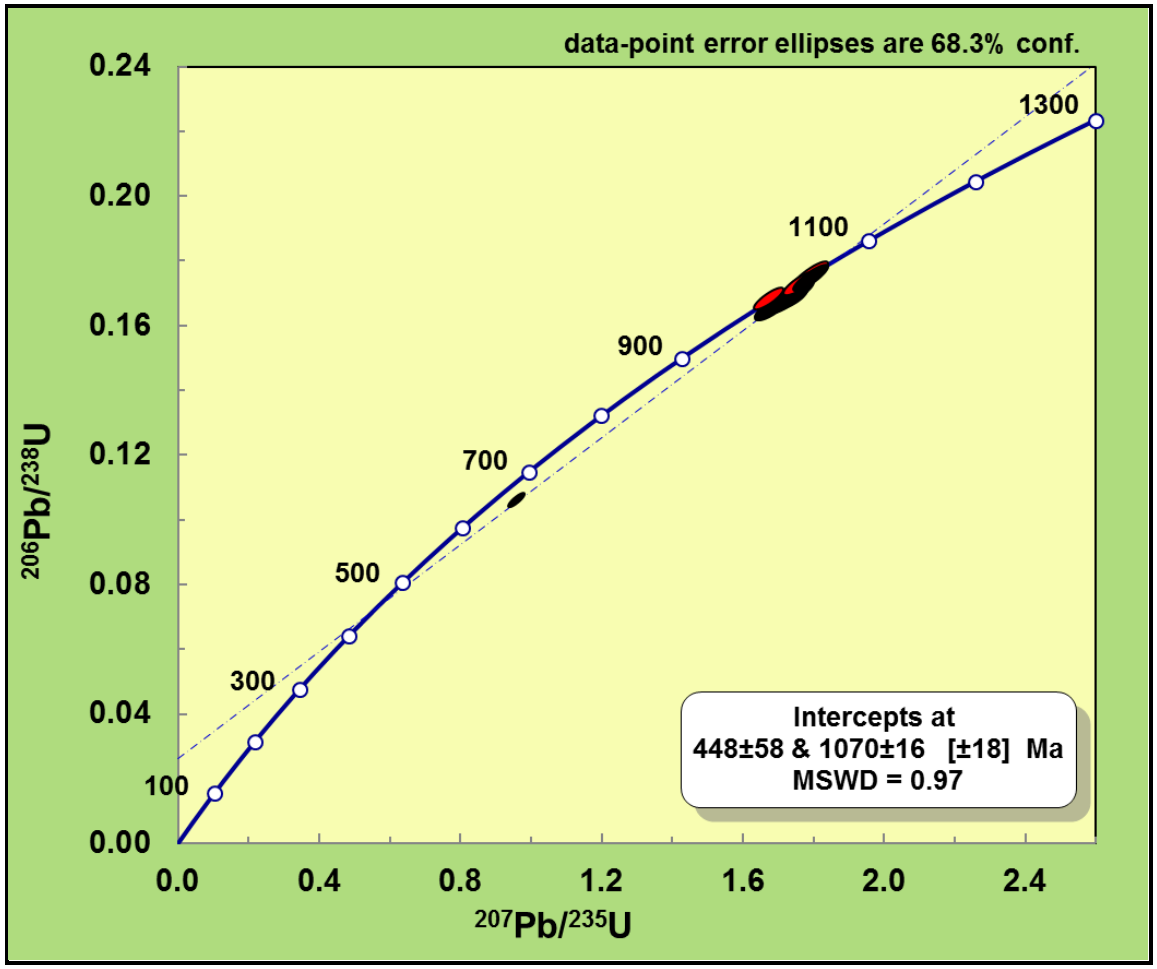

Fig. 5.27: Concordia plot for zircon grain spots from Sample BM256. Red ellipses represent concordant analyses and red ellipses represent discordant analyses.

5.3.3 OTHER ROCK TYPES

SAMPLE BM 200 (Refer to Table 5.15, Figs. 5.28, 5.29 & 5.30)

Sample BM 200 is a leucocratic, fine to medium grained foliated quartzo-feldspathic gneiss. In thin section the rock is composed of quartz (58%), plagioclase (14%), microcline (14%), biotite (4%), and a substantial amount of opaque minerals (11%). Zircons separated from this sample are transparent and some are dirty, euhedral shaped. In CL images show the zircons to be non-luminescent. The backscatter (BSE) images (Fig. 5.29A, B, & C) show euhedral, pyramidal shaped zircons with brighter cores that have abundant dark inclusions. The rims are darker with abundant fracturing and less inclusions when compared with the cores. The zircons are showing metamictimization. U concentrations range from 73 – 1820 ppm (average 849 ppm). Th concentrations range from 18 – 171 ppm. The Th/U ratios are from 0.10 – 0.90. These are xenocrystic zircons with the likelihood that the high U concentrations in the core generated radiation damage that is responsible for the fracturing of the rim (Corfu et al., 2003).

The analyses show two populations as indicated in a probability density diagram (Fig. 5.28). Of the thirty five analyses obtained seven were concordant. Of the seven, four are >900 Ma and their $^{207}Pb/^{206}Pb$ weighted average age is 1031 ± 34 Ma (MSWD = 4.0, 2 sigma). The remaining three are younger and yield a $^{206}Pb/^{238}U$ weighted average age of 607 ± 41 Ma (MSWD = 5.0, 2 sigma). The upper intercept $^{206}Pb/^{238}U$ age is 1097 ± 51 Ma and the lower intercept $^{206}Pb/^{238}U$ age is 479 ± 52 Ma (MSWD = 7.4, 2 sigma) (Fig. 5.30). Based on these

data, the margins of error/uncertainty in the weighted averages for the concordant grain populations and both (lower and upper) intercepts make it difficult to resolve or attach geological meaning to the ages, but the Mesoproterozoic ages may very well be associated with magmatism similar to the metagranites described above while the Cambrian dates may be associated with Gondwana assembly tectonothermal events.

Table 5.15: isotopic analyses for quartzofeldspathic gneiss Sample BM200

		CONCENTRATIONS (ppm)				ISOTOPIC RATIOS						ISOTOPIC AGES				
	Th/U	Pb	Th	U	$^{207}Pb/^{206}Pb$	1s %	$^{207}Pb/^{235}U$	1s %	$^{206}Pb/^{238}U$	1s %	$^{207}Pb/^{206}Pb$	2s abs	$^{206}Pb/^{238}U$	2s abs	$^{207}Pb/^{235}U$	2s abs
SAMPLE SPOT		ppm	ppm	ppm							age		age		age	
200_09a	0.03	107	29	1155	0.0608	0.86	0.773	1.60	0.0923	1.35	632	19	569	15	582	14
200_23b	0.04	185	83	1930	0.0641	0.81	0.824	1.53	0.0932	1.30	746	17	575	14	610	14
200_08	0.02	128	28	1334	0.0620	0.70	0.796	1.59	0.0932	1.43	673	15	575	16	595	14
200_24a	0.07	134	100	1391	0.0628	0.72	0.810	1.56	0.0936	1.38	700	15	577	15	602	14
200_16a	0.08	170	146	1739	0.0630	0.78	0.820	1.38	0.0944	1.13	707	17	582	13	608	13
200_11	0.05	175	96	1820	0.0615	0.78	0.806	1.61	0.0951	1.41	657	17	585	16	600	15
200_20	0.05	66	32	679	0.0644	0.72	0.849	1.55	0.0957	1.37	755	15	589	15	624	14
200_14	0.05	139	72	1409	0.0608	0.63	0.806	1.35	0.0962	1.19	632	14	592	13	600	12
200_17a	0.04	84	32	865	0.0664	0.93	0.889	2.06	0.0971	1.84	820	19	597	21	646	19
200_26	0.04	159	70	1570	0.0628	0.87	0.845	1.60	0.0977	1.35	700	18	601	15	622	15
200_25b	0.09	180	151	1764	0.0649	1.09	0.883	1.71	0.0988	1.32	771	23	607	15	643	16
200_05a	0.05	166	90	1639	0.0606	0.80	0.827	1.49	0.0990	1.26	626	17	609	15	612	14
200_12a	0.01	122	18	1216	0.0635	1.12	0.872	3.15	0.0997	2.94	723	24	612	34	636	29
200_21a	0.09	153	126	1467	0.0665	0.69	0.934	1.47	0.1019	1.30	823	14	625	16	670	14
200_18	0.07	102	71	949	0.0622	0.72	0.874	1.59	0.1020	1.41	680	15	626	17	638	15
200_21b	0.10	42	40	391	0.0653	0.77	0.934	1.56	0.1038	1.36	783	16	637	16	670	15
200_07	0.07	142	89	1336	0.0668	1.07	0.960	1.78	0.1043	1.43	830	22	640	17	683	18
200_15	0.05	178	85	1596	0.0643	0.60	0.965	1.61	0.1090	1.50	750	13	667	19	686	16
200_04	0.06	132	73	1213	0.0655	0.93	0.992	2.23	0.1098	2.03	792	20	671	26	700	22
200_01a	0.06	142	70	1184	0.0673	1.36	1.065	1.94	0.1148	1.39	847	28	701	18	736	20
200_22b	0.29	18	45	154	0.0693	1.43	1.105	2.34	0.1158	1.85	906	29	706	25	756	25
200_12b	0.30	20	43	145	0.0725	1.14	1.289	2.04	0.1290	1.69	1000	23	782	25	841	23
200_13	0.40	14	37	93	0.0726	1.19	1.426	1.88	0.1425	1.45	1004	24	859	23	900	22
200_01a	0.36	16	41	113	0.0741	1.39	1.462	2.28	0.1432	1.81	1044	28	863	29	915	27
200_16b	0.45	16	48	106	0.0754	1.08	1.550	2.19	0.1491	1.90	1080	22	896	32	950	27
200_25a	0.60	11	39	64	0.0776	1.14	1.719	1.95	0.1608	1.57	1136	23	961	28	1016	25
200_09c	0.62	23	88	143	0.0797	1.48	1.767	2.33	0.1609	1.80	1189	29	962	32	1033	30
200_02	0.56	39	120	217	0.0721	1.20	1.754	2.16	0.1765	1.79	989	24	1048	35	1029	28
200_03	0.70	35	136	196	0.0735	0.98	1.772	1.75	0.1749	1.45	1029	20	1039	28	1035	23
200_05a	0.48	31	82	171	0.0741	1.04	1.788	1.88	0.1752	1.57	1043	21	1041	30	1041	24
200_09b	0.46	19	49	105	0.0743	1.08	1.807	1.95	0.1766	1.63	1049	22	1048	31	1048	25
200_17b	0.40	52	121	301	0.0740	0.84	1.747	1.61	0.1712	1.37	1042	17	1019	26	1026	21
200_23a	0.51	13	37	73	0.0724	1.15	1.705	1.98	0.1708	1.61	998	23	1017	30	1010	25
200_24b	0.45	67	171	383	0.0738	0.70	1.730	1.44	0.1701	1.26	1036	14	1013	24	1020	18

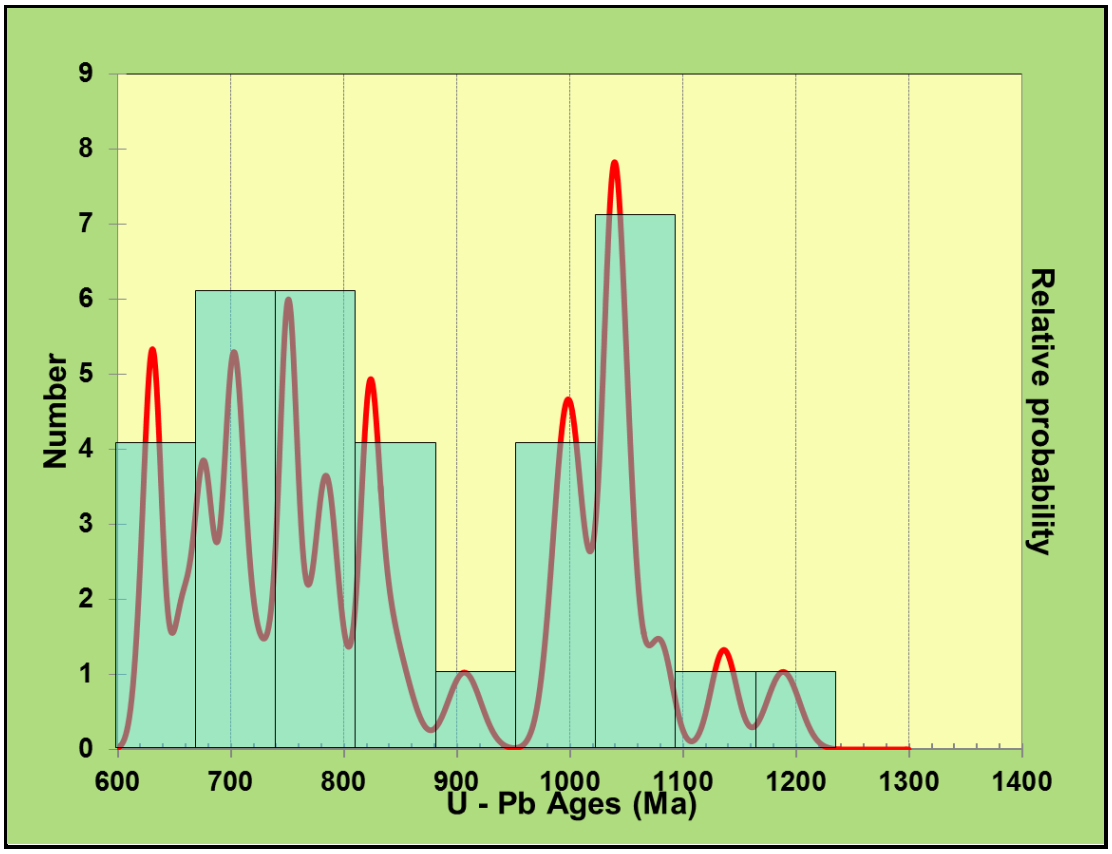

Fig. 5.28: Probability density diagram for zircons in Sample BM 200 showing two populations

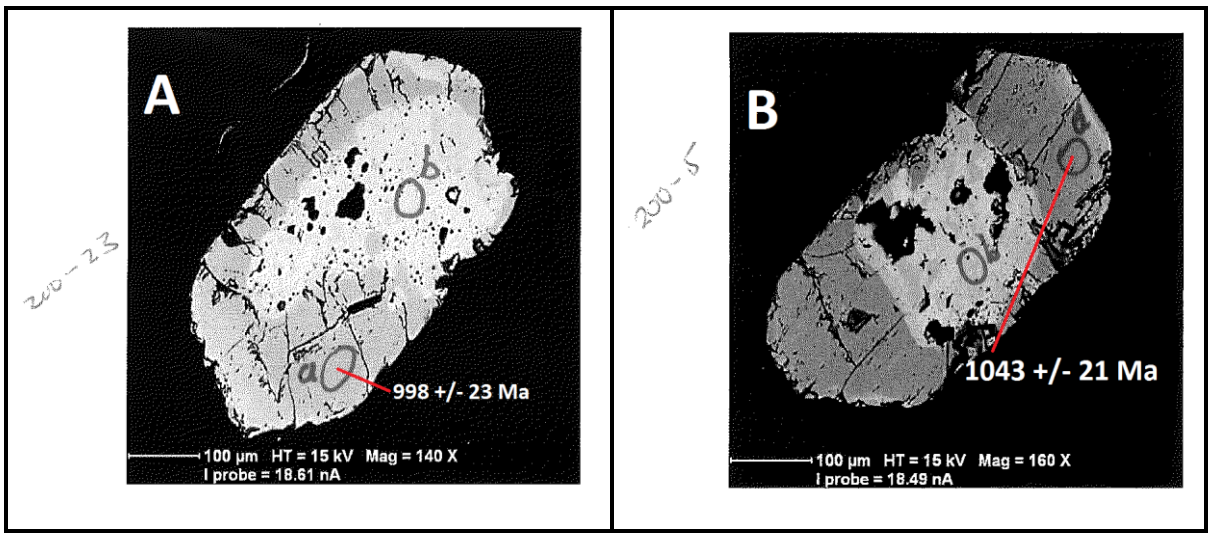

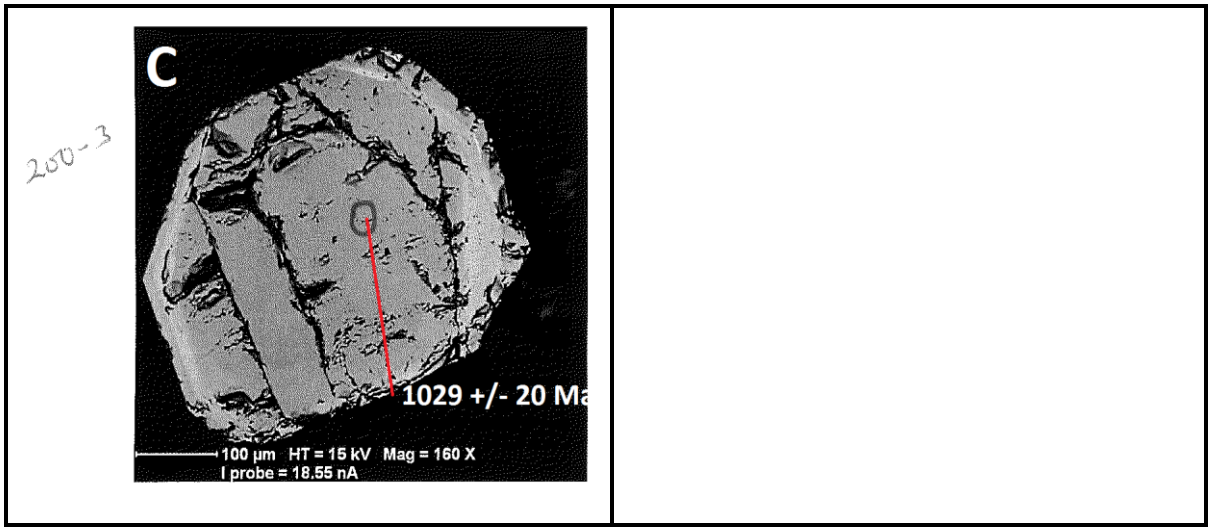

Fig. 5.29: Representative zircons from quartzofeldspathic Sample BM200 from southern Malawi.

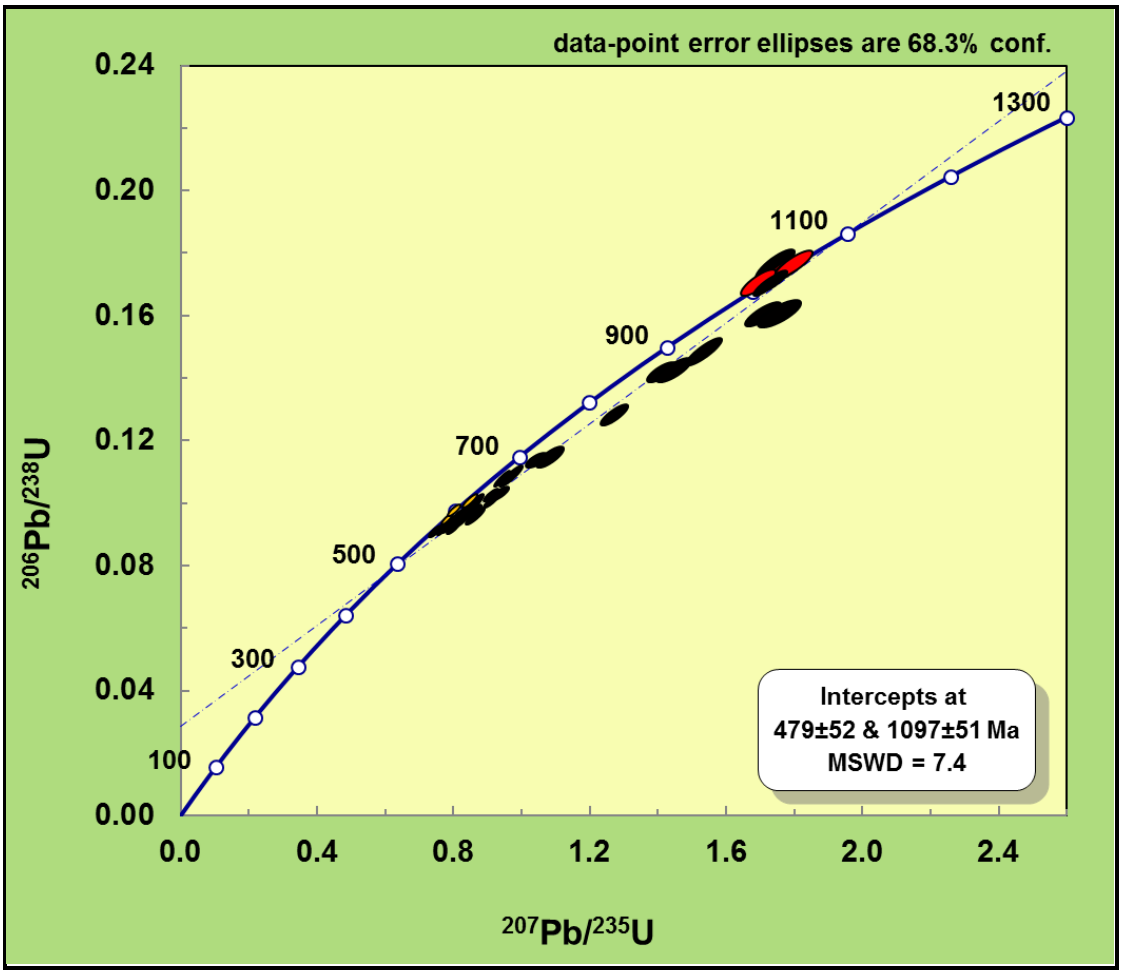

Fig. 5.30: Concordia plot of zircon grain analyses from Sample BM200. Red ellipses are analyses > 900 Ma and concordant and yellow ellipses are concordant population analyses <700 Ma. Black ellipses are discordant.

SAMPLE BM221 (Refer to Table 5.16 & Figs.5.31 and 5.32)

Sample BM221 is leucocratic, medium to coarse grained, foliated leucogranite gneiss comprising plagioclase feldspar (23%), microcline (25%), quartz (43%) biotite (4%) with

accessory epidote and unknown opaques. Euhedral and pyramidal shaped zircons were separated from this sample and in CL they are dark in the core and mantle but have a thin bright rim (Fig. 5.31C). Some of the zircons show growth and oscillatory zoning (Fig. 5.31B). The mantles and rims in some of the zircons display regular fractured patterns than the cores. U ranges from 685 – 5629 ppm and Th concentrations range from 58 -1125 ppm. The Th/U ratios range from 0 – 0.34. Twenty two analyses were carried out on these zircons with four grains being concordant. The $^{206}Pb/^{238}U$ weighted average age for the concordant grains is 737 ± 53 Ma (MSWD = 13, 2 sigma). The upper intercept $^{206}Pb/^{238}U$ age is 764 ± 20 (MSWD = 3.3, 2 sigma) (Fig. 5.32). The margins of uncertainty in the analyses are disappointingly large hence the ages do not provide significant temporal constraints. However Rodinia break-up events which could have affected this region are reported to have started between 750 – 600 Ma and this could be related to such tectonothermal events (Torsvik et al., 1996).

Table 5.16: Isotopic analyses for leucogranite Sample BM221

		CONCENTRATIONS (ppm)						ISOTOPIC RATIOS						ISOTOPIC AGES					
	Th/U	Pb	Th	U	$^{207}Pb/^{206}Pb$	1s %	$^{207}Pb/^{235}U$	1s %	$^{206}Pb/^{238}U$	1s %	$^{207}Pb/^{206}Pb$	2s abs	$^{206}Pb/^{238}U$	2s abs	$^{207}Pb/^{235}U$	2s abs
SAMPLE SPOT		ppm	ppm	ppm								age		age		age		
221_01a	0.12	337	537	4653	0.0670	0.86	0.662	1.55	0.0717	1.29	838	18	446	11	516	12
221_01b	0.03	256	79	2580	0.0653	0.82	0.899	1.97	0.0998	1.79	784	17	613	21	651	19
221_02c	0.05	220	105	1931	0.0660	0.88	1.023	1.63	0.1125	1.37	805	18	687	18	715	17
221_03a	0.05	209	117	2161	0.0652	0.80	0.859	1.89	0.0955	1.71	782	17	588	19	629	18
221_03b	0.06	215	97	1731	0.0643	0.86	1.099	1.55	0.1239	1.29	753	18	753	18	753	16
221_04a	0.27	225	691	2553	0.0670	0.83	0.818	2.49	0.0886	2.35	837	17	547	25	607	23
221_04b	0.20	246	671	3369	0.0675	0.87	0.689	2.61	0.0741	2.46	852	18	461	22	532	21
221_05a	0.05	333	205	3799	0.0661	0.77	0.803	2.07	0.0881	1.92	809	16	545	20	598	19
221_05b	0.34	272	831	2441	0.0655	0.89	0.996	1.54	0.1103	1.25	790	19	675	16	702	15
221_06a	0.05	181	73	1461	0.0648	0.82	1.088	1.60	0.1219	1.38	768	17	741	19	748	17
221_06b	0.10	382	481	4947	0.0676	0.79	0.720	1.74	0.0772	1.55	857	16	480	14	551	15
221_06b	0.18	231	526	2858	0.0691	0.94	0.743	1.61	0.0781	1.31	901	19	485	12	564	14
221_07a	0.06	141	77	1206	0.0642	0.90	1.008	1.58	0.1140	1.30	747	19	696	17	708	16
221_07b	0.29	72	200	685	0.0665	1.02	0.934	2.32	0.1020	2.08	821	21	626	25	670	22
221_07b	0.09	77	69	750	0.0637	0.95	0.891	1.57	0.1016	1.25	731	20	624	15	647	15
221_09a	0.08	210	127	1684	0.0667	0.90	1.130	1.57	0.1230	1.29	827	19	748	18	768	17
221_09b	0.04	271	78	2083	0.0644	0.76	1.133	1.63	0.1276	1.45	755	16	774	21	769	17
221_11a	0.03	220	73	2266	0.0644	0.88	0.846	1.66	0.0953	1.41	753	19	587	16	622	15
221_11b	0.04	282	102	2716	0.0650	0.81	0.914	1.74	0.1021	1.53	773	17	626	18	659	17
221_11c	0.03	137	58	2129	0.0679	0.88	0.591	1.66	0.0632	1.41	865	18	395	11	472	12
221_12b	0.08	190	151	1828	0.0649	0.87	0.924	1.76	0.1034	1.53	771	18	634	18	665	17
221_12c	0.07	270	224	3011	0.0641	0.83	0.774	1.72	0.0875	1.51	746	17	541	16	582	15

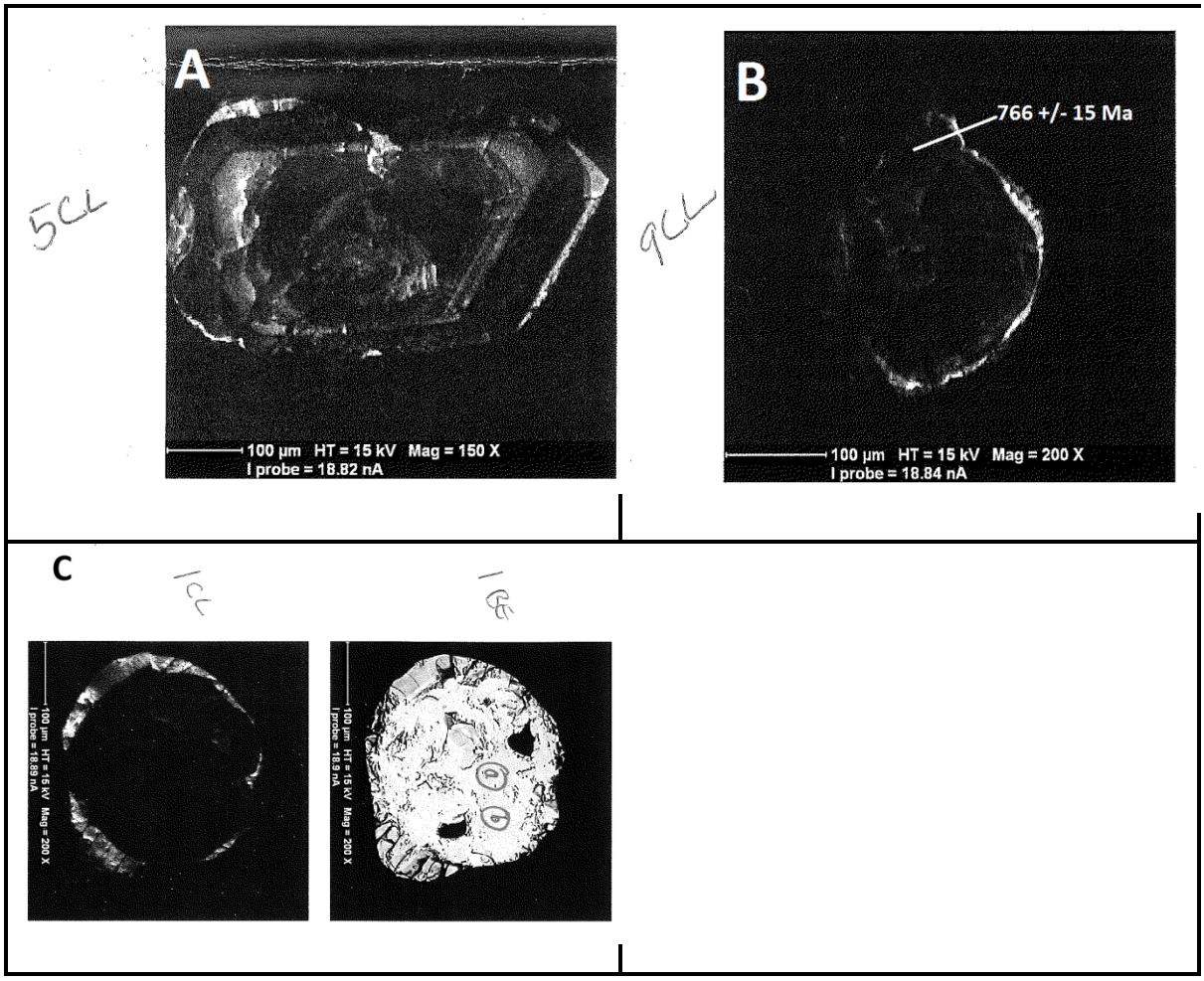

Fig. 5. 31: Representative zircons from hornblende biotite gneiss Sample BM221.

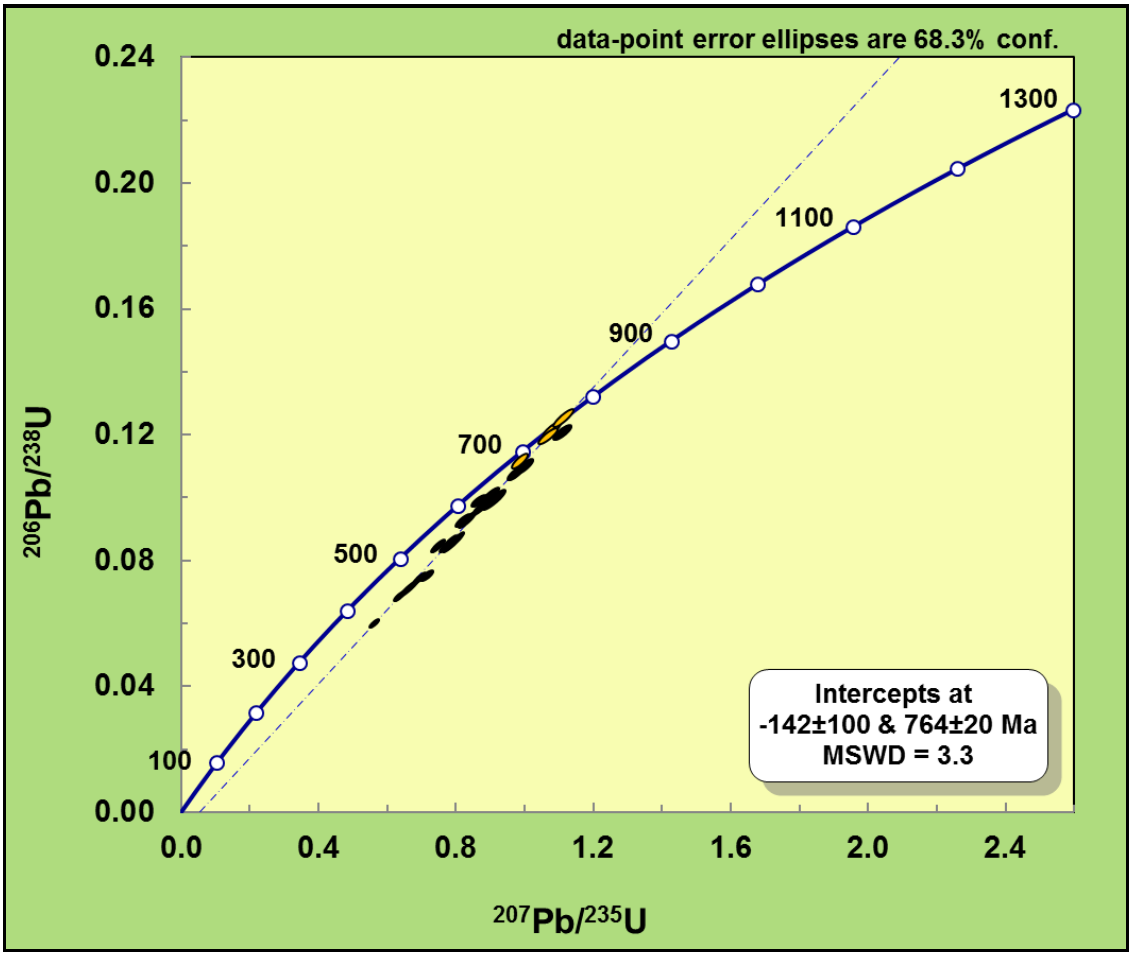

Fig. 5. 32: Concordia plot for zircons from sample BM221. Yellow ellipses stand for concordant analyses and black ones indicate discordant.

SAMPLE BM223A (Refer to Table 5.17 & Figs. 5.33 and 5.34)

Sample 223A is a medium grained, buff to pink coloured gneiss with K-feldspar (60%), quartz (17%), plagioclase feldspar (15%) hornblende (17%) and biotite (5%). Zircon and magnetite are accessory phases. Only two zircon crystals were separated from this sample; one pyramidal in shape with rounded edges (Fig. 5.33A), and the other sharply pyramidal (Fig. 5.33B). The former is 80µ - 200µ in width and 230µ in length and in CL image it shows a brighter core with some oscillatory zoning and a dark outer rim. The other zircon is 100µ in width and 300µ in length. This zircon has a brighter core and darker rim and ill-defined oscillatory zoning. The darker phases are featureless with no growth zoning and are therefore metamorphic zircon (Wu et al., 2004) overgrowing the oscillatory zoned magmatic zircons. The U concentrations are from 182 – 1398 ppm and Th concentrations are from 70 – 214 ppm. The Th/U ratios range from 0.15 – 0.60. Five analyses were obtained from the zircons, four of them concordant. Three concordant spots analyses yielded a weighted average $^{207}Pb/^{206}$ Pb age of 956±12 Ma (MSWD = 0.93, 2 sigma) interpreted as the crystallisation of age of the leucogranite. The other grain yields a date of 541 ± 17 Ma. The five analyses yielded an upper intercept $^{206}Pb/^{238}U$ age of 969 ± 53 Ma and a lower intercept of 589 ± 42 Ma (MSWD = 0.070, 2 sigma) (Fig. 5.34). The gneiss protolith was thus crystallised at 969 ± 53 Ma and lost Pb in a subsequent metamorphic event at 589 ± 42 Ma. New zircon growth during this metamorphic event occurred which yields the 541 ± 17 Ma age.

Table 5.17: Isotopic analyses for hornblende biotite gneiss Sample 223A

		CONCENTRATIONS (ppm)					ISOTOPIC RATIOS				ISOTOPIC AGES					
	Th/U	Pb	Th	U	$^{207}Pb/^{206}Pb$	1s %	$^{207}Pb/^{235}U$	1s %	$^{206}Pb/^{238}U$	1s %	$^{207}Pb/^{206}Pb$	2s abs	$^{206}Pb/^{238}U$	2s abs	$^{207}Pb/^{235}U$	2s abs
SAMPLE SPOT		ppm	ppm	ppm							age		age		age	
223a_01b	0.52	34	110	212	0.0709	1.03	1.538	1.82	0.1574	1.49	954	21	942	26	946	22
223a_01c	0.46	65	182	394	0.0713	1.02	1.590	1.71	0.1618	1.37	966	21	967	25	966	21
223a_02a	0.39	28	70	182	0.0705	1.40	1.458	2.19	0.1501	1.68	943	29	901	28	913	26
223a_02b	0.60	43	164	272	0.0706	1.12	1.511	1.82	0.1553	1.43	945	23	931	25	935	22

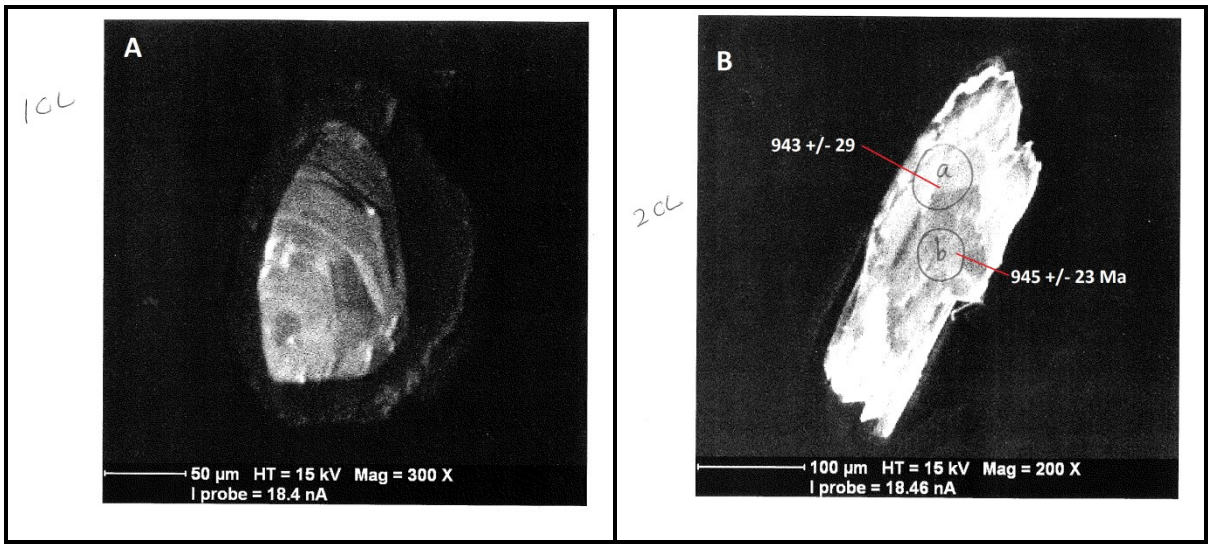

Fig. 5.33: Representative zircon grains from leucogranite gneiss Sample BM223A from southern Malawi

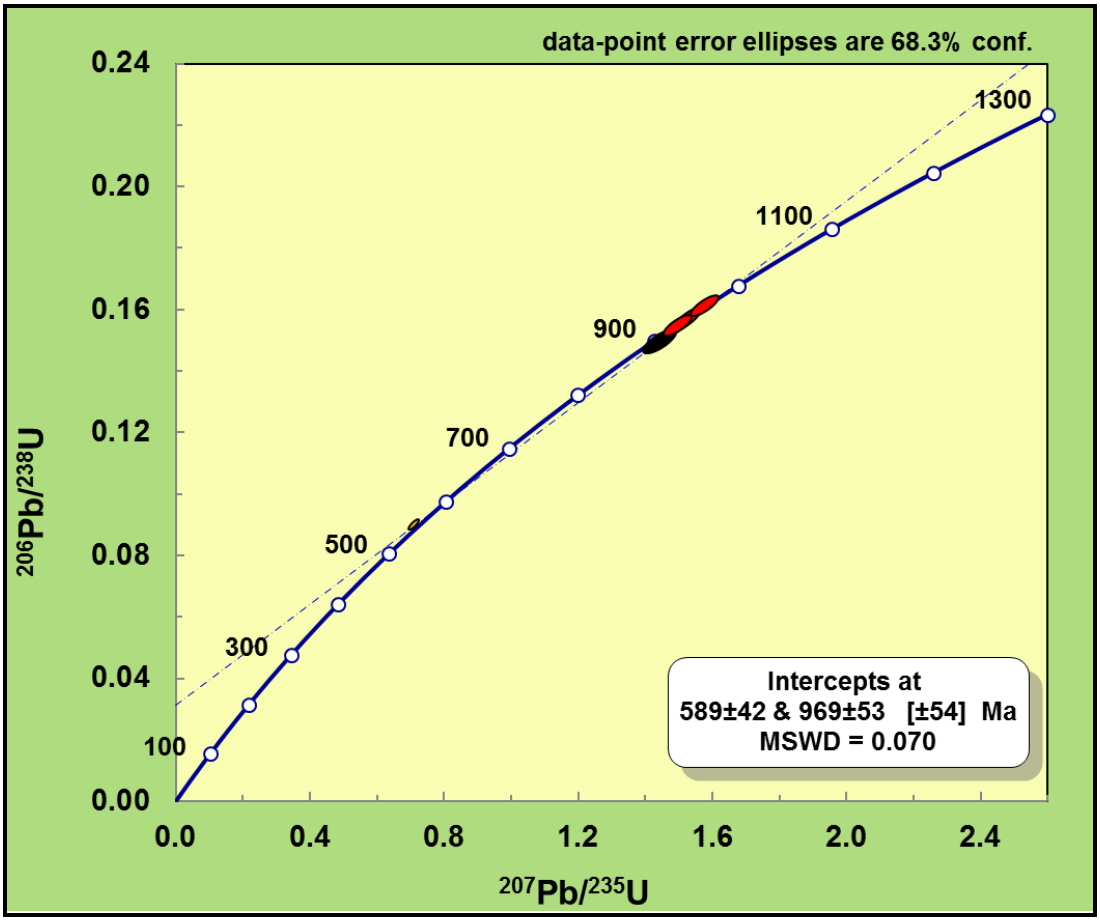

Fig. 5.34: Concordia plot for zircon grain spots for Sample BM223A. Red ellipses stand for concordant grain analyses and black one stand for discordant ones.

SAMPLE 289 (Refer to Table 5.18 & Figs. 5.35 & 5.36)

Sample BM 289 is a leucocratic, medium to coarse grained, well foliated perthitic syenite. In thin section the rock comprises of 40 % K-feldspar, perthitic feldspar (36%), plagioclase feldspar (5%), quartz (8%), biotite (5%), and pyroxene (3%). Accessory minerals include zircon and opaque minerals.

In CL images, zircons show euhedral, pyramidal shapes, and oscillatory zoning. These are magmatic zircons (Fig. 5.35A). Others exhibit alternating darker and brighter phases. The brighter phases have oscillatory zoning but the darker are featureless. These are inherited zircons overgrown by metamorphic phases (Fig. 5.35B). U concentrations are from 19 – 435 ppm whilst Th ranges from 45 – 621 ppm. The Th/U ratios range from 0.29 – 2.40. Of the twenty one analyses taken seventeen were concordant. A weighted average $^{206}Pb/^{238}U$ age of 530.6 ± 3.4 Ma was obtained which is interpreted as a crystallisation age of the perthitic syenite.

Table 5.18: Isotopic analyses for perthitic syenite Sample BM289

	CONCENTRATIONS (ppm)					ISOTOPIC RATIOS					ISOTOPIC AGES					
	Th/U	Pb	Th	U	$^{207}Pb/^{206}Pb$	1s %	$^{207}Pb/^{235}U$	1s %	$^{206}Pb/^{238}U$	1s %	$^{207}Pb/^{206}Pb$	2s abs	$^{206}Pb/^{238}U$	2s abs	$^{207}Pb/^{235}U$	2s abs
SAMPLE SPOT		ppm	ppm	ppm							age		age		age	
289_01a	0.53	33	197	369	0.0587	1.05	0.698	1.76	0.0864	1.42	554	23	534	15	538	15
289_01b	2.06	3	67	32	0.0585	1.66	0.689	2.25	0.0855	1.53	547	36	529	15	532	18
289_02a	1.38	3	51	37	0.0578	1.63	0.681	2.36	0.0855	1.71	521	36	529	17	527	19
289_02b	0.56	25	158	283	0.0573	1.07	0.680	1.80	0.0861	1.45	502	24	532	15	527	15
289_03a	1.48	38	621	420	0.0602	1.09	0.717	1.65	0.0864	1.24	609	24	534	13	549	14
289_03b	1.09	31	369	339	0.0584	1.12	0.690	1.77	0.0857	1.38	546	24	530	14	533	15
289_04	2.06	2	55	27	0.0600	1.94	0.701	2.67	0.0848	1.84	603	42	525	19	539	22
289_05a	0.48	36	193	401	0.0579	1.17	0.693	1.75	0.0868	1.30	525	26	537	13	534	14
289_05b	1.57	7	126	80	0.0583	1.45	0.686	2.05	0.0854	1.45	540	32	528	15	530	17
289_06a	0.48	19	105	218	0.0576	1.17	0.681	1.78	0.0858	1.34	516	26	530	14	528	15
289_07a	0.43	30	146	341	0.0580	1.21	0.688	1.76	0.0861	1.29	529	26	532	13	532	14
289_07b	2.22	6	156	70	0.0577	1.54	0.678	2.19	0.0853	1.55	518	34	528	16	526	18
289_08	1.81	6	118	65	0.0581	1.36	0.698	2.00	0.0872	1.46	532	30	539	15	537	17
289_09a	1.14	9	108	95	0.0763	2.95	0.947	3.32	0.0901	1.53	1103	59	556	16	677	32
289_09b	0.48	34	189	395	0.0589	1.07	0.689	1.72	0.0850	1.35	562	23	526	14	532	14
289_11a	0.29	22	69	237	0.0589	1.12	0.699	1.71	0.0861	1.30	563	24	532	13	538	14
289_11b	0.33	38	143	435	0.0588	1.07	0.688	1.66	0.0849	1.26	561	23	525	13	532	14
289_13a	1.62	5	93	57	0.0585	1.46	0.691	2.07	0.0858	1.48	547	32	530	15	533	17
289_13b	0.47	31	166	349	0.0577	1.20	0.676	1.75	0.0849	1.27	519	26	526	13	524	14
289_14a	2.40	2	45	19	0.0613	2.56	0.707	3.12	0.0837	1.78	650	55	518	18	543	26
289_14b	0.44	28	139	318	0.0592	1.06	0.704	1.71	0.0864	1.34	574	23	534	14	541	14

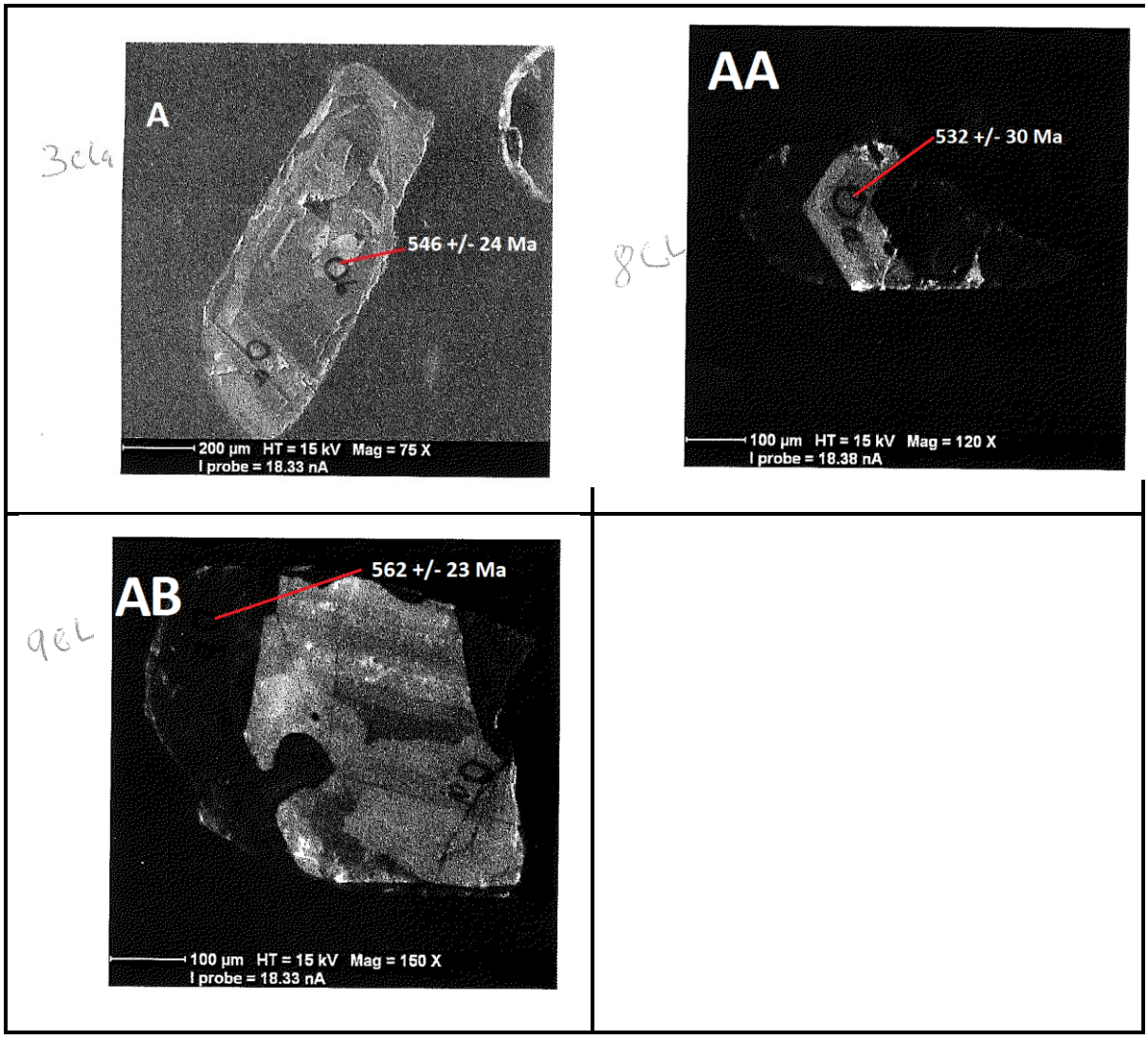

Fig. 5.35: Representative zircons from perthitic syenite Sample BM289.

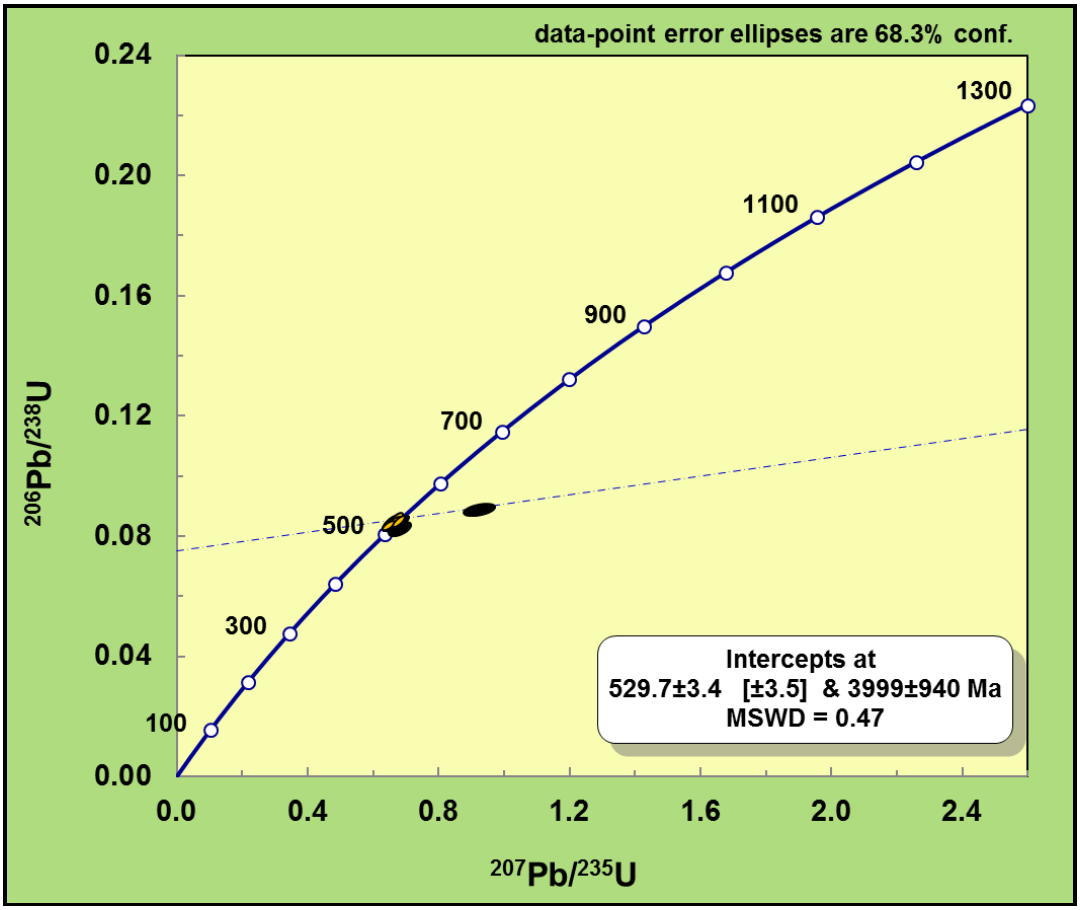

Fig. 5. 36: Concordia plot for zircons from Sample BM289. Yellow ellipses stand for concordant analyses. Black ellipses represent discordant analyses.

SAMPLE BM 240 (Refer to Table 5.19 & Figs. 5.37 and 5.38)

Sample BM 240 is a brown to pink, coarse grained, massive, homogeneous granite with euhedral and subhedral K-feldspars (75%), subhedral and anhedral quartz (13%), plagioclase feldspar (2%), hornblende (6%) and euhedral biotite (4%). Accessory minerals include zircon and magnetite. Zircons from this rock are euhedral, prismatic shaped. In CL images (Fig. 5.37) they display alternating phases of dark and bright zones with well-defined oscillatory zoning and dark coloured inclusions. The zircons range from 250 µ - 400µ in width and reach 600µ in length. U concentrations are from 48 – 269 ppm in nineteen analyses and one was 1620 ppm. Th ranges from 37 – 271 ppm. Th/U ratios are 0.53 – 1.15. Pb concentrations are from 1 – 5 ppm in nineteen analyses and 40 ppm in one spot. The analyses yielded a lower intercept $^{206}Pb/^{238}U$ age of 118.1 ± 1.2 Ma (MSWD = 1.5, 2 Sigma) (Fig. 5.38) which in interpreted as the crystallisation age of the granite (Fig. 21). Based on the mineralogy and texture together with its zircon U-Pb age, this granite is Cretaceous as opposed to the others which are Mesoproterozoic.

Table 5.19: Isotopic analyses for granite Sample BM240

		CONCENTRATIONS (ppm)							ISOTOPIC RATIOS			ISOTOPIC AGES				
	Th/U	Pb	Th	U	$^{207}Pb/^{206}Pb$	1s %	$^{207}Pb/^{235}U$	1s %	$^{206}Pb/^{238}U$	1s %	$^{207}Pb/^{206}Pb$	2s abs	$^{206}Pb/^{238}U$	2s abs	$^{207}Pb/^{235}U$	2s abs
SAMPLE SPOT		ppm	ppm	ppm							age		age		age	
240_01	0.82	1	41	50	0.0505	4.33	0.133	5.07	0.0191	2.64	218	100	122	6	127	12
240_02	1.06	1	69	64	0.0557	4.63	0.137	5.14	0.0178	2.23	442	103	114	5	130	12
240_03	1.03	2	86	83	0.0478	3.42	0.125	4.14	0.0190	2.34	90	81	122	6	120	9
240_04	0.77	2	60	78	0.0513	3.26	0.132	3.86	0.0187	2.08	255	75	119	5	126	9
240_05	0.88	1	54	61	0.0509	4.16	0.126	5.13	0.0180	2.99	236	96	115	7	121	12
240_06	0.76	1	53	70	0.0478	3.11	0.122	4.19	0.0185	2.81	91	74	118	7	117	9
240_07	0.68	1	46	67	0.0457	4.12	0.121	4.74	0.0192	2.34	-20	100	123	6	116	10
240_08	0.84	3	133	157	0.0487	2.34	0.126	3.22	0.0188	2.22	131	55	120	5	120	7
240_09	1.15	4	271	236	0.0492	2.42	0.124	3.09	0.0183	1.92	155	57	117	4	119	7
240_10	0.53	1	37	70	0.0535	3.45	0.143	4.10	0.0194	2.22	350	78	124	5	136	10
240_10b	n/a	1	n/a	64	0.0541	2.79	0.132	3.42	0.0177	1.98	374	63	113	4	126	8
240_10c	n/a	2	n/a	94	0.0482	2.95	0.125	3.36	0.0188	1.60	110	70	120	4	120	8
240_11	0.69	5	187	269	0.0476	2.35	0.120	2.92	0.0182	1.74	82	56	116	4	115	6
240_14b	1.15	3	166	145	0.0488	2.17	0.123	2.73	0.0183	1.66	136	51	117	4	118	6
240_17	n/a	3	n/a	181	0.0486	1.86	0.122	2.41	0.0182	1.53	128	44	116	4	117	5
240_4b	n/a	1	n/a	67	0.0520	3.09	0.132	3.79	0.0184	2.20	284	71	117	5	126	9
240_4c	n/a	1	n/a	48	0.0619	4.21	0.161	4.67	0.0189	2.01	671	90	121	5	152	13
240_9c	n/a	2	n/a	86	0.2568	1.74	0.862	2.42	0.0244	1.68	3227	27	155	5	631	22
240_9d	n/a	40	n/a	1620	0.2285	6.92	0.742	7.49	0.0236	2.87	3042	111	150	9	564	63
240_9e	n/a	1	n/a	59	0.1619	3.93	0.495	4.52	0.0222	2.24	2476	66	141	6	408	30

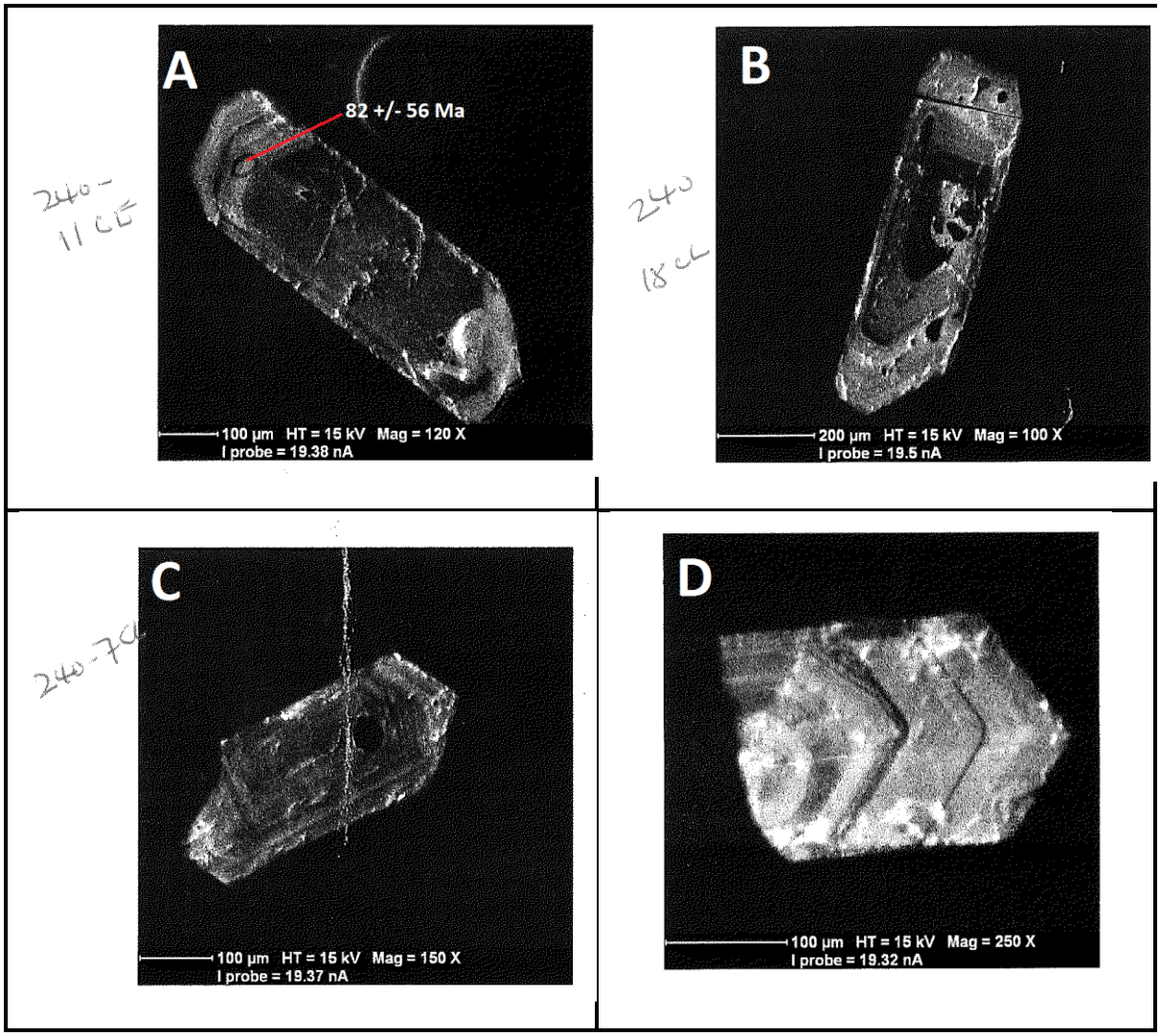

Fig. 5.37: Representative zircons from granite Sample BM240 from southern Malawi

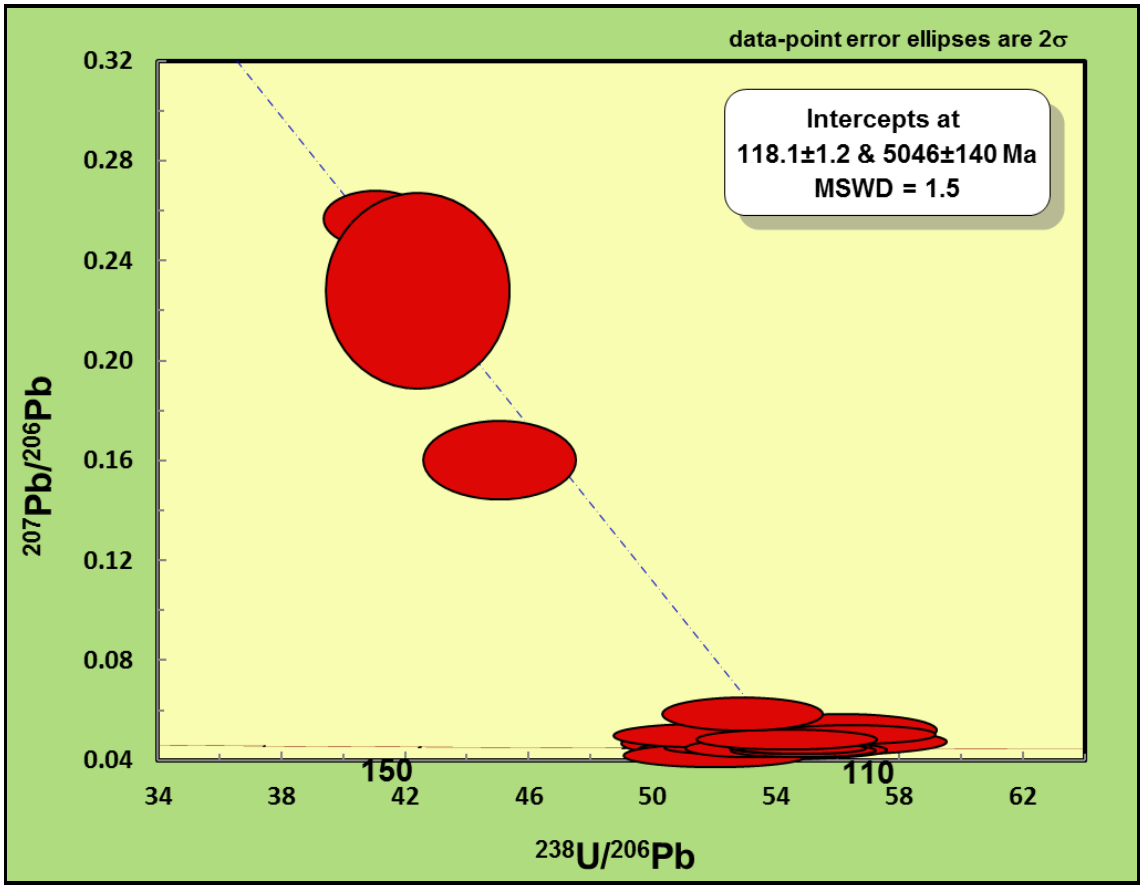

Fig. 5.38: Concordia plot for zircon grain analyses for granite Sample BM240 from southern Malawi

5.4 SUMMARY

The age data for this study are summarised and indicated in Table 5.20, and Fig. 5.39 is a map showing the ages in the different lithologic units with the sample localities.

Table 5.20: Table showing summarised age data for the southern Malawi rocks (LA-ICP-MS Single zircon U-Pb).

Sample	Age	2s	Type	MSWD	n total	n used in age calculation	Interpretation
BM 163	1038.2	6.8	Upper Intercept	1.18	24	24	Emplacement Age
BM 174	1035.6	8.3	Upper Intercept	1.2	32	32	Emplacement Age
BM 179	1047	13	Upper Intercept	1.01	24	24	Emplacement Age
BM 200	1031	19	Weighted Average (U poor population)	4.3	35	7	?
	530	24	Lower Intercept (U rich population)	25	35	29	?
	1278	61	Upper Intercept (U rich population)	2.9	35	29	?
	(TWO POPULATIONS - NOT DETRITAL)						
BM 209	1033	20	Upper Intercept	1.7	24	23	Emplacement Age
BM 213C	1088	23	Upper Intercept	1.5	25	25	Emplacement Age
BM 213X	1034	17	Upper Intercept	1.08	24	24	Emplacement Age
BM 221	764	20	Upper Intercept	3.3	22	22	
	756.2	8.6	Weighted Average	0.94	22	4	Emplacement Age
BM 223A	956	12	Weighted Average	0.93	5	3	Emplacement Age
BM 233	dog's breakfast	0	UNRESOLVABLE COMMON LEAD				?
BM 240	118.1	1.2	Lower Intercept	1.5	17	16	Emplacement Age
BM 249	1036	15	Upper Intercept	2	26	26	Emplacement Age
BM 252	1128	30	Upper Intercept	1.1	21	21	Emplacement Age
	515	18	Lower Intercept	1.1	21	21	Metamorphism Age
	535.9	6.7	Weighted Average	0.57	21	8	Emplacement Age
	(TWO POPULATIONS)						
BM 256	1070	16	Upper Intercept	0.97	17	17	Emplacement Age
BM 281	594	65	Upper Intercept	1.4	17	17	?
BM 282A	not simple enough to reduce to single values,	0	0	0	0	0	?
BM 282B	not simple enough to reduce to single values,	0	0	0	0	0	?
BM 289	530.6	3.4	Weighted Average	0.31	21	17	Emplacement Age

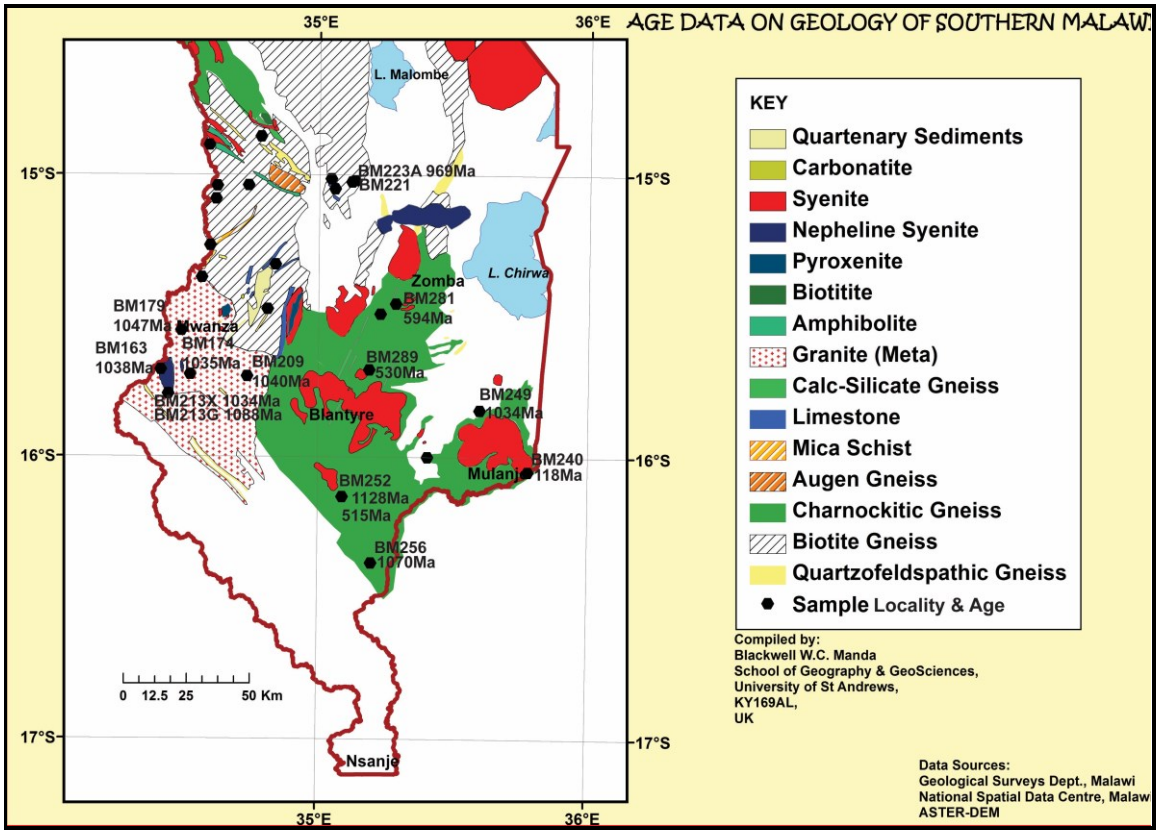

Fig. 5.39: Study map displaying the sample localities and ages for the lithologic units in southern Malawi

5.5 DISCUSSION AND IMPLICATIONS

LA-ICP-MS single zircon U-Pb dating was employed on calc-alkaline and associated supracrustal rocks in the study to provide constraints on the timing and nature of tectono-thermal events in southern Malawi in order to add understanding of the geodynamic evolution of the Mozambique Belt. Zircons have been characterised using back scatter images (BSE) and cathodo-luminescence (CL), which in turn guided the isotopic dating process providing constraints on the timing of magmatism and thermo-tectonic events. The study combines zircon types and morphology, and age data in seeking refinement of our knowledge of the geodynamic history. The working hypothesis in this study is that the southern Malawi region is a multiply metamorphosed terrane with granulite facies metamorphism and this would be tested by U-Pb zircon high precision age dating. The aim was to constrain the timing of calc-alkaline magmatism and associated tectono-thermal events in southern Malawi, and to determine the relationship between the magmatism and that in the neighbouring/adjacent areas within the Mozambique Belt.

Results in this study indicate tectonothermal events in three periods: Mesoproterozoic stretching from 1128 Ma to 1033 Ma; Neoproterozoic (956 Ma – 594 Ma); and Cambrian (530 Ma – 515 Ma). The Mesoproterozoic ones are magmatic events occurring over a period of nearly a hundred million years in three pulses at 1128 Ma, 1088 - 1070 Ma, and 1033 – 1047 Ma. The oldest (1128 Ma) is the emplacement of a charnockitic gneiss (sample BM252) occurring southwest of Mulanje. All the metagranite samples have emplacement dates within the Mesoproterozoic.

The emplacement of the protolith of hornblende biotite gneiss occurred ~956 Ma, with a leucogranite intruding at ca. 756 Ma. Charnockitic gneiss BM281 intruded much later (ca. 600

Ma) about 50 million years before the end of the Neoproterozoic. This study also found evidence for Pan-African magmatism and metamorphism spanning the late Neoproterozoic into the Cambrian (594 Ma to 515 Ma) on the basis of ages for the perthitic syenites and a charnockitic gneiss. In addition, one granite from Mulanje Mountain yielded a Cretaceous age of 118 ± 2 Ma. The data for rocks in southern Malawi display no evidence for the presence of late Archean reworked crustal precursors as suggested by Andreolli (1984). Previous studies using high precision geochronology in southern Malawi have found no evidence of Mesoproterozoic high grade metamorphism consistent with continental collision, but have confirmed Neoproterozoic – Cambrian metamorphism that overprinted the earlier magmatism (Kröner et al., 2001, 2003; Johnson et al., 2005; Ashwal et al., 2007).

The research found zircons that have variable amounts of U, ranging from 4 – 5629 ppm, and Th, from 0 – 3680 ppm. The zircons have variable Th/U ratios with ranges from 0 to 2.92. Metamorphic zircons were found to have the lowest Th/U ratio values (<0.02) as in sample BM252 whereas magmatic zircons have higher ratios (>0.30). The magmatic zircons are generally euhedral/subhedral and often pyramidal in shape, and they display oscillatory zoning in various degrees. Some grains show inherited cores whilst others display variable overgrowths. Metamorphic zircons were found to be rounded, often with featureless cores and mantles, but sometimes as overgrowths. The presence of inherited cores indicates heterogeneous sources of magmatic material i.e. calk-alkaline arc material (Liang Ma et al., 2013) from the lower crust.

Earlier dating by Kröner et al. (2001) yielded crystallisation dates for calc-alkaline magmatism between 1040 – 999 Ma. Johnson et al. (2005) dated calc-alkaline magmatism with ages between 1393 Ma and 1037 Ma in the Southern Irumide Belt to the west of the study area. Emplacement of calc-alkaline granitoids in the Nampula and Lurio Belt in Mozambique has been dated as Mesoproterozoic at c. 1148 Ma and 1009 Ma. Jacobs et al. (2001) concluded from U-Pb SHRIMP data that Mesoproterozoic rocks are the oldest in the Dronning Maud Land with metavolcanic rocks at c.1130 Ma and syntectonic granites and plutons at c. 1080 Ma. Kröner (2003) took note of occurrence of "rare" lithologic units belonging to the Irumide-age magmatism (crystallisation ages ~1009 – 1094 Ma) south of Mozambique. Bingen et al. (2009) noted the occurrence of calc-alkaline complexes in Mozambique, namely, Unango, Marrupa, and Nampula, and suggested their formation in active margin environments during the Mesoproterozoic (Irumide orogeny, ~1020 – 950 Ma) alongside terranes adjacent to the western side of southern Malawi otherwise named the Southern Irumide Belt (SIB). It must be noted, however, that Neoproterozoic magmatism has also been recorded in Malawi at c. 755 – 555 Ma (Kröner, et al., 2001) and in East Antarctica Jacobs et al. (2001) dated an anorthosite and a charnockite at c. 600 Ma. A comparative table for the Malawi U –Pb age data with some data on magmatism from other regions is presented in Table 5.21.

Table 5.21: Magmatism U - Pb age (Ma) data from Malawi and other regions

MALAWI		OUTHERN IRUMID		TANZANIA		MOZAMBIQUE		ANTARCTICA	
AGE	2S	AGE	2S	AGE	2S	AGE	2S	AGE	2S
1038	6.8	1393	22	633	N/A	1008	9	1850	N/A
1036	15	1082	7	639	N/A	1013	10	527	N/A
594	65	1066	21	642	N/A	1032	10	534	N/A
540	0	1071	8	843	N/A	1034	14	1059	N/A
1031	19	1083	8	1817	N/A	1037	10	527	N/A
1036	8.3	1050	20	1824	N/A	1039	11		
118	1.2	1046	3	1870	N/A	1040	8		
531	3.4	1070	3	1877	N/A	1047	8		
1047	13	1088	20	1898	N/A	1062	13		
1070	16	1051	12	1910	N/A	532	13		
756	8.6	1064	15	1921	N/A	538	10		
956	12	1037	8	1999	N/A	507	3		
1035	21	1040	21	2519	N/A	508	4		
1034	17	1105	22	2648	N/A	511	12		
1033	20	1094	2	2683	N/A	1042	9		
		1105	9	2685	N/A	1048	1		
		1125	15	2713	N/A	1057	9		
				2707	N/A	1060	17		
				2742	N/A	1072	8		
						1087	16		
						1123	9		

Sample BM221, a leucogranite, yielded a $^{206}Pb/^{238}U$ weighted average age of 737±53Ma, which has minimal geological significance on account of margins of uncertainty and error. Ashwal et al., (2007) dated magmatic zircons from a nepheline-monzonite gneiss in Mwanza – southern Malawi. Their analyses yielded a U-Pb isotopic analyses (by TIMS) upper intercept age of 730 ± 4 Ma (MSWD = 1.7) which was interpreted as a crystallisation age of the zircons, and this was a reflection of a continental rifting event during the Rodinia breakup period in the Neoproterozoic. Their SHRIMP spot analyses yielded a mean age of 729 ± 7 Ma (MSWD = 0.37). The leucogranite gneiss in this study therefore although poorly constrained may be consistent with Rodinia breakup events.

The significance of the Cretaceous date (118 ± 2 Ma) from a granite on Mulanje Mountain close to the Mozambique border east of the study area fits with known magmatism during the Upper Jurassic to Cretaceous in the Chilwa Alkaline Province in southern Malawi and adjacent parts of Mozambique (Platt et al., 1986).

Data from charnockitic sample BM252 yielded a lower intercept age of 515 ± 18 Ma interpreted as an age of metamorphism. A monazite $^{207}Pb/^{235}U$ age of 522 ± 17 Ma confirmed amphibolite metamorphism in the area (Ashwal et al., 2007) and it was suggested that it was a result of collisional suturing events associated with amalgamation of East and West Gondwana. Peak regional granulite facies metamorphism in the central part of Tanzania has been dated at c 640 Ma (Sommer et al., 2003). Granulite facies metamorphism was dated as Mesoproterozoic at c. 1080 in East Antarctica (Dronning Maud Land) with subsequent metamorphic events dated at c. 570 – 550 Ma and 530 – 515 Ma (Jacobs et al., 2001). The date from the charnockitic sample BM252 is thus consistent within errors with the monazite date by Ashwal et al., 2007 but both (515 ± 18 Ma and 522 ± 17 Ma, respectively) are younger than those documented in previous

studies in southern Malawi i.e. 571–549 Ma, but are closer to those known for the Central Dronning Maud Land/East Antarctica (570 – 550 Ma; 530–515 Ma). They are also younger than the dates from Tanzania which have given ages of ca. 640 Ma.

The findings are in marked contrast to Andreolli (1984) who used Rb-Sr whole rock dating to come up with a date of 850 – 1085 Ma in Malawi and those of Sacchi et al. (1984) and Pinna et al. (1993) with similar dates in northern Mozambique, that had been interpreted as reflection of high grade metamorphism belonging to a Kibaran (Mesoproterozoic) orogenic belt with a possible link to the rocks Dronning Maud Province of Antarctica.

The absence of isotopic ages of Archean ages in the studied lithologic units would suggest that all the magmatic and metamorphic events are related to younger igneous and tectono-thermal events, likely a result from crustal thickening in arc margin (subduction) environment (Muhongo et al., 1994). The crystallisation ages in the Mesoproterozoic would also imply crustal growth by additions of calc-alkali magmas in arc environments. The Neoproterozoic ages may mean two things: growth of new zircon during the Pan African Orogen or emplacement of new magmatic material (crustal addition) during that time. Isotopic data may be required to affirm sources of this magmatism in the Neoproterozoic (rather than being addition of new magmatic material it could be recycling of crustal material). Calc-alkaline magmatism coupled with the occurrence of marbles, calc-silicates and pelitic gneisses suggests arc-margin environments with shelf conditions in area. The subduction-related setting is consistent with other Mesoproterozoic terranes in Tanzania, Mozambique, Madagascar and Antarctica.

5.6 CONCLUSION AND RECOMMENDATIONS

Calc-alkaline magmatism in subduction related environment in southern Malawi has been dated in this study as late Mesoproterozoic (1033 – 1128 Ma), late Neoproterozoic (594 Ma) and during the Cambrian (535 Ma). Metamorphism related to collisional tectonics has been dated as Pan –African (Cambrian 515 ± 18 Ma). These findings are consistent with other previous studies in the area and in the adjacent regions (Bingen et al., 2009; Johnson et. al., 2005; Jacobs et al., 2001; Kröner et al., 2001), but contrast Andreolli (1984), Sacchi et al. (1984), and Pinna et al. (1993) who had interpreted their Rb-Sr whole rock dates as signifying high grade metamorphism belonging to a Kibaran (Mesoproterozoic) orogenic belt.

This study did not find evidence for different age crustal blocks in southern Malawi as the metagranites to the west and charnockitic gneisses to the east yielded Mesoproterozoic emplacement ages and Pan-African (Cambrian) metamorphism ages. A more detailed U-Pb work program on a regular grid coupled with other isotope dating methods (Sm-Nd, Lu-Hf) would be required to provide a detailed understanding of the geological relationships in the area. LA-ICP-MS has provided reliable high precision data in a relatively short time and would therefore be ideal to utilise in carrying out more work in south Malawi and the adjacent areas to the north. Monazite U-Pb dating would provide more robust data on metamorphism than zircon U-Pb, and that would be complementary to this study.

5.7 REFERENCES

Andreolli, M. A. G., (1984), Petrochemistry, Tectonic Evolution and Metasomatic Mineralizations of Mozambique Belt Granulites from S Malawi and Tete (Mozambique), Precambrian Research, Vol. 25, Issue 1-3, pp. 161-186.

Ashwal L.D., R. A. Armstrong et al., (2006), Geochronology of Zircon Megacrysts from Nepheline-bearing Gneisses as Constraints on Tectonic Setting: Implications for Resetting of the U-Pb and Lu-Hf Isotopic Systems, Contrib Mineral Petrol (2007) 153:389–403, DOI 10.1007/s00410-006-0153-

Bickford M. E., (1988) "The Formation of Continental Crust: Part 1. A Review of Some Principles; Part 2. An Application to the Proterozoic Evolution of Southern North America", Geological Society of America Bulletin 1988; 100, no. 9; 1375-1391, doi: 10.1130/0016-7606(1988)100<1375: TFOCCP>2.3.CO; 2

Bingen, B., J. Jacobs, et al. (2009). "Geochronology of the Precambrian Crust in the Mozambique Belt in NE Mozambique, and Implications for Gondwana Assembly." Precambrian Research 170(3–4): 231-255.

Bloomfield, K. (1965), The Geology of the Kirk Range – Lisungwe Valley Area, Bulletin 7, Geological Survey Department, Malawi, Government Printer, Zomba, Malawi.

Bloomfield, K., (1970), The Geology of the Zomba Area, Bulletin 16, Geological Survey of Malawi, Government Printer, Zomba, Malawi.

Evans, R. K., (1965), The Geology of the Shire Highlands, Bulletin 18, Geological Survey of Malawi, Government Printer, Zomba, Malawi.

Garson, M. S. et al., (1969), The Geology of the Mulanje Area, Bulletin 21, Geological Survey of Malawi, Government Printer, Zomba, Malawi.

Cao Xiaofeng, Lü Xinbiao, Liu Shentai, Zhang Ping, Gao Xiang, Chen Chao, Mo Yalong, (2011) LA-ICP-MS Zircon Dating, Geochemistry, Petrogenesis and Tectonic Implications of the Dapingliang Neoproterozoic Granites at Kuluketage Block, NW China. Precambrian Research, 186 (2011) 205–219.

Cawood P. A. and A. A. Nemchin, Paleogeographic Development of the East Laurentian Margin: Constraints from U-Pb dating of Detrital Zircons in the Newfoundland Appalachians, Geological Society of America Bulletin 2001;113, no. 9;1234-1246, doi: 10.1130/0016-7606(2001)113<1234:PDOTEL>2.0.CO;2.

Cordani U.G., Benjamin B. Brito-Neves and Manoel S.D'Agrella-Filho, (2003), From Rodinia to Gondwana: A Review of the Available Evidence from South America, Gondwana Research, Vol 6, No. 2, pp. 275-283. International Association for Gondwana Research, Japan.ISSN: 1342-937X.

Corfu F., J. M. Hanchar, P.W.O. Hoskin, and P. Kinny (2003), Atlas of Zircon Textures. Zircon, Reviews in Mineralogy and Geochemistry, 53, Chapter 16, 469 – 500, DOI: 10.2138/rmg.2003.53.16

Faure, G and T. Mensing, (2005), Isotopes: Principles and Applications, 3rd Edition, John Wiley & Sons, INC., New Jersey, USA.

Fisher C. M., Hanchar J. M., Samson S. D., Dhuime B., Blichert-Toft J., Vervoort J. D., Lam R., Synthetic zircon doped with hafnium and rare earth elements: A reference material for in situ hafnium isotope analysis, Chemical Geology, Volume 286, Issues 1–2, 26 June 2011, Pages 32–47.

Hawkesworth C. J. & Kemp A. I. S., Evolution of the continental crust, NATURE, Vol 443, 19 October 2006, doi:10.1038/nature05191

Helo, C., Hegner, E., Kröner, A., Badarch, G., Tomurtogoo, O., Windley, B. F., Dulski, P., (2006), Geochemical Signature of Paleozoic Accretionary Complexes of the Central Asian Orogenic Belt in South Mongolia: Constraints on Arc Environments and Crustal Growth, Chemical Geology, Volume 227, Issue 3-4, pp 236-257.

Hiess J., Condon D. J., McLean N. and Noble S. R., (2012), 238U/235U systematics in terrestrial U-bearing minerals, Science Magazine, New York, N.Y.), v. 335, no. 6076, p. 1610 – 4, doi: 1126/science.1215507.

Jackson S. E., Pearson N. J., Griffin W. L., Belousova E. A., The application of laser ablation-inductively coupled plasma-mass spectrometry to in situ U–Pb zircon geochronology, Chemical Geology, Volume 211, Issues 1–2, Pages 1-184 (8 November 2004) Original Research Article, Pages 47-69.

Jacobs J., C. Mark Fanning, Friedhelm Henjes-Kunst, Martin Olesch, and Hans-Ju¨ rgen Paech, Continuation of the Mozambique Belt into East Antarctica: Grenville-Age Metamorphism and Polyphase Pan-African High-Grade Events in Central Dronning Maud Land, The Journal of Geology, Vol. 106, No. 4 (July 1998), pp. 385-406, The University of Chicago Press, Stable URL: http://www.jstor.org/stable/10.1086/516031, Accessed: 10/12/2015 18:21

Johnson S. P, T. Rivers & B. De Waele (2005), A Review of the Mesoproterozoic to Early Paleozoic Magmatic and Tectonothermal History of South–Central Africa: Implications for Rodinia and Gondwana, Journal of the Geological Society, London, Vol. 162, 2005, pp. 433–450. Printed in Great Britain.

Kröner A., A.P. Willner , E. Hegner, 1, P. Jaeckel, A. Nemchin, Single Zircon Ages, PT Evolution and Nd Isotopic Systematics of High-grade Gneisses in Southern Malawi and their Bearing on the Evolution of the Mozambique Belt in Southeastern Africa, Precambrian Research 109 (2001) 257–291, 2001 Elsevier Science B.V.

Kröner A., & U. Cordani, (2003), African, Southern Indian and South American Cratons were not part of the Rodinia Supercontinent: Evidence from Field Relationships and Geochronology, Tectonophysics 375 (2003) 325– 352.

Liang Ma, Shao-Yong Jiang, Bao-Zhang Dai, Yao-Hui Jiang, Ming-Lan Hou, Wei Pu, Bin Xu, (2013), Multiple Sources for the Origin of Late Jurassic Linglong Adakitic Granite in the Shandong Peninsula, Eastern China: Zircon U–Pb Geochronological, Geochemical and Sr–Nd–Hf Isotopic Evidence, Lithos 162–163 (2013) 251–263

Ludwig, K.R., 2003, Isoplot 3.00: A geochronological toolkit for Microsoft Excel: Berkeley Geochronology Centre Special Publication 4, 70 p.

Mezger, K., Krogstad, E. J., Interpretation of discordant U-Pb zircon ages: An evaluation, J. Metamorphic Geol., 1997, 15: pp. 127 - 140.

Muhongo S. & J.-L. Lenoir (1994), Pan-African Granulite-Facies Metamorphism in the Mozambique Belt of Tanzania: U-Pb Zircon Geochronology, Journal of the Geological Society, London, Vol. 151, 1994, Pp. 343-347.

Nebel-Jacobse Y, Scherera E. E., Mu¨nkera Carsten, Mezger K, (2005), Separation of U, Pb, Lu, and Hf from single zircons for combined U–Pb dating and Hf isotope measurements by TIMS and MC-ICPMS, Chemical Geology 220 (2005) 105– 120.

Nowell, G and Parrish, R.R., 2001, Simultaneous Acquisition of Isotope Compositions and Parent/Daughter Ratios by non-isotope-dilution-mode Plasma Ionisation Multi-collector Mass Spectrometer (PIMMS), in Plasma Source Mass Spectrometer: The New Millenium, edited by G. Holland and S.D. Tanner, Proceedings of the 7th International Conference of Plasma Source Mass Spectrometry: The Millenium Conference, Royal Society of Chemistry, Special Publication 267, pp 298 - 310

Pinna, P., G. Jourde, et al. (1993). "The Mozambique Belt in northern Mozambique: Neoproterozoic (1100–850 Ma) crustal growth and tectogenesis, and superimposed Pan-African (800–550 Ma) tectonism." Precambrian Research 62(1–2): 1-59.

Platt R. G. and A. R. Woolley, (1986), The mafic mineralogy of the peralkaline syenites and granites of the Mulanje complex, Malawi, Mineralogical Magazine, March 2006, Vol. 50, pp 85 - 99

Rajesh H. M., (2007), The petrogenetic characterization of intermediate and silicic charnockites in high-grade terrains: a case study from southern India, Contributions to Mineral Petrology (2007) 154:591–606.

Ring U., Kröner A., Toulkeridis U. T., (1997), Paleoproterozoic granulite-facies metamorphism and granitoid intrusions in the Ubendian-Usagaran Orogen of northern Malawi, east-central Africa, Precambrian Research 85 (1997) 27-51.

Ring, U., Kroner A., Layer P., Buchwaldt R., Toulkeridis T., (1999), "Deformed A-type granites in northern Malawi, east-central Africa: pre- or syntectonic?" Journal of the Geological Society 156: 695-714.

Ring U., Kröner A., Buchwaldt R., Toulkeridis T., Layer P. W., (2002), Shear-zone patterns and eclogite-facies metamorphism in the Mozambique belt of northern Malawi, east-central Africa: implications for the assembly of Gondwana, Precambrian Research 116 (2002) 19–56.

Sláma J., Košler J., Condon D. J., Crowley J. L., Gerdes A., Hanchar J. M., Horstwood M. S.A., Morris G. A., Nasdala L., Norberg N., Schaltegger U., Schoene B., Tubrett M. N., Whitehouse M. J., (2008), Plešovice zircon — A new natural reference material for U–Pb and Hf isotopic microanalysis, Chemical Geology, Volume 249, Issues 1–2, Pages 1-236.

Sommer H., A. Kröner, C. Hauzenberger, S. Muhongo and M. T. D. Wingate, (2003), Metamorphic petrology and zircon geochronology of high-grade rocks from the central Mozambique Belt of Tanzania: crustal recycling of Archean and Paleoproterozoic material during the Pan-African orogeny, Journal of metamorphic Geology, 2003, 21, 915–934 doi:10.1046/j.1525-1314.2003.00491.x

Spencer, C.J., Cawood, P.A., Hawkesworth, C.J., Prave, A.R., Roberts, N.M.W., Horstwood, M.S.A., et al., 2015. Generation and preservation of continental crust in the Grenville Orogeny. Geosci. Front., 1–16, http://dx.doi.org/10.1016/j.gsf.2014.12.001

Sreejith C., et al., (2013), Petrogenesis of high-K metagranites in the Kerala Khondalite Belt, southern India: a possible magmatic-arc link between India, Sri Lanka, and Madagascar, Journal of Geodynamics 63 (2013) 69– 82

Tanaka T., Togashi S., Kamioka H., Amakawa H., Kagami H., Hamamoto T., Yuhara M., Orihashi Y., Yoneda S., Shimizu H., Kunimaru T., Takahashi K., (2000), JNdi-1: a neodymium isotopic reference in consistency with LaJolla neodymium, Chemical Geology - CHEM GEOL , vol. 168, no. 3, pp. 279-281, 2000, DOI: 10.1016/S0009-2541(00)00198-4

Walshaw, R.D. (1965) The geology of the Ntcheu-Balaka area Bulletin 19, Geological Survey Department, Malawi, Government Printer, Zomba, Malawi.

Wiedenbeck M., Hanchar J. M., Peck W. H., Sylvester P., Valley J., Whitehouse M., Kronz A., Morishita Y., Nasdala L., Fiebig J., Franchi I., Girard J.-P., Greenwood R.C., Hinton R., Kita N., Mason P.R.D., Norman M., Ogasawara M., Piccoli P.M., Rhede D., Satoh H., Schulz-Dobrick B., Skår O., Spicuzza M.J., Terada K., Tindle A., Togashi S., Vennemann T., Xie Q., and Zheng Y.-F., (2004), Further Characterisation of the 91500 Zircon Crystal, Geostandards and Geoanalytical Research, Volume 28, Issue 1, pages 9–39, DOI: 10.1111/j.1751-908X.2004.tb01041.x.

Wilson M. (2007), Igneous Petrogenesis, Springer, The Netherlands.

Wu, Y.B., Zheng, Y.F., 2004. Genesis of zircon and its constraints on interpretation of U–Pb age. Chinese Science Bulletin 49, 1554–1569.

Xiang W., Griffin W.L., Jie C., Pinyun, H., Xiang, L. I., (2011), U and Th Contents and Th/U Ratios of Zircon in Felsic and Mafic Magmatic Rocks: Improved Zircon-Melt Distribution Coefficients, Acta Geologica Sinica - English Edition, Blackwell Publishing Co Ltd., Vol 85 (1), pp. 164-174. DOI: 10.1111/j.1755-6724.2011.00387.x

Chapter 6: Sm – Nd and Lu – Hf Radiogenic Isotope Geochemistry

6.1 INTRODUCTION

Aims of this chapter

The objective of this chapter is to present new Sm – Nd whole rock major and single zircon Lu – Hf isotope data to constrain the sources and the timing of thermal events leading to granitoid magmatism in southern Malawi, and to use these data to characterise the regional geodynamic setting. The main aim of the chapter is to test two hypotheses. First, the hypothesis that contemporary crust in this region is derived from re-melting and re-working of older crust derived from mantle and upper crust levels of the lithosphere is tested using Nd isotope modelling. Second, the hypothesis that different crustal growth zones and magmatic intervals exist in this region and that resulting granitoids are an expression of collision-continental arc margin environments. This is tested using Lu-Hf dating and modelling in combination with geochronological constraints (Chapter 5). This area is important as it falls within the East African Orogen which comprises deformed and metamorphosed Precambrian rocks and is generally considered to be the principal collision zone during late Neoproterozoic amalgamation of Gondwana thus recording evidence of the genesis and evolution of the belt (Vogt et al., 2006; Kröner, 2001). The chapter reports and interprets geochemical results from Laser Ablation Inductively Coupled Plasma Mass Spectrometry (LA-ICP-MS) of granitoid samples from southern Malawi.

6.2 BACKGROUND

The samarium-neodymium isotope system

The Sm – Nd isotope system is normally considered a useful guide to the source of magma (Rollinson, 1993). Sm and Nd are relatively immobile compared with Rb, Sr, Th, U, and Pb consequently they are often more robust indicators in rocks that have gone through disturbances of metamorphism or fluid interaction (Rollinson, 1993). The system remains largely unperturbed during low temperature metamorphism and is particularly useful for tracing sources of magma in such rocks (Rollinson, 1993; Dickin, 2005), with application to the evolution and genesis of lower crustal sources and basement compositions of crustal terranes (Faure, 2005; Dickin, 2005).

Samarium-147 undergoes alpha-decay to neodymium-143, with a decay constant of 6.54×10^{-12} year $^{-1}$ (Faure et al., 2005). The initial $^{143}Nd/^{144}Nd$ ratio of any magmatic sample can be calculated from the measured isotopic ratios of $^{143}Nd/^{144}Nd$ and $^{147}Sm/^{144}Nd$ if its age is known. This ratio is then compared to mantle composition at the same time using the epsilon (εNd) notation (Rollinson, 1993; Stern, 2002), which is a measure of the difference between the $^{143}Nd/^{144}Nd$ ratio of a sample and a reference sample. In this chapter the Chondritic Uniform Reservoir (CHUR) is used as the reference (Rollinson, 1993). The εNd (t) of a sample is the εNd at time of formation (t) and is calculated from the initial $^{143}Nd/^{144}Nd$ of a sample and the $^{143}Nd/^{144}Nd$ of CHUR at the same time using the formula:

$\varepsilon Nd(t) = [((^{143}Nd/^{144}Nd \text{ (rock, t)})/(^{143}Nd/^{144}Nd \text{ (CHUR, t)})) - 1] \times 10^4$ (Rollinson, 1993).

The lutetium – hafnium isotope system

Lutetium (Lu), is the heaviest of the rare earth elements (REEs) at the end of the lanthanide series. ^{176}Lu, one of its naturally occurring isotopes, is radioactive and decays to stable ^{176}Hf, providing the basis for the Lu – Hf dating method (Faure et al., 2005, Dickin, 2005). Hf is also an important tracer of the sources of magma and Hf isotope data have been used to test Nd evidence for early crustal evolution with the result that whole-rock Sm–Nd systems have been shown in some cases to have been disturbed (Dickin, 2005).

The Lu – Hf system is analogous to the Sm - Nd system in that both elements are comparatively immobile and refractory. Their daughter isotopes are compatible with crustal minerals leading to lower ^{143}Nd/^{144}Nd and ^{176}Hf/^{177}Hf in the crust than in the mantle (White, 2007). The half-life of ^{176}Lu is only one third as long as that of ^{147}Sm and Lu – Hf fractionation is greater than that of Sm – Nd resulting in greater disparity in ^{176}Hf/^{177}Hf than in ^{143}Nd/^{144}Nd. This makes Hf isotope ratios more robust isotopic indicators of crust-building processes (White, 2007). Hf isotope ratios can be expressed using the epsilon (εHf) notation in a formulation analogous to Nd (parts per 10,000 deviation from the chondritic evolution line).

Model ages

Nd model ages, which indicate when a sample was separated from its mantle source, can be calculated based on the model parameters and measured ^{147}Sm/^{144}Nd and ^{143}Nd/^{144}Nd ratios (Rollinson, 1993; Stern, 2002). Depleted mantle model (TDM) ages are sometimes designated as "crust formation ages" and are calculated on the assumption that magma was derived from depleted mantle asthenosphere (De Paolo, 1981; Dhuime et al., 2011). The calculation of depleted mantle model ages (Nd and Hf) assumes that the isotope composition of the new crustal material is similar to that of the depleted mantle at the same time (Dhuime et al., 2011). The alternative assumption is that the Earth's primitive mantle had the same isotopic composition as the average chondritic meteorite at the time of formation of the earth (4.5 Ga), which gives the T_{CHUR} model ages (Rollinson, 1993). There is evidence, however, showing that island arcs which are equivalent to the new continental crust have different isotopic ratios from the depleted mantle and for this reason yet another model age is based on new continental crust that is more isotopically enriched than the depleted mantle (Dhuime et al., 2011). This proposal notates these model ages as TDM_{nc}.

6.3 ANALYTICAL METHODS

Non-ignited bulk rock samples were digested in HF-HNO3 to provide the solution for Sm - Nd analyses at the Natural Environment Research Council Isotope Geoscience Laboratory (NIGL), Nottingham in the UK. The concentration of light rare earth elements (LREEs) was undertaken using Eichrom AG50 cation exchange columns. Sm and Nd were loaded onto double-rhenium filament assemblies and analysed in multi-dynamic mode on a Thermo Scientific Triton thermal ionization mass spectrometer. ^{143}Nd/^{144}Nd is reported normalized to a preferred value of 0.512115 for the JNd-i standard (Tanaka et al., 2000). Measured ^{143}Nd/^{144}Nd ratios for the La Jolla standard are 0.512106 ± 0.000010 (2 sigma = 18 ppm, n = 15).

Zircon ablation spots with near concordant (> 95 % concordance) U–Pb analyses from each of the samples were re-analysed for their Lu–Hf isotopic compositions. Isotope analyses were carried out using a Thermo Scientific Neptune Plus MC-ICP-MS coupled to a New Wave Research UP193UC excimer laser ablation system and a TwoVol2 ablation cell. Helium was used as the carrier gas through the ablation cell with Ar makeup gas being connected via a T-piece and sourced from a Cetac Aridus II desolvating nebulizer. After initial set-up and tuning, the nebulizer was aspirating air during the ablation analyses. Masses ^{172}Yb, ^{173}Yb, ^{175}Lu,

^{176}Hf+Yb+Lu, ^{177}Hf, ^{178}Hf, ^{179}Hf and ^{180}Hf were measured simultaneously using a 1 second integration time during a static, 30 second ablation analysis utilising a 35 μm diameter spot and a fluence of 8-10 J/cm^2 (see Spencer et al., 2015 for full methods).

A standard–sample–standard bracketing technique, using zircons Mudtank and 91500 as reference materials, was employed to monitor accuracy and precision of internally corrected Hf isotope ratios and instrumental drift with respect to the Lu/Hf ratio. Hf reference solution JMC475 (both doped with 2 ppb Yb and undoped) was analysed during each analytical session to allow normalization of the laser ablation Hf isotope data. Correction for ^{176}Yb on the ^{176}Hf peak was made using a ^{176}Yb/^{173}Yb ratio calibrated for Hf mass bias using Yb-doped JMC475 solutions (cf. Nowell and Parrish, 2001). Additionally, Plešovice and Yb-doped synthetic zircons (Zr141 and Zr142; Fisher et al., 2010) were analysed to assess the accuracy of the Hf ratio normalization and Yb ratio correction, respectively. ^{176}Lu interference on the ^{176}Hf peak was corrected by using the measured ^{175}Lu and assuming ^{176}Lu/^{175}Lu = 0.02653. Systematic uncertainties of Hf and Lu isotope ratios were propagated using quadratic addition, incorporating the external variance of the reference material during each analytical session.

Results of Hf analyses over nine sessions spanning three weeks, for 91500, Mudtank, Plesovice, and Yb-doped synthetic zircons, are presented below (Table 6.1). Hf ratios of Mudtank are self-normalized. Two Yb-doped synthetic zircons containing varying amounts of Yb were also analysed. The lower Yb zircon (Zr141, Yb/Hf = ~0.08) yielded a precise and accurate arithmetic mean within uncertainty of the preferred value. The higher Yb zircon (Zr142, Yb/Hf = ~0.16) yielded a greater degree of scatter over the three week period and returned > 200 ppm reproducibility within each daily session. Only 2 of the 341 sample analyses had Yb/Hf ratios beyond the range of Zr141 and even for these analyses the average Hf isotope ratio did not deviate from the range determined from the low Yb/Hf samples. It is therefore concluded that for this dataset the Yb/Hf isobaric interference is accurately corrected.

Table 6.1: Measured Lu–Hf data for reference materials for normalization (91500) and assessment of secondary reference materials (Mudtank, Plesovice, and Zr141). In the table MSWD = Mean square weight deviation. MC = Multicollector.

Standard	Measured (MC-ICP-MS)	±2s (%)	MSWD	Preferred	n MC
91500	0.282301	0.010	0.89	0.282307	206
Mudtank	0.282509	0.008	0.55	0.282507	143
Plesovice	0.282484	0.009	1.18	0.282482	98
Zr141	0.282128	0.008	0.77	0.28214	46

6.4 RESULTS

6.4.1 Sm – Nd analyses

Results for whole rock Sm – Nd isotopic analyses on granitoids from Southern Malawi are presented in Table 6.2. Neodymium epsilon (εNd(t)) values are calculated at magmatic crystallisation ages as determined by U – Pb single zircon dating for each sample. Samples with $^{147}Sm/^{144}Nd > 0.165$ are considered to yield unreliable model ages (Stern, 2002) however all the samples in this study are <0.16 except for sample BM252. The whole rock Sm – Nd data show elemental quantities of Sm ranging from 0.9 – 33 ppm and Nd ranges from 5.4 – 154 ppm. The $^{147}Sm/^{144}Nd$ ratios range from 0.0986 to 0.1814 and ratios for $^{143}Nd/^{144}Nd$ range from 0.512104 to 0.512811. Calculated TDM model ages range from 1153 to 1801 Ma with the mean at 1535 Ma. The εNd(o) values are all negative and have a wide range from -10.31 to -2.24. The εNd(t) values range from -4.95 to +5.78 suggestive of substantial contributions to the crust from depleted mantle sources with some contributions from crustal sources. A $^{147}Sm/^{144}Nd$ vs $^{143}Nd/^{144}Nd$ correlation diagram (Figure 6.1) is presented indicating a rather poor positive correlation of the two isotopes, however this is to be expected for rocks of different ages on an isochron plot. Included on this diagram are data from published literature from Malawi by Kröner (2003) and that dataset and the new data in this thesis show similar variability over approximately the same ranges.

Table 6.2: LA-ICP-MS Sm - Nd isotope data for southern Malawi granitoids

Sample	87Sr/86Sr_tr	± 2SE	Sm ppm	± 2SE	Nd ppm	± 2SE	147Sm/144Nd	143Nd/144Nd	± 2SE	U - Pb Age	εNd(o)	εNd(t)	Model Age	143Nd/144Nd (t, CHUR)	143Nd/144Nd(t,rock)
BM163	0.707839	0.000008	7.501154	0.00395	31.9747	0.0019	0.141819799	0.512409246	0.000007	1038	-4.4623	2.83726	1567.68538	0.511298155	0.511443224
BM174	0.715412	0.000007	7.113064	0.00221	32.3938	0.00285	0.13273897	0.512291243	0.000006	1036	-6.7642	1.72263	1613.33115	0.511300746	0.511388824
BM281	0.707296	0.000009	4.801445	0.00304	24.0675	0.00176	0.120593944	0.512109238	0.00001	594	-10.315	-4.5428	1699.72897	0.511872382	0.511639848
BM282A	0.704952	0.000009	5.146668	0.00428	20.1361	0.00109	0.154517233	0.512523249	0.000007	540	-2.2384	0.6736	1610.76706	0.511942106	0.511976591
BM200	0.764564	0.000005	7.13761	0.00114	33.5404	0.0025	0.128649234	0.512473247	0.00001	1031	-3.2138	5.78217	1211.85828	0.511307222	0.511602868
BM249	0.712732	0.000006	12.76077	0.08603	58.3519	0.00526	0.132197597	0.512270242	0.000006	1036	-7.1738	1.38389	1641.65367	0.511300746	0.511371504
BM240	0.709484	0.000093	18.15895	0.19426	78.7213	0.00836	0.13944886	0.512419246	0.000007	118	-4.2672	-3.406	1497.48326	0.512486144	0.512311589
BM289	0.718988	0.000122	32.82047	0.86408	153.39	0.03383	0.129341369	0.512150239	0.000007	531	-9.5147	-4.9504	1801.47422	0.511953725	0.511700289
BM179	0.715762	0.000006	7.343694	0.00542	34.1248	0.0033	0.130091626	0.512311243	0.000009	1047	-6.374	2.56023	1526.29746	0.511286499	0.5114174
BM256	0.725572	0.000009	6.538025	0.00238	28.3402	0.00228	0.139460567	0.512329244	0.000008	1070	-6.0229	1.82293	1681.1721	0.511256705	0.511349904
BM221	0.718058	0.000008	0.887055	2.7E-05	5.44022	0.00019	0.098568086	0.512278242	0.000006	756	-7.0178	2.4749	1153.40884	0.51166306	0.511789691
BM223A	0.709847	0.000008	11.98502	0.0252	66.018	0.00873	0.109740762	0.51217624	0.000007	956	-9.0075	1.63536	1425.55891	0.511404332	0.511487965
BM213G	0.712894	0.000008	7.687673	0.00386	35.4368	0.00328	0.131143802	0.512324244	0.000009	1088	-6.1204	3.01963	1521.81402	0.511233386	0.511387759
BM213X	0.708681	0.000005	8.208708	0.04817	34.552	0.00305	0.14362032	0.512395245	0.000008	1034	-4.7354	2.2962	1637.97664	0.511303336	0.511420742
BM209	0.711999	0.000007	5.964451	0.00616	26.8379	0.00205	0.134349739	0.512398245	0.000009	1033	-4.6769	3.5771	1441.78608	0.511304631	0.51148753

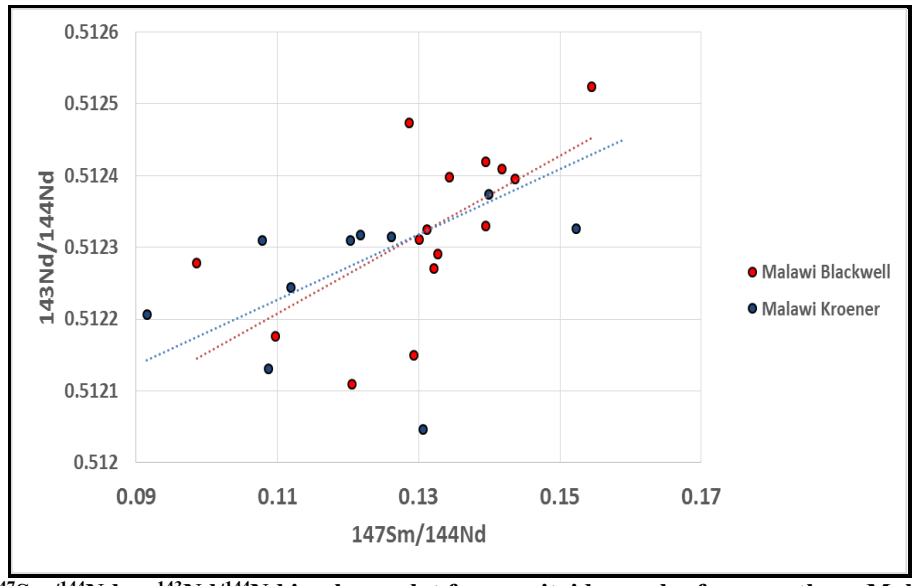

Figure 6.1: $^{147}Sm/^{144}Nd$ vs $^{143}Nd/^{144}Nd$ isochron plot for granitoid samples from southern Malawi using combined data from this study and from Kröner et al. (2003)

6.4.2 Sm – Nd DATA DISTRIBUTION

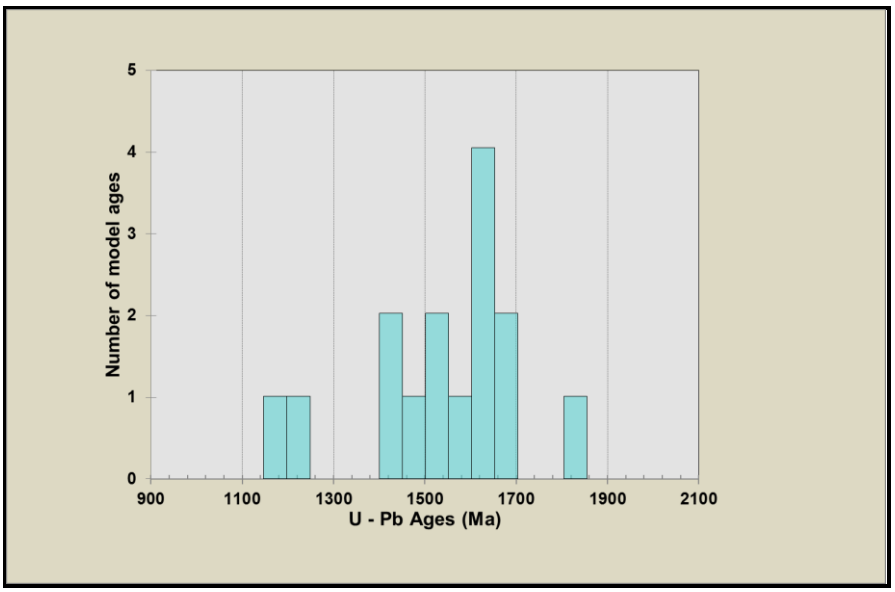

Figure 6.2: Sm –Nd model ages distribution for granitoids from southern Malawi

The distribution of the Sm – Nd model age data is shown in Figure 6.2. The oldest model ages (Paleoproterozoic) are from the central part of the study area - a perthitic syenite BM289 from Chiradzulu hill to the north of Blantyre (1801 Ma) and from a charnockitic gneiss BM281 (1700 Ma) further north (about 60 kilometers from Blantyre). The youngest model ages are from a hornblende gneiss sample BM221 (model age 1153 Ma) from a locality about 60

kilometers north of Zomba and a quartzo-feldspathic gneiss sample BM200 (1212 Ma) from an area north of Mwanza west of the study area.

6.4.3 INITIAL EPSILON (εNd(t)) VALUES

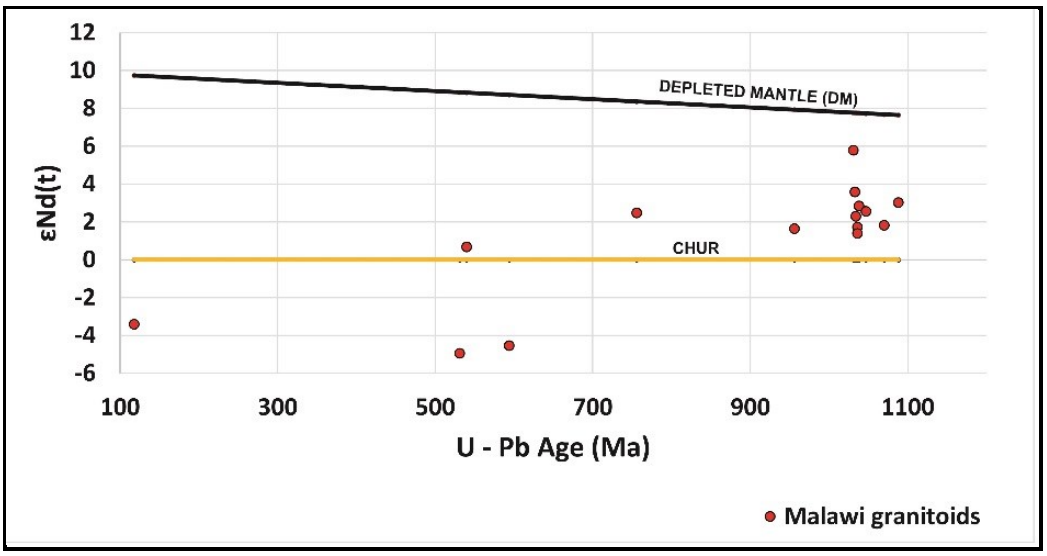

Figure 6.3: εNd(t) vs U - Pb age evolution diagram for southern Malawi granitoids

Figure 6.3 shows the εNd(t) values plotted against the U – Pb ages. Granitoids of Mesoproterozoic age and some of Neoproterozoic age have relatively primitive origins in the mantle whereas towards the end of the Mesoproterozoic and during the Neoproterozoic magmatism was largely due to recycling of older crust with only a small amount from juvenile material.

Sm – Nd isotopic data on granitoids from Malawi by Kröner (2003) has been utilised to calculate εNd(t) values comparable to those in this study and are plotted in Figure 6.4. The data from Kröner shows εNd (t) values ranging from -3.70 to +3.73 against the U – Pb ages. The data from the study of Kröner (2003) is consistent with this study in showing a small amount of crustal addition during the Neoproterozoic.

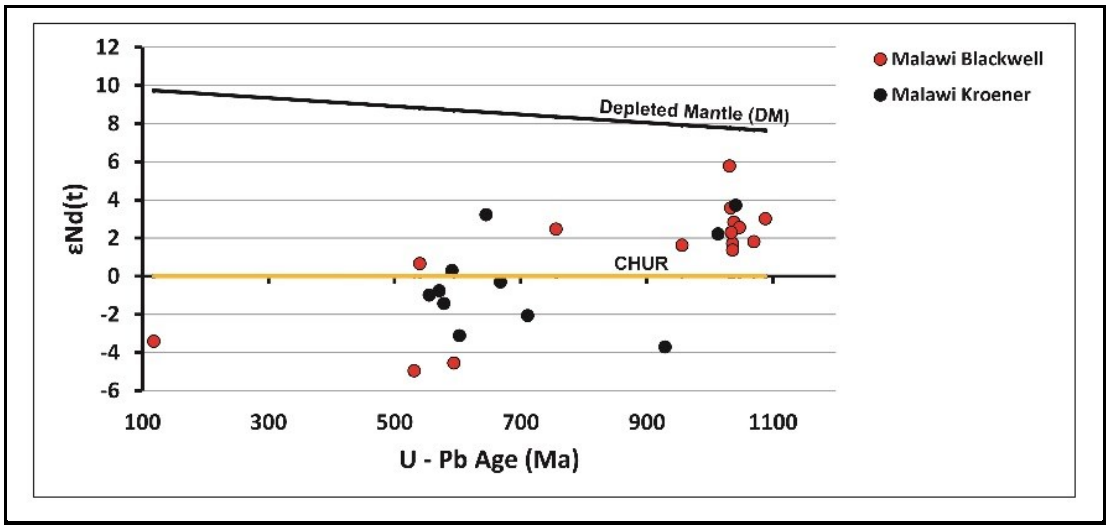

Figure 6.4: εNd(t) vs U - Pb age evolution diagram for southern Malawi granitoids for both this study and that of Kröner (2003).

6.4.4 CHARNOCKITIC GNEISSES

Sample BM249: The U – Pb age for this charnockitic gneiss sample is 1036 Ma with an initial εNd (t) value of +1.4 and a crustal model age of 1642 Ma. The positive εNd (t) value of the sample suggests derivation from magma-depleted sources in the mantle (Faure et al., 2005).

Sample BM281: This rock is a charnockitic gneiss with a U –Pb age of 594 Ma. Whole rock Sm - Nd analyses were carried out yielding an initial εNd (t) value of -4.5 and a crustal model age of 1700 Ma. The negative εNd (t) value of the sample suggests derivation of the gneiss protolith from a source with lower Sm/Nd ratio than CHUR – i.e. an enriched mantle or a crustal source (Rollinson 1994; Faure et al., 2005).

Sample BM282A: This sample is a charnockitic gneiss with a U –Pb age of 540 Ma, whose initial εNd (t) has the value of +0.7 with a crustal model age of 1611 Ma. The positive εNd (t) value of the sample is suggestive of origins of protolith of the gneiss from juvenile material.

These three charnockites BM249, BM281 and BM282A have very different U-Pb ages (1036, 592 and 540 Ma respectively) indicating separate thermal events yet their crustal model ages are not very different (1642, 1700 and 1611 Ma respectively) while there is some variation in their εNd(t) values (+1.4, -4.5 and +0.7 respectively). These data suggest that the sources for the charnockites may have separated from the mantle at around 1650±50 Ma. The sources of the charnockites vary from enriched mantle or crustal remelts to depleted mantle.

6.4.5 METAGRANITES

Sample BM163: This metagranite with a U – Pb age of 1038 Ma yielded an initial εNd (t) value of +2.8 and a crustal model age of 1568 Ma. The positive εNd (t) value of the sample suggests derivation of this metagranite from juvenile material (Faure et al., 2005).

Sample BM174: The U – Pb age for this metagranite sample is 1036 Ma and the whole rock Sm - Nd analyses yielded an initial εNd (t) value of +1.7 with a crustal model age of 1613 Ma that is not very different from the U-Pb age. The positive εNd (t) value of the sample suggests an origin in magma-depleted sources in the mantle (Faure et al., 2005).

Sample BM179: The sample is a metagranite with U –Pb age of 1047 Ma. The whole rock Sm - Nd analyses yielded an initial εNd (t) value of +2.6 with a crustal model age of 1526 Ma. The positive εNd (t) value suggests a protolith in mantle material (Faure et al., 2005).

Sample BM209: This sample is a metagranite with U –Pb age of 1033 Ma. The whole rock Sm - Nd analyses yielded an initial εNd (t) value of +3.6 and a crustal model age of 1442 Ma. The positive εNd (t) value of the sample means suggests origins from magma-depleted mantle sources (Faure et al., 2005).

Sample BM213G: This sample is a metagranite with a U – Pb age of 1035 ± 12 Ma and an initial εNd (t) value of +3.0 with a crustal model age of 1522 Ma. The positive εNd (t) value of the sample indicates derivation of this metagranite from juvenile material (Faure et al., 2005; Rollinson, 1994).

Sample BM213X: This sample is an enclave taken from a metagranite outcrop and it yielded U – Pb age of 1034 Ma and an initial εNd (t) value of +2.3 with a crustal model age of 1638 Ma.

The positive εNd (t) value suggests origins of this metagranite enclave from mantle-depleted sources (Faure et al., 2005).

Sample BM256: The U – Pb age for this metagranite sample is 1070 Ma and an initial εNd (t) value of +1.8 with a crustal model age of 1681 Ma. A positive εNd (t) value of the sample is suggestive of origins from magma-depleted sources in the mantle (Faure et al., 2005).

Five of the metagranites (BM163, BM174, BM179, BM209 and BM213G) have U-Pb ages between 1033 and 1047 Ma. Collectively they have crustal model ages of 1442 to 1613 Ma and εNd(t) from +1.7 to +3.6. The data suggest derivation of these granites from a slightly depleted source that separated from the mantle at around 1500Ma to be remobilised at around 1040 Ma. The metagranite enclave BM213X shares these characteristics although it has a slightly older crustal model age of 1638 Ma. One metagranite (BM256) has a slightly older U – Pb age of 1070 Ma and a slightly older model age of 1681 Ma.

6.4.6 OTHER ROCKS

Sample BM200: This sample is a quartzo-feldspathic gneiss with a U –Pb age of 1031 Ma. Whole rock Sm - Nd analyses yielded an initial εNd (t) value of +5.8 and a crustal model age of 1568 Ma. The U-Pb age of this gneiss is the same as those of the cluster of metagranites described above and its Nd isotope characteristics are similar although the protolith for the gneiss appears to have been derived from slightly more depleted mantle material.

Sample BM223A: The rock sample is a leucogranite gneiss with U – Pb age of 956 Ma and an initial εNd (t) value of +1.6 with a crustal model age of 1426 Ma. The positive εNd (t) value of the sample suggests origins of the protolith from depleted juvenile material (Faure et al., 2005). Although this leucogranite is almost 80 Ma younger than the metagranites its Nd isotope systematics are broadly similar suggesting that a later thermal event produced magmas from the same source or that the metagranites were re-melted at this time and had little time to develop distinct Nd isotope characteristics.

Sample BM221: The rock is a foliated hornblende biotite gneiss with U – Pb age of 756 Ma. The Sm - Nd whole rock analyses carried out yielded an initial εNd (t) value of +2.5 suggesting derivation of the protolith from juvenile material (Faure et al., 2005). The sample gives a crustal model age of 1153 Ma. This gneiss sample represent a very much younger event and a distinctly younger model age, so are unlikely to be connected to the major event that produced the metagranites.

Sample BM289: The rock is foliated perthitic syenite with a U – Pb age of 531 Ma and an initial εNd (t) value of -5.0 with a crustal model age of 1801 Ma. The negative εNd (t) value of the sample means the Nd is derived from magma with Sm/Nd ratio less than that of CHUR (Faure et al., 2005; Rollinson, 1994), or recycling of crustal rocks (Faure et al., 2005). This syenite sample is also very distinct from all the other samples in representing a much younger tectonothermal event with clear Nd isotope evidence of crustal recycling as the dominant source.

Sample BM240: The rock is an unfoliated granite with a relatively young U – Pb age of 118 Ma. The whole rock Sm - Nd analyses yielded an initial εNd (t) value of -3.4 and a crustal model age of 1497 Ma. The negative εNd (t) value of the sample means the Nd is derived from magma with Sm/Nd ratio less than that of CHUR (Faure et al., 2005; Rollinson, 1994) suggestive of recycling of crustal rocks during orogenesis by regional metamorphism and partial melting of terrigenous sediments (Faure et al., 2005).

Three gneisses, a syenite and an unfoliated granite have very different U-Pb ages. Quartzofeldspathic gneiss BM200 has a U-Pb age of 1031Ma with an initial εNd (t) value of +5.8 and a crustal model age of 1568 Ma. These characteristics similar to several metagranites and a charnockitic gneiss indicating that BM200 belongs to this magmatic episode. A leucocratic gneiss (BM223A) yields a U-Pb age of 956 Ma, εNd (t) value of +1.6 and a crustal model age of 1426 Ma. These characteristics do not match any of the other samples and appear to represent a discrete event. A foliated hornblende biotite gneiss (BM221) has U–Pb age of 756 Ma, an initial εNd (t) value of +2.5 and a crustal model age of 1153 Ma. This also appears to represent a separate event. **A** foliated perthitic syenite (BM289) gives a U–Pb age of 531 Ma, an initial εNd (t) value of -5.0 and a crustal model age of 1801 Ma, and this also appears to be a unique event. Finally a very young event is represented by an unfoliated granite (B250) with a U–Pb age of 118 Ma, an initial εNd (t) value of -3.4 and a crustal model age of 1497 Ma. This group of five diverse samples appear to represent five different events, at least based on U-Pb ages and Nd isotope systematics, with one of these events coinciding with the main group of metagranites.

6.5 Lu – Hf ISOTOPIC ANALYSES

In contrast to Sm-Nd isotope analysis which was conducted on bulk whole rocks samples Lu-Hf analyses were performed using a laser spot on zircon grains. Thus the data are reported below in terms of the results of spot analyses on zircons extracted from whole rocks.

6.5.1 CHARNOCKITIC GNEISSES

Sample BM249: Ten Lu-Hf spot analyses were carried out on concordant grains yielding initial εHf(t) values from +5.5 to +7.8, a weighted mean of +6.4 and Hf new continental crustal model ages (TDM_{nc}) from 1 Ma. The mean model age is 1330 Ma. The depleted mantle model ages (TDM) range from 1754 to 1910 Ma. The mean depleted mantle model age (TDM) is 1836 Ma. The data are presented in Table 6.3. The positive εHf(t) values of the sample suggests derivation of this charnokitic gneiss almost exclusively from juvenile material.

Table 6.3: Lu-Hf isotopic analyses for a charnockitic gneiss sample BM249 from southern Malawi. In the table, s = standard error. Hf/Hf(t) = Hf ratio at time (t) i.e. at age of crystallisation. Hf/Hf CHUR (t) = Hf ratios based on CHUR at time (t). Hf/Hf DM(t) = Hf ratio based on Depleted Mantle model at time (t).

	SAMPLE BM249 Charnockitic gneiss, LAT. -15.8338600, LONG. +35.5992400																
Hf	Spot	176Hf/177Hf	1s%	176Lu/177Hf	1s%	U-Pb Spot	Age	1s	eHf	2s+	2s	TDM	TDMnc	Hf/Hf (t)	Hf/Hf CHUR(t)	Hf/Hf DM(t)	
BM249	14	0.282308	0.0041	0.00094357	4.4	14	1036	15	5.7	1.2	0.8	1880	1351	0.282289	0.282129	0.282502	
BM249	35	0.282293	0.0032	0.000351677	2.7	35	1036	15	5.5	0.9	0.6	1910	1364	0.282286	0.282129	0.282502	
BM249	19	0.282345	0.0046	0.001098269	6.4	19	1036	15	6.9	1.3	0.9	1808	1317	0.282323	0.282129	0.282502	
BM249	20	0.282351	0.0053	0.000871505	8.2	20	1036	15	7.2	1.4	1.1	1796	1312	0.282334	0.282129	0.282502	
BM249	21	0.282372	0.0048	0.001160725	6.9	21	1036	15	7.8	1.3	1.0	1754	1293	0.282349	0.282129	0.282502	
BM249	29	0.282320	0.0035	0.001151116	2.2	29	1036	15	6.0	1.0	0.7	1857	1340	0.282297	0.282129	0.282502	
BM249	36	0.282306	0.0046	0.000656271	15.3	36	1036	15	5.8	1.3	0.9	1884	1353	0.282293	0.282129	0.282502	
BM249	24	0.282360	0.0039	0.001835252	3.5	24	1036	15	6.9	1.1	0.8	1778	1304	0.282324	0.282129	0.282502	
BM249	40	0.282346	0.0028	0.001141508	3.0	40	1036	15	6.9	0.9	0.6	1806	1316	0.282324	0.282129	0.282502	
BM249	26	0.282305	0.0037	0.00044392	4.2	26	1036	15	5.9	1.1	0.7	1886	1353	0.282296	0.282129	0.282502	

Sample BM281: Four Lu – Hf spot analyses from this metagranite sample's concordant zircon grains were carried out. They yielded initial εHf(t) values from +6.4 to + 7. 3 with a mean of +6.8 and Hf new continental crustal model ages (TDM_{nc}) from 1348 to 1380 Ma. The mean model age is 1363 Ma. The depleted mantle model ages (TDM) range from 1832 to 1901 Ma with a mean of 1865 Ma. The data are displayed in Table 6.4. The positive εHf(t) values of the sample suggests derivation of this metagranite almost exclusively from juvenile material.

Table 6.4: Lu-Hf isotopic analyses for a charnockitic sample BM281 from southern Malawi. For column headings, see Table 6.3.

	SAMPLE BM281. Charnockitic gneiss. LAT. -15.4565600. LONG. +35.2863100															
Hf	Spot	176Hf/177Hf	1s%	176Lu/177Hf	1s%	U-Pb Spot	Age	1s	eHf	2s+	2s	TDM	TDMnc	Hf/Hf (t)	Hf/Hf CHUR(t)	Hf/Hf DM(t)
BM281	4.2	0.282297	0.0065	0.000400935	4.7	4.2	1070	16	6.4	1.7	1.3	1901	1380	0.282289	0.282108	0.282477
BM281	4.3	0.282307	0.0060	0.000746104	8.7	4.3	1070	16	6.5	1.6	1.2	1881	1371	0.282292	0.282108	0.282477
BM281	6.1	0.282326	0.0060	0.000825907	1.4	6.1	1070	16	7.2	1.6	1.2	1844	1353	0.282310	0.282108	0.282477
BM281	6.3	0.282332	0.0060	0.000983588	1.2	6.3	1070	16	7.3	1.6	1.2	1832	1348	0.282312	0.282108	0.282477

Sample BM282A: Eighteen Lu-Hf spot analyses were carried out on two populations of concordant grains from this sample - a charnockitic gneiss. The older population yielded initial εHf(t) values of +8.9 to +9.2 with a mean of +9.2 and crustal model ages (TDM_{nc}) 1318 to 1346 Ma. The mean model age is 1335 Ma. The younger population analyses yielded initial εHf(t) values from +1.1 to +3.8 with a mean of +2.3 and the Hf new continental crustal model ages (TDM_{nc}) range from 845 to 912 Ma and a mean model age of 883 Ma. The depleted mantle model ages (TDM) for the older population range from 1730 to 1791 Ma with a mean of 1335 Ma whilst the younger population range from 1389 to 1535 Ma and their mean is 1472 Ma. The data are shown in Table 6.5. The old populations are from the cores of the zircon grains and their U –Pb ages are Mesoproterozoic (1100 Ma) whilst the younger are from the rim with U–Pb age of 530 Ma.

Table 6.5: Lu-Hf Isotopic analyses for a charnockitic gneiss sample BM282A from southern Malawi. For column headings, see Table 6.3.

	SAMPLE BM282A. Charnockitic gneiss. LAT. -15.4925100. LONG. +35.2291100															
Hf	Spot	176Hf/177Hf	1s%	176Lu/177Hf	1s%	U-Pb Spot	Age	1s	eHf	2s+	2s	TDM	TDMnc	Hf/Hf (t)	Hf/Hf CHUR(t)	Hf/Hf DM(t)
BM282A	1	0.282544	0.0067	0.000423049	1.7	1	540		3.4	2.0	1.3	1415	857	0.282540	0.282445	0.282862
BM282A	2	0.282500	0.0072	0.00042401	1.0	2	540		1.8	2.1	1.4	1502	897	0.282496	0.282445	0.282862
BM282A	6	0.282503	0.0066	0.0003519	2.2	6	540		1.9	1.9	1.3	1496	894	0.282500	0.282445	0.282862
BM282A	8	0.282505	0.0062	0.000334593	1.3	8	540		2.0	1.9	1.2	1492	892	0.282502	0.282445	0.282862
BM282A	9	0.282501	0.0066	0.000494198	2.9	9	540		1.8	1.9	1.3	1500	896	0.282496	0.282445	0.282862
BM282A	10	0.282517	0.0066	0.000380744	1.1	10	540		2.4	2.0	1.3	1468	881	0.282513	0.282445	0.282862
BM282A	11	0.282557	0.0066	0.00056727	8.5	11	540		3.8	1.9	1.3	1389	845	0.282551	0.282445	0.282862
BM282A	12	0.282538	0.0059	0.000251906	2.2	12	540		3.2	1.8	1.2	1427	862	0.282536	0.282445	0.282862
BM282A	16	0.282498	0.0062	0.000495159	4.6	16	540		1.7	1.9	1.2	1506	898	0.282493	0.282445	0.282862
BM282A	17	0.282502	0.0061	0.000333632	1.0	17	540		1.9	1.9	1.2	1498	895	0.282499	0.282445	0.282862
BM282A	19	0.282483	0.0056	0.000605729	2.7	19	540		1.1	1.7	1.1	1535	912	0.282477	0.282445	0.282862
BM282A	21	0.282538	0.0062	0.000581692	4.9	21	540		3.1	1.9	1.2	1427	862	0.282532	0.282445	0.282862
BM282A	22	0.282518	0.0064	0.000393243	2.4	22	540		2.5	1.9	1.3	1466	880	0.282514	0.282445	0.282862
BM282A	29	0.282504	0.0063	0.0003394	3.3	29	540		2.0	1.9	1.3	1494	893	0.282501	0.282445	0.282862
BM282A	13	0.282384	0.0066	0.001100888	5.0	13	1100		9.7	1.6	1.3	1730	1318	0.282361	0.282089	0.282455
BM282A	14	0.282353	0.0059	0.000588422	5.5	14	1100		8.9	1.5	1.2	1791	1346	0.282341	0.282089	0.282455
BM282A	15	0.282360	0.0058	0.000895133	2.2	15	1100		9.0	1.5	1.2	1777	1339	0.282342	0.282089	0.282455
BM282A	30	0.282363	0.0060	0.00071726	1.7	30	1100		9.2	1.5	1.2	1772	1337	0.282348	0.282089	0.282455

6.5.2 METAGRANITES

Sample BM 163: BM163 is a metagranite. Ten Lu-Hf spot analyses were carried out on concordant grains from this sample and yielded initial εHf (t) values of +5.2 to +6.8 with a mean εHf(t) of +6.1. The analyses also yielded Hf (TDM_{nc}) model ages between 1330 to 1374 Ma with a mean of 1351 Ma. The corresponding Hf (TDM) model ages range from 1833 to 1920 Ma with a mean of 1877 Ma. The data are shown in Table 6.6. The positive εHf(t) values of the sample suggests derivation of this metagranite almost exclusively from juvenile material.

Table 6.6: Lu-Hf isotopic analyses for metagranite sample BM163 from southern Malawi. For column headings, see Table 6.3.

	SAMPLE BM163 Metagranite. LAT. -15.6912700. LONG +34.4177300															
Hf	Spot	176Hf/177Hf	1s%	176Lu/177Hf	1s%	U-Pb Spot	Age	1s	eHf	2s+	2s	TDM	TDMnc	Hf/Hf (t)	Hf/Hf CHUR(t)	Hf/Hf DM(t)
BM163	2	0.282298	0.0037	0.000287524	1.1	2	1038	7	5.8	1.4	0.7	1900	1361	0.282292	0.282128	0.282500
BM163	3	0.282323	0.0034	0.000354956	1.1	3	1038	7	6.6	1.3	0.7	1851	1338	0.282316	0.282128	0.282500
BM163	7	0.282332	0.0035	0.000457977	1.3	7	1038	7	6.9	1.4	0.7	1833	1330	0.282323	0.282128	0.282500
BM163	9	0.282297	0.0028	0.000336225	1.7	9	1038	7	5.7	1.1	0.6	1902	1362	0.282290	0.282128	0.282500
BM163	10	0.282330	0.0030	0.000771725	1.0	10	1038	7	6.6	1.2	0.6	1837	1332	0.282315	0.282128	0.282500
BM163	12	0.282329	0.0025	0.000442056	2.5	12	1038	7	6.8	0.9	0.5	1839	1333	0.282320	0.282128	0.282500
BM163	14	0.282284	0.0027	0.000385862	1.1	14	1038	7	5.2	1.0	0.5	1927	1374	0.282276	0.282128	0.282500
BM163	15	0.282308	0.0023	0.000529156	1.1	15	1038	7	6.0	0.9	0.5	1880	1352	0.282297	0.282128	0.282500
BM163	16	0.282288	0.0032	0.000310001	2.1	16	1038	7	5.4	1.2	0.6	1920	1370	0.282282	0.282128	0.282500
BM163	18	0.282306	0.0030	0.000758613	3.7	18	1038	7	5.8	1.2	0.6	1884	1354	0.282291	0.282128	0.282500

Sample BM174: Ten Lu-Hf spot analyses were carried out on seven concordant zircon grains from a metagranite sample BM174. εHf values from this sample are between +3.9 to +5.7 with a mean εHf(t) of +4.8 and Hf crustal model ages (TDM_{nc}) between 1355 and 1399 Ma. The mean model age is 1379 Ma. The depleted mantle model ages (TDM) range from 1890 to 1984 Ma and a mean of 1942 Ma. The data are shown in Table 6.7. The positive εHf(t) values of the sample suggests derivation of this metagranite almost exclusively from juvenile material.

Table 6.7: Lu-Hf isotopic analyses for metagranite sample BM174 from southern Malawi. For column headings, see Table 6.3.

	SAMPLE BM174. Metagranite. LAT. -15.7080300. LONG. +34.5266700															
Hf	Spot	176Hf/177Hf	1s%	176Lu/177Hf	1s%	U-Pb Spot	Age	1s	eHf	2s+	2s	TDM	TDMnc	Hf/Hf (t)	Hf/Hf CHUR(t)	Hf/Hf DM(t)
BM174	1	0.282292	0.0035	0.001047073	3.5	1	1036	8	5.0	1.4	0.7	1912	1365	0.282271	0.282129	0.282502
BM174	2	0.282283	0.0030	0.000503869	1.0	2	1036	8	5.1	1.2	0.6	1929	1373	0.282273	0.282129	0.282502
BM174	4	0.282259	0.0039	0.000645289	4.0	4	1036	8	4.1	1.6	0.8	1976	1395	0.282246	0.282129	0.282502
BM174	5	0.282261	0.0032	0.000428007	1.0	5	1036	8	4.4	1.3	0.6	1972	1393	0.282252	0.282129	0.282502
BM174	6	0.282282	0.0044	0.000536648	4.1	6	1036	8	5.0	1.8	0.9	1931	1374	0.282271	0.282129	0.282502
BM174	8	0.282278	0.0032	0.000509488	1.0	8	1036	8	4.9	1.3	0.6	1939	1378	0.282268	0.282129	0.282502
BM174	9	0.282255	0.0035	0.000833537	5.0	9	1036	8	3.9	1.5	0.7	1984	1399	0.282238	0.282129	0.282502
BM174	11	0.282269	0.0030	0.000701483	1.6	11	1036	8	4.5	1.2	0.6	1957	1386	0.282255	0.282129	0.282502
BM174	12	0.282303	0.0048	0.00063967	5.4	12	1036	8	5.7	1.9	1.0	1890	1355	0.282290	0.282129	0.282502
BM174	13	0.282286	0.0030	0.000451421	6.1	13	1036	8	5.2	1.2	0.6	1924	1371	0.282277	0.282129	0.282502

Sample BM179: From this metagranite sample seven Lu-Hf spot analyses were carried out on concordant grains yielding initial εHf(t) values of +3.8 to +5.4 (mean εHf(t) is +4.7). The analyses also yielded Hf crustal model ages (TDM_{nc}) between 1365 to 1402 Ma and a mean of 1384 Ma. Depleted mantle ages (TDM) range from 1912 to 1992 Ma with a mean of 1952 Ma. The data are shown in Table 6.8. The positive εHf(t) values of the sample suggests derivation of this metagranite almost exclusively from juvenile material.

Table 6.8: Lu-Hf isotopic analyses for metagranite sample BM179 from southern Malawi. For column headings, see Table 6.3.

	SAMPLE BM179 Metagranite. LAT -15.5522500. LONG. 4933800															
Hf	Spot	176Hf/177Hf	1s%	176Lu/177Hf	1s%	U-Pb Spot	Age	1s	eHf	2s+	2s	TDM	TDMnc	Hf/Hf (t)	Hf/Hf CHUR(t)	Hf/Hf DM(t)
BM179	8	0.282251	0.0034	0.000561935	7.4	8	1036	8	3.9	1.4	0.7	1992	1402	0.282240	0.282129	0.282502
BM179	12	0.282272	0.0030	0.000487947	1.2	12	1036	8	4.7	1.2	0.6	1951	1383	0.282262	0.282129	0.282502
BM179	19	0.282292	0.0028	0.000479518	1.7	19	1036	8	5.4	1.1	0.6	1912	1365	0.282282	0.282129	0.282502
BM179	22.1	0.282281	0.0037	0.00040272	4.8	22.1	1036	8	5.1	1.5	0.7	1933	1375	0.282273	0.282129	0.282502
BM179	22.2	0.282251	0.0041	0.000683688	3.8	22.2	1036	8	3.8	1.6	0.8	1992	1402	0.282237	0.282129	0.282502
BM179	23	0.282274	0.0030	0.00060689	3.5	23	1036	8	4.7	1.2	0.6	1947	1382	0.282262	0.282129	0.282502
BM179	24	0.282276	0.0034	0.000355892	1.7	24	1036	8	4.9	1.3	0.7	1943	1380	0.282269	0.282129	0.282502

Sample BM209: Sample 209 is a metagranite and eleven Lu-Hf spot analyses were carried out on concordant grains which yielded initial εHf(t) values of +5.8 to +7.8 with a mean of +6.8. The analyses also yielded Hf crustal model ages (TDM_{nc}) between 1365 to 1402 Ma and a mean model age of 1327 Ma. Depleted mantle model ages (TDM) range from 1774 to 1890 Ma and the mean model age is 1833 Ma. The data are shown in Table 6.9. The positive εHf(t) values of the sample suggests derivation of this metagranite almost exclusively from juvenile material.

Table 6.9: Lu-Hf isotopic analyses for metagranite sample BM209 from southern Malawi. For column headings, see Table 6.3.

	SAMPLE BM209 Metagranite. LAT -15.7139300. LONG. +34.7369600															
Hf	Spot	176Hf/177Hf	1s%	176Lu/177Hf	1s%	U-Pb Spot	Age	1s	eHf	2s+	2s	TDM	TDMnc	Hf/Hf (t)	Hf/Hf CHUR(t)	Hf/Hf DM(t)
BM209	3	0.282341	0.0041	0.000698673	4.9	3	1033	20	6.9	2.2	0.8	1816	1319	0.282327	0.282131	0.282504
BM209	4	0.282362	0.0060	0.000573174	8.6	4	1033	20	7.8	3.0	1.2	1774	1300	0.282351	0.282131	0.282504
BM209	6.1	0.282348	0.0032	0.000446739	2.0	6.1	1033	20	7.4	1.8	0.6	1802	1313	0.282339	0.282131	0.282504
BM209	6.2	0.282303	0.0035	0.000397101	2.6	6.2	1033	20	5.8	1.9	0.7	1890	1354	0.282295	0.282131	0.282504
BM209	6.3	0.282320	0.0041	0.000331542	2.7	6.3	1033	20	6.4	2.2	0.8	1857	1338	0.282313	0.282131	0.282504
BM209	8.1	0.282332	0.0041	0.000467343	1.9	8.1	1033	20	6.8	2.2	0.8	1833	1328	0.282323	0.282131	0.282504
BM209	8.2	0.282322	0.0046	0.000448612	4.1	8.2	1033	20	6.4	2.4	0.9	1853	1337	0.282313	0.282131	0.282504
BM209	11	0.282329	0.0034	0.000367131	2.3	11	1033	20	6.7	1.9	0.7	1839	1330	0.282322	0.282131	0.282504
BM209	13.1	0.282339	0.0037	0.000481391	1.7	13.1	1033	20	7.0	2.0	0.7	1820	1321	0.282329	0.282131	0.282504
BM209	15	0.282340	0.0032	0.000390545	3.0	15	1033	20	7.1	1.8	0.6	1818	1320	0.282332	0.282131	0.282504
BM209	18	0.282319	0.0037	0.000394291	2.4	18	1033	20	6.4	2.0	0.7	1859	1339	0.282311	0.282131	0.282504

Sample BM213G: Nine Lu-Hf spot analyses were carried out on concordant grains of BM213G which is a coarse grained leucocratic metagranite, yielding initial εHf(t) values of +6.0 to +8.4 and a mean of +6.9. The analyses also yielded Hf crustal model ages (TDM_{nc}) between 1349 to 1402 Ma. The average model age is 1389 Ma. The depleted mantle model ages (TDM) range from 1814 to 1947 Ma and with a mean of 1898 Ma. The data are shown in Table 6.10. The positive εHf(t) values of the sample suggests derivation of this leucocratic metagranite almost exclusively from juvenile material.

Table 6.10: Lu-Hf isotopic analyses for metagranite sample BM213G from southern Malawi. For column headings, see Table 6.3.

	SAMPLE BM213G. Metagranite. LAT. -15.7769000. LONG. +34.4452700															
Hf	Spot	176Hf/177Hf	1s%	176Lu/177Hf	1s%	U-Pb Spot	Age	1s	eHf	2s+	2s	TDM	TDMnc	Hf/Hf (t)	Hf/Hf CHUR(t)	Hf/Hf DM(t)
BM213G	1	0.282284	0.0048	0.000415832	1.3	1	1088	23	6.3	2.6	1.0	1927	1402	0.282275	0.282096	0.282464
BM213G	2	0.282274	0.0041	0.000414896	2.7	2	1088	23	6.0	2.3	0.8	1947	1411	0.282265	0.282096	0.282464
BM213G	3	0.282295	0.0044	0.000467343	3.0	3	1088	23	6.7	2.5	0.9	1906	1392	0.282285	0.282096	0.282464
BM213G	4	0.282342	0.0035	0.00046266	8.6	4	1088	23	8.4	2.1	0.7	1814	1349	0.282332	0.282096	0.282464
BM213G	5	0.282279	0.0057	0.000397101	3.0	5	1088	23	6.2	3.0	1.1	1937	1406	0.282271	0.282096	0.282464
BM213G	8	0.282315	0.0032	0.000282841	1.1	8	1088	23	7.5	2.0	0.6	1867	1374	0.282309	0.282096	0.282464
BM213G	22	0.282295	0.0025	0.000373687	3.6	22	1088	23	6.8	1.7	0.5	1906	1392	0.282287	0.282096	0.282464
BM213G	23	0.282320	0.0048	0.000371814	1.1	23	1088	23	7.7	2.6	1.0	1857	1369	0.282312	0.282096	0.282464
BM213G	24	0.282285	0.0035	0.0003484	4.4	24	1088	23	6.4	2.1	0.7	1925	1401	0.282278	0.282096	0.282464

Sample BM213X: From this metagranite enclave sample five Lu-Hf spot analyses were carried out on concordant grains yielding initial εHf(t) values of +4.5 to +7.0, a mean of +5.7 and Hf crustal model ages (TDM_{nc}) between 1321 to 1387 Ma. The mean model age for this metagranite enclave is 1353 Ma. Depleted mantle model ages (TDM) are from 1822 to 1961 Ma and their mean is 1888 Ma. The data are shown in Table 6.11. The positive εHf(t) values of the sample suggests derivation of this metagranite almost exclusively from juvenile material.

Table 6.11: Lu-Hf isotopic analyses for metagranite enclave sample BM213X from southern Malawi. For column headings, see Table 6.3.

	SAMPLE BM213X Metagranite enclave. LAT. -15.7769000. LONG. +34.4452700															
Hf	Spot	176Hf/177Hf	1s%	176Lu/177Hf	1s%	U-Pb Spot	Age	1s	eHf	2s+	2s	TDM	TDMnc	Hf/Hf (t)	Hf/Hf CHUR(t)	Hf/Hf DM(t)
BM213X	1	0.282338	0.0066	0.000474835	2.8	1	1034	17	7.0	3.0	1.3	1822	1323	0.282328	0.282131	0.282503
BM213X	2	0.282340	0.0050	0.000559126	4.6	2	1034	17	7.0	2.4	1.0	1818	1321	0.282329	0.282131	0.282503
BM213X	4	0.282302	0.0060	0.000566618	3.3	4	1034	17	5.7	2.8	1.2	1892	1355	0.282291	0.282131	0.282503
BM213X	5.1	0.282274	0.0046	0.000380243	2.0	5.1	1034	17	4.8	2.2	0.9	1947	1380	0.282266	0.282131	0.282503
BM213X	9	0.282267	0.0051	0.000409276	3.8	9	1034	17	4.5	2.5	1.0	1961	1387	0.282259	0.282131	0.282503

Sample BM256: This sample is a metagranite from which eight Lu-Hf spot analyses were carried out on concordant grains. These yielded initial εHf(t) values from +5.1 and +6.5, a mean of +6.1 and they also yielded Hf crustal model ages (TDM_{nc}) from 1375 to 1415 Ma with a mean model age of 1396 Ma. Depleted mantle model ages (TDM) range from 1891 to 1977 Ma and the mean is 1937 Ma. The data are shown in Table 6.12. The positive εHf(t) values of the sample suggests derivation of this metagranite almost exclusively from juvenile material.

Table 6.12: Lu-Hf isotopic analyses for metagranite sample BM256 from southern Malawi. For column headings, see Table 6.3.

	SAMPLE BM256. Metagranite. LAT. -16.3755300. LONG. +35.1994800															
Hf	Spot	176Hf/177Hf	1s%	176Lu/177Hf	1s%	U-Pb Spot	Age	1s	eHf	2s+	2s	TDM	TDMnc	Hf/Hf (t)	Hf/Hf CHUR(t)	Hf/Hf DM(t)
BM256	1	0.282288	0.0060	0.000517273	1.6	1	1070	16	6.0	1.6	1.2	1919	1388	0.282278	0.282108	0.282477
BM256	2	0.282258	0.0066	0.000381705	4.6	2	1070	16	5.1	1.7	1.3	1977	1415	0.282250	0.282108	0.282477
BM256	3	0.282280	0.0063	0.000439394	1.3	3	1070	16	5.8	1.6	1.3	1934	1395	0.282271	0.282108	0.282477
BM256	4	0.282272	0.0064	0.000540349	9.7	4	1070	16	5.4	1.7	1.3	1950	1402	0.282261	0.282108	0.282477
BM256	5	0.282290	0.0063	0.000761488	3.0	5	1070	16	5.9	1.6	1.3	1915	1386	0.282275	0.282108	0.282477
BM256	6	0.282275	0.0065	0.000679762	12.2	6	1070	16	5.4	1.8	1.3	1944	1399	0.282261	0.282108	0.282477
BM256	7	0.282263	0.0065	0.000558617	2.9	7	1070	16	5.1	1.7	1.3	1968	1410	0.282252	0.282108	0.282477
BM256	8	0.282302	0.0061	0.000586499	10.5	8	1070	16	6.5	1.7	1.2	1891	1375	0.282290	0.282108	0.282477

6.5.3 OTHER ROCKS

Sample BM200: Fifteen Lu-Hf spot analyses were carried out on two populations of concordant grains from this quartzo-feldspathic gneiss. The older population yielded initial εHf(t) values of +7.7 to +10.3 and new crustal model ages (TDM_{nc}) 1227 to 1293 Ma. The mean model average is 1254 Ma. The normal depleted mantle model ages (TDM) have ages from 1443 to 1761 Ma and the mean is 1616 Ma. The high positive εHf(t) values of the sample suggests derivation of this gneiss almost exclusively from juvenile material. The younger population analyses also yielded initial εHf(t) values of -3.5 to +2.5 and Hf crustal model ages (TDM_{nc}) between 882 to 1003 Ma. The mean model age (TDM_{nc}) is 929 Ma. The data are shown in Table 6.13.

Table 6.13: Lu-Hf isotopic analyses for a quartzo-feldspathic sample BM200 from southern Malawi. For column headings, see Table 6.3.

	SAMPLE BM200. Quartzofeldspathic gneiss. LAT. -15.3636700. LONG. +34.5678000																
Hf	Spot	176Hf/177Hf	1s%	176Lu/177Hf	1s%	U-Pb Spot	Age	1s	eHf	2s+	2s	TDM	TDMnc	Hf/Hf (t)	Hf/Hf CHUR(t)	Hf/Hf DM(t)
BM200	1.1	0.282510	0.0044	0.000725833	6.3	1.1	530	24	1.8	2.2	0.9	1483	882	0.282503	0.282451	0.282870
BM200	3	0.282433	0.0039	0.001506923	1.3	3	1031	19	9.6	2.0	0.8	1635	1235	0.282403	0.282133	0.282505
BM200	5.1	0.282455	0.0053	0.000961846	2.8	5.1	530	24	-0.2	2.5	1.1	1591	932	0.282445	0.282451	0.282870
BM200	9.2	0.282440	0.0103	0.00084384	2.4	9.2	1031	19	10.3	4.6	2.1	1621	1229	0.282423	0.282133	0.282505
BM200	9.3	0.282530	0.0134	0.000885985	7.0	9.3	530	24	2.5	5.8	2.7	1443	864	0.282521	0.282451	0.282870
BM200	11	0.282499	0.0042	0.001274657	4.3	11	530	24	1.2	2.1	0.8	1505	892	0.282486	0.282451	0.282870
BM200	12.2	0.282499	0.0051	0.000935622	5.8	12.2	530	24	1.4	2.5	1.0	1505	892	0.282489	0.282451	0.282870
BM200	13	0.282402	0.0027	0.000956227	2.6	13	530	24	-2.1	1.5	0.5	1696	980	0.282392	0.282451	0.282870
BM200	16.1	0.282384	0.0030	0.001164143	2.8	16.1	530	24	-2.8	1.6	0.6	1731	996	0.282372	0.282451	0.282870
BM200	17.2	0.282442	0.0037	0.000944051	2.5	17.2	1031	19	10.3	2.0	0.7	1617	1227	0.282423	0.282133	0.282505
BM200	19	0.282401	0.0035	0.000831664	2.7	19	530	24	-2.1	1.8	0.7	1698	980	0.282392	0.282451	0.282870
BM200	20	0.282528	0.0065	0.000775471	1.6	20	530	24	2.4	3.0	1.3	1447	866	0.282520	0.282451	0.282870
BM200	23.2	0.282377	0.0035	0.000763296	1.9	23.2	1031	19	8.1	1.9	0.7	1745	1286	0.282362	0.282133	0.282505
BM200	24.2	0.282369	0.0025	0.000744564	2.9	24.2	1031	19	7.9	1.5	0.5	1761	1293	0.282354	0.282133	0.282505
BM200	25.1	0.282370	0.0046	0.001721395	22.7	25.1	530	24	-3.5	2.5	0.9	1759	1008	0.282353	0.282451	0.282870

Sample BM221: The sample is a hornblende biotite gneiss and two Lu-Hf spot analyses were carried out on concordant grains which yielded initial εHf(t) values of +4.3 and +4.6 and a mean of +4.5. The analyses also yielded Hf crustal model ages (TDM_{nc}) of 1057 and 1064 Ma. The mean model age is 1060 Ma. Depleted mantle model ages range from 1585 to 1599 and their mean is 1592 Ma. The data are shown in Table 6.14. The positive εHf(t) values of the sample suggests derivation of this hornblende biotite gneiss almost exclusively from juvenile material.

Table 6.14: Lu-Hf isotopic analyses for a leucogranite gneiss sample BM221 from southern Malawi. For column headings, see Table 6.3.

	SAMPLE BM221. Hornbl-biot gneiss. LAT. -15.0201600. LONG. +35.1322900															
Hf	Spot	176Hf/177Hf	1s%	176Lu/177Hf	1s%	U-Pb Spot	Age	1s	eHf	2s+	2s	TDM	TDMnc	Hf/Hf (t)	Hf/Hf CHUR(t)	Hf/Hf DM(t)
BM221	5.1	0.282458	0.0019	0.00145475	3.2	5.1	756	9	4.6	0.5	0.4	1585	1057	0.282437	0.282308	0.282706
BM221	5.2	0.282451	0.0027	0.00151336	11.0	5.2	756	9	4.3	0.6	0.5	1599	1064	0.282429	0.282308	0.282706

Sample BM223A: From this leucogranite sample four Lu-Hf spot analyses were carried out on concordant grains and they yielded initial εHf(t) values of +5.5 to +8.1 with a mean of +6.9 and Hf crustal model ages (TDM_{nc}) between 1209 to 1271 Ma with a mean of 1251 Ma. Depleted mantle model ages (TDM) range from 1670 to 1813 Ma with a mean of 1762 Ma. The data are shown in Table 6.15. The positive εHf(t) values of the sample suggests derivation of this leucogranite almost exclusively from juvenile material.

Table 6.15: Lu-Hf isotopic analyses for a hornblende biotite gneiss sample BM223A from southern Malawi. For column headings, see Table 6.3.

	SAMPLE BM223A, Leucogranite gneiss, LAT -15.0246800, LONG +35.1206600															
Hf	Spot	176Hf/177Hf	1s%	176Lu/177Hf	1s%	U-Pb Spot	Age	1s	eHf	2s+	2s	TDM	TDMnc	Hf/Hf (t)	Hf/Hf CHUR(t)	Hf/Hf DM(t)
BM223A	1.1	0.282415	0.0025	0.00031805	2.6	1.1	956	12	8.1	0.6	0.5	1670	1209	0.282409	0.282181	0.282560
BM223A	1.2	0.282342	0.0034	0.00039588	4.5	1.2	956	12	5.5	0.8	0.7	1813	1275	0.282335	0.282181	0.282560
BM223A	1.3	0.282361	0.0041	0.00043719	3.4	1.3	956	12	6.1	1.0	0.8	1776	1258	0.282353	0.282181	0.282560
BM223A	2.1	0.282354	0.0161	0.00066204	10.4	2.1	956	12	5.7	3.4	3.2	1790	1264	0.282342	0.282181	0.282560

Sample BM233: The zircons in this quartzofeldspathic gneiss are of two U – Pb age groups; one group with age 780 Ma and the other 550 Ma but both groups yield more or less similar model ages. This sample is a quartzo-felspathic gneiss from which nine Lu-Hf spot analyses were carried out on concordant grains. These yielded initial εHf(t) values of -3.7 and +6.5 and they also yielded Hf new continental crustal model ages (TDM_{nc}) from 988 to 1037 Ma and its mean model age is 1022 Ma. Depleted mantle model ages (TDM) range from 1490 to 1794 Ma. The mean model age is 1701 Ma. The data are shown in Table 6.16.

Table 6.16: Lu-Hf isotopic analyses for a quartzo-feldspathic gneiss sample BM233 from southern Malawi. For column headings, see Table 6.3.

	SAMPLE BM233. Quartzo-felds gneiss. LAT - 15.0852700. LONG. +34.6192100															
Hf	Spot	176Hf/177Hf	1s%	176Lu/177Hf	1s%	U-Pb Spot	Age	1s	eHf	2s+	2s	TDM	TDMnc	Hf/Hf (t)	Hf/Hf CHUR(t)	Hf/Hf DM(t)
BM233	5	0.282352	0.0028	0.001737244	2.4	5	550		-3.7	1.2	0.6	1794	1036	0.282334	0.282439	0.282855
BM233	6	0.282380	0.0027	0.001485497	5.4	6	550		-2.6	1.1	0.5	1739	1011	0.282365	0.282439	0.282855
BM233	18.1	0.282356	0.0027	0.001790092	4.8	18.1	550		-3.6	1.1	0.5	1786	1032	0.282337	0.282439	0.282855
BM233	18.2	0.282374	0.0025	0.001923652	4.1	18.2	550		-3.0	1.1	0.5	1751	1016	0.282354	0.282439	0.282855
BM233	21	0.282360	0.0027	0.001356742	4.2	21	550		-3.3	1.1	0.5	1778	1029	0.282346	0.282439	0.282855
BM233	30	0.282366	0.0025	0.001111721	3.9	30	550		-3.0	1.1	0.5	1766	1023	0.282354	0.282439	0.282855
BM233	44	0.282405	0.0035	0.001629627	5.9	44	550		-1.8	1.3	0.7	1690	988	0.282388	0.282439	0.282855
BM233	37.1	0.282506	0.0034	0.002013973	4.0	37.1	780		6.5	1.1	0.7	1490	1027	0.282476	0.282293	0.282688
BM233	37.2	0.282495	0.0027	0.002001482	3.6	37.2	780		6.1	1.0	0.5	1512	1037	0.282466	0.282293	0.282688

Sample BM240: Seven Lu-Hf spot analyses were carried out on concordant grains from this granite sample yielding initial εHf(t) values of -7.2 and -3.8, a mean of -5.4 and Hf new continental crustal model ages (TDM_{nc}) from 561 to 629 Ma with the mean model age is 602 Ma. Depleted mantle model ages (TDM) range from 1293 to 1479 Ma and the mean is 1383 Ma. The data are shown in Table 6.17. The U – Pb age for this sample is 118 Ma against a model age (TDM_{nc}) of 602 Ma. The negative εHf(t) suggest therefore derivation from crustal material.

Table 6.17: Lu-Hf isotopic analyses for a granite sample BM240 from southern Malawi. For column headings, see Table 6.3.

	SAMPLE BM240, GRANITE. LAT. -16.0511100. LONG. +35.7783500														
Hf	Spot	176Hf/177Hf	1s%	176Lu/177Hf	1s%	U-Pb Spot	Age	1s	eHf	2s+	2s	TDM	TDMnc	Hf/Hf (t)	Hf/Hf CHUR(t)	Hf/Hf DM(t)
BM240	3	0.282512	0.0041	0.00147493	12.7	3	118	1	-7.2	1.6	0.8	1479	645	0.282509	0.282711	0.283166
BM240	6	0.282572	0.0048	0.00064666	1.3	6	118	1	-5.0	1.8	1.0	1360	591	0.282570	0.282711	0.283166
BM240	8	0.282601	0.0053	0.00082154	1.2	8	118	1	-4.0	1.9	1.1	1302	565	0.282599	0.282711	0.283166
BM240	9.3	0.282530	0.0055	0.00110596	8.3	9.3	118	1	-6.5	1.9	1.1	1443	629	0.282527	0.282711	0.283166
BM240	9.1	0.282534	0.0062	0.00312281	2.4	9.1	118	1	-6.5	2.0	1.2	1435	625	0.282527	0.282711	0.283166
BM240	14.2	0.282606	0.0041	0.00092531	1.4	14.2	118	1	-3.8	1.6	0.8	1293	561	0.282604	0.282711	0.283166
BM240	14.1	0.282567	0.0053	0.00063321	1.5	14.1	118	1	-5.1	1.9	1.1	1370	596	0.282565	0.282711	0.283166

Sample BM289: Seven Lu – Hf spot analyses were carried out from this perthitic syenite sample's concordant zircon grains. They yielded initial εHf(t) values from -2.7 to + 1.4 with a mean of +1.6 and Hf crustal model ages (TDM_{nc}) from 889 to 1001 Ma. The mean is 970 Ma. Depleted mantle model ages (TDM) range from 1496 to 1742 Ma with a mean of 1675 Ma. The data are displayed in Table 6.18. The negative εHf(t) suggest origins from more evolved crustal material for this perthitic syenite.

Table 6.18: Lu-Hf Isotopic analyses for a perthitic syenite sample BM289 from southern Malawi. For column headings, see Table 6.3.

	SAMPLE BM289. Perthitic syenite. LAT. -15.6907200. LONG. +35.1889900														
Hf	Spot	176Hf/177Hf	1s%	176Lu/177Hf	1s%	U-Pb Spot	Age	1s	eHf	2s+	2s	TDM	TDMnc	Hf/Hf (t)	Hf/Hf CHUR(t)	Hf/Hf DM(t)
BM289	8	0.282399	0.0061	0.000493236	1.5	8	531	3	-2.0	1.7	1.2	1701	982	0.282394	0.282451	0.282869
BM289	9	0.282394	0.0066	0.000372091	3.5	9	531	3	-2.1	1.8	1.3	1711	987	0.282390	0.282451	0.282869
BM289	3	0.282503	0.0068	0.001253763	1.4	3	531	3	1.4	1.9	1.4	1496	889	0.282491	0.282451	0.282869
BM289	4	0.282407	0.0065	0.000389397	1.0	4	531	3	-1.7	1.8	1.3	1685	975	0.282403	0.282451	0.282869
BM289	5	0.282378	0.0068	0.000405742	4.6	5	531	3	-2.7	1.9	1.4	1742	1001	0.282374	0.282451	0.282869
BM289	6	0.282391	0.0069	0.000313441	4.7	6	531	3	-2.2	1.9	1.4	1717	990	0.282388	0.282451	0.282869
BM289	7	0.282414	0.0074	0.000997049	1.3	7	531	3	-1.6	2.0	1.5	1671	969	0.282404	0.282451	0.282869

6.6 Depleted Mantle Model Ages (TDM) vs Depleted Mantle Model Ages – New Continental Crust (TDM_{nc})

Model ages calculated from the alternative continental crust model (TDM_{nc}) are younger by up to 300 Ma compared with those calculated from the depleted mantle (TDM) and are closer to the geological record (Dhuime et al., 2011). In this study both the depleted mantle based model ages (TDM) and those based on the new continental crust (TDM_{nc}) have been calculated for the Lu-Hf data (and presented in accompanying Tables). Fig. 6.5 is a comparison of the Neodymium (Nd) model age, Hafnium (Hf) model age based on the depleted mantle (Hf TDM) and the Hf model age based on the new continental crust (Hf TDM_{nc}). The Nd model ages show poor agreement with U-Pb emplacement age whereas the two Hf model ages show parallel trends (Fig. 6.6). The new continental crust model ages show a good positive correlation with emplacement age although the ages are too high by about 600 Ma at the younger end and about 250 Ma at the older end. This correlation appears to be real and not some artefact of the method possibly reflecting regular events removing magma from the mantle between 1400 Ma and about 900 Ma and recycled in the crust a few hundred Ma later.

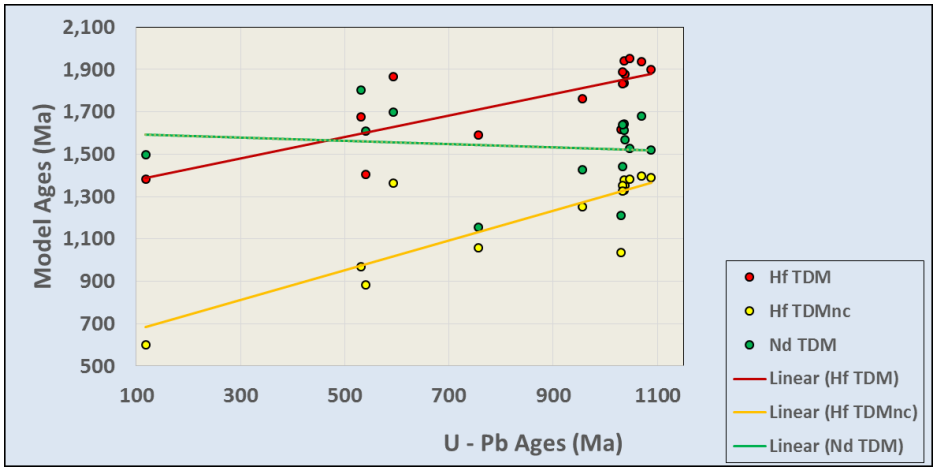

Fig. 6.5: Showing comparisons between the neodymium and hafnium model ages on granitoids from southern Malawi

6.7 DISCUSSION

The use of the Sm –Nd model age data has an underlying assumption of a single stage model of crustal magma extraction from the mantle but this assumption is challenged by well proven multi-stage extraction models (Stern, 2002; Faure, 2005). Where the mantle composition is known and the time between the model age and crystallisation age is short, model age data can provide robust information on crust forming events (Stern, 2002), however caution needs to be exercised when these assumptions do not hold true and this probably applies to most of the findings for the Malawi granitoids discussed above.

Regional comparisons may provide useful correlations. Sm – Nd data for Tanzania (Moller et al., 1998), Antarctica (Will et al., 2010), India (Tomson et al., 2013) and Mongolia (Li et al., 2013) taken from the published literature has been compiled alongside data from Malawi (this study and published (Kröner, 2001)). εNd(t) values were calculated from this dataset and are plotted against U – Pb ages in Fig. 6.8. The data from India and Antarctica shows positive and negative εNd(t) values in the Archean period implying juvenile material contributions and recycling of older crust at that time, whilst data from Tanzania indicates negative values during that period signifying only recycling of older crust. During the Neoproterozoic the Indian data displays a significant range of negative εNd(t) values and a marked absence of positive values in the Meso- and Neoproterozoic periods implying no crustal additions during these periods. Similarly data from Mongolia suggest no crustal additions during the Meso- and Neoproterozoic periods but recycling of older crust.

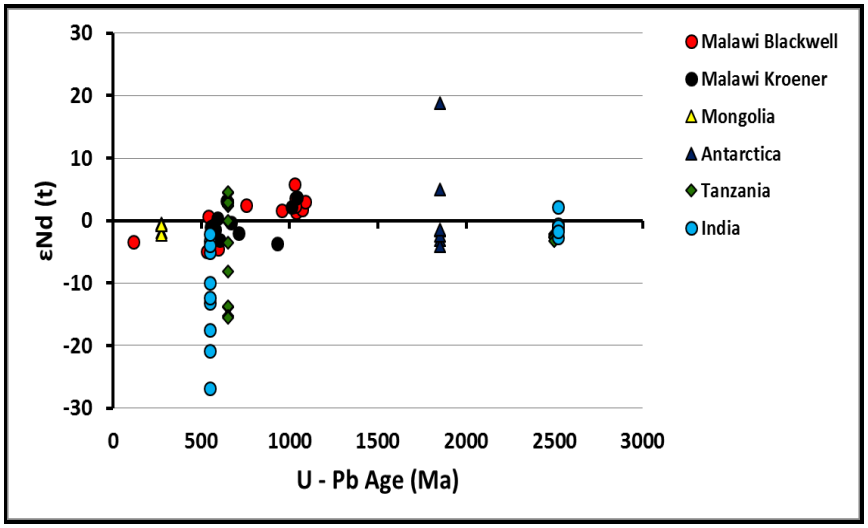

Fig. 6.6: εHf(t) vs U -Pb age evolution diagram for the southern Malawi granitoids in comparison with analogous data from other regions. Data from this study; Kröner et al., 2001; Shan et al., 2013; Tomson et al., 2013; Moeller et al., 1998)

From the available data in this study the southern Malawi area is largely a block where Mesoproterozoic crust dominates (Figure 6.6). The depleted model ages (TDM_{nc}) for the arc margin type granitoids (561 to 1415 Ma) imply very little or no addition of pre-Paleoproterozoic material to the crust, an inference supported by U – Pb dating in this study and other studies (Kröner, 2001; Muhongo, 2003). Importantly, the Mesoproterozoic granitoids all show positive εNd(t) values but there is a significant difference between crustal extraction age and crystallisation age, which can be interpreted as mixing between juvenile melts and recycled crust all from within the Mesoproterozoic (Faure, 2005, p. 206).

Whilst the data are far from exhaustive the presence of positive εNd(t) values during the Mesoproterozoic in Malawi is clearly important (Fig. 6.7), along with crustal additions in Tanzania. One implication deriving from this is that at the end of the Mesoproterozoic southern Malawi experienced calc-alkaline magmatism from juvenile material in an arc margin environment, an event shared with some parts of Tanzania but missing in India, Antarctica and Mongolia. This may reinforce the notion that tectono-thermal events that led to break-up and amalgamation of Rodinia and Gondwana were not uniform across the East African Orogen/Mozambique Belt (Ashwal et al., 2005). More data for the other regions might establish new crustal linkages as is the case for Malawi and Tanzania.

Figure 6.7 is a correlation diagram of εHf(t) and εNd(t) for the southern Malawi granitoids. Positive correlations have been reported between initial hafnium and neodymium isotopes in depleted mantle rocks as well as those derived from the crust (Andersen et al., 2002). Fig. 6.7 shows a positive correlation with the exception of one sample BM281 which is a charnockitic gneiss. It is not known yet why this sample is anomalous.

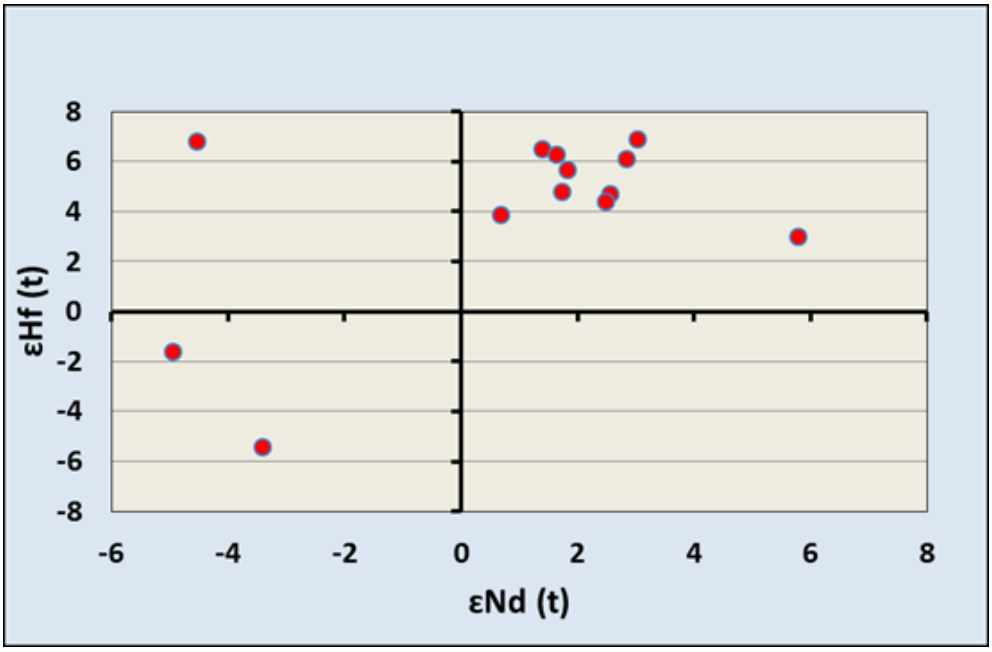

Fig. 6.7: εNd(t) vs εHf(t) correlation diagram for granitoid samples from southern Malawi

6.8 CONCLUSIONS

Epsilon values for these radiogenic isotope systems based on different model assumptions indicate that crust building took place principally through addition of mantle material with a lesser role for crustal recycling.

Radiogenic isotope model ages for the granitoids are older than their U-Pb crystallisation ages testifying to the complexity of the crust-building process in southern Malawi during the Mesoproterozoic.

Of the various Nd and Hf model ages the Hf TDM_{nc} model ages correlate best with U-Pb crystallisation ages for the granitoids although the Hf ages are significantly older. Intrusions that are younger in terms of U-Pb crystallisation age tend to have Hf TDM_{nc} ages that are older by about 600 Ma whereas older intrusions ages tend to have Hf TDM_{nc} model ages that are older by about 250 Ma.

The evolution of εHf(t) with time as constrained by U-Pb ages in zircons indicates an increasing role for crustal recycling with time, with the youngest granitoids being essentially crustal melts.

6.9 REFERENCES

Ashwal L. D., Armstrong R. A., et al., (2006) Geochronology of Zircon Megacrysts from Nepheline-bearing Gneisses as Constraints on Tectonic Setting: Implications for Resetting of the U-Pb and Lu-Hf Isotopic Systems, Contributions to Mineral Petrology (2007) 153:389–403, DOI 10.1007/s00410-006-0153-

Andersen T., Griffin W. L. & Pearson N. J., Crustal Evolution in the SW Part of the Baltic Shield: the Hf Isotope Evidence, J. Petrology (2002) 43 (9): 1725-1747. doi: 10.1093/petrology/43.9.1725

DePaolo D. J., (1981), Neodymium Isotopes in the Colorado Front Range and Crust-Mantle evolution in the Proterozoic, Nature Vol 291

Dhuime B., Hawkesworth C., Cawood Peter, (2011), When Continents Formed, GEOCHEMISTRY, Perspectives, Volume 331, pp.154 – 155.

Dickin A. L., (2005), Isotope Geology, 2nd Edition, Cambridge University Press, New York.

Faure G., & Mensing T. M., (2005), Isotopes: Principles and Applications, 3rd Edition, John Wiley & Sons, INC. New Jersey, USA.

Harrison T. M., Schmitt A. K., McCulloch M. T., Lovera O. M., 2008, Early (≥4.5 Ga) formation of terrestrial crust: Lu–Hf, δ18O, and Ti thermometry results for Hadean zircons, Earth and Planetary Science Letters 268 (2008) 476–486.

Kröner, A., A. P. Willner, et al. (2001). "Single zircon ages, PT evolution and Nd isotopic systematics of high-grade gneisses in southern Malawi and their bearing on the evolution of the Mozambique belt in south-eastern Africa." Precambrian Research 109(3-4): 257-291.

Moeller A., Mezger K., & Schenk V., 1998, Crustal Age Domains and the Evolution of the Continental Crust in the Mozambique Belt of Tanzania: Combined Sm–Nd, Rb–Sr, and Pb–Pb Isotopic Evidence, Journal of Petrology, Vol. 39, No.4 pp. 749–783, 1998

Muhongo, S., C. Hauzenberger, et al. (2003). "Vestiges of the Mesoproterozoic events in the Neoproterozoic Mozambique belt: The East African perspective in the Rodinia puzzle." Gondwana Research 6(3): 409-416.

Shan Li, Simon A. Wilde, Tao Wang, Qianqian Guo, 2013, Incremental growth and origin of the Cretaceous Renjiayingzi pluton, southern Inner Mongolia, China: Evidence from structure, geochemistry and geochronology, Journal of Asian Earth Sciences 75 (2013) 226–242.

Stern R. J., 2002, Crustal evolution in the East African Orogen: a neodymium isotopic perspective, Journal of African Earth Sciences, 34 (2002) 109–117.

Tomson, J.K., Bhaskar Rao Y.J., Vijaya Kumara T., Choudhary A.K., 2013, Geochemistry and neodymium model ages of Precambrian charnockites, Southern Granulite Terrain, India: Constraints on terrain assembly, Precambrian Research 227 (2013) 295–315.

White, M. M., 2007, Geochemistry, An online textbook eventually to be published by John-Hopkins University Press.

Will T.M., Frimmela H.E., Zeha A., Roux P. Le, E. Schmädicke, Geochemical and isotopic constraints on the tectonic and crustal evolution of the Shackleton Range, East Antarctica, and correlation with other Gondwana crustal segments, Precambrian Research 180 (2010) 85–112, doi:10.1016/j.precamres.2010.03.005.

Chapter 7: Synopsis and Perspectives

7.1 Project summary

The ultimate objective of this research is to enhance our understanding of the crustal evolution of the Mozambique Belt, a principal suture in Gondwana assembly, thereby providing constraints to global paleogeography during the Proterozoic, a first order control on Earth's system major changes to the surface and solid Earth's processes at a key time in Earth history (Cawood and Buchan, 2007; Collins and Pisarevsky, 2005). The study provides constraints on the timing, sources and nature of the tectono-thermal events responsible for magmatism in the Mozambique Belt in southern Malawi. The hypothesis to be tested were threefold. Firstly, that the region is a multiply metamorphosed terrane with granulite facies metamorphism – and would be tested by U - Pb zircon high precision age dating. Secondly, that contemporary crust in this region is derived from re-melting and re-working of older crust derived from mantle and upper crust levels of the lithosphere and was to be tested using Nd isotope modelling. Thirdly, that different crustal growth zones and intervals exist in this region and that granitoids are an expression of collision-continental arc margin environments, and this would be tested using Lu-Hf dating and modelling in combination with geochronological constraints (Chapter 5).

Prior to this study, the bedrock geology of this area was generally understood from a broad regional scale, that the area was underlain by basement complex gneisses intruded by various orthogneisses which were believed to be mainly Archean – Precambrian (Bloomfield, 1974; Andreolli, 1984; Kröner et al., 2001). The southern Malawi area is important as it lies within the East African Orogen, which comprises deformed and metamorphosed Precambrian rocks and is generally considered to be the principal suture zone during late Neoproterozoic amalgamation of Gondwana thus recording evidence of the genesis and evolution of the belt (Vogt et al., 2006; Kröner, 2001). To add our understanding of the geodynamic history of the southern Malawi terrane of the Mozambique Belt and further constrain existing tectonic models, various samples of granitoids and supracrustals were collected for petrographic, geochemical and geochronological analyses from the main lithological units in the area.

This thesis therefore is a presentation of results for my PhD study and a discussion of the implications for existing tectonic models on Rodinia and Gondwana break-up and amalgamation. The thesis mainly reports on new Laser Ablation Inductively Coupled Plasma Mass Spectrometer (LA-ICP-MS) single zircon U – Pb data, new whole rock major and trace element analyses, and radiogenic isotope (samarium - neodymium (Sm-Nd) and lutetium-hafnium (Lu-Hf)) data from southern Malawi. Single zircon U – Pb data report crystallization and metamorphism ages from grano-dioritic to quartz-monzo-dioritic meta-granites, charnockitic gneisses and some hornblende biotite gneiss rocks which stratigraphically are deemed the oldest rocks in the area. The major and trace element geochemistry data apart from enabling comparison in between similar aged and compositionally like rock units (Grantham et al., 2011), provides pointers to the geo-tectonic settings where the lithologies were formed. The Sm – Nd and Lu – Hf isotope data points us to the sources of magmatism and provides knowledge of the involvement of older crust in the formation of the new crust (Grantham et al., 2011). These sets of data are correlated with data from other regions in the Mozambique Belt to help us understand the nature of the cratonic boundaries.

7.2 Geochemistry

The geochemistry study shows that the charnockitic gneisses from southern Malawi are intermediate to acidic with relative enrichment in LILEs and depletion in HFSEs with moderately negative anomalies in Th, Nb, P, Zr and Ti. The REE spider plots show enrichment in the LREEs and depleted HREEs with negative Eu anomalies. The meta-granites are largely metaluminous with a few peraluminous, I-type granites belonging to the calc-alkaline series. They are enriched in LILEs, depleted in the HFSEs (Nb, Ta, P, and Ti), and show consistently negative Eu anomalies in the REE patterns. The meta-granites and the charnockitic gneisses are collectively calc-alkaline series rocks with continental arc margin signatures pointing to a volcanic arc setting. Both the charnockitic gneisses and the meta-granites from Malawi are geochemically similar to published literature Tanzania charnockitic gneisses and Mozambique meta-granites. In broader terms the chemistry of the charnockitic gneisses is most similar to a group termed metamorphic charnokites (Kilpatrick et al., 1992).

7.3 Geochronology

The LA-ICP-MS single zircon U-Pb results in this study show tectono-thermal events in four periods: Mesoproterozoic stretching from 1128 ± 30 Ma to 1033 ± 20 Ma; Neoproterozoic (956 ± 12 Ma – 594 ± 65 Ma); and Cambrian (530 ± 3 Ma – 515 ± 12 Ma), and Cretaceous (118 ± 2 Ma). Magmatism during the Mesoproterozoic spanned a period of nearly a hundred years in three pulses at 1128 ± 30 Ma, 1070 Ma, and 1033 – 1047 Ma. The oldest (1128 ± 30 Ma) is the emplacement of a charnockitic gneiss (sample BM252) occurring southwest of Mulanje. All the meta-granite samples have emplacement dates within the Mesoproterozoic. The emplacement of the protolith of hornblende biotite gneiss occurred ~956 Ma, with a leucogranite intruding at ca. 756 Ma and charnockitic gneiss sample BM281 intruded much later (ca. 600 Ma). Pan-African magmatism has been dated for a perthitic syenite from Chiradzulu Hill to the north of Blantyre at 594 Ma. The Cretaceous emplacement date (118 ± 2 Ma) of Mulanje Mountain granite close to the Mozambique border east of the study area is consistent with magmatism during the Upper Jurassic to Cretaceous in the Chilwa Alkaline Province in southern Malawi and adjacent parts of Mozambique (Platt et al., 1986).

Metamorphism is dated from a charnockitic sample BM252 that yielded a lower intercept age of 515 ± 18 Ma. A monazite $^{207}Pb/^{235}U$ age of 522 ± 17 Ma confirmed amphibolite metamorphism in the area (Ashwal et al., 2007) and it was suggested that it was a result of collisional suturing events associated with amalgamation of East and West Gondwana. Peak regional granulite facies metamorphism in the central part of Tanzania has been dated at c 640 Ma (Sommer et al., 2003). Granulite facies metamorphism was dated as Mesoproterozoic at c. 1080 in East Antarctica (Dronning Maud Land) with subsequent metamorphic events dated at c. 570 – 550 Ma and 530 – 515 Ma (Jacobs et al., 2001). The date from the charnockitic sample BM252 is thus consistent within errors with the monazite date by Ashwal et al., 2007 but both (515±18 Ma and 522 ± 17 Ma, respectively) are younger than those documented in previous studies in southern Malawi i.e. 571–549 Ma, but are closer to those known for the Central Dronning Maud Land/East Antarctica (570 – 550 Ma; 530–515 Ma). They are also younger than dates from Tanzania which have given ages of ca. 640 Ma.

7.4 Radiogenic Isotopes Ages

Radiogenic isotope data reveals slight differences in that older rocks of Mesoproterozoic age show positive εNd and εHf values signifying derivation from depleted mantle (juvenile) material, whilst the younger aged rocks display negative epsilon values suggestive of crustal

material recycling and mixing for their source and origins (Chapter 6 - Fig. 6.4). The data however does not show any clear crustal boundaries in southern Malawi. Radiogenic isotope model ages for the granitoids are older than their U-Pb crystallisation ages. Of the various Nd and Hf model ages the Hf TDM_{nc} model ages correlate best with U-Pb crystallisation ages for the granitoids although the Hf ages are significantly older (Chapter 6 - Fig. 6.5). Intrusions that are younger in terms of U-Pb crystallisation age tend to have Hf TDM_{nc} ages that are older by about 600 Ma whereas older intrusions ages tend to have Hf TDM_{nc} model ages that are older by about 250 Ma. The evolution of εHf(t) with time as constrained by U-Pb ages in zircons indicates an increasing role for crustal recycling with time, with the youngest granitoids being essentially crustal melts.

Three charnockitic gneisses, BM249, BM281 and BM282A yielded very different U-Pb ages (1036, 592 and 540 Ma respectively) indicating separate thermal events yet their crustal model ages are not very different (1642, 1700 and 1611 Ma respectively) while there is some variation in their εNd(t) values (+1.4, -4.5 and +0.7 respectively). The sources of the charnockites vary from enriched mantle or crustal remelts to slightly depleted mantle. These data suggest that the sources for the charnockites may have separated from the mantle at around 1650±50 Ma.

Four of the meta-granites (BM163, BM174, BM179 and BM209) have U-Pb ages between 1033 and 1047 Ma. Collectively they have crustal model ages of 1442 to 1613 Ma and εNd(t) from +1.7 to +3.6. The data suggest derivation of these granites from a slightly depleted source that separated from the mantle at around 1500 Ma to be remobilised at around 1040 Ma. The metagranite enclave BM213X shares these characteristics although it has a slightly older crustal model age of 1638 Ma.

Three gneisses, a syenite and an unfoliated granite have very different U-Pb ages. Quartzofeldspathic gneiss BM200 has a U-Pb age of 1031Ma with an initial εNd (t) value of +5.8 and a crustal model age of 1568 Ma. These characteristics are similar to several meta-granites and a charnockitic gneiss indicating that BM200 belongs to this magmatic episode. A leucocratic gneiss (BM223A) yields a U-Pb age of 956 Ma, εNd (t) value of +1.6 and a crustal model age of 1426 Ma. These characteristics do not match any of the other samples and appear to represent a discrete event. A foliated hornblende biotite gneiss (BM221) has U–Pb age of 756 Ma, an initial εNd (t) value of +2.5 and a crustal model age of 1153 Ma. This also appears to represent a separate event. A foliated perthitic syenite (BM289) gives a U–Pb age of 531 Ma, an initial εNd (t) value of -5.0 and a crustal model age of 1801 Ma, and this also appears to be a unique event. Finally a very young event is represented by an unfoliated granite (BM240) with a U–Pb age of 118 Ma, an initial εNd (t) value of -3.4 and a crustal model age of 1497 Ma. This group of five diverse samples appear to represent five different events, at least based on U-Pb ages and Nd isotope systematics, with one of these events coinciding with the main group of metagranites.

The geochronology, radiogenic isotope and geochemistry data in the thesis is summarized in integrated Table 7.1.

Table 7.1: Thesis data summary for the southern Malawi granitoids. In the table CA = Calk-alkaline; TH = Tholeiitic. NA = Data was not available/not taken. VAG = Volcanic Arc Granite; WPG = Within Plate Granite.

THESIS DATA SUMMARY											
SAMPLE	ROCK TYPE	U-Pb (Ma)	error (2s)	TDMnc(Nd	εNd(t)	Mnc(Hf)εH	εHf(t)	SiO2%	A/CNK	Series	Tectonic setting indicator
BM249	Charnokitic gneiss	1036	21	1642	+1.4	1293-1364	+6.4	57.73	1.16	CA	VAG
BM281	Charnokitic gneiss	594	65	1700	-4.5	1348-1380	+6.8	57.41	1.02	CA	VAG
BM282A	Charnokitic gneiss	540		1611	+0.7	1335, 883	+9.2, +2.3	56.52	0.97	CA	VAG
BM163	Metagranite	1038.2	6.8	1568	+2.8	1351	+6.1	54.96	0.86	CA	VAG
BM174	Metagranite	1036.6	8.3	1613	+1.7	1379	+4.8	62.91	1.02	CA	VAG
BM179	Metagranite	1047	13	1526	+2.6	1384	+4.7	64.33	1.19	CA	VAG
BM209	Metagranite	1033	20	1442	+3.6	1327	+6.8	60.68	0.89	CA	VAG
BM213G	Metagranite	1035	12	1522	+3.0	1389	+6.9	61.04	0.96	CA	VAG
BM213X	Metagranite enclave	1034	17	1638	+2.3	1353	+5.7	56.31	0.83	CA	VAG
BM256	Metagranite	1070	16	1681	+1.8	1396	+6.1	63.44	0.88	CA	VAG
BM200	QF gneiss	1031	19	1568	+5.8	1254, 929	NA	NA	1.13	NA	NA
BM223A	Horn-biotite gneiss	956	12	1426	+1.6	1251	+6.9	60.39	0.87	CA	VAG
BM221	Horn-biotite gneiss	756	8.4	1153	+2.5	1060	4.5	75.01	0.99	CA	WPG
BM289	Perthitic gneiss	531	3.4	1801	-5.0	970	+1.6	67.48	1.13	CA	VAG
BM240	Unfoliated granite	118	1.2	1497	-3.4	602	-5.4	64.04	1.01	CA	WPG
BM233	QF gneiss	NA		NA	NA	NA	NA	NA	1.3	NA	NA
BM252	Charnockitic gneiss	1128	30	NA	NA	NA	NA	63.44	1.3	TH	VAG

7.5 Crustal Evolution Path

Fig.7.1 is a εHf(t) vs U –Pb age evolution diagram for the southern Malawi granitoids. They show positive εHf(t) values in three major age populations; in the Mesoproterozoic (~1040 Ma), in the Neoproterozoic (~760 Ma), and in the Cambrian (~530 Ma). Negative εHf(t) values also occur during the Cambrian and in the Jurassic (~120 Ma). An important relationship shown by this diagram is the steep reworking trend in the data with a Lu/Hf ratio of 0.015 projecting back to an average model age of ~1.5 Ga.

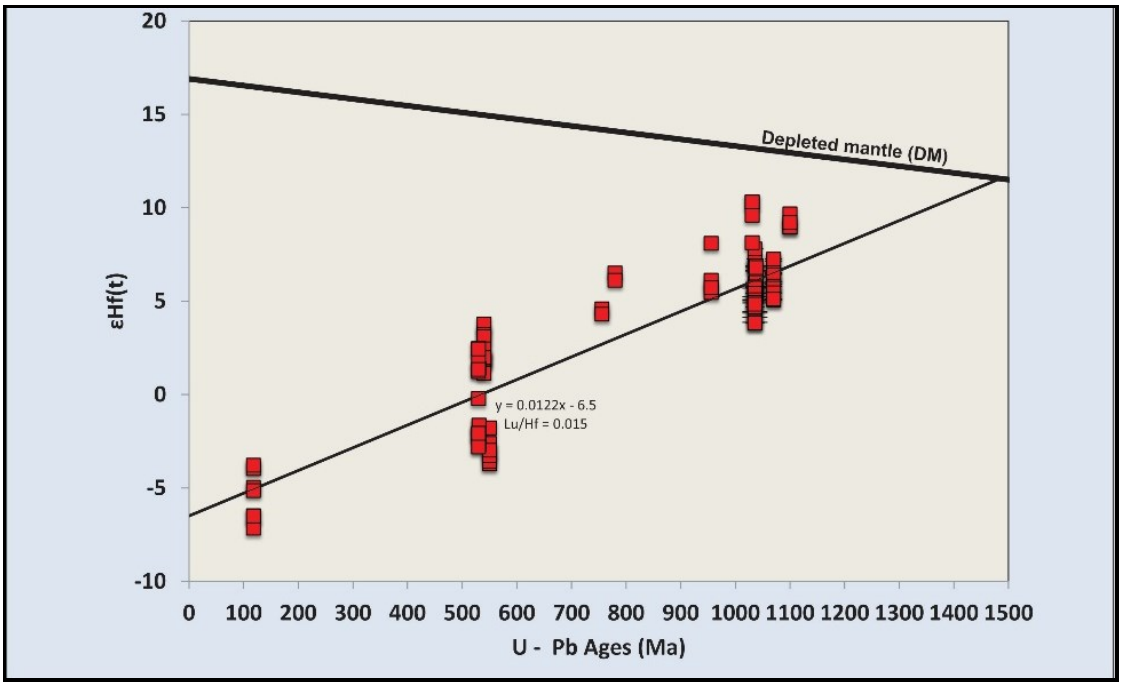

Fig. 7.1: εHf(t) vs U-Pb age evolution diagram for the southern Malawi granitoids

7.6 Regional Implications

U – Pb age data from Malawi (this study) is plotted in a histogram (Fig. 7.2) alongside data from the Southern Irumide Belt (SIB) to the west of Malawi in Mozambique and Zambia (Johnson et al., 2006), Mozambique Belt (Tanzania) (Sommer et al., 2003), and Mozambique Belt (Mozambique) (Bingen et al., 2009). The data indicates that there are no magmatic events in the southern Malawi region pre- 1100 Ma. The magmatism in southern Malawi closely resembles that of the Mozambique Belt (Mozambique) where magmatism ends at around 1200 Ma. The data from neighbouring Southern Irumide Belt (SIB) to the west of Malawi in Mozambique and Zambia shows magmatism between 950 – 1450 Ma and none in the Paleoproterozoic and Archean periods. The data from the Mozambique Belt (Tanzania) is marked by absence of magmatism at around 1000 Ma – a period when there is magmatic activity in Malawi, Mozambique and SIB. The Tanzania data shows magmatism in the Paleoproterozoic and Archean periods. A time-space plot (Fig. 7.3) shows the magmatism and metamorphism indicated from the U – Pb age data. Both, magmatism and metamorphism, are dated during the Pan African in Malawi, Mozambique Belt in Mozambique and Tanzania. These events are missing in the SIB based on the provided U –Pb data. Magmatism is evident around 1000 Ma in southern Malawi, in the SIB and in Mozambique but absent in the Mozambique Belt (Tanzania). From this data it is evident that the southern Malawi area has a Mozambique Belt imprint whilst the Southern Irumide Belt does not, which suggests that the boundary between the Mozambique Belt and the "Kibaran" Southern Irumide Belt (SIB) lies somewhere near the border of southern Malawi and western Mozambique.

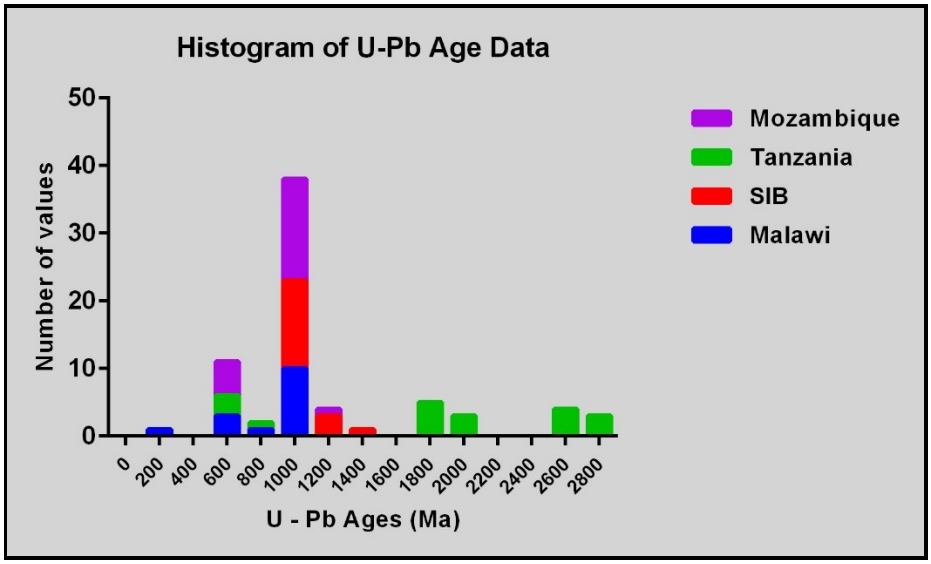

Fig. 7. 2: Histograms of U - Pb ages for Mozambique Belt (Malawi, Mozambique & Tanzania) and South Irumide Belt (W. Mozambique & Zambia). Data sources: (Blackwell Manda - this study; Johnson et al., 2006; Sommers et al., 2007; Bingen et al., 2009).

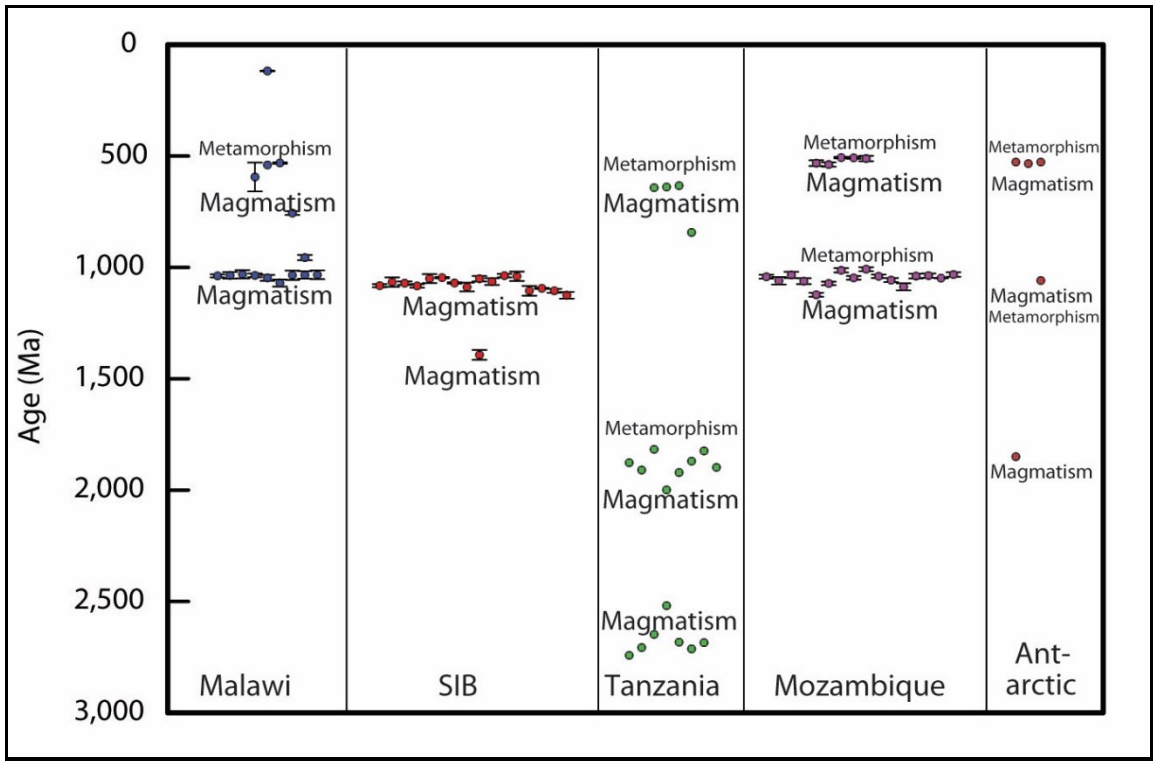

Fig. 7.3: Time Space plot for U - Pb age data for Malawi (this study), Southern Irumide Belt (SIB), Tanzania, Mozambique, and Antarctica. Data sources: (Blackwell Manda - this study; Johnson et al., 2006; Sommer et al., 2003; Bingen et al., 2009).

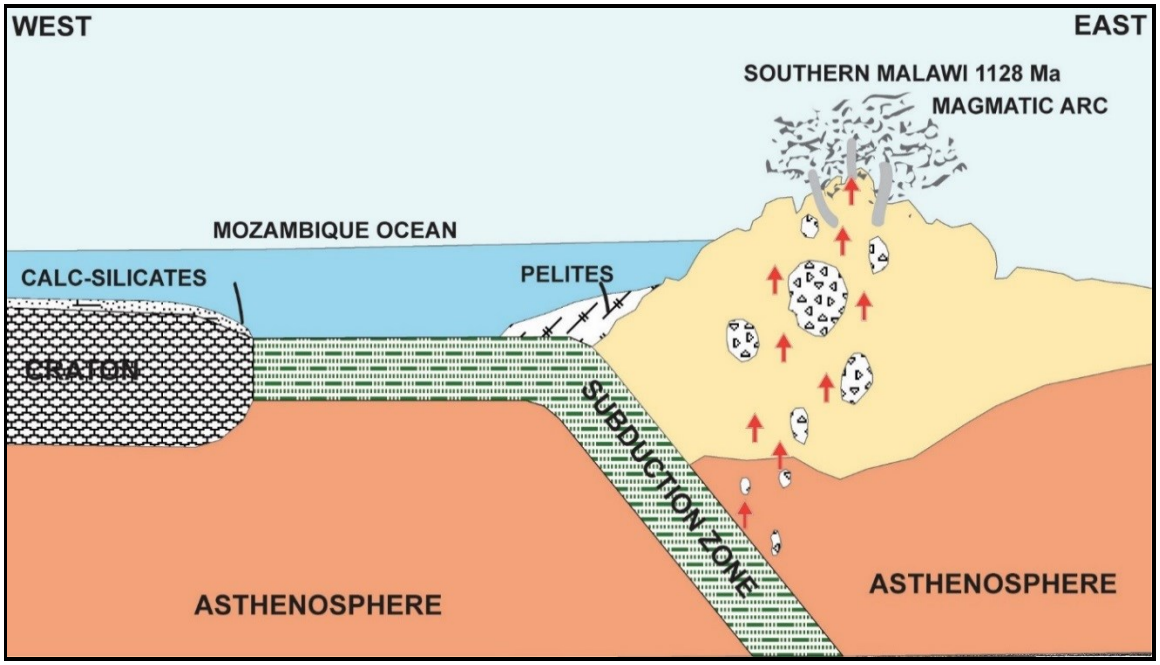

Fig. 7. 4: Schematic diagram showing a genetic model and tectonic setting of southern Malawi during the Mesoproterozoic. The oldest (1128 ± 30 Ma) is the emplacement of a charnockitic gneiss (sample BM252) occurring southwest of Mulanje. The emplacement of the protolith of hornblende biotite gneiss occurred ~956 Ma.

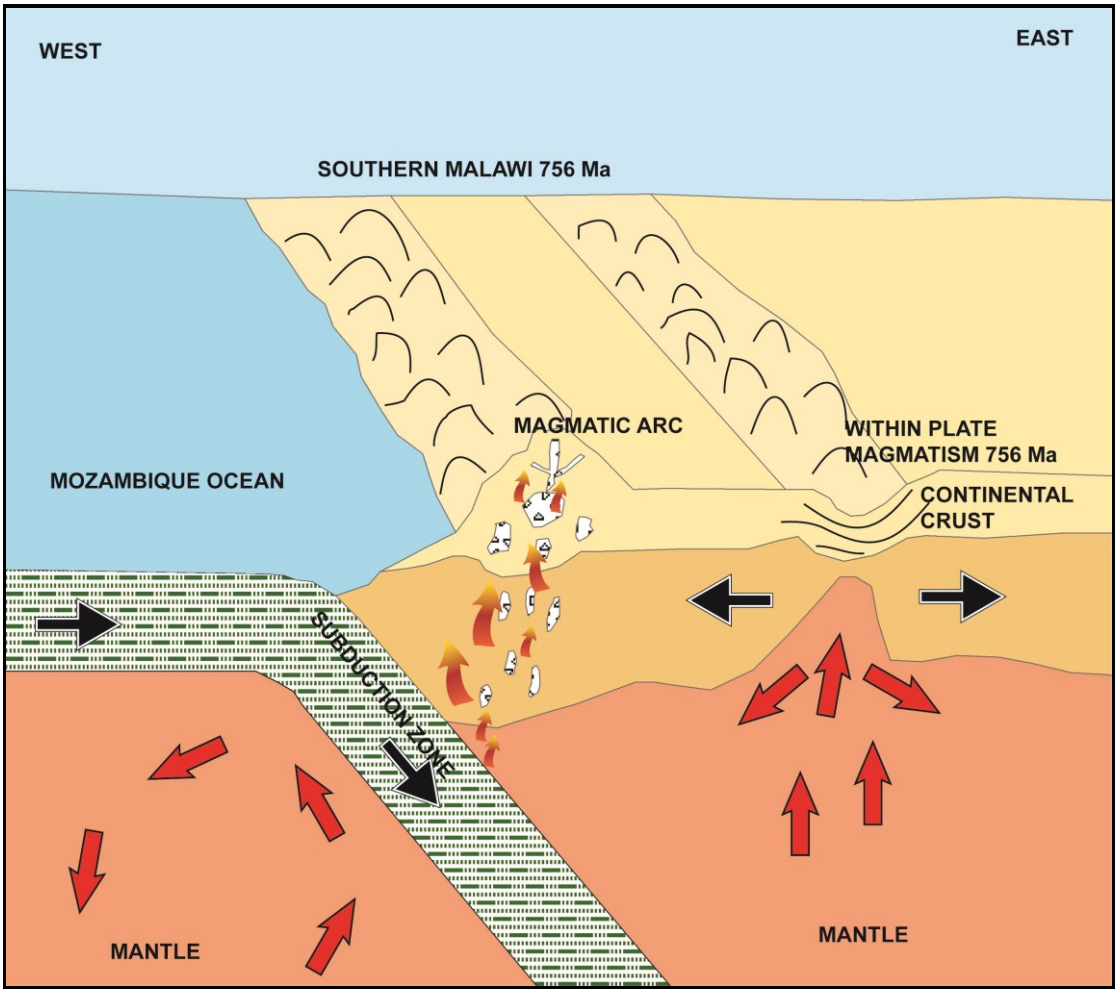

Fig. 7.5: Schematic diagram showing a genetic model and tectonic setting of southern Malawi during the Neoproterozoic. Mantle superplume could have been responsible for Rodinia break-up which may correspond to the rifting in Malawi c. 765 Ma.

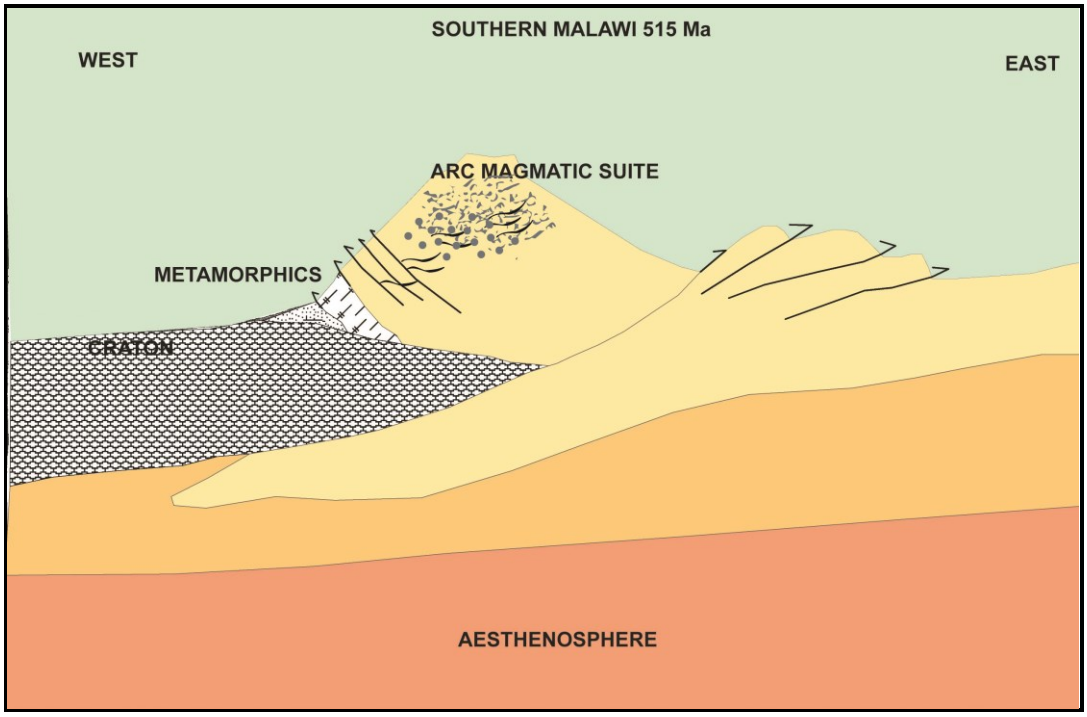

Fig. 7.6: Schematic diagram showing a genetic model of southern Malawi during the Neoproterozoic - Cambrian period.

The genesis of depleted mantle material is directly connected to subduction tectonics that ultimately ends in ocean closures, continent collisions and continental amalgamations (Pollock et al., 2015). Nd and Hf model ages between 1800 and 1150 Ma for southern Malawi with positive epsilon values are therefore associated with juvenile material from arc margin tectonics during Rodinia assembly and breakup (Fig. 7.4). Various arguments have been put forward regards specifics in the Rodinia supercontinent fit and chronological issues of its disintegration, but general consensus has it that initial break-up occurred at 725 – 750 Ma (Torsvik et al., 1996). Magmatism in the Neoproterozoic i.e. 756 Ma in southern Malawi (Fig. 7.5) has been attributed to events related to Rodinia breakup (Ashwal et al., 2007) although the spatial relationships between these southern Malawi events and those of other Rodinia blocks could not be ascertained. Interesting to note in our compared data (Fig. 7.3) is that this type of magmatism is absent in the neighbouring SIB and Mozambique but can be seen in Tanzania. A perthitic syenite BM289 yielded a crystallisation age of 531 ± 3.4 Ma and these intrusions have been associated with reactivated rifting (Bloomfield, 1965; Evans, 1965; Garson et al., 1965). Similarly the Cretaceous granite BM240 dated 118 ± 1.2 is associated with reactivation of the East African Valley rift.

The metamorphism date during the Cambrian period (515 ± 12 Ma) in this study is interpreted as relating to collisional events of Gondwana assembly, consistent with similar events in the Mozambique Belt in Tanzania and Mozambique (Fig. 7.3). The date is younger than previous dates by other authors (Ashwal et al., 2007; Kröner, et al., 2001) but it is now established that the timing of metamorphism in the Mozambique Belt has spatial and temporal variations (i.e. diachronous). Even younger dates of metamorphism (505 Ma, 497 ± 8 and 453 ± 17 Ma) have been reported from Mozambique (Ashwal et al., 2007).

7.7 CONCLUSION

The main conclusion of this study is that the charnokitic gneisses and meta-granites of southern Malawi bear the characteristics of an origin in a continental arc mainly by crustal melting but with the possibility of mantle inputs, with model ages from late Paleoproterozoic to early Mesoproterozoic, varied emplacement ages mainly from Mesoproterozoic to Cambrian and one emplacement date from the Cretaceous. They share chemical characteristics with Andean type granitoids and some aspects of the chemistry resembles tonalite-trondhjemite-granite (TTG) suites mapped in the Mozambique Belt in Kenya, Tanzania, Mozambique, and Antarctica (Muhongo, 2003; Grantham et al., 2003; Westerhof, et al., (2007) although the data are not sufficiently compelling to assign the Malawi rocks to classic TTGs. Metamorphism is dated in the Cambrian (515 ± 12 Ma).

Previous studies using high precision geochronology in southern Malawi have found no evidence of Mesoproterozoic high grade metamorphism consistent with continental collision, but have confirmed Neoproterozoic – Cambrian metamorphism that overprinted the earlier magmatism (Kröner et al., 2001, 2003; Johnson et al., 2005; Ashwal et al., 2007). Consistent with the foregoing this study of the amphibolite-granulite-facies rocks in southern Malawi also shows no evidence for the presence of late Archean reworked crustal precursors as suggested by Andreolli (1984).

7.8 RECOMMENDATIONS

The following are recommendations for further work in southern Malawi:

1. Refinement of the timing constraints on the calc-alkaline magmatism using methods which are an order of magnitude higher in precision than LA-ICP-MS such as chemical abrasion–isotope dilution–thermal ionization mass spectrometry (CA-ID-TIMS).

2. Need to obtain a wide range of geochronological constraints that reflect full range of cooling history.

3. A more detailed grid type of mapping and geochronology of the border areas of western Malawi in the southern region and Mozambique to define the boundaries between the Mesoproterozoic SIB and Mozambique belts.

4. The Rodinia break-up and subsequent rift related magmatic events from 756 Ma needs further petrological, geochemistry, and geochronological work.

7.9 REFERENCES

Andreolli, M. A. G., (1984), Petrochemistry, Tectonic Evolution and Metasomatic Mineralizations of Mozambique Belt Granulites from S Malawi and Tete (Mozambique), Precambrian Research, Vol. 25, Issue 1-3, pp. 161-186.

Ashwal L.D., R. A. Armstrong et al., (2006), Geochronology of Zircon Megacrysts from Nepheline-bearing Gneisses as Constraints on Tectonic Setting: Implications for Resetting of the U-Pb and Lu-Hf Isotopic Systems, Contrib Mineral Petrol (2007) 153:389–403, DOI 10.1007/s00410-006-0153-

Cawood P. A. & Buchan C., (2007), Linking accretionary orogenesis with supercontinent assembly, Earth-Science Reviews, Volume 82, Issues 3–4, June 2007, Pages 217–256

Collins, A. S. and S. A. Pisarevsky (2005). "Amalgamating eastern Gondwana: The evolution of the Circum-Indian Orogens." Earth-Science Reviews **71**(3–4): 229-270.

Grantham G.H., Manhica A.D.S.T., Armstrong R.A., Kruger F.J., Loubser M., (2011), New SHRIMP, Rb/Sr and Sm/Nd isotope and whole rock chemical data from central Mozambique and western Dronning Maud Land, Antarctica: Implications for the nature of the eastern margin of the Kalahari Craton and the amalgamation of Gondwana, Journal of African Earth Sciences 59 (2011) 74–100.

Grantham G. H., Maboko M. & Eglington B. M. (2003), A review of the evolution of the Mozambique Belt and implications for the amalgamation and dispersal of Rodinia and Gondwana, Geological Society, London, Special Publications, 206, 401-425. 0305-8719/03/$15

Jacobs J., C. Mark Fanning, Friedhelm Henjes-Kunst, Martin Olesch, and Hans-Ju¨ rgen Paech, Continuation of the Mozambique Belt into East Antarctica: Grenville-Age Metamorphism and Polyphase Pan-African High-Grade Events in Central Dronning Maud Land, The Journal of Geology, Vol. 106, No. 4 (July 1998), pp. 385-406, The University of Chicago Press, Stable URL: http://www.jstor.org/stable/10.1086/516031, Accessed: 10/12/2015 18:21

Johnson S. P., Rivers T. & De Waele B., 2005, A review of the Mesoproterozoic to early Palaeozoic magmatic and tectono-thermal history of south–central Africa: implications for Rodinia and Gondwana, Journal of the Geological Society, London, Vol. 162, 2005, pp. 433–450.

Kilpatrick J. A. and Ellis D. J., (1992), C-Type Magmas: Igneous Charnockites and their Extrusive Equivalents, Transactions of the Royal Society of Edinburgh: Earth Sciences, 83, 155-153, 1992.

Kröner A., Willner A. P., Hegner E., Jaeckel P., Nemchin A., (2001). "Single Zircon Ages, PT Evolution and Nd Isotopic Systematics of High-Grade Gneisses in Southern Malawi and their Bearing on the Evolution of the Mozambique Belt in South-eastern Africa." Precambrian Research **109**(3-4): 257-291.

Kröner A., & U. Cordani, (2003), African, Southern Indian and South American Cratons were not part of the Rodinia Supercontinent: Evidence from Field Relationships and Geochronology, Tectonophysics 375 (2003) 325– 352.

Muhongo S., Hauzenberger C., and Sommer H., (2003), Vestiges of the Mesoproterozoic Events in the Neoproterozoic Mozambique Belt: the East African Perspective in the Rodinia Puzzle, Gondwana Research, V 6, No. 3, pp. 409-41 6.

Pollock J.C., Sylvester P.J., and Barr S.M., (2015), Lu–Hf zircon and Sm–Nd whole-rock isotope constraints on the extent of juvenile arc crust in Avalonia: examples from Newfoundland and Nova Scotia, Canada, Can. J. Earth Sci. 52: 161–181 (2015) dx.doi.org/10.1139/cjes-2014-0157.

Sommer H., A. Kröner, C. Hauzenberger, S. Muhongo and M. T. D. Wingate, (2003), Metamorphic petrology and zircon geochronology of high-grade rocks from the central Mozambique Belt of Tanzania: crustal recycling of Archean and Paleoproterozoic material during the Pan-African orogeny, Journal of metamorphic Geology, 2003, 21, 915–934 doi:10.1046/j.1525-1314.2003.00491.x

Torsvik T.H., M.A. Smethurst, J.G. Meert, R. Van der Voo, W.S. McKerrow, M.D. Brasier, B.A. Sturt, H.J. Walderhaug, (1996), Continental break-up and collision in the Neoproterozoic and Palaeozoic — A tale of Baltica and Laurentia, Earth-Science Reviews, Volume 40, Issues 3–4, June 1996, Pages 229-258.

Vogt, M., Kroner, A., Poller, U., Sommer, H., Muhongo, S., Wingate, M.T.D., (2006) Archaean and Paleoproterozoic Gneisses Reworked During a Neoproterozoic (Pan-African) High-Grade Event in the Mozambique Belt of East Africa: Structural Relationships and Zircon Ages from the Kidatu Area, Central Tanzania, Journal of African Earth Sciences 45, pp. 139–155.

Westerhof, A. B. Phil, Lehtonen, M. I., Mäkitie, H., Manninen, T., Pekkala, Y., Gustafsson, B. & Tahon, A. (2007), The Tete-Chipata Belt: A New Multiple Terrane Element from Western Mozambique and Southern Zambia, GTK Consortium Geological Surveys in Mozambique 2002–2007, edited by Yrjö Pekkala, Tapio Lehto & Hannu Mäkitie